ELASTIC LATERAL-TORSIONAL BUCKLING OF CELLULAR BEAMS

LUANA VIDOTI DA SILVA

Final thesis submitted to

Escola Superior de Tecnologia e Gestão

Instituto Politécnico de Bragança

For the fulfilment of the Master Degree in

Construction Engineering

June 2022

ELASTIC LATERAL-TORSIONAL BUCKLING OF CELLULAR BEAMS

LUANA VIDOTI DA SILVA

Final thesis submitted to

Escola Superior de Tecnologia e Gestão

Instituto Politécnico de Bragança

For the fulfilment of the Master Degree in

Construction Engineering

In the ambit of the double diploma with the

Universidade Tecnológica Federal do Paraná

Supervisors:

Prof. Dr. Luís Manuel Ribeiro Mesquita

Prof. Dr. Ronaldo Rigobello

June 2022

ACKNOWLEDGMENTS

I want to thank my parents, Mara Roberta and Guilherme, and my brother, Matheus, for always encouraging me in my decisions and giving me all support to face the difficulties encountered. Without them, nothing would be possible. They are my motivation!

I thank my supervisor, Dr. Luís Mesquita, for his patience and help. Always teaching and giving me the necessary support to develop this work.

To the Instituto Politécnico de Bragança (IPB) for the reception in Portugal and for offering me so much during this period. To my supervisor, Dr. Ronaldo Rigobello, and the Universidade Tecnológica Federal do Paraná (UTFPR) for all these years of graduation and the opportunity of the double degree.

I thank my boyfriend, Ricardo Jorge, and all my family and friends from Ilha Solteira- SP, Campo Mourão-PR, and Bragança, Portugal, for making my journey lighter and happier!

RESUMO

Este estudo apresenta uma análise numérica de vigas sólidas e alveolares através do software ANSYS e compara os seus resultados com os resultados obtidos através dos métodos simplificados do Eurocódigo 3 parte 1-1 e do guia SCI P385. Um novo método de cálculo (método 3) para as propriedades geométricas das vigas alveolares é abordado no estudo. A comparação entre os métodos analíticos e numérico tem como objetivo analisar o comportamento e a influência da nova constante de torção abordada nos valores do momento crítico para encurvadura lateral torsional (ELT) e no angulo de torção não uniforme da viga. O tipo de aço escolhido foi o S355 e os perfis do modelo de referência para as vigas solidas e alveolares foram o IPE 200 (RM1) e o HE 200 A (RM2). No total, 316 simulações numéricas foram realizadas, variando o comprimento da viga e os parâmetros geométricos da viga alveolar (diâmetro do furo, espaçamento entre os furos e altura da viga). Concluiu-se que na análise do momento critico para ELT dos RM1 e RM2, a nova constante de torção abordada pelo método 3 apresentou o melhor resultado entre todos os métodos abordados em todos os estudos de caso. Analisou-se também a influência da variação dos parâmetros geométricos utilizando esta nova constante no cálculo do método analítico. Quanto maior o diâmetro do furo, menor a diferença relativa entre a maioria dos casos baseados no perfil HE 200 A. Já nos casos baseados no perfil IPE 200, o valor médio do diâmetro do furo, apresentou uma menor diferença relativa. A variação do espaçamento entre os furos e a altura final da viga não provocou grandes diferenças relativas. Quanto maior o espaçamento entre os furos e a altura da viga, maior a diferença relativa entre a maioria dos casos. Em todos os casos das análises do ângulo de torção não uniforme, a nova constante de torção abordada apresentou a maior diferença relativa entre os métodos analítico e numérico. Esse comportamento pode ser devido a uma diferença no desenvolvimento do modelo numérico com o analítico, que pode ser observada também nos resultados dos casos de viga sólida. Essa diferença é reduzida através da normalização pelos resultados da viga sólida. A nova constante apresentou melhores resultados com uma menor diferença relativa apenas para a viga de L=1[m].

Palavras-chave: Vigas alveolares, Encurvadura lateral torsional, Ângulo de torção não uniforme, Constante de torção, Simulação numérica.

ABSTRACT

This study performed a numerical analysis of solid and cellular beams using the ANSYS software and compared its results with the ones obtained from the simplified methods of Eurocode 3 part 1-1 and the SCI P385 guide. A new calculation method (method 3) for the torsion constant of cellular beams is approached in the study. The comparison between the analytical and numerical methods aims to analyze the behavior and the influence of the new torsion constant approached on the values of the critical moment for lateral-torsional buckling (LTB) and the non-uniform angle of torsion of the beam. The type of steel chosen was S355 and the reference model profiles for solid and cellular beams were IPE 200 (RM1) and HE 200 A (RM2). In total, 316 numerical simulations were performed, varying the beam length and the cellular beam geometric parameters (hole diameter, hole spacing, and beam height). It was concluded that in the analysis of the critical moment for LTB of RM1 and RM2, the new torsion constant approached by method 3 presented the best result among all methods approached in all case studies. The influence of the geometric parameter's variation was also analyzed using this new constant in the analytical method calculation. The larger the hole diameter, the smaller the relative difference between most cases based on the HE 200 A profile. In the cases based on the IPE 200 profile, the average value of the hole diameter presented a smaller relative difference. The variation of the spacing between the holes and the final height of the beam did not cause a great relative differences. The greater the spacing between the holes and the height of the beam, the greater the relative difference between most cases. In all cases of non-uniform torsion angle analyses, the new torsion constant discussed presented the greatest relative difference between the analytical and numerical methods. This behavior may be due to a difference in the development of the numerical model with the analytical one, which can also be observed in the results of the solid beam cases. This difference is reduced through normalization by the results of the solid beam. The new constant presented better results with a smaller relative difference only for the beam of L=1[m].

Keywords: Cellular beams, Lateral-torsional buckling, Non-uniform angle of torsion, Torsion constant, Numerical simulation

INDEX

ACKNOWLEDGMENTS ..... **I**
RESUMO ..... **II**
ABSTRACT ..... **III**
INDEX ..... **IV**
LIST OF FIGURES ..... **VI**
LIST OF TABLES ..... **X**
SIMBOLOGY ..... **XIII**
ABREVIATIONS ..... **XVI**
1. INTRODUCTION **1**
1.1. Contextualization 1
1.2. Objectives 2
1.3. Thesis structure 3
2. LITERATURE REVIEW **5**
2.1. Characterization of cellular beams 5
2.1.1. Application fields 5
2.1.2. Fabrication process 6
2.1.3. Geometric characteristics 7
2.2. Lateral torsional buckling 10
2.3. Uniform and non-uniform torsion 11
2.4. Finite element method 14
2.5. State of art 15
3. SAFETY VERIFICATION OF SOLID AND CELLULAR BEAMS ACCORDING TO THE EUROCODE **25**
3.1. Bending moment 25
3.2. Lateral-torsional buckling 25
4. TORSION CONSTANT OF CELLULAR BEAMS **29**
4.1. Method 1 29
4.2. Method 2 30
4.3. Method 3 31
5. NUMERICAL ANALYSIS OF SOLID AND CELLUAR BEAMS **33**

5.1. Strategy 33
5.2. Study cases 33
5.3. Simulation program in ANSYS software 35
5.3.1. Element type 35
5.3.2. Material and geometric properties of the elements 36
5.3.3. Mesh 36
5.3.4. Boundary conditions to study cases of elastic critical moment. 37
5.3.5. Boundary conditions to study cases of non-uniform torsion angle 41
5.4. Results of analytical and numerical methods 41
5.4.1. Critical moment for LTB of solid beam cases 41
5.4.2. Critical moment for LTB of cellular beam cases 45
5.4.3. Variation of the diameter of the hole 55
5.4.4. Variation of the spacing between the holes 61
5.4.5. Variation of the final height of the cellular beam 67
5.4.6. Non-uniform angle of torsion of solid beam cases 74
5.4.7. Non-uniform angle of torsion of cellular beam cases 78
6. CONCLUSIONS 86
6.1. Main conclusions 86
6.2. Future lines of investigation 88
REFERENCES 89
ANNEXES 93

LIST OF FIGURES

Figure 1. Application fields of cellular beams: (a) service integration with ceiling attached to structure; (b) curved cellular beam roof structure, adapted from [1]. 6
Figure 2. Fabrication process: (a) cellular beams; (b) castellated beams, adapted from [1]. 7
Figure 3. 2T approach to calculate the LTB resistance, adapted from [9]. 8
Figure 4. Geometric dimensions of the cellular beam in front view. 8
Figure 5. Geometric dimensions of the cellular beam in cross-section. 8
Figure 6. Lateral–torsional buckling failure of a cellular beam loaded by a bending moment, [9]. 10
Figure 7. I section beam subject to uniform torsion, [18]. 11
Figure 8. I section beam subject to a torque at mid-span, [18]. 11
Figure 9. I section beam subject to a torque at the free end and torsion and warping is restraint in the other end (non-uniform torsion), [18]. 13
Figure 10. Solutions for the angle ϕ and its derivatives for two specific cases, [18]. 13
Figure 11. Finite element models of different structures: (a) multi-story building; (b) connection in a conduit; (c) an airplane wing, adapted from [19]. 14
Figure 12. Critical LTB moment: comparison of numerically obtained values Mcr, abq with analytically obtained values $Mcr, 2T$, and Mcr, avg, [9]. 21
Figure 13. Equivalent rectangular openings for the calculation of weighted average $\mathrm{It, avg1}$. 30
Figure 14. Equivalent rectangular openings for the calculation of weighted average $\mathrm{It, avg2}$ 30
Figure 15. Area of integration for calculation of torsional constant $\mathrm{It, hole}$. 31
Figure 16. Equivalent rectangular openings for the calculation of the torsion constant $\mathrm{It, hole}$. 32
Figure 17. Dimensions of the beam's profiles IPE 200 and HE 200 A in millimeters. . 34
Figure 18. SHELL181 element geometry, adapted from [47]. 35
Figure 19. Mesh edge sizing of solid beam cases with different elements sizes: (a) 10 [mm]; (b) 15 [mm]. 36
Figure 20. Mesh edge sizing with different elements sizes: (a) 10 [mm]; (b) 5 [mm]. 36
Figure 21. Mesh of the numerical beam model with 1[m] length: (a) RM1 solid case; (b) RM1 cellular case. 37

Figure 22. Web fragment mesh of RM1 cellular case. 37
Figure 23. RM2 solid beam study case with the three-first beam lengths: (a) Without APDL command; (b) After applied APDL command. 38
Figure 24. RM1 cellular beam study case with L=1 [m]: (a) Without APDL command; (b) After applied APDL command. 39
Figure 25. RM2 cellular beam study case with the four-first beam lengths: (a) Without APDL command; (b) After applied APDL command. 40
Figure 26. Lateral-torsional buckling of RM1 solid beam case of L=3 [m]. 43
Figure 27.Lateral-torsional buckling of RM2 solid beam case of L=3 [m]. 43
Figure 28. Comparison of critical moment between EC3 and numerical analysis for the solid beams cases RM1 and RM2. 43
Figure 29. Relative difference between the critical moments of the analytical and numerical methods for the solid beam cases RM1 and RM2. 45
Figure 30. Lateral-torsional buckling of RM1 cellular beam case of L=3 [m]. 45
Figure 31. Lateral-torsional buckling of RM2 cellular beam case of L=3 [m]. 46
Figure 32. Comparison of critical moment between EC3 method, with the different torsion constants, and numerical analysis for the cellular beam cases RM1 and RM2.. 48
Figure 33. Relative difference of the critical moments between the three different weighted average methods of torsion constant with the constant I_t, $2T$. 49
Figure 34. Analytical critical moment, without the APDL command, divided by the ANSYS critical moment of solid and cellular beam study cases of RM1, varying the torsion constant. 52
Figure 35. Analytical critical moment, without the APDL command, divided by the ANSYS critical moment of solid and cellular beam study cases of RM2, varying the torsion constant. 52
Figure 36. Analytical critical moment, with the APDL command, divided by the ANSYS critical moment of solid and cellular beam study cases of RM1, varying the torsion constant. 53
Figure 37. Comparison between the critical moment of the RM1 cellular beam study case with 1.5[m] of length.: (a) Without APDL command; (b) After applied APDL command. 54
Figure 38. Analytical critical moment, with the APDL command, divided by the ANSYS critical moment of solid and cellular beam study cases of RM2, varying the torsion constant. 54

Figure 39. Comparison between the critical moment of the RM2 cellular beam study case with 3[m] of length.: (a) Without APDL command; (b) After applied APDL command. 55
Figure 40. Lateral-torsional buckling of $a0 = 0.8h$ cellular beam case based on RM1 of L=3 [m]..... 56
Figure 41. Lateral-torsional buckling of $a0 = 1.3h$ cellular beam case based on RM1 of L=3 [m]..... 57
Figure 42. Analytical critical moment, using the torsion constant $It, avg3$, divided by the ANSYS critical moment of the $a0 = 0.8h$, $a0 = 1.3h$, and RM1 cellular beam cases. 58
Figure 43. Lateral- torsional buckling of $a0 = 0.8h$ cellular beam case based on RM2 of L=3 [m]..... 59
Figure 44. Lateral- torsional buckling of $a0 = 0.8h$ cellular beam case based on RM2 of L=3 [m]..... 60
Figure 45. Analytical critical moment, using the torsion constant $It, avg3$, divided by the ANSYS critical moment of the $a0 = 0.8h$, $a0 = 1.3h$, and RM2 cellular beam cases. 61
Figure 46. Lateral-torsional buckling of $S = 1.1a0$ cellular beam case based on RM1 of L=3 [m]..... 63
Figure 47. Lateral-torsional buckling of $S = 1.7a0$ cellular beam case based on RM1 of L=3 [m]..... 63
Figure 48. Analytical critical moment, using the torsion constant $It, avg3$, divided by the ANSYS critical moment of the $S = 1.1a0$, $S = 1.7a0$, and RM1 cellular beam cases. 63
Figure 49. Lateral- torsional buckling of $S = 1.1a0$ cellular beam case based on RM2 of L=3 [m]..... 65
Figure 50. Lateral- torsional buckling of $S = 1.7a0$ cellular beam case based on RM2 of L=3 [m]..... 66
Figure 51. Analytical critical moment, using the torsion constant $It, avg3$, divided by the ANSYS critical moment of the $S = 1.1a0$, $S = 1.7a0$, and RM2 cellular beam cases. 67
Figure 52. Lateral-torsional buckling of $H = 1.3h$ cellular beam case based on RM1 of L=3 [m]..... 69
Figure 53. Lateral-torsional buckling of $H = 1.6h$ cellular beam case based on RM1 of L=3 [m]..... 69
Figure 54. Analytical critical moment, using the torsion constant $It, avg3$, divided by the ANSYS critical moment of the $H = 1.3h$, $H = 1.3h$, and RM1 cellular beam cases.... 69

Figure 55. Lateral- torsional buckling of H = 1.3h cellular beam case based on RM2 of L=3 [m]..... 71
Figure 56. Lateral- torsional buckling of H = 1.6h cellular beam case based on RM2 of L=3 [m]..... 72
Figure 57. Analytical critical moment, using the torsion constant It, avg3, divided by the ANSYS critical moment of the H = 1.3h, H = 1.3h, and RM2 cellular beam cases.... 73
Figure 58. Non-uniform torsion of RM1 solid beam case of L=1 [m]..... 75
Figure 59. Non-uniform torsion of RM2 solid beam case of L=1 [m]..... 75
Figure 60. Analytical angle of torsion $\Phi(z)_{,SCI}$ divided by the ANSYS angle of torsion $\Phi(z)_{,ANSYS}$ of solid beam study cases with L=10[m]..... 76
Figure 61. Analytical angle of torsion $\Phi(z)_{,SCI}$ divided by the ANSYS angle of torsion $\Phi(z)_{,ANSYS}$ of solid beam study cases with L=5[m]..... 77
Figure 62. Analytical angle of torsion $\Phi(z)_{,SCI}$ divided by the ANSYS angle of torsion $\Phi(z)_{,ANSYS}$ of solid beam study cases with L=1[m]..... 77
Figure 63. Non-uniform torsion of RM1 cellular beam case of L=1 [m]..... 79
Figure 64. Non-uniform torsion of RM2 cellular beam case of L=1 [m]..... 80
Figure 65. Analytical angle of torsion $\Phi(z)_{,SCI}$ divided by the ANSYS angle of torsion $\Phi(z)_{,ANSYS}$ of cellular RM1 study case with L=10[m], normalized by the values of the same case of solid beam 82
Figure 66. Analytical angle of torsion $\Phi(z)_{,SCI}$ divided by the ANSYS angle of torsion $\Phi(z)_{,ANSYS}$ of cellular RM2 study case with L=10[m], normalized by the values of the same case of solid beam 82
Figure 67. Analytical angle of torsion $\Phi(z)_{,SCI}$ divided by the ANSYS angle of torsion $\Phi(z)_{,ANSYS}$ of cellular RM1 study case with L=5[m], normalized by the values of the same case of solid beam..... 83
Figure 68. Analytical angle of torsion $\Phi(z)_{,SCI}$ divided by the ANSYS angle of torsion $\Phi(z)_{,ANSYS}$ of cellular RM2 study case with L=5[m], normalized by the values of the same case of solid beam..... 84
Figure 69. Analytical angle of torsion $\Phi(z)_{,SCI}$ divided by the ANSYS angle of torsion $\Phi(z)_{,ANSYS}$ of cellular RM1 study case with L=1[m], normalized by the values of the same case of solid beam..... 85
Figure 70. Analytical angle of torsion $\Phi(z)_{,SCI}$ divided by the ANSYS angle of torsion $\Phi(z)_{,ANSYS}$ of cellular RM2 study case with L=1[m], normalized by the values of the same case of solid beam..... 85

LIST OF TABLES

Table 1. Variation of geometric dimensions of cellular beams according to application and objective, [3]. 7
Table 2. Recommended values for imperfection factors for lateral-torsional buckling curves, [37]. 26
Table 3. Recommended values for lateral-torsional buckling curves for cross-sections, [37]. 27
Table 4. Values of factors C1 and kz corresponding to end moment and support conditions, adapted from [42]. 28
Table 5. Values of factors C1, C2 and kz corresponding to loading and support conditions, adapted from [44]. 28
Table 6. Study cases of the critical moment analyzes 34
Table 7. Study cases of the non-uniform angle of torsion analyzes 34
Table 8. Comparison between the critical moments of the analytical and numerical methods for the solid beam cases RM1 and RM2. 42
Table 9. Relative difference between the critical moments of the analytical and numerical methods for the solid beam cases RM1 and RM2. 44
Table 10. Comparison of critical moment between EC3 method, with the different torsion constants, and numerical analysis for the cellular beam case RM1. 46
Table 11. Comparison of critical moment between EC3 method, with the different torsion constants, and numerical analysis for the cellular beam case RM2. 47
Table 12. Relative difference of the critical moments between the three different weighted average methods of torsion constant with the constant It, 2T. 49
Table 13. Relative difference of the critical moment between the numerical and the analytical analyzes, with the different torsion constants, for the cellular beam case RM1. 50
Table 14. Relative difference of the critical moment between the numerical and the analytical analyzes, with the different torsion constants, for the cellular beam case RM2. 51
Table 15. Comparison of critical moment between EC3 method, with the torsion constant It, avg3, and numerical analysis for the a0 = 0.8h, a0 = 1.3h, and RM1 cellular beam cases. 56

Table 16. Relative difference of the critical moment between the numerical and the analytical analyzes, using the torsion constant $I_{t,avg3}$, for the $a0 = 0.8h$, $a0 = 1.3h$, and RM1 cellular beam cases. 57
Table 17. Comparison of critical moment between EC3 method, with the torsion constant $I_{t,avg3}$, and numerical analysis for the $a0 = 0.8h$, $a0 = 1.3h$, and RM2 cellular beam cases. 59
Table 18. Relative difference of the critical moment between the numerical and the analytical analyzes, using the torsion constant $I_{t,avg3}$, for the $a0 = 0.8h$, $a0 = 1.3h$, and RM2 cellular beam cases. 60
Table 19. Comparison of critical moment between EC3 method, with the torsion constant $I_{t,avg3}$, and numerical analysis for the $S = 1.1a0$, $S = 1.7a0$, and RM1 cellular beam cases. 62
Table 20.Relative difference of the critical moment between the numerical and the analytical analyzes, using the torsion constant $I_{t,avg3}$, for the $S = 1.1a0$, $S = 1.7a0$, and RM1 cellular beam cases. 64
Table 21. Comparison of critical moment between EC3 method, with the torsion constant $I_{t,avg3}$, and numerical analysis for the $S = 1.1a0$, $S = 1.7a0$, and RM2 cellular beam cases. 65
Table 22. Relative difference of the critical moment between the numerical and the analytical analyzes, using the torsion constant $I_{t,avg3}$, for the $S = 1.1a0$, $S = 1.7a0$, and RM2 cellular beam cases. 66
Table 23. Comparison of critical moment between EC3 method, with the torsion constant $I_{t,avg3}$, and numerical analysis for the $H = 1.3h$, $H = 1.6h$, and RM1 cellular beam cases. 68
Table 24. Relative difference of the critical moment between the numerical and the analytical analyzes, using the torsion constant $I_{t,avg3}$, for the $H = 1.3h$, $H = 1.6h$, and RM1 cellular beam cases. 70
Table 25. Comparison of critical moment between EC3 method, with the torsion constant $I_{t,avg3}$, and numerical analysis for the $H = 1.3h$, $H = 1.6h$, and RM2 cellular beam cases. 71
Table 26. Relative difference of the critical moment between the numerical and the analytical analyzes, using the torsion constant $I_{t,avg3}$, for the $H = 1.3h$, $H = 1.6h$, and RM2 cellular beam cases. 72

Table 27. Comparison between the non-uniform angle of torsion of the analytical and numerical methods for the solid beam cases RM1 and RM2 with L=10 [m]. 74
Table 28. Relative difference between the non-uniform angle of torsion of the analytical and numerical methods for the solid beam cases RM1 and RM2. 76
Table 29. Comparison between the non-uniform angle of torsion of the analytical and numerical methods for the cellular beam case RM1 with L=10 [m]..... 78
Table 30. Comparison between the non-uniform angle of torsion of the analytical and numerical methods for the cellular beam case RM2 with L=10 [m]..... 79
Table 31. Relative difference between the non-uniform angle of torsion of the analytical and numerical methods for the cellular beam cases RM1 and RM2 with L=10[m]. 80
Table 32. Relative difference between the non-uniform angle of torsion of the analytical and numerical methods for the cellular beam cases RM1 and RM2 with L=5[m]. 81
Table 33. Relative difference between the non-uniform angle of torsion of the analytical and numerical methods for the cellular beam cases RM1 and RM2 with L=1[m]. 81

SIMBOLOGY

Latin alphabet letters

$A, B, C, D,$ E, F	constants of differential equation that depend on load distribution and end conditions;
A_f	area of one flange;
A_T	area of tee section;
A_{wT}	area of a web of tee section;
a	factor that multiplies the angle of torsion;
a_0	diameter of hole opening;
b_f	width of flange;
C_1, C_2	factors depending on the loading and end restraint conditions;
C_b	moment-gradient coefficient;
D_d	Value of the directional deformation of the numerical model;
d	distance of cellular beam web height divided in the middle subtracting the hole opening;
E	modulus of elasticity of steel;
f_y	yield strength of steel;
G	shear modulus of steel;
H	final height of cellular beam;
h	height of solid beam;
h_w	height of web cellular beam;
h_{wT}	height of web tee section;
I_i	moment of inertia of the cross-section relative to the i axis;
$I_{T,i}$	moment of inertia of a tee section relative to the i axis;
I_t	torsion constant of solid beam;
$I_{t,hole}$	new torsion constant of cellular beam of Method 3;
$I_{t,2T}$	torsion constant of cellular beam of 2T approach;
$I_{t,avg1}$	torsion constant of weighted average of the Method 1;
$I_{t,avg2}$	torsion constant of weighted average of the Method 2;
$I_{t,avg3}$	torsion constant of weighted average of the Method 3;
I_w	warp constant of solid beam;

$I_{w,2T}$	warp constant of cellular beam;
$[K]$	structural stiffness matrix;
k_z, k_w	effective length factors;
L	total length of the beam;
$M_{b,Rd}$	resistant moment of lateral-torsional buckling;
M_{cr}	elastic critical moment of lateral-torsional buckling;
$M_{c,Rd}$	resistant bending about one principal axis of a cross-section;
$M_{pl,Rd}$	plastic moment resistance;
n	number of cellular beam holes;
r	radius of hole opening;
S	distance between holes;
$[S]$	stress stiffness matrix;
w	length of the intermediate web post;
w_{end}	length of the end web post;
T_{sv}	St Venant's torsion;
T_n	non-uniform torsion;
T_w	warping torsion;
t_f	flange thickness;
t_w	web thickness;
W_y	appropriate section modulus as follows: $W_y = W_{pl,y}$ for Class 1 or 2 cross-sections, $W_y = W_{el,y}$ for Class 3 cross-sections and $W_y = W_{eff,y}$ for Class 4 cross-sections;
z	distance along the length of the beam;
Z_c	centroid of tee section;
Z_g	distance between the point of load application and the shear center.

Greek alphabet letters

α	imperfection factor;
α_{LT}	imperfection factor for lateral-torsional buckling;
β	severity factor;
γ_{M0}	partial safety factor for resistance of bending moment;
γ_{M1}	partial safety factor for resistance of lateral-torsional buckling;
$\bar{\lambda}_{LT}$	non-dimensional slenderness to lateral-torsional buckling;
λ_i	the i^{th} eigenvalue used to multiply the loads that generated $[S]$;
v	Poisson's ratio;
ϕ	angle of torsion;
ϕ_{LT}	value to determine the factor χ_{LT} ;
χ_{LT}	reduction factor for lateral-torsional buckling;
ψ_i	the i^{th} eigenvector of displacements.

ABREVIATIONS

APDL	ANSYS Parametric Design Language;
EC3	Eurocode 3;
EN	European Standard
ENV	European pre-Standard
FEM	Finite Element Method;
LTB	Lateral-torsional buckling;
RD [%]	Percentage of relative difference;
RM	Refence model of cellular beam, study case a_0=1h, S=1,4a_0 e H=1,5h;
RM2	IPE 200 refence model of cellular beam;
RM1	HE 200 A refence model of cellular beam;
SCI	Steel Construction Institute.

1. INTRODUCTION

1.1. Contextualization

In 1910, Chicago Bridge and Iron Works were the first to use beams with expanded web sections and repeating web openings. Soon after, G.M. Boyd also developed independently this idea in Argentina in 1935, and was later patented in the United Kingdom, [1].

Then, it was during World War II that the open web-expanded steel beams were initially used in structures, to increase the stiffness and strength of the original beam. Therefore, since the 1950s, structural engineers crave a high strength to weight ratio of open web-expanded steel beams to design even lighter and with better cost-efficient steel structures. In the beginning, the cellular beams with circular openings were used for the architectural application, because exposed steelwork with circular web openings in the beams was considered aesthetically pleasing. The pioneer was the castellated beams with hexagonal opening. However, even with a simple process of manufacturing that needs just one cut with a zigzag pattern, the castellated beams did not reach the moment of inertia and modulus values of the cellular beam section, due to its final height, [2].

Currently, the open web-expanded steel beams are increasingly being used in civil construction. These beams are lightweight and long-spanning structural elements that enable the design of vast column-free spaces with composite or non-composite systems. Furthermore, their web openings allow the installation of mechanical, electrical, and plumbing pipes and ducts within the depth of the beam, allowing for compact ceiling systems and maximized floor-to-ceiling heights. [3].

The beams can have different forms of opening like circles, hexagons, and rectangles. This work specifically studies the cellular beams with circular openings. Usually, the cellular beams are manufactured starting from steel hot-rolled I-section members of which the web is thermally cut according to a certain pattern, and then the obtained halves are shifted and rewelded, [4].

Despite their advantages, web openings must be considered in the design of structures. There is still no specific standard for cellular beams. The only design guides for safety verification of steel beams with web openings at room temperature are a proposal to complement Eurocode 3, Eurocode 3 part 1-13 [5], which has not yet is in circulation, and Annex N of the ENV 1993 version - 1-1: 1992 [6].

Although the lateral-torsional buckling (LTB) is a global failure mode that already exists for solid beams, the cellular beam web openings influence this mode. Thus, the cellular beams' geometric properties should be analyzed, varying the diameter and the number of web openings, spacing between the web openings, the final height of the cellular beam, and other parameters that depend on them.

Therefore, this work aims to study and improve the existing knowledge of the behavior of cellular beams, focusing on the strength of the beam in its lateral-torsional buckling instability mode. For such a purpose, is approached a new calculation method of torsion constant of cellular beam and performed numerical simulations using the Finite Element Method (FEM).

1.2. Objectives

Intend to analyze the influence of a new approach of calculation method of the torsion constant varying the geometric parameters of the cellular beam in the elastic critical moment for lateral-torsional buckling and the non-uniform torsion angle. A numerical model will be proposed by the FEM, varying some geometric parameters of the cellular beam, such as length, final height, diameter and spacing between the holes. The following specific objectives were addressed to achieve the success of this work:

1. Create a numerical model to analyze the elastic critical moment for lateral-torsional buckling and the non-uniform angle of torsion of the solid and cellular beams using the ANSYS Mechanical software;

2. Present a new calculation method from the weighted average of the torsion constant for cellular beams;
3. Compare the numerical results with the analytical results of simplified calculation methods of the Eurocode 3 part 1-1 and the SCI P385 guide, varying the value of the torsion constant between the different calculation methods of this constant;
4. Analyze the influence of the geometric parameters of the cellular beam at the critical moment for lateral-torsional buckling.

1.3. Thesis structure

The work is organized in 6 chapters. This present chapter is the first, which has a contextualization and motivation to study the lateral-torsional buckling of cellular beams and presents the objectives to be accomplished with the work.

Chapter 2 presents the literature review, where the cellular beams are characterized by application fields, fabrications process, and geometric characteristics. The lateral-torsional buckling global instability mode and the uniform and non-uniform torsion angle of a beam according to the SCI P385 guide also are presented. Explain how works the FEM and shows the steps to create a numerical model, ending with the state of art, which has the results of recent studies about cellular beam and LTB.

In chapter 3, safety verification of solid and cellular beams according to the Eurocode 3 part 1-1 is shown. The design resistance for bending and the resistance of lateral-torsional buckling are presented, showing the calculation of the elastic critical moment.

In the fourth chapter, three different methods of torsion constant calculating are approached. The first two have already been approached in other studies, and both use the same constant, only differentiating on the weighted averages. The third and new method continues using the weighted average, but a new torsion constant is presented, different from the previously utilized.

Chapter 5 contains the numerical analysis of solid and cellular beams in the software ANSYS, describing the study cases and showing how the numerical model was designed. Also is presented and compared the results of analytical and numerical

methods. Finally, chapter 6 presents the main conclusions of this work about LTB of cellular beams and suggestions for investigation in future studies.

2. LITERATURE REVIEW

2.1. Characterization of cellular beams

I-shaped steel sections are extensively used as main structural elements in building structures, especially cellular beam elements, which have advantages with the web openings. Without increasing the floor-to-floor height, the cellular beams allow the passage and installation of piping, ductworks, and electrical conduits. Furthermore, web openings reduce the amount of structural steel used, [7].

In modern constructions with long spans to be covered, the cellular steel beams fabricated from standard hot rolled I-sections are commonly used. It happens because cellular steel beams create flexibility in the use of the floor area and flexibility in running services such as ventilation ducts with the possibility for alterations. Greater flexural stiffness, larger section modulus, optimum self-weight-depth ratio, economic construction, and aesthetic architectural appearance are other advantages of cellular beams, [8].

2.1.1. Application fields

Cellular beams allow few amounts of columns and footings to be able to support longer-spanning sections, creating additional column-free space and a floor with flexible space. The ability to use longer and lighter spans makes fewer members necessary for a given system, saving construction costs of the structure. Parking garages, industrial and warehouse facilities, office buildings, schools, and hospitals are structures with long open space requirements where cellular beams are ideal, [1].

It is common to use cellular beams in roof support systems, as shown in Figure 1. These beams provide the functionality of trusses with one simple prefabricated element and the possibility of a span up to 40 meters, being used as simply supported members, cantilever elements, or as part of a moment or portal frames of the structure. Moreover, cellular beams are commonly used in floor support systems, accommodating the building systems (heating, ventilation, air conditioning, etc.) as well as structural support within minimal ceiling spaces, [3].

(a) (b)

Figure 1. Application fields of cellular beams: (a) service integration with ceiling attached to structure; (b) curved cellular beam roof structure, adapted from [1].

2.1.2. Fabrication process

This study focuses on cellular beams, in which the holes in the web of the profile are circular. However, also there are beams with rectangular, sinusoidal, and hexagonal openings, which were pioneers and are known as castellated beams.

Figure 2 shows the fabrication of cellular and castellated beams. The fabrication process is similar between these two types of cellular beams but is not identical. Castellated beams need just one cut with a zigzag pattern, and then the two halves are offset, the waste at the beam ends is removed, and the two sections are welded back together to form the castellated section. On the other hand, cellular beams need two cutting passes with a circular pattern instead of the zigzag, producing more waste than castellated beams, [1].

The cellular beam height will be 40 to 60% higher than its parent section height, resulting in more economical material use when the beam is loaded in strong axis bending, [9]. Furthermore, the circular opening increases the overall beam depth, the moment of

inertia, and section modulus while reducing the overall weight of the beam. So, cellular beams produce a more efficient and economical solution than castellated beams, due to their flexible geometry, [2].

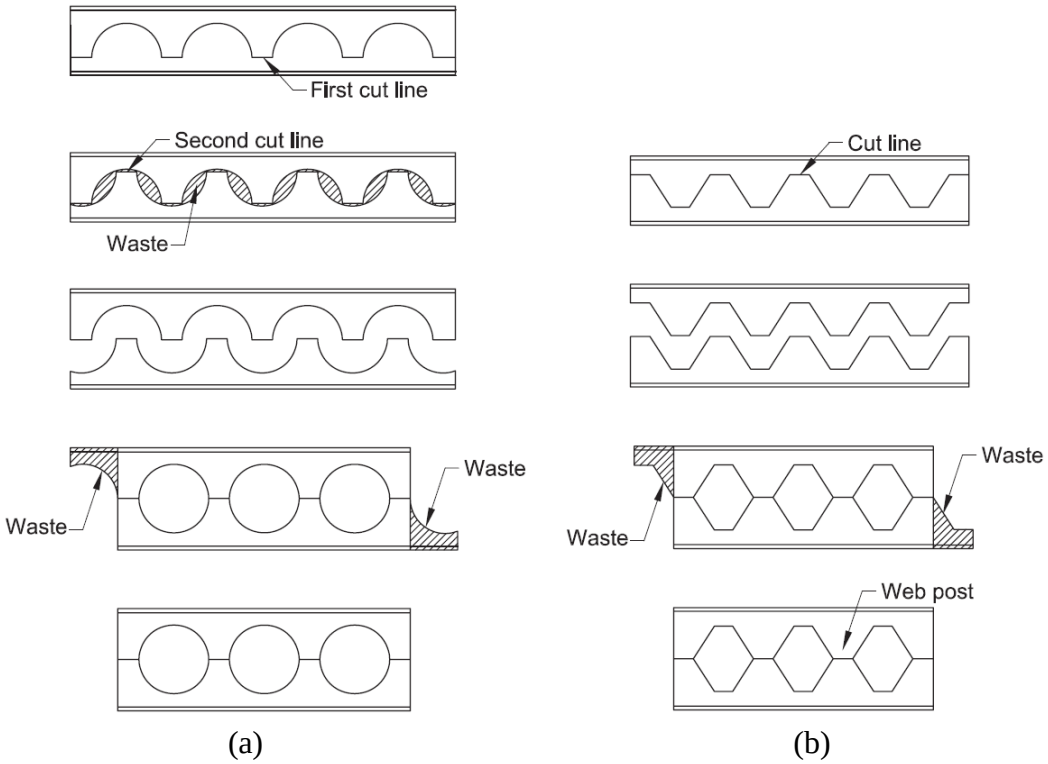

Figure 2. Fabrication process: (a) cellular beams; (b) castellated beams, adapted from [1].

2.1.3. Geometric characteristics

Depending on the design for a given section, infinite opening combinations, sizes, and spacings can be implemented, [3]. Table 1 shows the ranges of dimensions variation changing according to their applications and objective. These dimensions are the diameter a_0 of the hole openings, the distance S between them, the height h of the profile of the solid beam that gives rise to the cellular beam, and the final height H of the cellular beam.

Table 1. Variation of geometric dimensions of cellular beams according to application and objective, [3].

Applications	**Objective**	a_0	S	H
Roofing, footbridges, and wide-span purlins	Optimization of the height/weight ratio	$1.0 - 1.3h$	$1.1 - 1.3a_0$	$1.4 - 1.6h$
Floors, parking structures and offshore structures	Optimization of the load/weight ratio	$0.8 - 1.1h$	$1.2 - 1.7a_0$	$1.3 - 1.4h$

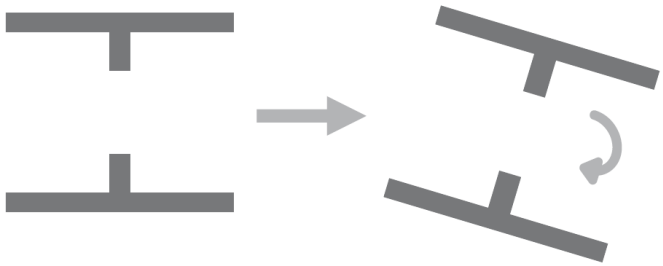

Figure 3. 2T approach to calculate the LTB resistance, adapted from [9].

Figure 4 and Figure 5 show the geometric dimensions of the cellular beam, which vary with the requirements of each design and are necessary for the cross-section strength calculation.

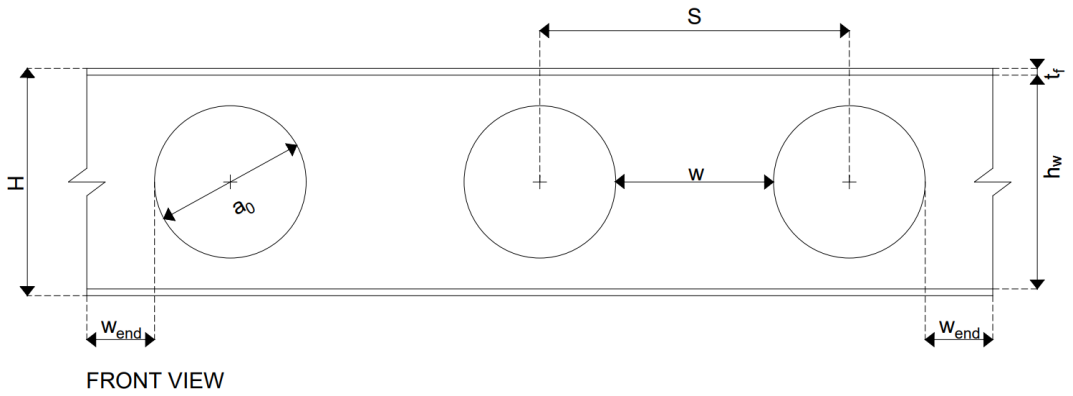

Figure 4. Geometric dimensions of the cellular beam in front view.

Therefore, with these dimensions and using the 2T approach, it is possible to define some geometric properties of the cellular beams disregarding the radius of agreement between the flange and the web.

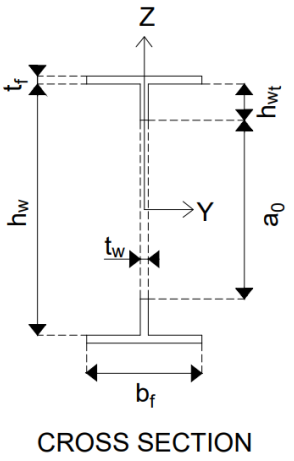

Figure 5. Geometric dimensions of the cellular beam in cross-section.

Equations 1 to 3 show the area A_{wT} of the tee section web, the area A_f of one flange, and the total area A_T of the tee section.

$$A_{wT} = t_w h_{wT} \tag{1}$$

$$A_f = b_f t_f \tag{2}$$

$$A_T = A_{wT} + A_f \tag{3}$$

It is also possible to determine the centroid Z_c of the tee section. Equation 4 shows this calculation:

$$Z_c = \frac{A_f \frac{(h_w + t_f)}{2} + A_{wT}\left(\frac{h_{wT}}{2} + \frac{t_f}{2}\right)}{A_{wT} + A_f} \tag{4}$$

Equations 5 to 7 show the plastic section modulus $W_{pl,y}$ of the cross-section, the moment of inertia $I_{T,z}$ of a tee section relative to the z-axis, and the moment of inertia I_z of the cross-section relative to the z-axis

$$W_{pl,y} = 2A_T Z_c \tag{5}$$

$$I_{T,Z} = \frac{t_f b_f^3}{12} + \frac{h_{wT} t_w^3}{12} \tag{6}$$

$$I_Z = 2I_{T,Z} \tag{7}$$

Although some studies calculate the warp constant $I_{w,2T}$ subtracting the hole of the cellular beam as shown in Equation 8, [10], [11], other studies consider a different method of calculation that does not discount the hole of the cellular beam, being the same constant for solid and cellular beams.

$$I_{w,2T} = \frac{t_f b_f^3 \left(h_w + t_f\right)^2}{24} - \frac{(a_0 t_w)^3}{144} \quad (8)$$

This work will use this second method, presented in Equation 9, [12]–[15].

$$I_{w,2T} = \frac{t_f b_f^3 \left(h_w + t_f\right)^2}{24} \quad (9)$$

Finally, the torsion constant $I_{t,2T}$ of cellular beam also is an important geometric property that can be calculated by Equation 10, [14].

$$I_{t,2T} = \frac{2}{3} b_f t_f^3 + \frac{1}{3}(h_w - a_0) t_w^3 \quad (10)$$

2.2. Lateral torsional buckling

The change in the opening geometry of the cellular beam influences its failure behavior. Among the main and potential instability modes of cellular beams, are included the Vierendeel Mechanism, the web-post buckling, and the LTB, [16]. The first two are local failure modes that specifically occur because of the web openings, while the LTB is a global failure mode that already exists for solid beams. However, there is difference between the LTB of solid and cellular beams due to web openings, [13].

This global buckling failure mode results, at the same time, in a sideways displacement and a torsional rotation of the cross-section, as can be seen in Figure 6. LTB occurs when the movement of the buckled compressed part of the beam is restrained by the other part of the beam that is still in tension, [13].

Furthermore, the final height of the cellular beam is an important geometric parameter due to your influence on the LTB. As the cellular beams are slenderer and higher than solid beams, they are more prone to LTB.

Figure 6. Lateral–torsional buckling failure of a cellular beam loaded by a bending moment, [9].

2.3. Uniform and non-uniform torsion

The total resistance of a beam to torsional loading is composed of the sum of uniform torsion and warping torsion. Nevertheless, there are cases in which only uniform torsion occurs, and they also can be called pure torsion or St Venant torsion, on account of the theory developed initially by St Venant, [17].

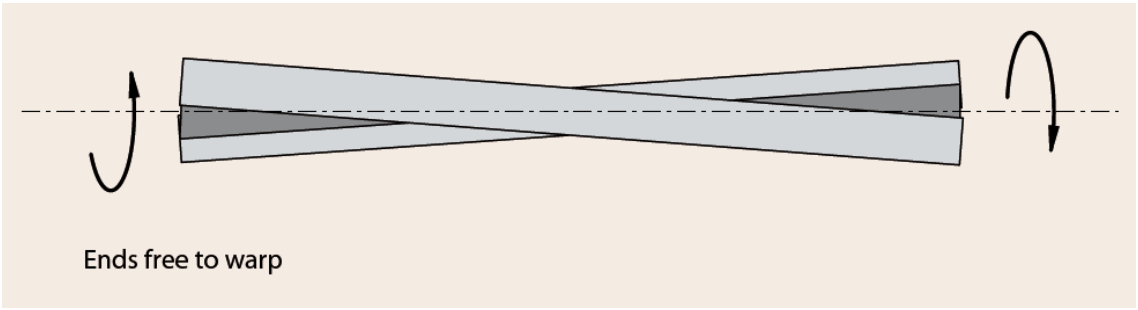

Figure 7. I section beam subject to uniform torsion, [18].

In this case of uniform torsion (Figure 7), the rate of change of the angle of twist is constant along the member and the applied torque is resisted entirely by shear stresses distributed throughout the cross-section. The St Venant torsion T_{sv} can be determined by Equation 11, [17].

$$T_{sv} = GI_t\phi' \tag{11}$$

Where I_t is the torsional constant and ϕ' is the first derivative of the angle of torsion with respect to distance z along the beam.

Figure 8 shows a simply supported beam with an applied torque at the center of the span, which is a case of non-uniform torsion. The beam is continuous at mid-span, so the warping is fully restrained at the location. Therefore, both flanges are constrained to bend in plan, and the beam twist at a varying rate over each half span, [18].

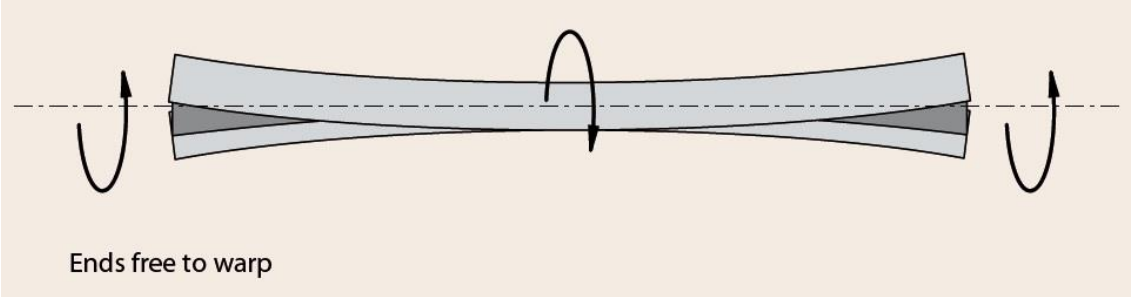

Figure 8. I section beam subject to a torque at mid-span, [18].

The non-uniform torsion T_n (Equation 12) is carried partly as St Venant torsion and partly as warping torsion at any cross-section, [17].

$$T_n = T_{sv} + T_w \tag{12}$$

The warping torsional constant is given by Equation 13.

$$T_w = -EI_w\phi''' \tag{13}$$

Where ϕ''' is the third derivative of the angle of rotation with respect to distance z along the beam.

Therefore, the calculation of the non-uniform torsion can be expressed in terms of the angle of rotation and its derivates as is shown in Equation 14, [18].

$$T_n = GI_t\phi' - EI_w\phi''' \tag{14}$$

Solving the differential equation for the variation of ϕ with the distance z along the beam gives solutions of the form shown in Equation 15, [18].

$$\phi = A\sinh\left(\frac{z}{a}\right) + B\cosh\left(\frac{z}{a}\right) + Cz^3 + Dz^2 + Ez + F \tag{15}$$

Where $a = \sqrt{\frac{EI_w}{GI_t}}$ and A to F are constants that depend on load distribution and end conditions.

Figure 9 shows a specific case that will be analyzed in this work. In this case, there are the torsional restraint and warping restraint at one end only, and the torque is applied at the free end.

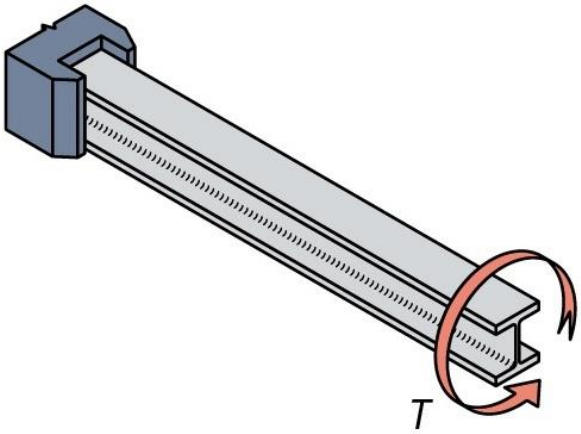

Figure 9. I section beam subject to a torque at the free end and torsion and warping is restraint in the other end (non-uniform torsion), [18].

According to the SCI P385 guide, applying the boundary conditions for this case, the angle of torsion can be calculated by Equation 16, [18].

$$\phi = \frac{T_n a}{GI_t}\left\{\tanh\left(\frac{L}{a}\right)\left[\cosh\left(\frac{z}{a}\right) - 1\right] - \sinh\left(\frac{z}{a}\right) + \frac{z}{a}\right\} \tag{16}$$

Figure 10 shows the graph with the solutions for the angle ϕ for two specific cases of cantilevers with warping fixity at support: loading by uniformly distributed torque and loading by point torque at the end.

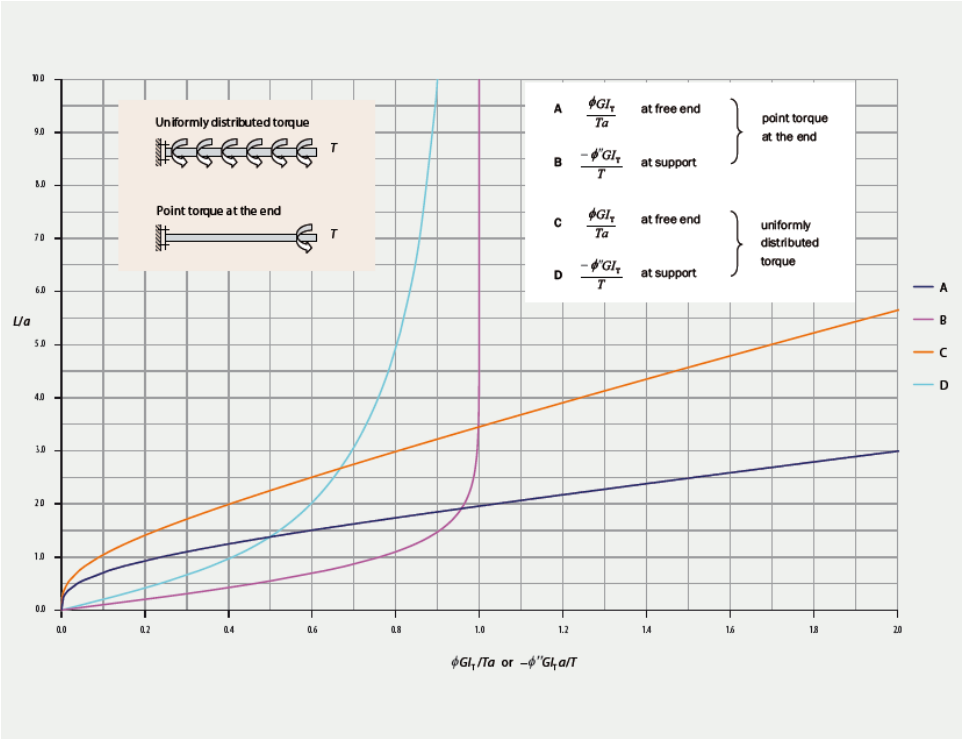

Figure 10. Solutions for the angle ϕ and its derivatives for two specific cases, [18].

2.4. Finite element method

The finite element method has become of great interest to many industries in solving practical analysis and highly complex design problems, offering many advantages with the appearance of high speed and large storage capacity of digital computers, [19].

The concept of the finite element method is based on a real structure that can be divided or discretized by a finite number of elements connected by its nodes, and also along its boundaries. Generally, the elements used in the design of a structure are bars, beams, two-dimensional elements, shells and plates under bending, and three-dimensional elements, [19].

Figure 11 (a) shows how a multi-story hotel building is modeled using bars, beams, columns, and slabs. The model of a nozzle in a thin-walled cylinder, created using triangular shell elements, is illustrated in Figure 11 ((b), and Figure 11 (c) illustrates the wing of an airplane, discretized by rectangular finite elements, [19].

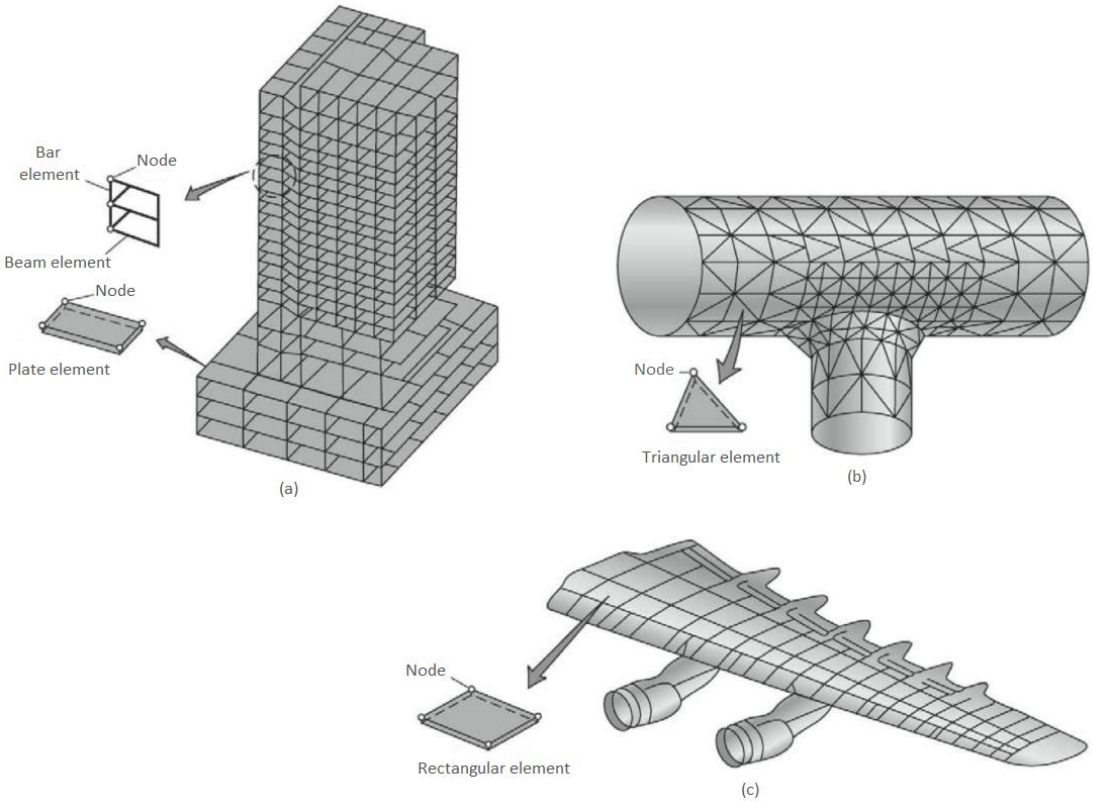

Figure 11. Finite element models of different structures: (a) multi-story building; (b) connection in a conduit; (c) an airplane wing, adapted from [19].

The boundary conditions are the specified values of the field variables on the boundaries of the field. Depending on the type of physical problem being analyzed, the field variables may include physical displacement, temperature, heat flux, and fluid velocity. Some steps in formulating a finite element analysis of a physical problem are common to all such analyzes. These steps described below are embodied in commercial finite element software, [20]:

- Define the geometric domain of the problem;
- Define the element type(s) to be used;
- Define the material properties of the elements;
- Define the geometric properties of the elements (length, area, and the like);
- Define the element connectivity (mesh the model);
- Define the physical constraints (boundary conditions);
- Define the loadings.

2.5. State of art

Djamel E. Kerdal studied the lateral-torsional buckling strength of castellated beams in 1982. This work aimed to provide the missing quantitative data on the lateral-torsional buckling strength of castellated sections that were available in the U.K. Two series of tests were performed, the first on small scales specially fabricated castellated beams of the same general proportions as full-scale beams, and a second on eight full-scale beams. The results of the first series suggested that the presence of holes in the web had a negligible effect on the beams' lateral stability. The second series of tests covered a wide range of beam slenderness and showed that all eight beams collapsed in a lateral-torsional mode. Finally, the experimentally observed maximum loads have been compared with the strengths predicted by various interpretations of the new draft steelwork British code, [21].

In 1984, D. Kerdal and D.A. Nethercot studied failure modes for castellated beams. Methods for predicting the loads at which each type of failure mode occurs were evaluated against the available experimental data and the limitations in a number of analytical approaches were discussed. It was possible to notice that when the critical span was subjected to an approximately uniform moment collapse was likely to occur either

by lateral-torsional instability in the case of unbraced beams or by the formation of a flexural mechanism for laterally restrained beams, [22].

The study concluded that both lateral-torsional instability and the formation of a flexural mechanism may be handled by an adaptation of established methods for plain webbed beams, providing the cross-sectional properties are those corresponding to the centerline of a castellation. Available methods in the time for the determination of collapse in the other modes, while rather less accurate, were adequate for design except in the case of web post-buckling due to compression, [22].

Paulo P. et al. analyzed experimentally the lateral-torsional buckling of solid beams with cross reinforcements in 2003. The expression of the critical moment for beams with reinforcements proposed, presented the same form of the original expression without reinforcements, verifying an alteration in the torsion constant and the moment of second order. Experimental tests of reinforced beam elements were carried out on a reaction frame, with two concentrated loads and two fork supports. The lateral buckling resistance of transversely reinforced beams increased with the number of reinforcements. Furthermore, when the reinforcements were located close to the supports and the places where efforts were applied, an increase in the value of the resistant moment could be expected, [23].

In 2004, Amin Mohebkhah studied the nonlinear lateral-torsional buckling of standard Iranian simply supported castellated beams with a wide variety of modified slenderness. This study developed a three-dimensional finite-element model using ANSYS for the analysis that investigated the effects of slenderness on the moment-gradient factor C_b. It was concluded that the value of C_b was not constant in the whole range of castellated beam's slenderness, while the American Institute of Steel Construction gives a constant value for any range of slenderness, which can lead to an unsafe design. The decrease in the C_b factor increases as the modified slenderness decreases, [24].

Therefore, instead of using a constant C_b factor for any of the cases, alternative equations for evaluating the C_b factor for each case in terms of the beam's modified slenderness were proposed. This reduction in the C_b factor value of the castellated beams might be due to web local buckling or yielding the tee sections above and below the holes inducing a premature instability. However, owing to the limited number of castellated beams studied herein, further research must be carried out to establish a better proposal

for the gradient moment factor in castellated beams, which covers all important loading cases, [24].

The problem of lateral-torsional buckling of steel solid beams at elevated temperatures was studied in 2004. Vila Real et al. did a numerical investigation of the lateral-torsional buckling of steel I-beams subjected to a temperature variation from room temperature up to 700 °C. The study used a geometrically and materially non-linear finite element program with the material properties of Eurocode 3, Part 1-2 and compared the numerical results with the results of the simple model presented in Eurocode 3, Part 1-2 (1995). The comparison showed unsafe results for a certain range of slenderness because the simple models based on the lateral-torsional buckling curve that was valid at room temperature led to a safety level that depends on the slenderness of the beam. Therefore, a new beam design lateral-torsional buckling curve was proposed that depends on the imperfection factor α. Moreover, was numerically confirmed the influence of the residual stresses in the lateral-torsional buckling of beams is bigger for intermediate slenderness, [25].

In 2007, according to Vila Real et al., numerical research works showed that the design equation that was present in the ENV 1993-1-2 of Eurocode 3 is over-conservative in the case of non-uniform bending and proved to yield unsafe results for beams under fire conditions. Although a significant improvement was generated when a new design equation was introduced in the EN 1993-1-2 of Eurocode 3, only the case of uniform bending distribution along the beams was considered in research work performed at the time, [26].

Thereat, Vila Real et al did an improved proposal for the lateral-torsional buckling of unrestrained steel beams subjected to fire, addressing the issue of the influence of the loading type, the steel grade, the pattern of the residual stresses (hot-rolled or welded sections) and the ratio between the depth and the width of the cross-section on the resistance of the beam. In the new proposal, the imperfection factor α shown in Equation 17, was rewritten as a function of a severity factor β, which is tabulated and calibrated through an extensive comparison with the results of FEM numerical simulations. The results of FEM numerical simulations of more than 5000 beams showed that the proposal was safe and accurate even though the influence of these factors when considered separately is rather limited, because the combination of these three factors had a more significant effect, [26].

$$\alpha = \beta\sqrt{235/f_y} \tag{17}$$

Ali Nadjai et al., in 2007, studied experimentally and numerically composite floor cellular steel beams at both ambient and elevated temperatures. In the experiment were tested four specimens with two different steel geometries on monotonic loading and at elevated temperatures. As expected, and designed, the beams failed by web-post buckling in all tests, and the instability resulted in a sudden loss of stiffness and strength in the beams. Then, a finite element model is then established with both material and geometrical non-linearity to compare against the experimental results. The comparison was very good in terms of failure modes, load-deflection behavior, and ultimate loads and gave confidence that the finite element modeling can be used for further parametric studies being capable to simulate the mechanical behavior of composite cellular beam sections in both cold and at elevated temperature conditions with relatively high accuracy, [27].

L. Simões da Silva et al. evaluated the partial safety factor γ_{M1}, that corresponds to the reliability targets recommended in EN 1990 (2002), for the lateral-torsional buckling resistance of steel I-beams, in 2009. For the study were performed 1331 numerical simulations using the finite element program SAFIR (2005). Results showed that considering the variability of the design model and the variability of the material properties of steel, a partial safety factor equal to 1.0 approximately meets the Eurocode reliability targets for the General Case and the General Case with the correction factor together, for steel S235 and S355. However, steel S460 requires a partial safety factor equal to 1.1 for these two methods. The Special Case required a partial safety factor equal to 1.1 for steel S235 and S355 and a partial safety factor equal to 1.2 for steel S460, [28].

In 2011, the interaction of buckling modes in castellated steel beams was investigated by Ehab Ellobody, combining lateral-torsional and distortional buckling modes. He developed an efficient nonlinear 3D finite element model for the analysis of simply supported beams, in which initial geometric imperfection and material nonlinearities were carefully considered. The failure loads predicted from the finite element analysis were compared with those predicted from Australian Standards AS4100 for steel beams under lateral buckling. It was shown that the Specification predictions are generally conservative for normal strength castellated steel beams, and quite conservative for high strength castellated steel beams failing by lateral-torsional buckling, [29].

Amr M.I. Sweedan investigated in 2011 the elastic lateral stability of I-shaped cellular steel beams. The study was carried out using three-dimensional finite element modeling of simply supported I-shaped cellular steel beams, and varying the cross-sectional dimensions, span lengths, and web perforation configurations. The results revealed that the moment-gradient coefficient C_b was significantly influenced by the beam geometry and slenderness and depends on the web perforation configuration. Variation of C_b was investigated relative to a non-dimensional factor α_{LB}that relates the warping rigidity to the torsional rigidity of cellular beams. A quantitative assessment of C_b showed that values that were slightly higher or lower than recommended code values for plain-webbed beams were associated with the purely elastic lateral-torsional buckling mode of long-span beams. The buckling of intermediate-span beams was controlled by the lateral distortional buckling mode. Meanwhile, in the case of short-span beams, no lateral buckling occurred and a significant reduction in the values took place because the buckling was dominated by the high level of web distortion associated with the high shear stresses induced in the web plates, [30]

The LTB resistance of cellular steel beams was investigated through both experimental, numerical, and analytical (design) aspects by Joanna Nseir et al. in 2012. To improve the design of beams that was done employing rough design rules which often lead to an unduly conservative girder, this study proposed and detailed a new set of design rules. First, a series of 3 full-scale tests was performed to the validation of purposely derived finite elements models, that showed a very good agreement with the tests and was used to gather a large set of numerical reference results varying some parameters. Then, a new set of dedicated design rules was derived and proved to be accurate results and may be recommended for practical design as well as for design code implementation, [31].

In 2013, Ferhat Erdal and Mehmet P. Saka did research where the ultimate load-carrying capacities of optimally designed steel cellular beams were performed under the action of the same concentrated loadings in a self-reacting frame. Twelve tests were carried out on full-scale non-composite cellular beams. The results showed that when there was no lateral support, the beams failed due to lateral-torsional buckling. So, lateral supports were governing factor for the analysis of beams, because when the lateral movement was prevented, the beams failed by web buckling failure mode. Furthermore, when the load was applied directly over the circular openings, the failure behavior was controlled by the Vierendeel bending mechanism. And when the concentrated load was applied directly over a web post, the beams failed by web-post buckling, [2].

In the same study, experimental work was performed using an ANSYS-workbench finite element program integrated software program to verify the test results and to a good degree with the nonlinear behavior of failure modes such as web-post buckling and Vierendeel bending. Failure loads obtained from experimental tests were compared with finite element analysis values for three cellular beams. The results demonstrated that the nonlinear analysis results correlated well with experimental ones and the discrepancies are within 10%, [2].

In 2015, Pattamad Panedpojaman did an investigation on lateral-torsional buckling resistance of EC3 for cellular beams using the General Method and Specific Method. The investigated parameters of cellular beams were the section dimension, the section ratio, the opening ratio, and the spacing ratio. The calculation resulted in terms of the maximum moment at the LTB failure was compared with a nonlinear finite element model. The 2T approach was used for the calculus and the LTB resistance only subjected to a constant bending moment was examined. Pattamad summarized that the General Method of EC3 was mostly slightly conservative, except for the non-dimensional slenderness lesser than 1.5, so it should be used to design the LTB resistance of cellular beams as a cost-effective and safe design. However, for the short non-dimensional slenderness the method should be modified due to its conservative resistance. The Specific Method mostly provided overestimated results compared with the results of the finite element and may be unsafe for the LTB design, [32].

A parametric study was executed for a large number of cellular beam geometries simply supported and loaded by a constant bending moment, using a validated numerical model Furthermore, it is numerically confirmed that the critical buckling moment M_{cr} of cellular beams can be calculated by the existing 2T design approach, which used the approach for I-section beams without openings, but including all necessary cross-sectional properties calculated at the 2T section at the center of the opening. The underestimation of the torsion constant by the 2T approach caused an underestimation of the numerical critical moment visible for larger slenderness values. Sonck also approached the weighted average to calculate the torsion constant for a beam with equivalent rectangular openings, obtaining a better result for the larger lengths. The agreement with the analytical expression using the weighted average approaches considerably improved for the longer beam lengths, as shown in Figure 12, [9].

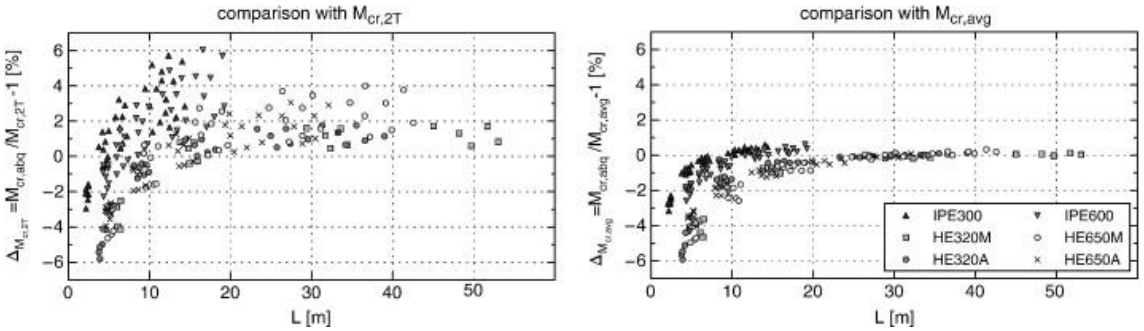

Figure 12. Critical LTB moment: comparison of numerically obtained values $M_{cr,abq}$ with analytically obtained values $M_{cr,2T}$, and $M_{cr,avg}$, [9].

Also was verified that this 2T approach could also be used for the calculation of the LTB resistance M_{Rd} although it was unclear which buckling curve to choose. In the study was found that the residual stress modification had a detrimental effect on the buckling resistance and the buckling curve c is chosen for all sections, [9].

In 2017, Dahmane Manal did one research work on the behavior of solid and cellular steel beams at high temperatures, using finite element simulations with ANSYS software. It was considered the transient temperature variation over time, the nonlinear material, and the geometric behavior, as well as the effect of initial geometric imperfections and residual stresses. The study showed that the LTB resistance is more influenced by geometric imperfections than the residual stress. The increase in the temperature and the length of the beam also affect the LTB stability, [33]

Using the finite element, Fatimah De'nan performed an analysis of lateral-torsional buckling behavior of I-beam in 2017. Five types of opening were adopted in the analysis, which were c-hexagon, octagon, hexagon, circle, square, and I-beam without web opening. Analysis results showed that the size of the web opening had a slight effect on the buckling moment resistance and the differences in buckling moment values decrease when the opening becomes larger such as the square opening. Moreover, it was noted that I-beam without web opening had the highest buckling moments resistance, and C-hexagon had the highest buckling moment compared to other web opening shapes. Furthermore, five shapes and three sizes of opening with 1.1 [m] of section length were used to find the optimum size and shapes of opening. Concluded that the optimum size is 100 [mm] of diameter opening due to the high values of the buckling moment compared with the others, [34].

The structural behavior of steel beams with openings in fire conditions was investigated by Sherif A.E. and Maha M.H. in 2018. The study employed the general finite element software ABAQUS to do the numerical mode, where four sizes of

perforated steel sections with seven different opening configurations were modeled and studied, and were examined the influence of applied load ratios. A restraint frame was used to prevent lateral movement of the test specimens, which results in one drastically different behavior when compared to unrestrained beams. The results showed that circular and castellated web opening shapes gave the best behavior of axial restraint perforated beams in fire, observing that their beam limit temperatures were about the same as for beams with no openings at the same applied load ratio. Moreover, the Vierendeel mechanism accompanied by buckling of the lower T-section was a common failure mode of the beams and the critical opening length had a higher effect on the structural behavior in the fire of the beams than all other geometrical parameters of the web openings, [35].

Also in 2018, O.F. Zaher et al. studied the behavior of structural arched cellular steel beams. An experimental program comprising four full-scale specimens was performed and a finite element model was proposed to analyze the behavior of arched cellular beams and to compare with the test results. To focus on local failures of the cellular arched beams around the openings, lateral buckling of the beams was prevented by lateral supports. The results from the experimental study indicated that there was a significant decrease in the ultimate strength of cellular beams compared to the solid. Furthermore, by increasing the subtended angle, the ultimate strength increased, as did the buckling load for the web posts. In addition, decreasing the radius of curvature is inversely proportional to the ultimate strength of the arched cellular beam. The proposed finite element model, which showed good accuracy, was in good agreement with the experimental, as were the failure modes, [36].

Felipe P.V. Ferreira et al. did a study in 2019 about the lateral-torsional buckling of cellular beams according to the possible updating of Eurocode 3 part 1-1 by modifying the distribution of residual stresses after the manufacturing process. The cellular steel beams were simply supported, with fork-supports at the end, and subjected to uniform bending, mid-span concentrated load, and uniformly distributed loads. This study concluded that the calculation prescription of the new proposal is effective, accurate, and conservative for LTB resistance in inelastic and elastic behavior. However, for stocky cellular steel beams, the Vierendeel mechanism and web post-buckling must be verified first, [12].

Jaqueline A. Silva studied numerically the stability of the cellular beams in a fire situation in 2019. The studies were focused on the thermomechanical behavior of the cellular beam for different geometries, varying the opening diameter, the spacing between

the openings, and the final height of the profile. The investigation was done applying the finite element method, using ANSYS software and a total of 201 simulations were performed. The results are compared with those proposed by the simplified methods of Eurocode 3 part 1-1 [37], Eurocode 3 part 1-2 [38] and guide SCI-P355 [39]. It is concluded that the collapse modes of the cellular beams are more related to the length of the beam than to the geometric parameters of the apertures themselves. Longer beams collapse by lateral-torsional buckling and on short beams collapse mode is local. The 2T approach applied to the calculation of the buckling-resistant moment by the Eurocode generated increased results when compared to the numerical simulation, [10].

In 2020 Daniel B. Costa investigated the resistant behavior of cellular beams using the finite element method in the ANSYS software. The main goal was to verify the moment of resistance to lateral-torsional buckling and to compare it with the results obtained through Eurocode 3 part 1-2. An IPE 220 profile beam made of S355 steel was chosen as the paternal beam, and cellular beams of different lengths and geometric parameters were investigated. It was noted that the failure mode for the shortest beams is due to the Vierendeel mechanism, and with the increase in length, we can verify the lateral-torsional buckling. Therefore, beam length was the most relevant factor for the appearance of a local or global instability mode, [40].

The differences and uncertainties between existing procedures to determine the LTB resistance of cellular beams at room temperature and the few studies in a fire situation, motivated a new study by Caroline C. Faria et al., in 2021, where was develop new procedures to evaluate the LTB resistance of cellular steel beams. These procedures were written as a unified formula for both room temperature and fire situation, and a numerical model was proposed and validated by comparison with numerical and experimental results available from the literature. Comparing the results of 1535 numerical models, the new proposal at room temperature presented a maximum difference equal to 4.8%. Under the fire situation, two procedures were proposed, called Proposal I (with one resistance curve) and Proposal II (with three resistance curves), based on 10,771 numerical models. The Proposal I presented differences with the numerical results between −40% and 7%, so gives mostly conservative results and is indicated for fast and practical calculations. Whereas Proposal II presented differences with the numerical results between −16% and 8%, so presents better agreement with the numerical models for each investigated temperature, [41]

Trayana Tankova et al. provided a study about lateral-torsional buckling of high strength steel beams, analyzing experimentally the resistance. In this study, 12 experiments were performed, considering steel grade, member slenderness, buckling mode, and cross-section class. The results showed that the material overstrength is present in the high-strength steel as well and the steel grade does not influence the distribution and magnitude. Also was observed a major impact on the distribution and magnitude by the cross-section dimensions of flange width and by section depth, as well as by the thickness of the welded plates and the welding process. As expected, all specimens failed in the lateral-torsional buckling mode, although tests on monosymmetric beams exhibited modes with local and global deformations. In general, it was possible to achieve higher resistance using high-strength steel, [42]

In 2021 Ashish P. Khatri et al., also numerically investigated the effect of the level of application of uniformly distributed load on the elastic moment gradient factor C_b of the cellular beams. A linear finite element three-dimensional model was developed in finite element software ANSYS for numerical analysis. This study was based on simply supported beams, varying the load application at different levels across the beam depth and considering other different parameters: beam slenderness, web slenderness, flange slenderness, and perforation configurations. The level of load with respect to the shear center position influences the moment gradient factors of beams that are used to calculate the elastic critical moment M_{cr}. This effect of load height on the moment gradient factor for plain-webbed beams can be obtained using a specific approached equation [43].

The numerical analysis indicated that stability loss in the case of longer span cellular beams is due to lateral-torsional buckling and the use of the specific approached equation in the determination of C_b values of longer span cellular beam results in close predictions to the results obtained from numerical analysis. In the case of a shorter span, stability loss is associated with the lowest considered web slenderness. The top flange loading condition is the most severe condition and is associated with the least values of moment gradient factors in comparison to shear center and bottom flange loading. In short, C_b factors of cellular beams are affected by flange slenderness, [43].

3. SAFETY VERIFICATION OF SOLID AND CELLULAR BEAMS ACCORDING TO THE EUROCODE

3.1. Bending moment

In agreement with Eurocode 3 part 1-1, the design resistance for bending about one principal axis of a cross-section $M_{c,Rd}$ is determined according to the class of the steel profile cross-section. For classes 1 and 2 the design resistance for bending is equal to plastic moment resistance $M_{pl,Rd}$ that is calculated by Equation 18, [37].

$$M_{c,Rd} = M_{pl,Rd} = \frac{W_{pl,y} f_y}{\gamma_{M0}} \tag{18}$$

Where $W_{pl,y}$ is the plastic section modulus previously defined for cellular beams, f_y is the yield strength of steel, and γ_{M0} is a partial safety factor for buildings recommended by Eurocode 3 equal to 1,0.

3.2. Lateral-torsional buckling

The resistance of lateral-torsional buckling $M_{b,Rd}$ is calculated using Equation 19, given in Eurocode 3 part 1-1, [37]. Eurocode 3 considers that the beams are laterally unrestrained and uses the same equation for solid and cellular beams. The difference is in geometric parameters of beams, like the constants of torsion and warp.

$$M_{b,Rd} = \frac{\chi_{LT} W_y f_y}{\gamma_{M1}} \tag{19}$$

Where γ_{M1} is a partial safety factor for buildings recommended by Eurocode 3 equal to 1,0 and χ_{LT} is the reduction factor for lateral-torsional buckling, which is determined by Equation 20 of the general case method.

$$\chi_{LT} = \frac{1}{\Phi_{LT} + \sqrt{\Phi_{LT}^2 - \bar{\lambda}_{LT}^2}} \text{ but } \chi_{LT} \leq 1{,}0 \tag{20}$$

To determine the reduction factor is necessary to calculate the value of Φ_{LT} given by Equation 21, where α_{LT} is an imperfection factor and $\bar{\lambda}_{LT}$ is the non-dimensional slenderness to lateral-torsional buckling given by Equation 22.

$$\Phi_{LT} = 0{,}5\left[1 + \alpha_{LT}\left(\bar{\lambda}_{LT} - 0{,}2\right) + \bar{\lambda}_{LT}^2\right] \tag{21}$$

$$\bar{\lambda}_{LT} = \sqrt{\frac{W_y f_y}{M_{cr}}} \tag{22}$$

The Eurocode 3 part 1-1 recommends the values given in Table 2 and Table 3 to obtain the imperfection factor of the lateral-torsional buckling curve and to define which buckling curve should be used. These values depend on the type of beam and its geometry section.

Table 2. Recommended values for imperfection factors for lateral-torsional buckling curves, [37].

Buckling curve	a	b	c	d
Imperfection factor α_{LT}	0,21	0,34	0,49	0,76

The elastic critical moment (M_{cr}) for lateral-torsional buckling, that is on Equation 23, is based on cross-sectional properties of the beam and considers the loading and support conditions, and the real moment distribution. To bi-symmetric cross-sections, the elastic critical moment is given by Equation 23, [44].

Table 3. Recommended values for lateral-torsional buckling curves for cross-sections, [37].

Cross-section	Limits	Buckling curve
Rolled I-sections	$h/b \leq 2$	a
	$h/b > 2$	b
Welded I-sections	$h/b \leq 2$	c
	$h/b > 2$	d
Other cross-sections	-	d

$$M_{cr} = C_1 \frac{\pi^2 E I_z}{(k_z L)^2} \left\{ \sqrt{\left[\left(\frac{k_z}{k_w} \right)^2 \frac{I_w}{I_z} + \frac{(k_z L)^2 G I_t}{\pi^2 E I_z} + \left(C_2 Z_g \right)^2 \right]} - C_2 Z_g \right\} \quad (23)$$

Where

$$G = \frac{E}{2(1+\upsilon)} \quad (24)$$

Thus, G is the shear modulus that depends on the modulus of elasticity ($E = 210000\ N/mm^2$) and of the Poisson's ratio ($\upsilon = 0{,}3$). In equation 8, I_z is the moment of area about the minor axis, I_w is the warping constant, I_t is the torsion constant, L is the length of the beam between points which have lateral restraint, C_1 and C_2 are factors depending on the loading and end restraint conditions (Table 4 and Table 5), k_z and k_w are effective length factors and z_g is the distance between the point of load application and the shear center.

For end-moment loading and transverse loads applied at the shear center $C_2 Z_g = 0$. Then, for these cases, the critical moment is given by Equation 25.

$$M_{cr} = C_1 \frac{\pi^2 E I_z}{(k_z L)^2} \sqrt{\left[\left(\frac{k_z}{k_w} \right)^2 \frac{I_w}{I_z} + \frac{(k_z L)^2 G I_t}{\pi^2 E I_z} \right]} \quad (25)$$

The factor k_z refers to end rotation on plan and k_w refers to end warping. Unless special provision for warping restraint is made, k_w should be taken as 1,0. And, for normal conditions of restraint at each end (fork support), k_z= k_w=1,0. Therefore, to determine the critical moment can be used Equation 26, [44].

$$M_{cr} = C_1 \frac{\pi^2 E I_z}{L^2} \sqrt{\left[\frac{I_w}{I_z} + \frac{L^2 G I_t}{\pi^2 E I_z}\right]} \tag{26}$$

Table 4. Values of factors C_1 and k_z corresponding to end moment and support conditions, adapted from [42].

End moment and support conditions	Bending moment diagram	*Value of* k_z	*Value of* C_1
	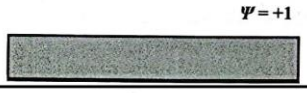	1,0 0,5	1,00 1,05
	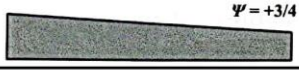	1,0 0,5	1,14 1,19
		1,0 0,5	1,31 1,37
		1,0 0,5	1,52 1,60
		1,0 0,5	1,77 1,86
		1,0 0,5	2,06 2,15
		1,0 0,5	2,35 2,42
		1,0 0,5	2,60 2,45
		1,0 0,5	2,60 2,45

Table 5. Values of factors C_1, C_2 and k_z corresponding to loading and support conditions, adapted from [44].

Loading and support conditions	*Bending moment diagram*	*Values of* k_z	*Value of factors*	
			C_1	C_2
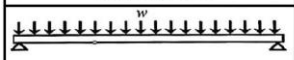		1,0 0,5	1,12 0,97	0,45 0,36
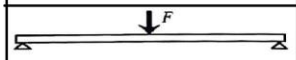		1,0 0,5	1,35 1,05	0,59 0,48
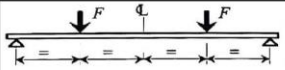		1,0 0,5	1,04 0,95	0,42 0,31

4. TORSION CONSTANT OF CELLULAR BEAMS

To get more accurate results on the critical moment of lateral-torsional buckling and the angle of non-uniform torsion, can be used an average weight to calculate the constant of torsion. Three different methods of torsion constant calculating are approached below. Two of them have already been approached in other studies, and both use the constant $I_{t,2T}$, only differentiating on the weighted averages. The third will be a new approach, in which the difference is in the torsion constant.

4.1. Method 1

The first method is calculated with a weighted average between the torsion constant corresponding to the portion of the beam where there are no holes in the web and the torsion constant $I_{t,2T}$ for a 2T approach. The torsion constant for the portion where there are no holes is equal to the torsion constant for solid beams $I_{t,sol}$ is shown in Equation 27.

$$I_{t,sol} = \frac{2}{3} b_f t_f^3 + \frac{1}{3} h_w t_w^3 \tag{27}$$

For this weighted average, a beam with square openings of sides equal to the diameter of the hole in the cellular beam is considered (Figure 13). Equation 28 shows this method of calculation, where n is the number of holes of the cellular beam and L the length of the beam.

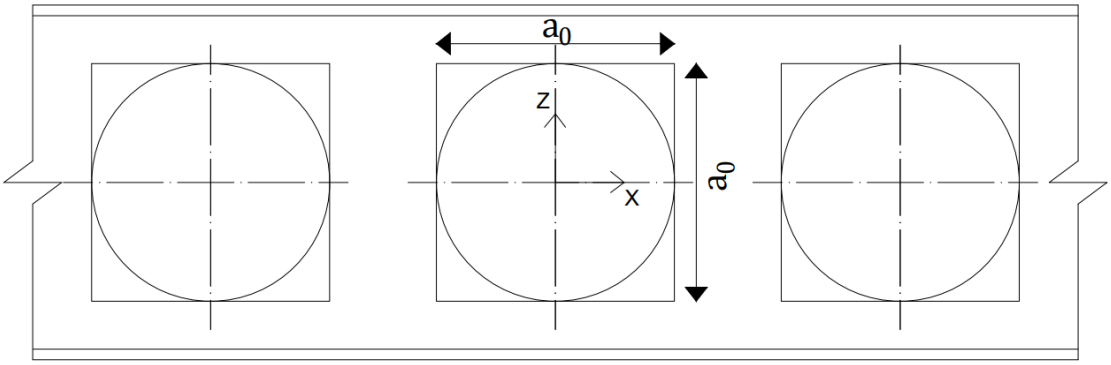

Figure 13. Equivalent rectangular openings for the calculation of weighted average $I_{t,avg1}$.

$$I_{t,avg1} = \frac{na_0}{L} I_{t,2T} + \left(1 - \frac{na_0}{L}\right) I_{t,sol} \tag{28}$$

4.2. Method 2

The study carried out by Delphine Sonck and Jan Belis in 2015 [9], numerically confirmed that the existing 2T design approach is efficient to calculate the critical buckling moment of cellular beams. Although, for the larger slenderness values (and relatively longer lengths), an underestimation of the numerical critical moment is visible, caused by the underestimation of the torsion constant by the 2T approach. To obtain a better fit for the larger lengths, Sonck also approached the weighted average to calculate the torsion constant for a beam with equivalent rectangular openings, as shown in Figure 14.

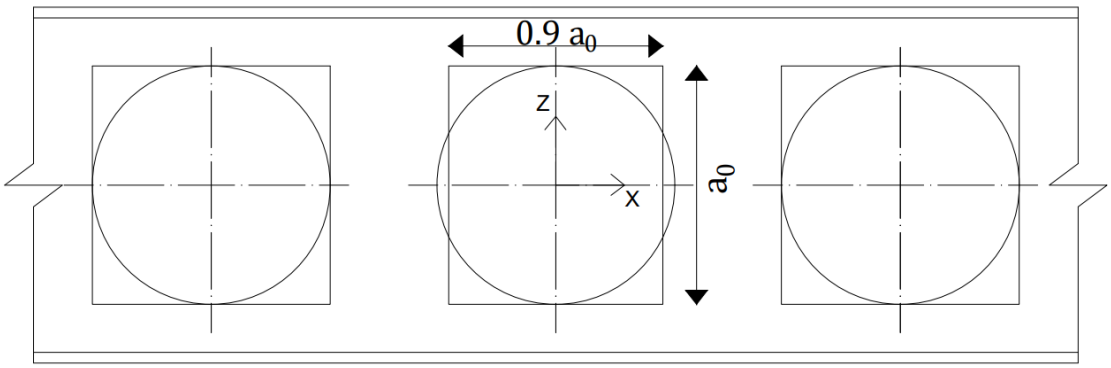

Figure 14. Equivalent rectangular openings for the calculation of weighted average $I_{t,avg2}$.

This approach that considers the approximation of Figure 14, results in the weighted average $I_{t,avg2}$ shown in Equation 29, [9].

$$I_{t,avg2} = 0{,}9\frac{na_0}{L}I_{t,2T} + \left(1 - 0{,}9\frac{na_0}{L}\right)I_{t,sol} \quad (29)$$

4.3. Method 3

The third method approaches a new torsion constant for the web portion with holes, different from the 2T approach. It is an exact integration of the torsion constant, subtracting the area of the circular hole. Figure 15 shows the area of integration, where $r = \frac{a_0}{2}$ and $d = \frac{h_w}{2} - z_i$

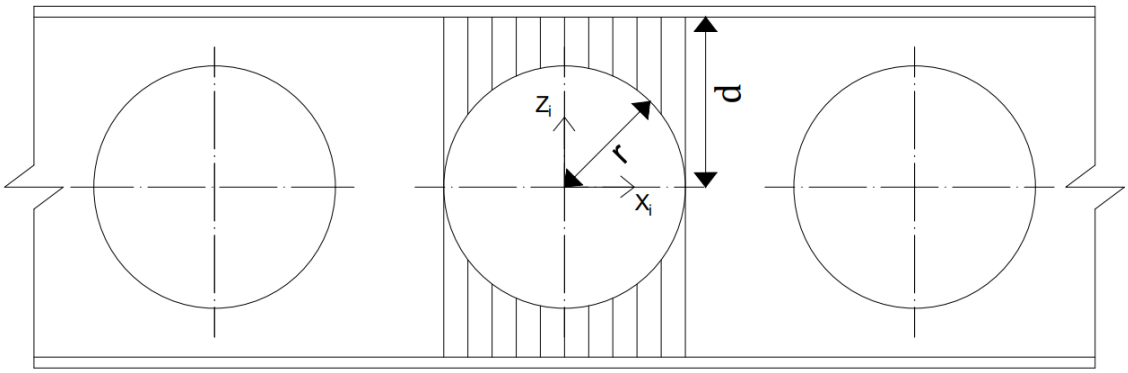

Figure 15. Area of integration for calculation of torsional constant $I_{t,hole}$.

From the equation of the circumference, Equation 30 is given.

$$z_i = \sqrt{r^2 - {x_i}^2} \quad (30)$$

Then, the distance d can be written by Equation 31.

$$d = \frac{h_w}{2} - \sqrt{r^2 - {x_i}^2} \quad (31)$$

Thus, the new torsional constant of the beam portion with the circular hole $I_{t,hole}$ is calculated by Equation 32.

$$I_{t,hole} = \frac{2}{3}b_f t_f^3 + \left[\int_{-r}^{r} 2\left(\frac{1}{3}d{t_w}^3\right)dx_i\right]\frac{1}{2r} \quad (32)$$

Substituting Equation 31 into 32, the Equation 33 is determined.

$$I_{t,hole} = \frac{2}{3} b_f t_f^3 + \frac{{t_w}^3}{3r}\left[\int_{-r}^{r}\left(\frac{h_w}{2} - \sqrt{r^2 - {x_i}^2}\right) dx_i\right] \tag{33}$$

Then, solving the integral, Equation 34 shows the final value of the torsional constant $I_{t,hole}$.

$$I_{t,hole} = \frac{2}{3} b_f t_f^3 + \frac{1}{3}\left(h_w - \frac{\pi a_0}{4}\right) t_w^3 \tag{34}$$

The difference between the constants $I_{t,2T}$ and $I_{t,hole}$ is on the value $\frac{\pi}{4}$ that multiplies a_0. Figure 16 shows equivalent rectangular openings for the calculation of the torsional constant $I_{t,hole}$.

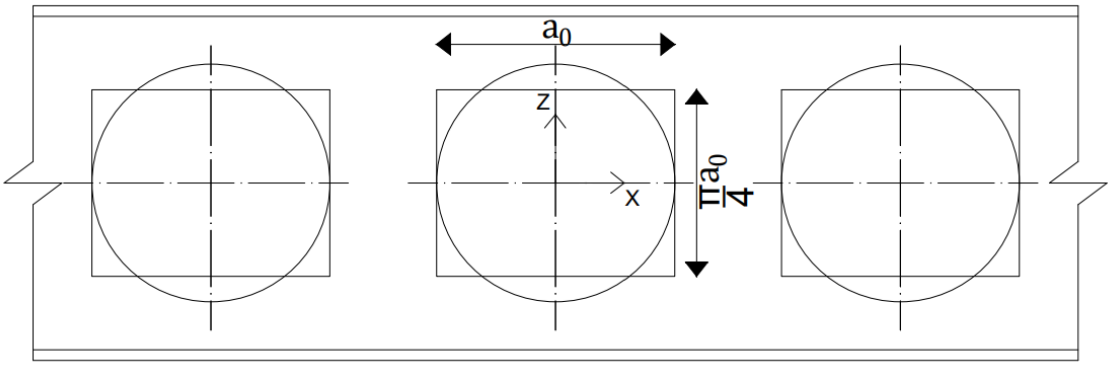

Figure 16. Equivalent rectangular openings for the calculation of the torsion constant. $I_{t,hole}$.

Although there is a difference between the constants, the equivalent rectangular openings for the weighted average calculation are the same in Figure 14. Equation 35 shows the weighted average calculation $I_{t,avg3}$ for the Method 3.

$$I_{t,avg3} = \frac{n a_0}{L} I_{t,hole} + \left(1 - \frac{n a_0}{L}\right) I_{t,sol} \tag{35}$$

5. NUMERICAL ANALYSIS OF SOLID AND CELLUAR BEAMS

5.1. Strategy

The study compares the results obtained by the numerical method MEF with the analytical method of simplified calculation of Eurocode 3 and SCI P385 guide, varying the three methods to calculate the torsion constant. Two different types of beam profiles were analyzed together with the effect of modifying the geometric parameters of the cellular beam on the results of resistance to lateral-torsional buckling (critical moment), and non-uniform angle of torsion.

5.2. Study cases

The analyzes were carried out on solid and cellular beams, based on two types of profiles in common that are adopted as reference models (RM). In solid beams, there is only length of beam variation. In cellular beams, the final height of the section, the diameter, and the spacing between the holes was also varied.

In the simulations, all beams are doubly symmetrical and the radius of agreement between the flange and the web was not considered. The chosen steel grade is S355, and the reference model profiles are IPE 200 (RM1) and HE 200 A (RM2).

Figure 17 shows the dimensions of the profiles. For pure bending, the class of RM1 and RM2 are 1 and 2, respectively.

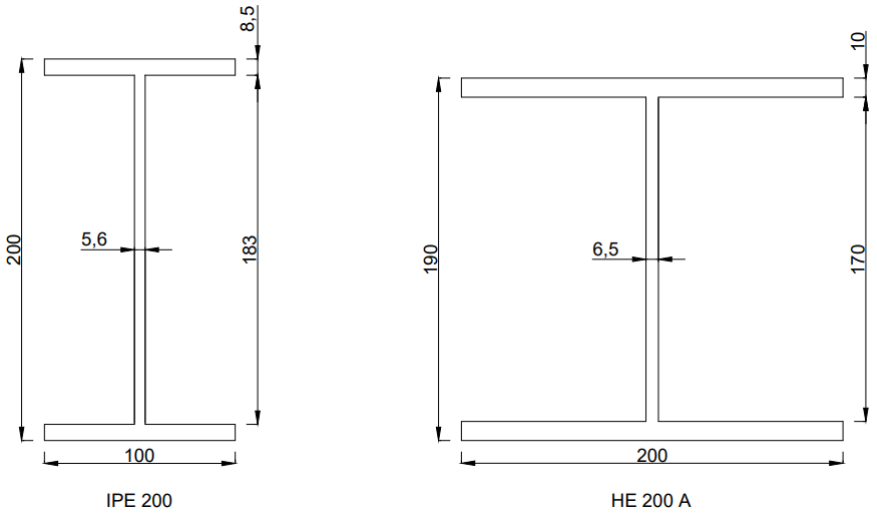

Figure 17. Dimensions of the beam's profiles IPE 200 and HE 200 A in millimeters.

Table 6 shows the study cases of critical moment analyzes, where the reference models RM1 and RM2 of cellular beams have intermediate values of the geometric parameters: $a_0 = 1.0h, S = 1.4a_0$ and $H = 1.5h$. The cellular beams are designed with as many holes as possible, respecting the distance S between them.

Table 6. Study cases of the critical moment analyzes

Case	Type	a_0	S	H	$L[m]$
RM	Solid	–	–	h	1, 1.5, 2, 2.5,…, 9, 9.5, 10
RM	Cellular	$1.0h$	$1.4a_0$	$1.5h$	1, 1.5, 2, 2.5,…, 9, 9.5, 10
$a_0 = 0.8h$	Cellular	$0.8h$	$1.4a_0$	$1.5h$	1, 1.5, 2, 2.5,…, 9, 9.5, 10
$a_0 = 1.3h$	Cellular	$1.3h$	$1.4a_0$	$1.5h$	1, 1.5, 2, 2.5,…, 9, 9.5, 10
$S = 1.1a_0$	Cellular	$1.0h$	$1.1a_0$	$1.5h$	1, 1.5, 2, 2.5,…, 9, 9.5, 10
$S = 1.7a_0$	Cellular	$1.0h$	$1.7a_0$	$1.5h$	1, 1.5, 2, 2.5,…, 9, 9.5, 10
$H = 1.3h$	Cellular	$1.0h$	$1.4a_0$	$1.3h$	1, 1.5, 2, 2.5,…, 9, 9.5, 10
$H = 1.6h$	Cellular	$1.0h$	$1.4a_0$	$1.6h$	1, 1.5, 2, 2.5,…, 9, 9.5, 10

In the non-uniform angle of torsion analyzes, the study cases were just with the RM and three-beam lengths of beam, as is shown in Table 7.

Table 7. Study cases of the non-uniform angle of torsion analyzes

Case	Type	a_0	S	H	$L[m]$
RM	Solid	–	–	h	1, 5, 10
RM	Cellular	$1.0h$	$1.4a_0$	$1.5h$	1, 5, 10

5.3. Simulation program in ANSYS software

Numerical simulations were performed with the ANSYS Mechanical 2021 R2 software, using shell elements in the numerical model, which is suitable for analyzing thin to moderately-thick shell structures.

These simulations were made for an elastic linear analysis, using the Eigenvalue Buckling analysis, that predicts the theoretical buckling strength of an ideal elastic and uses the Equation 36, [45]

$$([K] + \lambda_i[S])\{\psi_i\} = \{0\} \tag{36}$$

Where $[K]$ is the structural stiffness matrix, $[S]$ the stress stiffness matrix, λ_i is the i^{th} eigenvalue used to multiply the loads that generated $[S]$, and ψ_i is the i^{th} eigenvector of displacements. This procedure requires a pre-loaded environment from which it draws solution data for use in the Eigenvalue Buckling analysis, [46].

5.3.1. Element type

The chosen shell element is the SHELL181 (Figure 18) with three integration points located through the thickness. It is a four-node element with six degrees of freedom at each node: translations and rotations in the three directions and axes x, y, and z. This element is well-suited for linear, large rotation, and/or large strain nonlinear applications. The triangular option is not recommended because it should only be used as filler elements in mesh generation, [47].

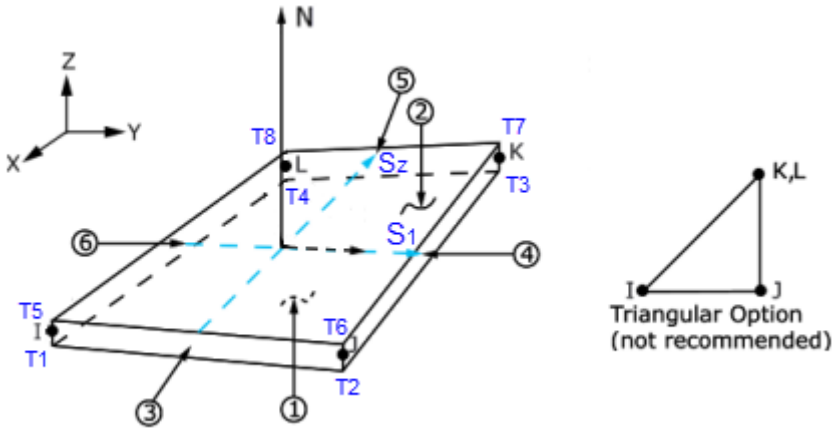

Figure 18. SHELL181 element geometry, adapted from [47].

5.3.2. Material and geometric properties of the elements

The adopted materials proprieties to all study cases were 210 GPa to the modulus of elasticity E, 0.3 to the Poisson's ratio v, and 355 MPa to the yield strength of steel f_y.

Cross-section is traced by the coordinates of the average surface of the profile and then the surface body thickness is defined according to the geometric dimensions of each profile.

5.3.3. Mesh

The mesh adopted was different between the cases of solid and cellular beams. In solid beam cases, the mesh was defined with elements size of 10 [mm] in edges along the beam length (Figure 19.a) and elements size of 15 [mm] in end edges (Figure 19.b).

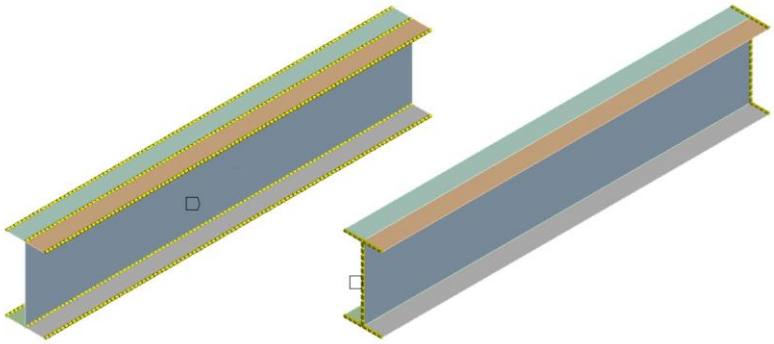

(a) (b)

Figure 19. Mesh edge sizing of solid beam cases with different elements sizes: (a) 10 [mm]; (b) 15 [mm].

In cellular beam cases, the mesh was defined with elements size of 5 [mm] in the edges of the holes (Figure 20.b) and 10 [mm] in the remaining edges of the beam (Figure 20.a).

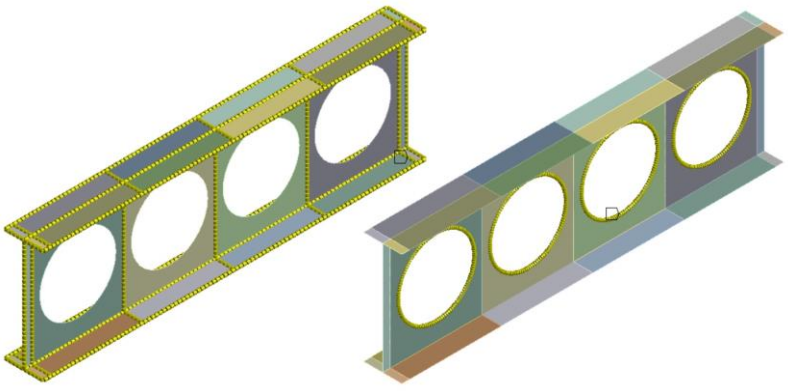

(a) (b)

Figure 20. Mesh edge sizing with different elements sizes: (a) 10 [mm]; (b) 5 [mm].

Figure 21 shows the mesh of the numerical beam model with 1[m] length to the solid and cellular case of RM1, and the mesh of the web-fragment of the cellular case is shown in Figure 22.

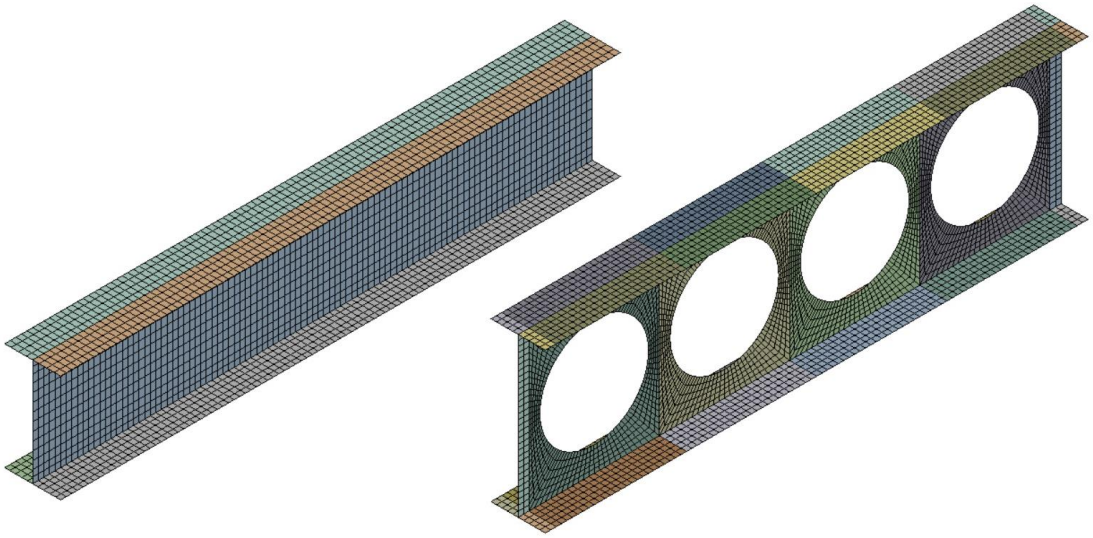

(a) (b)

Figure 21. Mesh of the numerical beam model with 1[m] length: (a) RM1 solid case; (b) RM1 cellular case.

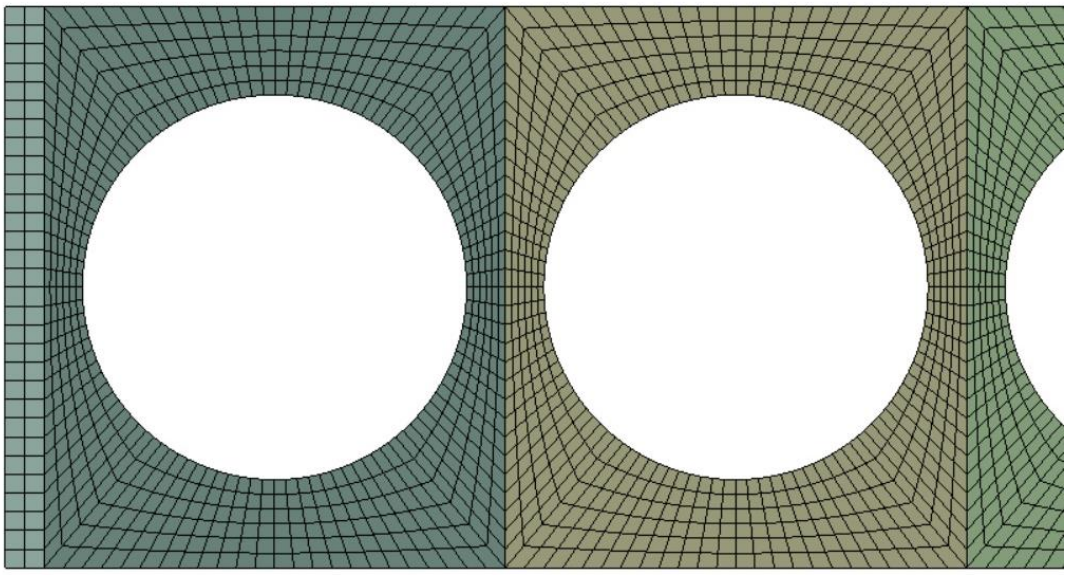

Figure 22. Web fragment mesh of RM1 cellular case.

5.3.4. Boundary conditions to study cases of elastic critical moment.

The boundary conditions are different between critical moment and non-uniform torsional angle study cases. For the critical moment cases, a unitary moment was applied at each end of the beam in opposite directions. The displacement in the y-axis direction

was constrained in the edges of the flange underneath of the two ends. The displacement in x-axis was also constrained in the web edges of the two ends. And the z-displacement was constrained at a vertex of one of the ends.

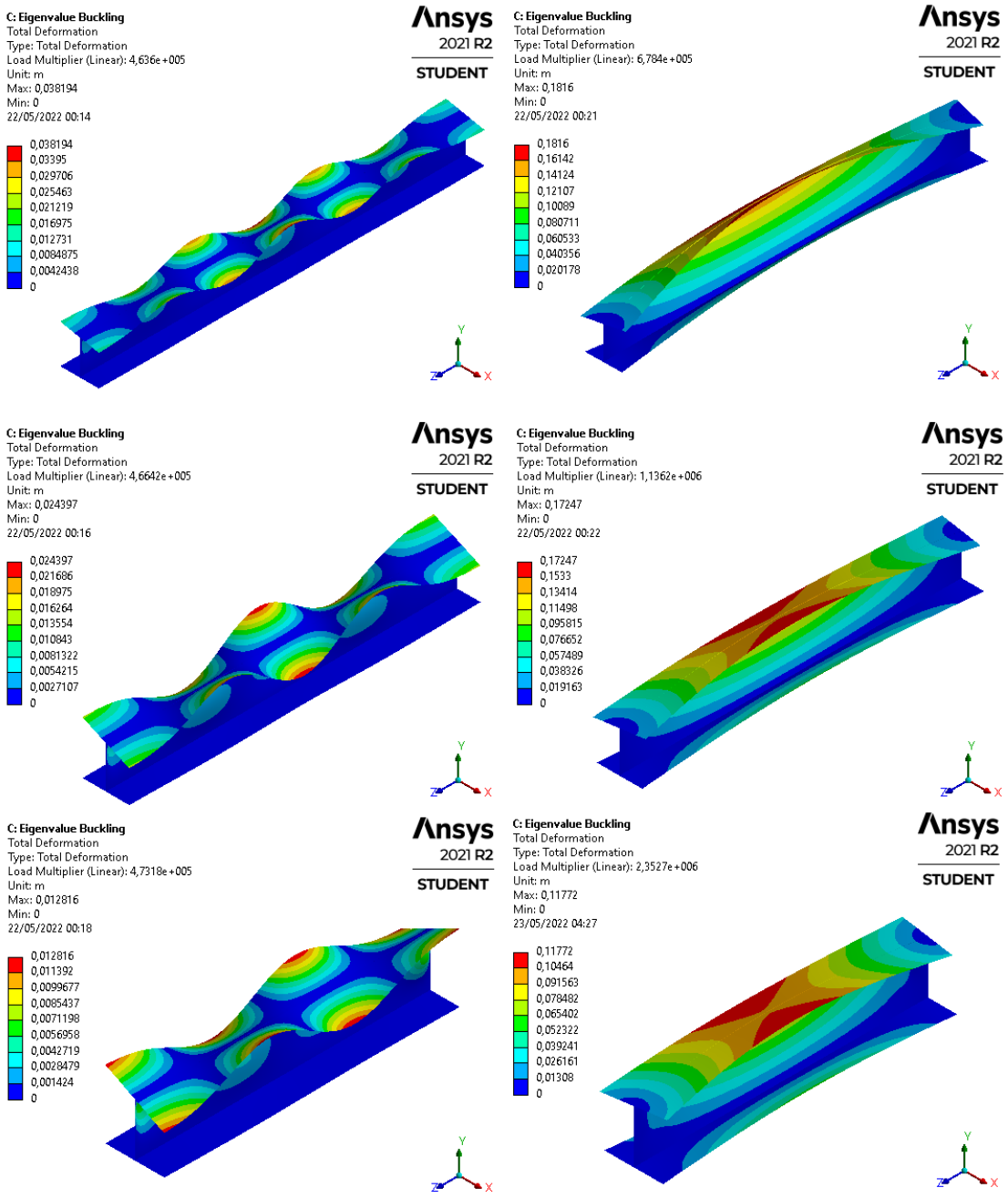

(a) (b)

Figure 23. RM2 solid beam study case with the three-first beam lengths: (a) Without APDL command; (b) After applied APDL command.

In some cases of short beam lengths, the first buckling mode was not the LTB. To avoid any local or distortional buckling in the cross section a rigid type constraint

equation was applied using the CERIG command, using the APDL (ANSYS Parametric Design Language) command in the static structural analysis. Annex A presents the structure of this APDL command.

All beam lengths for the RM1 solid beam case presented LTB in the first buckling mode. But, for the cases of RM2 solid beam with the three-first beam lengths (L=1 [m], L=1.5 [m], L=2 [m]), the first buckling mode was not LTB. Figure 23 shows the RM2 solid beam case before and after applying the APDL command. A pure LTB mode was not found for the first length of this case, but mode 5 was the closest, in which some local deformations in the web are visualized.

For the case of RM1 of the cellular beam, only the beam with length $L = 1$ [m] did not present LTB in the first buckling mode. Figure 24 shows the first buckling mode before and after applying the APDL command.

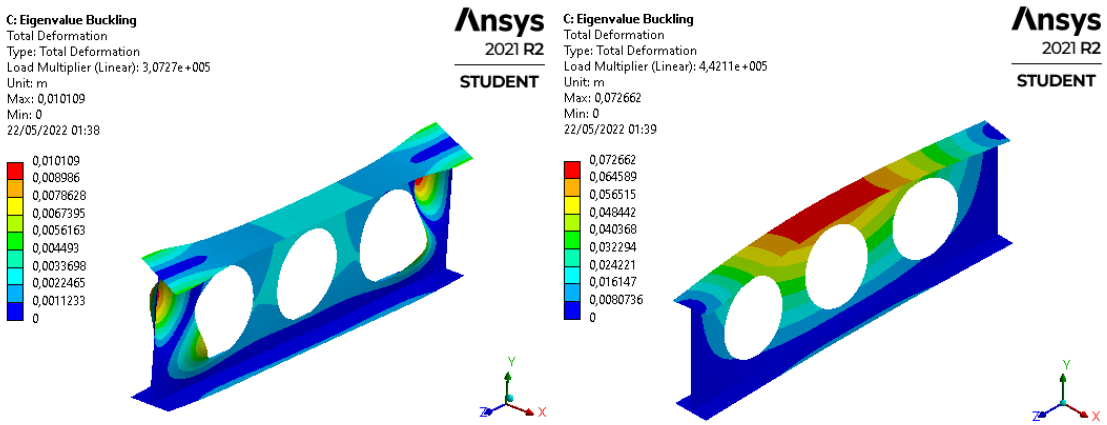

(a) (b)

Figure 24. RM1 cellular beam study case with L=1 [m]: (a) Without APDL command; (b) After applied APDL command.

Although, for the RM2 case of the cellular beam, the four-first lengths did not present LTB in the first buckling mode. Figure 25 shows the RM2 cellular beam case before and after applying the APDL command. As in the case RM2 for solid beam, a pure LTB mode was not found for the first length of this case, and mode 5, with some local deformations in the web, was the closest.

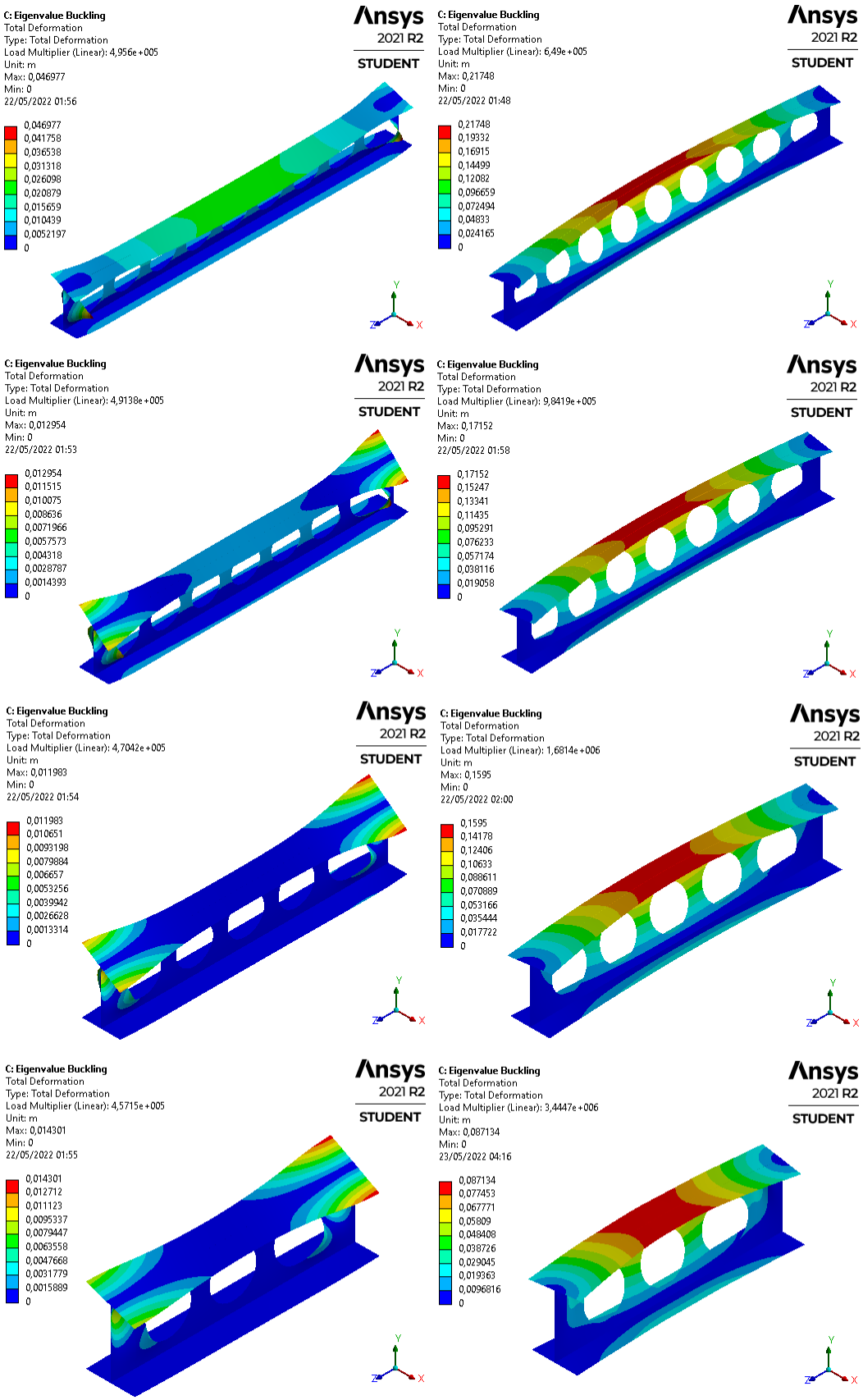

(a) (b)

Figure 25. RM2 cellular beam study case with the four-first beam lengths: (a) Without APDL command; (b) After applied APDL command.

5.3.5. Boundary conditions to study cases of non-uniform torsion angle

For the cases of non-uniform torsion angle, fixed support was applied in all the edges of one ends of the beam, restricting the torsion and the warping at that point of the beam. And a torsional moment of 100 [N.m] was applied at the free end of the beam.

5.4. Results of analytical and numerical methods

In sequence, the results of the analytical methods, Eurocode 3 [37] and SCI P385 [18], and the numerical described above are discussed and compared to analyze the effectiveness of the new weighted average of torsion constant $I_{t,avg3}$ developed by Method 3 in this study.

The reference models that give rise to the cellular beams are the reference model profiles IPE 200 (RM1) and HE 200 A (RM2). The analyzes are made in both types of beams, varying only the length in the solids, and all the geometric parameters (length, height, diameter, and the spacing between the holes) in the cellular beams.

5.4.1. Critical moment for LTB of solid beam cases

Table 8 shows the results of the critical moment for LTB of the solid beam cases and compares the Eurocode analytical method with the ANSYS numerical method.

The numerical model has results very close to the analytical one, showing that the critical moment decreases with the length increase of the beam. Figure 26 and Figure 27 illustrate the LTB of RM1 and RM2 solid beam cases of length L=3 [m], with the APDL command applied. Annexes F and G present the LTB of all lengths of RM1 and RM2 cases.

The two methods were also compared with the graph in Figure 28 where the critical moment M_{cr} is normalized by the plastic moment $M_{pl,Rd}$ and is in the function of the beam length L [m].

Table 8. Comparison between the critical moments of the analytical and numerical methods for the solid beam cases RM1 and RM2.

L [m]	M_{cr} [kN.m] Solid cases					
	Analytical EC3		Numerical ANSYS			
			Without APDL command		APDL command	
	RM1	RM2	RM1	RM2	RM1	RM2
1	302.43	2553.45	289.41	473.18	302.33	2352.67
1.5	145.25	1170.47	142.54	466.42	145.75	1136.23
2	89.54	685.45	88.02	463.60	89.74	678.39
2.5	63.17	459.99	62.12	435.16	63.26	457.93
3	48.39	336.64	47.52	325.69	48.33	335.88
3.5	39.11	261.48	38.40	255.09	39.01	261.07
4	32.81	212.01	32.21	207.62	32.69	211.70
4.5	28.27	177.50	27.79	174.15	28.18	177.22
5	24.85	152.31	24.44	149.56	24.75	152.00
5.5	22.19	133.24	21.81	130.90	22.07	132.92
6	20.05	118.36	19.70	116.33	19.92	118.06
6.5	18.30	106.46	17.98	104.66	18.17	106.15
7	16.84	96.76	16.55	95.13	16.72	96.44
7.5	15.60	88.69	15.33	87.22	15.48	88.38
8	14.53	81.88	14.29	80.54	14.42	81.58
8.5	13.60	76.07	13.39	74.84	13.50	75.77
9	12.79	71.04	12.60	69.91	12.71	70.75
9.5	12.07	66.66	11.90	65.61	11.99	66.37
10	11.43	62.79	11.27	61.81	11.35	62.50

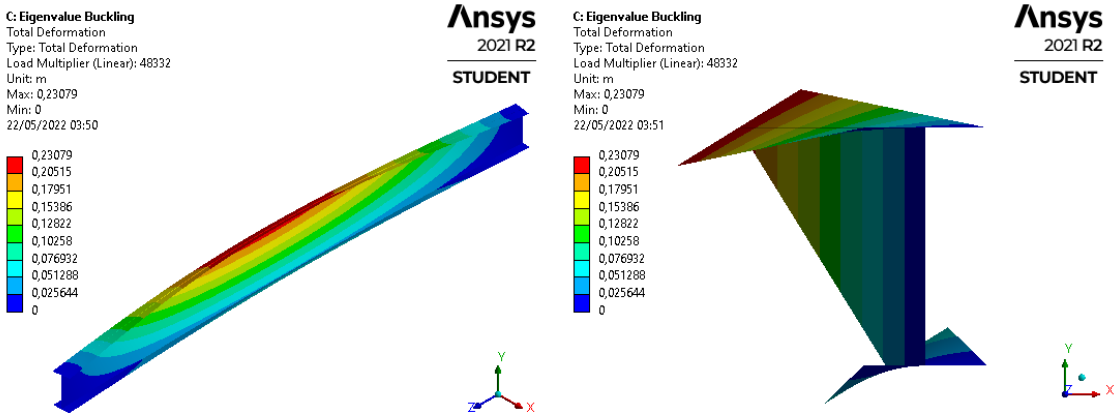

Figure 26. Lateral-torsional buckling of RM1 solid beam case of L=3 [m].

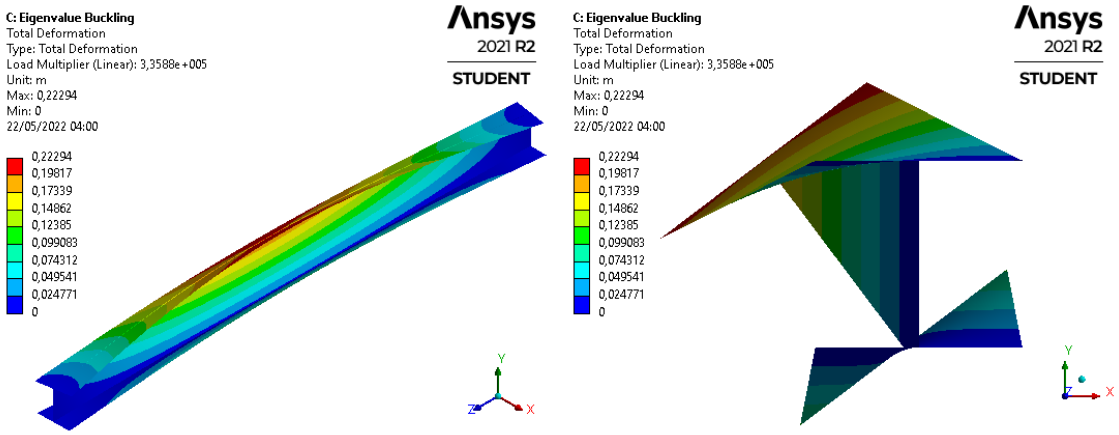

Figure 27.Lateral-torsional buckling of RM2 solid beam case of L=3 [m].

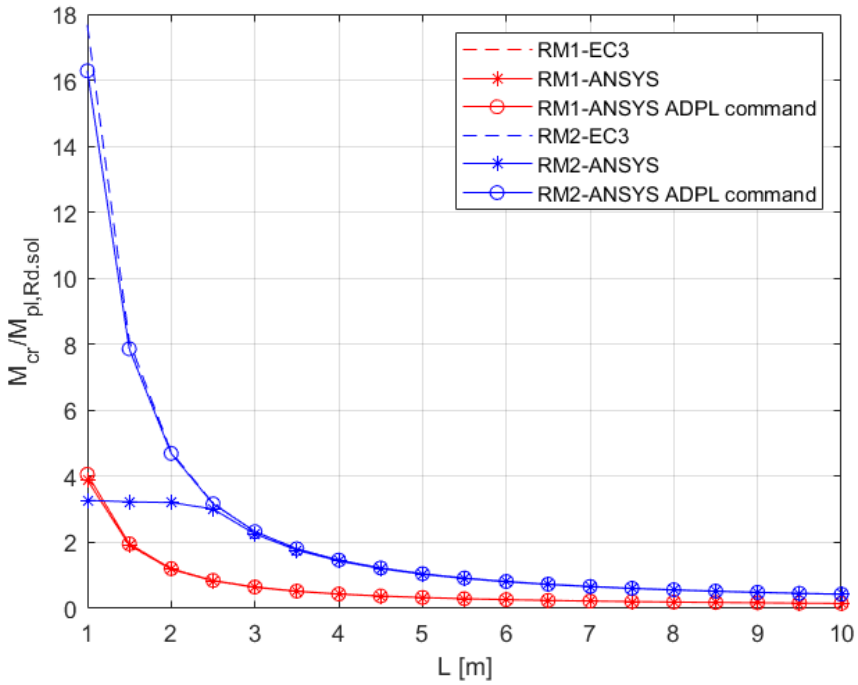

Figure 28. Comparison of critical moment between EC3 and numerical analysis for the solid beams cases RM1 and RM2.

Note that the difference between the values of the first beam lengths of the RM2 case is due to the first buckling mode not being LTB in the numerical simulation without the APDL command.

The relative difference between the analytical and numerical methods is shown in Table 9 and Figure 29.

Table 9. Relative difference between the critical moments of the analytical and numerical methods for the solid beam cases RM1 and RM2.

Relative difference [%]				
L [m]	Without APDL command		APDL command	
	RM1	RM2	RM1	RM2
1	4.31	81.47	0.03	7.86
1.5	1.86	60.15	-0.34	2.93
2	1.70	32.37	-0.22	1.03
2.5	1.68	5.40	-0.13	0.45
3	1.79	3.25	0.11	0.23
3.5	1.82	2.44	0.25	0.16
4	1.83	2.07	0.37	0.15
4.5	1.70	1.89	0.33	0.16
5	1.68	1.81	0.40	0.20
5.5	1.71	1.76	0.53	0.23
6	1.75	1.71	0.64	0.26
6.5	1.72	1.69	0.68	0.29
7	1.70	1.68	0.72	0.33
7.5	1.67	1.66	0.75	0.35
8	1.66	1.64	0.78	0.37
8.5	1.56	1.61	0.72	0.39
9	1.45	1.59	0.66	0.41
9.5	1.43	1.58	0.67	0.43
10	1.42	1.57	0.69	0.46

The results show that the relative difference between the analytical and numerical methods decreases with the APDL command and is less than 1% in almost all cases. Note that for three lengths (L=1.5 [m], L=2 [m], L=2.5 [m]) of the RM1 case, the values of the numerical critical moment are slightly higher than the analytical. Moreover, for length L=1 [m] of the RM2 case, the relative difference is higher than in all cases because mode 5 was not pure of LTB.

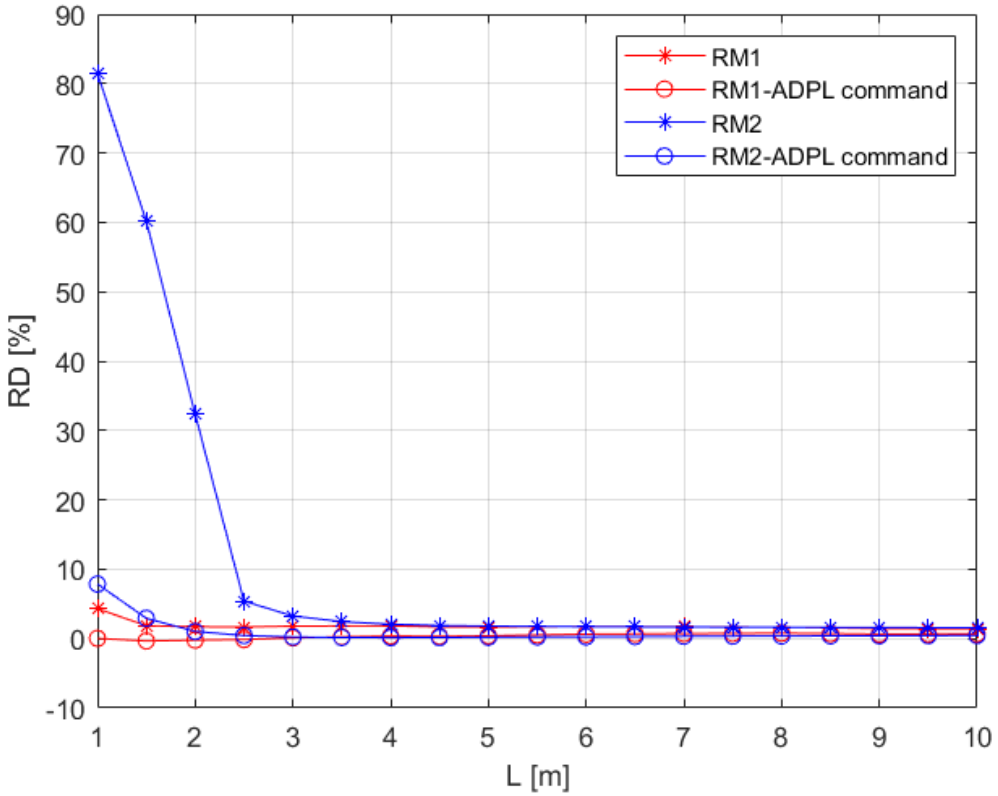

Figure 29. Relative difference between the critical moments of the analytical and numerical methods for the solid beam cases RM1 and RM2.

5.4.2. Critical moment for LTB of cellular beam cases

Table 10 and Table 11 show the values results of the critical moment for LTB of the cellular beam cases RM1 and RM2 and compare the analytical method of Eurocode, varying the constant of torsion, with the numerical method of ANSYS.

Annex B presents the table with these results of all the others study cases of Table 6.

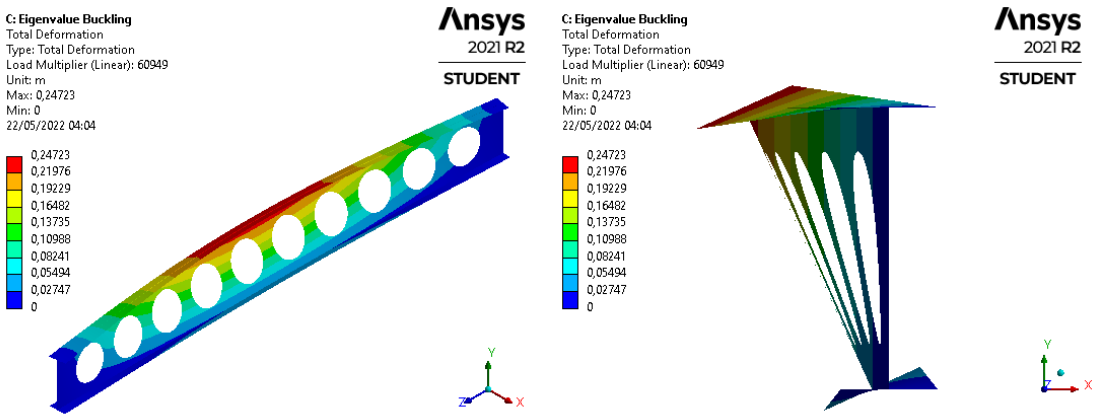

Figure 30. Lateral-torsional buckling of RM1 cellular beam case of L=3 [m].

Table 10. Comparison of critical moment between EC3 method, with the different torsion constants, and numerical analysis for the cellular beam case RM1.

	M_{cr} [kN.m] RM1 cellular case					
L [m]	Analytical EC3				Numerical ANSYS	
	$I_{t,2T}$	$I_{t,avg1}$	$I_{t,avg2}$	$I_{t,avg3}$	Without APDL command	APDL command
1	440.65	442.09	442.31	442.50	307.27	442.11
1.5	202.58	203.66	203.88	204.10	197.25	205.64
2	119.05	120.27	120.45	120.64	118.55	121.85
2.5	80.20	81.22	81.40	81.60	80.28	82.55
3	58.91	59.80	59.98	60.17	59.16	60.95
3.5	45.92	46.71	46.88	47.06	46.21	47.73
4	37.36	38.06	38.22	38.40	37.66	38.99
4.5	31.37	32.10	32.24	32.40	31.85	32.92
5	26.98	27.64	27.78	27.94	27.43	28.41
5.5	23.66	24.26	24.39	24.54	24.07	24.97
6	21.06	21.61	21.73	21.87	21.44	22.27
6.5	18.97	19.53	19.65	19.78	19.43	20.14
7	17.27	17.78	17.89	18.02	17.69	18.36
7.5	15.85	16.33	16.43	16.55	16.24	16.87
8	14.65	15.09	15.19	15.31	15.01	15.61
8.5	13.62	14.04	14.13	14.24	13.96	14.53
9	12.73	13.15	13.24	13.34	13.10	13.61
9.5	11.96	12.35	12.43	12.53	12.30	12.79
10	11.27	11.64	11.72	11.82	11.59	12.06

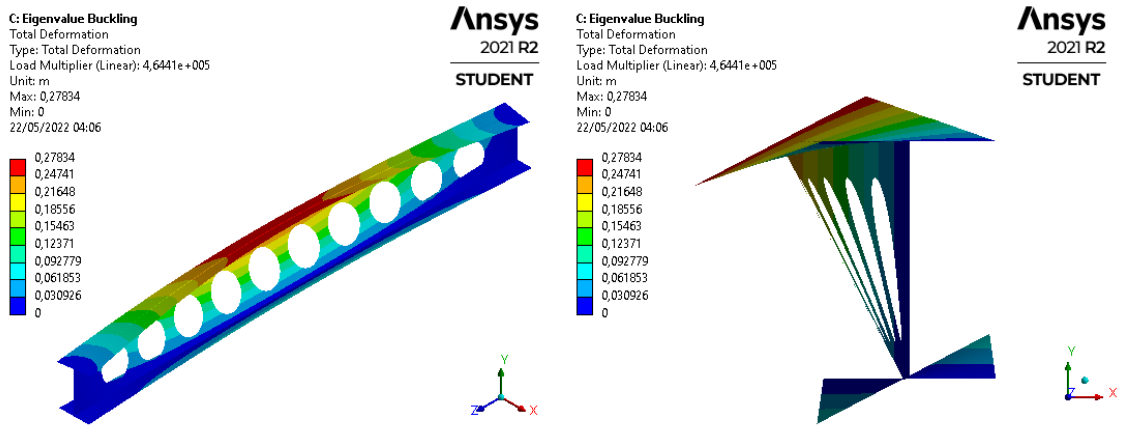

Figure 31. Lateral-torsional buckling of RM2 cellular beam case of L=3 [m].

Table 11. Comparison of critical moment between EC3 method, with the different torsion constants, and numerical analysis for the cellular beam case RM2.

L [m]	M_{cr} [kN.m] RM2 cellular case					
	Analytical EC3				Numerical ANSYS	
	$I_{t,2T}$	$I_{t,avg1}$	$I_{t,avg2}$	$I_{t,avg3}$	Without APDL command	APDL command
1	3841.00	3843.44	3843.77	3844.06	457.15	3444.69
1.5	1729.60	1731.53	1731.86	1732.21	470.42	1681.39
2	990.33	992.03	992.37	992.73	491.38	984.19
2.5	647.88	649.43	649.76	650.13	495.60	649.00
3	461.57	463.31	463.61	463.94	446.28	464.41
3.5	348.97	350.57	350.86	351.20	341.90	352.52
4	275.62	277.11	277.40	277.73	271.63	279.11
4.5	225.10	226.49	226.78	227.10	222.57	228.60
5	188.74	190.05	190.33	190.65	187.05	192.05
5.5	161.64	162.87	163.14	163.45	160.45	164.67
6	140.84	142.00	142.27	142.57	139.94	143.80
6.5	124.49	125.59	125.85	126.14	123.81	127.27
7	111.36	112.41	112.66	112.94	110.81	114.02
7.5	100.64	101.72	101.95	102.22	100.45	103.75
8	91.74	92.76	92.99	93.25	91.61	94.72
8.5	84.25	85.23	85.45	85.70	84.18	87.00
9	77.88	78.81	79.02	79.26	77.84	80.50
9.5	72.39	73.28	73.49	73.72	72.39	75.12
10	67.63	68.48	68.68	68.91	67.65	70.14

The results of cellular beams behaved like solid beams, showing that the critical moment decreases with the length increase of the beam. Figure 30 and Figure 31 illustrate the LTB of RM1 and RM2 cellular beam cases of length L=3 [m], with the APDL command applied. Annexes F and G present the LTB of all lengths of RM1 and RM2 cases.

The values of Table 10 and Table 11 are compared with the graph in Figure 32 where the critical moment is normalized by the plastic moment and is in function of the beam length L [m].

The difference between the values of the first beam length of RM1 case and four-first lengths of RM2 case also is due to the first buckling mode not being LTB in the numerical simulation without the APDL command.

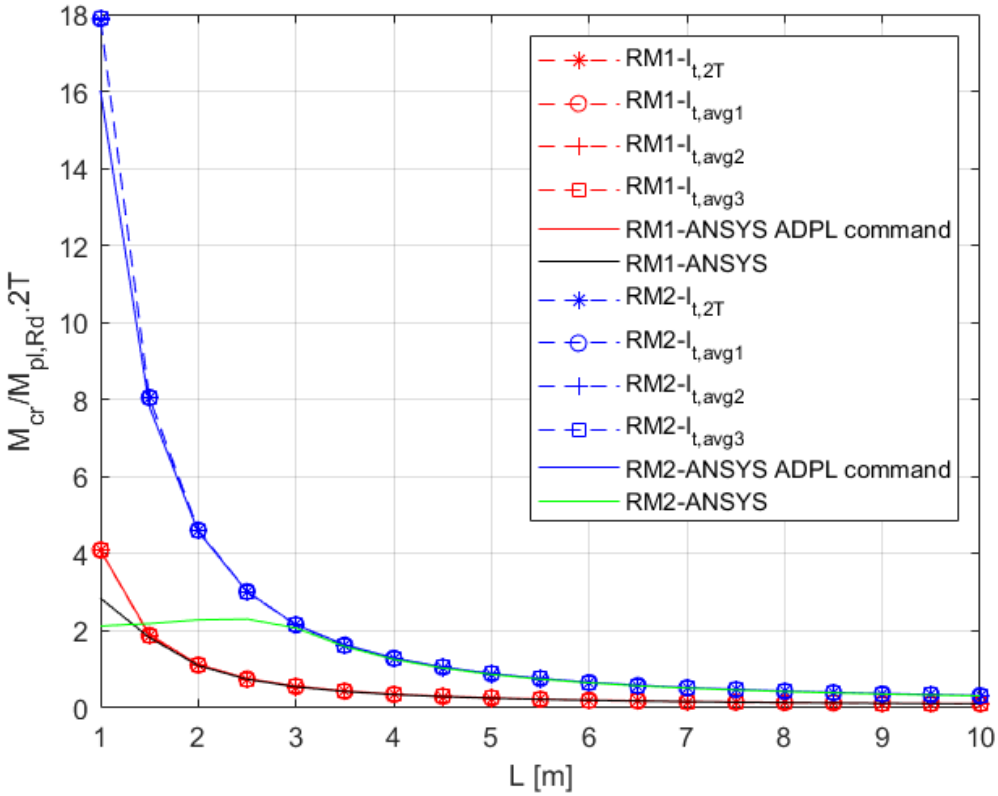

Figure 32. Comparison of critical moment between EC3 method, with the different torsion constants, and numerical analysis for the cellular beam cases RM1 and RM2.

The relative difference of the critical moment is compared between the three different weighted average methods of torsion constant with the constant $I_{t,2T}$. These values of relative percentage difference are in Table 12.

Figure 33 shows a graph with the values of Table 12, where some plateaus can be seen. This plateau happens because the number of cellular beam holes do not have a constant increase. In these cases, the number of holes increase by two in each length of beam and when has the plateau, the increase is by one hole.

All methods of weighted average have higher values to the critical moment than the constant $I_{t,2T}$, being the weighted average $I_{t,avg3}$ the furthest. This was expected because the weighted average $I_{t,avg3}$ is the closer constant of the cellular beam real model, increasing the rigidity of the beam and, consequently, increasing the critical moment. Also, note that the relative difference is less than 5% in all cases but is smallest in the RM2 profile than in the RM1.

Table 12. Relative difference of the critical moments between the three different weighted average methods of torsion constant with the constant $I_{t,2T}$.

L [m]	Relative difference [%]					
	RM1			RM2		
	$I_{t,avg1}$	$I_{t,avg2}$	$I_{t,avg3}$	$I_{t,avg1}$	$I_{t,avg2}$	$I_{t,avg3}$
1	-0.33	-0.38	-0.42	-0.06	-0.07	-0.08
1.5	-0.53	-0.64	-0.75	-0.11	-0.13	-0.15
2	-1.02	-1.17	-1.33	-0.17	-0.21	-0.24
2.5	-1.27	-1.50	-1.74	-0.24	-0.29	-0.35
3	-1.51	-1.81	-2.13	-0.38	-0.44	-0.51
3.5	-1.71	-2.08	-2.48	-0.46	-0.54	-0.64
4	-1.88	-2.32	-2.80	-0.54	-0.65	-0.77
4.5	-2.33	-2.79	-3.30	-0.62	-0.75	-0.89
5	-2.45	-2.96	-3.53	-0.69	-0.84	-1.01
5.5	-2.54	-3.10	-3.72	-0.76	-0.93	-1.12
6	-2.61	-3.21	-3.88	-0.83	-1.02	-1.23
6.5	-2.94	-3.55	-4.23	-0.89	-1.09	-1.33
7	-2.98	-3.62	-4.33	-0.94	-1.16	-1.42
7.5	-3.00	-3.67	-4.42	-1.08	-1.31	-1.57
8	-3.02	-3.72	-4.49	-1.12	-1.37	-1.65
8.5	-3.03	-3.75	-4.55	-1.16	-1.42	-1.72
9	-3.27	-3.98	-4.78	-1.20	-1.47	-1.78
9.5	-3.27	-4.00	-4.81	-1.23	-1.51	-1.84
10	-3.26	-4.01	-4.84	-1.26	-1.55	-1.89

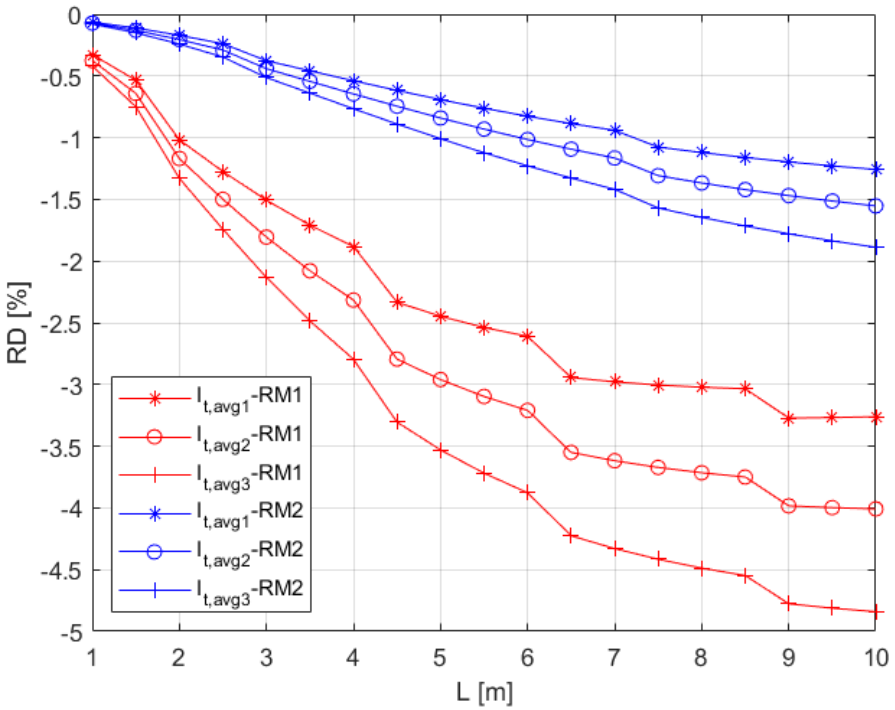

Figure 33. Relative difference of the critical moments between the three different weighted average methods of torsion constant with the constant $I_{t,2T}$.

Table 13 and Table 14 compare and calculate the relative difference of the critical moment between the numerical and the analytical analyzes, with the different torsion constants, for the cellular beam cases RM1 and RM2.

Table 13. Relative difference of the critical moment between the numerical and the analytical analyzes, with the different torsion constants, for the cellular beam case RM1.

L [m]	Relative difference [%] RM1							
	Without APDL command				APDL command			
	$I_{t,2T}$	$I_{t,avg1}$	$I_{t,avg2}$	$I_{t,avg3}$	$I_{t,2T}$	$I_{t,avg1}$	$I_{t,avg2}$	$I_{t,avg3}$
1	-43.41	-43.88	-43.95	-44.01	0.33	0.01	-0.04	-0.09
1.5	-2.70	-3.25	-3.36	-3.47	1.49	0.96	0.85	0.75
2	-0.43	-1.45	-1.60	-1.76	2.30	1.30	1.15	1.00
2.5	0.10	-1.17	-1.39	-1.64	2.84	1.60	1.39	1.15
3	0.41	-1.09	-1.39	-1.71	3.34	1.88	1.59	1.28
3.5	0.63	-1.07	-1.44	-1.84	3.79	2.15	1.79	1.40
4	0.80	-1.07	-1.50	-1.98	4.18	2.38	1.96	1.50
4.5	1.52	-0.77	-1.23	-1.73	4.73	2.50	2.06	1.58
5	1.63	-0.78	-1.28	-1.84	5.01	2.69	2.20	1.66
5.5	1.71	-0.78	-1.33	-1.94	5.25	2.85	2.32	1.73
6	1.77	-0.79	-1.38	-2.04	5.45	2.98	2.42	1.79
6.5	2.34	-0.53	-1.13	-1.79	5.79	3.02	2.45	1.81
7	2.37	-0.54	-1.16	-1.86	5.94	3.14	2.54	1.87
7.5	2.38	-0.55	-1.20	-1.93	6.05	3.23	2.60	1.91
8	2.39	-0.56	-1.24	-1.99	6.15	3.31	2.66	1.94
8.5	2.39	-0.57	-1.27	-2.05	6.23	3.39	2.72	1.97
9	2.82	-0.36	-1.05	-1.83	6.45	3.39	2.72	1.98
9.5	2.80	-0.38	-1.09	-1.88	6.49	3.43	2.75	1.99
10	2.78	-0.39	-1.12	-1.93	6.53	3.49	2.79	2.01

The relative differences are less than 4 % in all cases, except for the first length of RM2, that do not have pure LTB in its failure mode. To better understand these differences, graphs are illustrated with the analytical critical moment divided by the numerical critical moment in the function of the beam length and varying the torsion constant. Figure 34 and Figure 35 show the results of RM1 and RM2 study cases respectively, without APDL command.

Table 14. Relative difference of the critical moment between the numerical and the analytical analyzes, with the different torsion constants, for the cellular beam case RM2.

L [m]	Relative difference [%] RM2							
	Without APDL command				APDL command			
	$I_{t,2T}$	$I_{t,avg1}$	$I_{t,avg2}$	$I_{t,avg3}$	$I_{t,2T}$	$I_{t,avg1}$	$I_{t,avg2}$	$I_{t,avg3}$
1	-740.21	-740.75	-740.82	-740.88	-11.51	-11.58	-11.59	-11.59
1.5	-267.67	-268.08	-268.16	-268.23	-2.87	-2.98	-3.00	-3.02
2	-101.54	-101.89	-101.96	-102.03	-0.62	-0.80	-0.83	-0.87
2.5	-30.73	-31.04	-31.11	-31.18	0.17	-0.06	-0.12	-0.17
3	-3.43	-3.82	-3.88	-3.96	0.61	0.24	0.17	0.10
3.5	-2.07	-2.54	-2.62	-2.72	1.01	0.55	0.47	0.37
4	-1.47	-2.02	-2.13	-2.25	1.25	0.72	0.61	0.49
4.5	-1.14	-1.76	-1.89	-2.04	1.53	0.92	0.80	0.66
5	-0.90	-1.60	-1.75	-1.92	1.72	1.04	0.90	0.73
5.5	-0.74	-1.51	-1.68	-1.87	1.84	1.09	0.93	0.74
6	-0.64	-1.48	-1.67	-1.88	2.06	1.25	1.06	0.86
6.5	-0.54	-1.44	-1.64	-1.88	2.19	1.32	1.12	0.89
7	-0.50	-1.45	-1.67	-1.93	2.34	1.42	1.20	0.95
7.5	-0.18	-1.26	-1.49	-1.76	3.00	1.95	1.73	1.48
8	-0.14	-1.26	-1.51	-1.79	3.15	2.07	1.83	1.56
8.5	-0.08	-1.25	-1.51	-1.80	3.16	2.04	1.78	1.50
9	-0.05	-1.25	-1.52	-1.83	3.26	2.10	1.84	1.54
9.5	-0.01	-1.24	-1.52	-1.84	3.64	2.45	2.18	1.87
10	0.03	-1.23	-1.52	-1.86	3.58	2.37	2.08	1.76

Figure 34 shows that the analytical critical moment without the APDL command is greater than the numerical one, except for the constant $I_{t,2T}$. Although the difference between the methods of the constants with the weighted averages is small, the method of the constant $I_{t,avg3}$ is the one that was furthest from the reference value line 1.

In Figure 35, the results of the first beam lengths of RM2, with big relative differences, do not appear in the range of the graph axis for better visualization of the relative difference between the torsion constants. The analytical critical moment without the APDL command also is greater than the numerical one, except for the last beam length of the constant $I_{t,2T}$. Moreover, the method of the constant $I_{t,avg3}$ continues to be the one that was furthest from the reference value line 1.

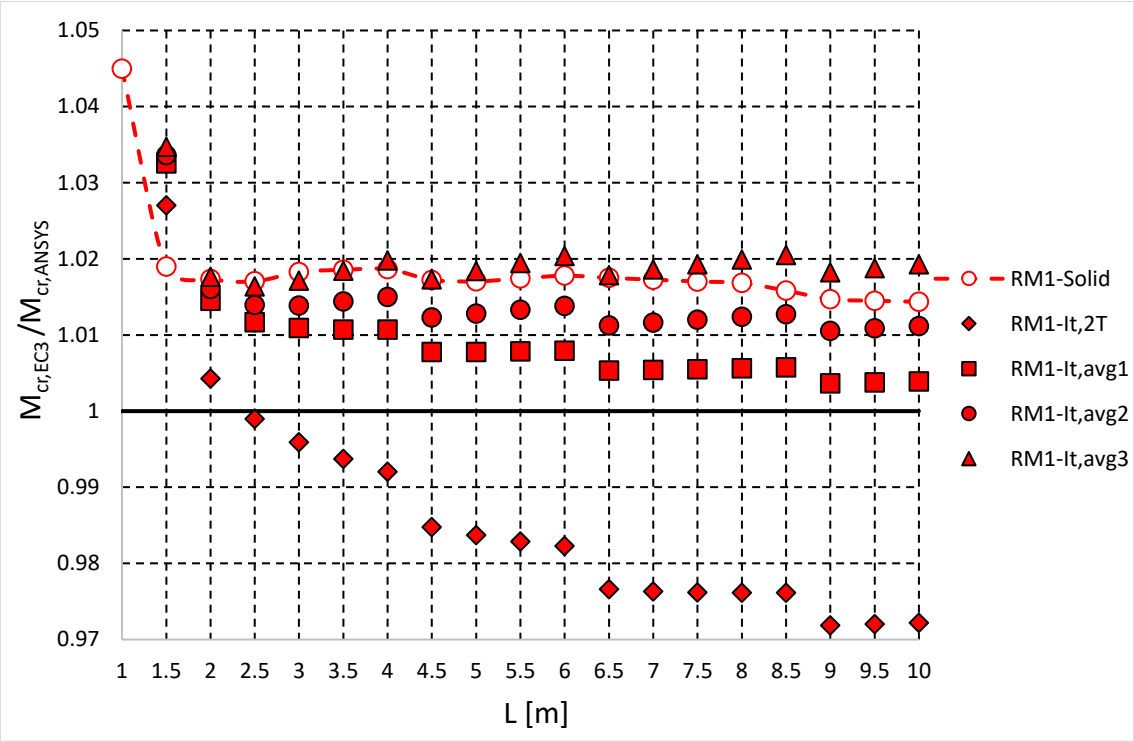

Figure 34. Analytical critical moment, without the APDL command, divided by the ANSYS critical moment of solid and cellular beam study cases of RM1, varying the torsion constant.

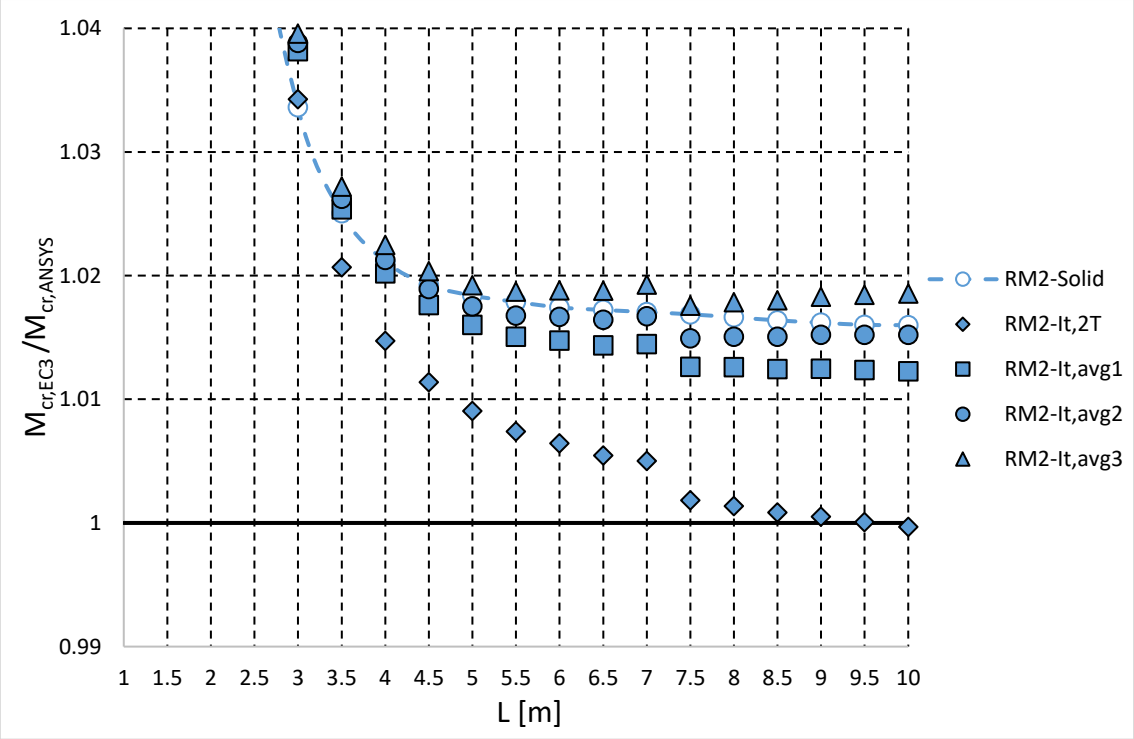

Figure 35. Analytical critical moment, without the APDL command, divided by the ANSYS critical moment of solid and cellular beam study cases of RM2, varying the torsion constant.

The results of the study cases of RM1, with the APDL command applied, are shown in Figure 36. Only the solid beam case (except for three beam lengths) has the

analytical critical moment smaller than the numerical. As was expected, the method of the constant $I_{t,avg3}$ is the closest to the reference value line 1 than all other torsion constants.

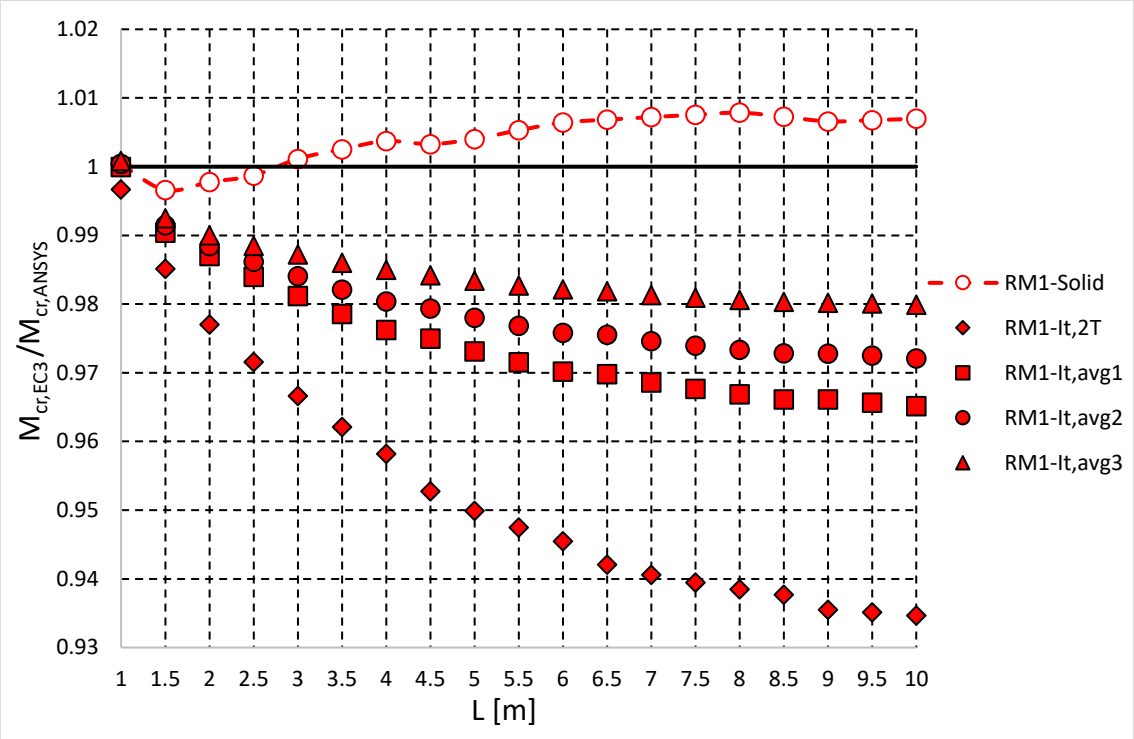

Figure 36. Analytical critical moment, with the APDL command, divided by the ANSYS critical moment of solid and cellular beam study cases of RM1, varying the torsion constant.

This good result happens because in the numerical model without the APLD command, even though it appeared to be pure LTB mode, some small local deformations in web also are present. This fact can be seen in Figure 37, which shows the comparison between the critical moment of the RM1 cellular beam study case with L=1.5[m] before and after applying the command.

The results of the study cases of RM2, with the APDL command applied, are shown in Figure 38. The solid beam case and the three-first length of the cellular beam cases have the analytical critical moment smaller than the numerical. As was also expected, the method of the constant $I_{t,avg3}$ is the closest to the reference value line 1 than all other torsion constants.

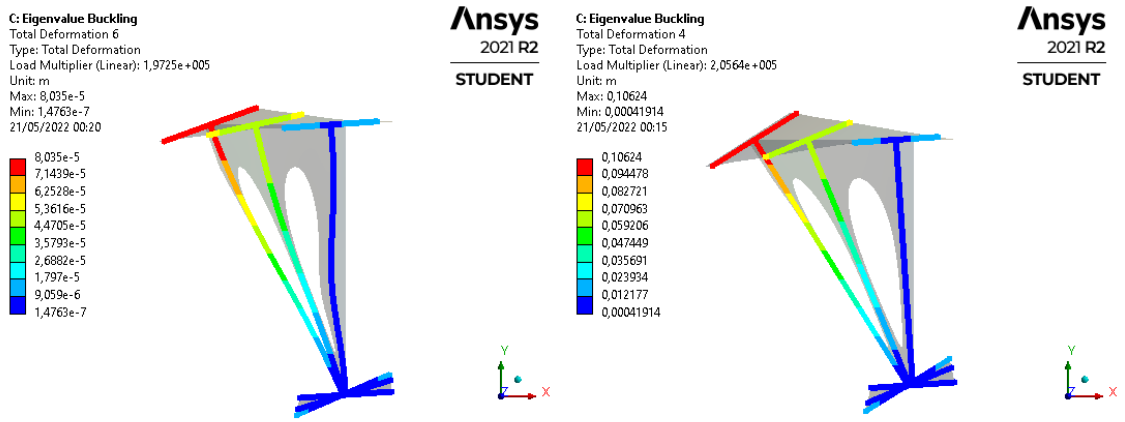

Figure 37. Comparison between the critical moment of the RM1 cellular beam study case with 1.5[m] of length.: (a) Without APDL command; (b) After applied APDL command.

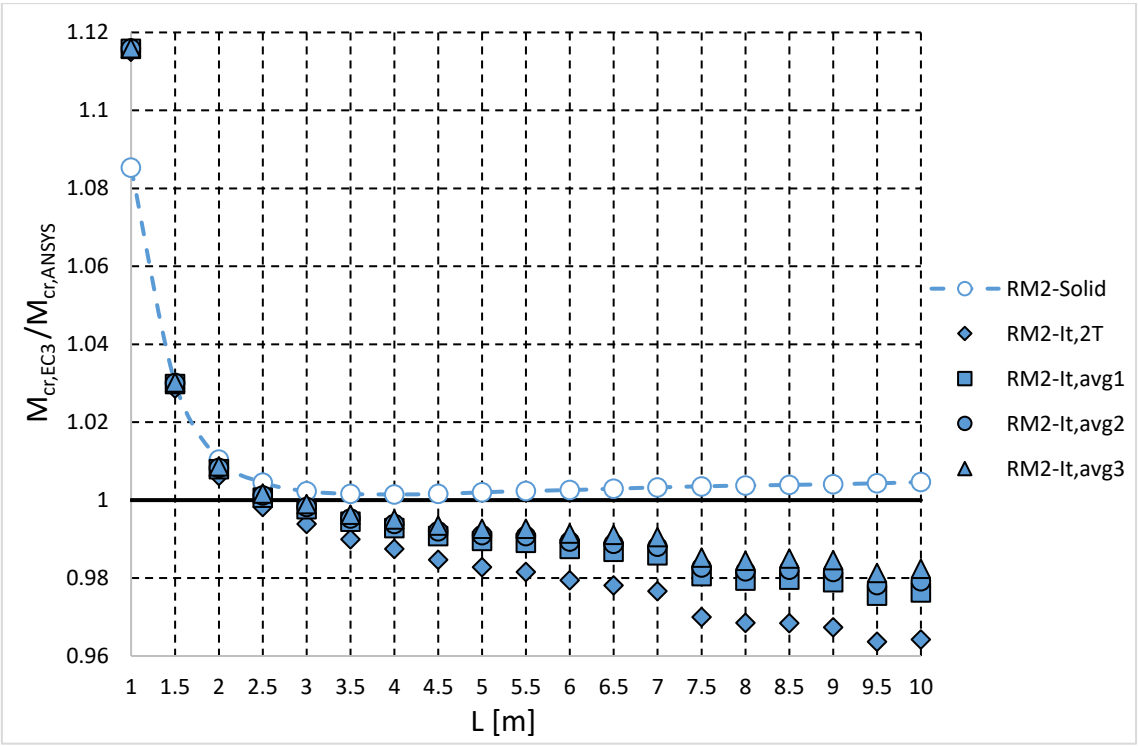

Figure 38. Analytical critical moment, with the APDL command, divided by the ANSYS critical moment of solid and cellular beam study cases of RM2, varying the torsion constant.

The same behavior described above of RM1 happens in the RM2 cellular beam case. Figure 39 explains this good result showing the comparison between the critical moment of the RM2 cellular beam study case with 3[m] of length before and after applying the command.

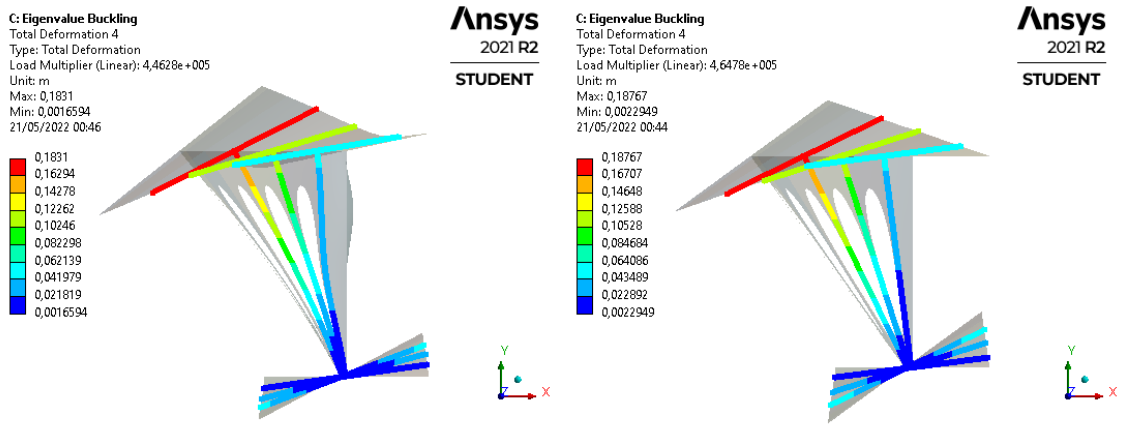

Figure 39. Comparison between the critical moment of the RM2 cellular beam study case with 3[m] of length.: (a) Without APDL command; (b) After applied APDL command.

Annex D presents the graphs of the analytical critical moment divided by the ANSYS critical moment (with the APDL command) and varying the torsion constant, of all the other cases of Table 6. These other cases have same behavior to the reference model cases described above.

After concluding that the constant $I_{t,avg3}$ presents the best results for the comparisons between the elastic critical moment for LTB, the influence of the geometric parameters of the other cases is also analyzed and compared with the numerical results with the APDL command.

5.4.3. Variation of the diameter of the hole

The first parameter to be evaluated is the diameter of the hole on the web. Table 15 shows the results of the critical moment for LTB of $a_0 = 0.8$h and $a_0 = 1.3$h cellular beam cases based on the RM1 and compares the Eurocode analytical method, using the torsion constant $I_{t,avg3}$, with the ANSYS numerical method.

The results show that the critical moment decreases with the length increase of the beam and the analytical critical moment is greater than the numerical just in the case of L=1[m]. Figure 40 and Figure 41 illustrate the LTB of $a_0 = 0.8$h and $a_0 = 1.3$h cellular beam cases based on the RM1 of length L=3 [m]. Annexes F and G present the LTB of all lengths of RM1 and RM2 cases.

Table 16 shows the relative difference of the critical moment between the numerical and the analytical analyzes, using the torsion constant $I_{t,avg3}$, for the $a_0 = 0.8$h and $a_0 = 1.3$h cellular beam cases based on the RM1.

Table 15. Comparison of critical moment between EC3 method, with the torsion constant $I_{t,avg3}$, and numerical analysis for the $a_0 = 0.8$h, $a_0 = 1.3$h, and RM1 cellular beam cases.

L [m]	M_{cr} [kN.m]					
	Analytical EC3 $I_{t,avg3}$			Numerical ANSYS APDL command		
	$a_0 = 0.8$h	$a_0 = 1.3$h	RM1	$a_0 = 0.8$h	$a_0 = 1.3$h	RM1
1	442.75	442.27	442.50	442.18	442.63	442.11
1.5	204.50	204.07	204.10	206.53	206.08	205.64
2	120.85	120.05	120.64	122.71	121.39	121.85
2.5	81.88	81.21	81.60	83.27	82.27	82.55
3	60.40	59.92	60.17	61.74	60.88	60.95
3.5	47.33	46.71	47.06	48.46	47.59	47.73
4	38.68	38.14	38.40	39.75	38.79	38.99
4.5	32.62	32.00	32.40	33.62	32.63	32.92
5	28.12	27.62	27.94	29.03	28.21	28.41
5.5	24.73	24.28	24.54	25.59	24.85	24.97
6	22.08	21.59	21.87	22.82	22.05	22.27
6.5	19.94	19.50	19.78	20.87	19.95	20.14
7	18.19	17.78	18.02	18.82	18.21	18.36
7.5	16.70	16.30	16.55	17.47	16.67	16.87
8	15.46	15.09	15.31	16.05	15.45	15.61
8.5	14.40	14.02	14.24	14.97	14.37	14.53
9	13.48	13.12	13.34	14.03	13.47	13.61
9.5	12.66	12.34	12.53	13.17	12.63	12.79
10	11.94	11.62	11.82	12.52	11.91	12.06

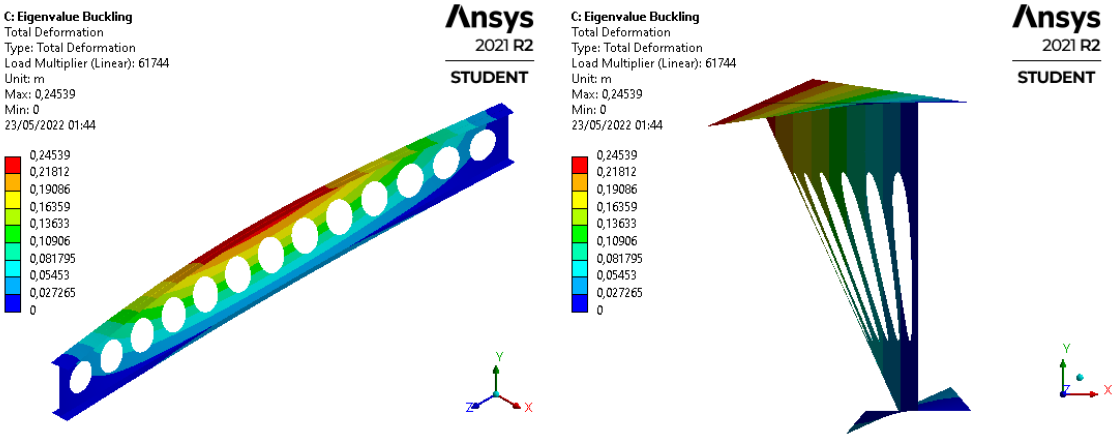

Figure 40. Lateral-torsional buckling of $a_0 = 0.8$h cellular beam case based on RM1 of L=3 [m].

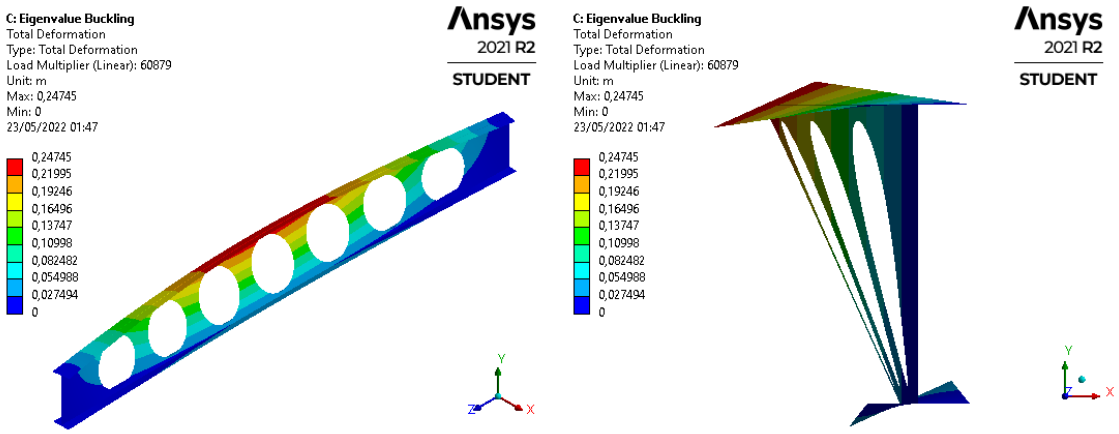

Figure 41. Lateral-torsional buckling of $a_0 = 1.3$h cellular beam case based on RM1 of L=3 [m].

Table 16. Relative difference of the critical moment between the numerical and the analytical analyzes, using the torsion constant $I_{t,avg3}$, for the $a_0 = 0.8$h, $a_0 = 1.3$h, and RM1 cellular beam cases.

L [m]	Relative difference [%]		
	APDL command		
	$I_{t,avg3}$		
	$a_0 = 0.8$h	$a_0 = 1.3$h	RM1
1	-0.13	0.08	-0.09
1.5	0.98	0.97	0.75
2	1.52	1.10	1.00
2.5	1.67	1.29	1.15
3	2.17	1.58	1.28
3.5	2.33	1.85	1.40
4	2.69	1.70	1.50
4.5	2.99	1.93	1.58
5	3.14	2.11	1.66
5.5	3.33	2.30	1.73
6	3.27	2.09	1.79
6.5	4.43	2.25	1.81
7	3.38	2.36	1.87
7.5	4.40	2.21	1.91
8	3.63	2.32	1.94
8.5	3.78	2.43	1.97
9	3.90	2.55	1.98
9.5	3.92	2.33	1.99
10	4.63	2.45	2.01

These relative differences increase with increasing beam length and are less than 4 % in most cases. Figure 42 shows the analytical critical moment divided by the numerical critical moment in the function of the beam length.

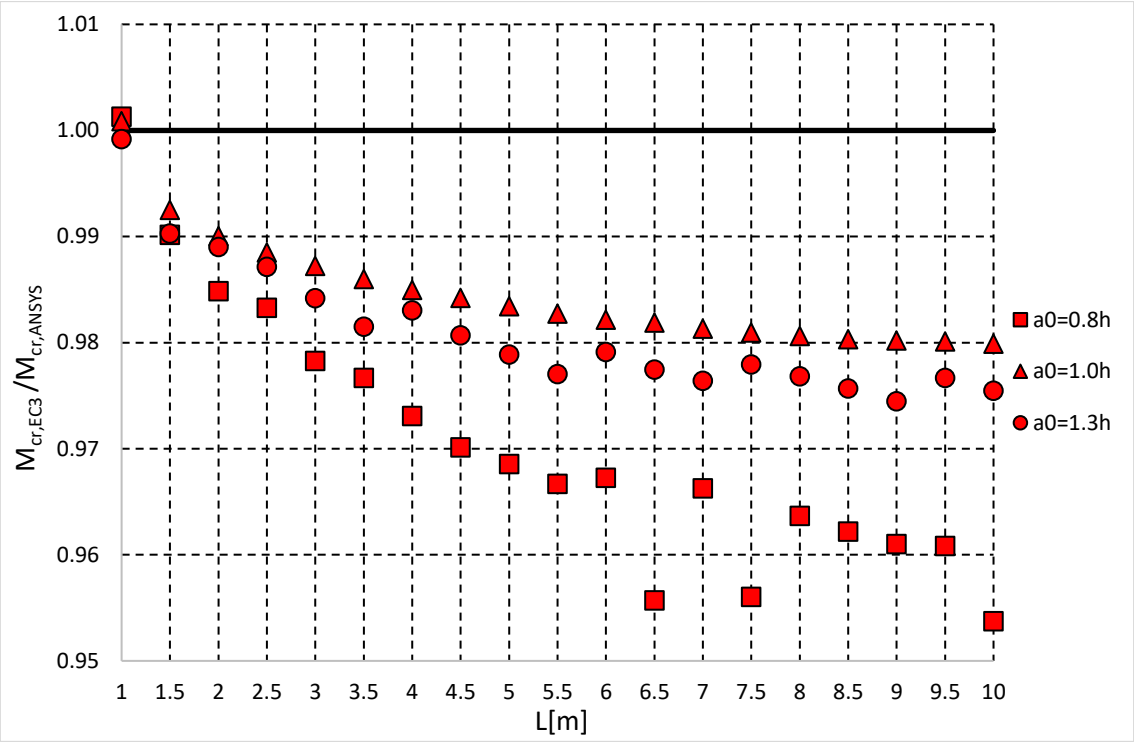

Figure 42. Analytical critical moment, using the torsion constant $I_{t,avg3}$, divided by the ANSYS critical moment of the $a_0 = 0.8$h, $a_0 = 1.3$h, and RM1 cellular beam cases.

The intermediate value for the diameter of the hole $a_0 = 1.0$h represented in the RM1 cellular beam case resulted in the smallest relative difference. The case $a_0 = 1.3$h, with the largest diameter, showed the greatest relative difference and case $a_0 = 0.8$h, with the smallest diameter, was in the middle of the other two cases. Moreover, the increase of the number of holes in each beam length is variable and causes this illustrated behavior in this figure, which is not constant and is more visible in some points, like L=7.5[m].

The same analyzes are done for the HE 200 A beam profile. Table 17 shows the results of the critical moment for LTB of $a_0 = 0.8$h and $a_0 = 1.3$h cellular beam cases based on the RM2 and compares the Eurocode analytical method, using the torsion constant $I_{t,avg3}$, with the ANSYS numerical method.

The results also show that the critical moment decreases with the length increase of the beam and the analytical critical moment is greater than the numerical just in the four-first beam lengths of these cases. Figure 43 and Figure 44 illustrate the LTB of $a_0 = 0.8$h and $a_0 = 1.3$h cellular beam cases based on the RM2 of length L=3 [m]. Annexes F and G present the LTB of all lengths of RM1 and RM2 cases.

Table 17. Comparison of critical moment between EC3 method, with the torsion constant $I_{t,avg3}$, and numerical analysis for the $a_0 = 0.8$h, $a_0 = 1.3$h, and RM2 cellular beam cases.

L [m]	M_{cr} [kN.m]					
	Analytical EC3			Numerical ANSYS		
	$I_{t,avg3}$			APDL command		
	$a_0 = 0.8$h	$a_0 = 1.3$h	RM2	$a_0 = 0.8$h	$a_0 = 1.3$h	RM2
1	3844.45	3843.73	3844.06	3476.57	3547.77	3444.69
1.5	1732.82	1731.27	1732.21	1679.68	1678.04	1681.39
2	993.20	992.18	992.73	983.22	982.65	984.19
2.5	650.70	649.79	650.13	649.86	648.35	649.00
3	464.34	463.11	463.94	465.75	464.45	464.41
3.5	351.54	350.57	351.20	353.63	351.78	352.52
4	278.14	276.97	277.73	280.40	278.09	279.11
4.5	227.56	226.50	227.10	229.88	228.10	228.60
5	191.05	189.95	190.65	193.24	191.38	192.05
5.5	163.88	162.88	163.45	165.87	163.91	164.67
6	143.02	141.93	142.57	144.94	142.91	143.80
6.5	126.54	125.60	126.14	128.39	126.61	127.27
7	113.36	112.48	112.94	115.12	113.38	114.02
7.5	102.57	101.64	102.22	104.30	102.42	103.75
8	93.57	92.75	93.25	95.22	93.86	94.72
8.5	86.03	85.16	85.70	87.62	86.25	87.00
9	79.57	78.79	79.26	81.07	79.45	80.50
9.5	74.04	73.23	73.72	75.44	73.88	75.12
10	69.23	68.47	68.91	70.60	69.27	70.14

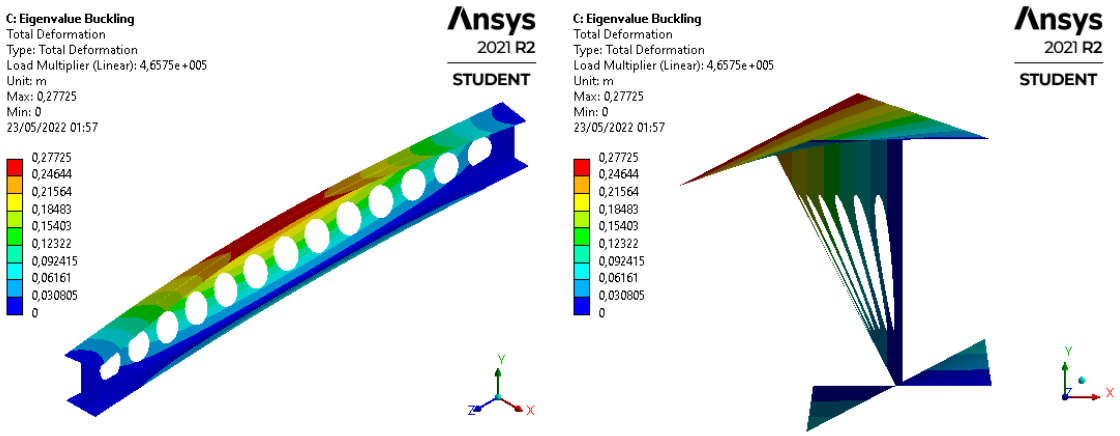

Figure 43. Lateral- torsional buckling of $a_0 = 0.8$h cellular beam case based on RM2 of L=3 [m].

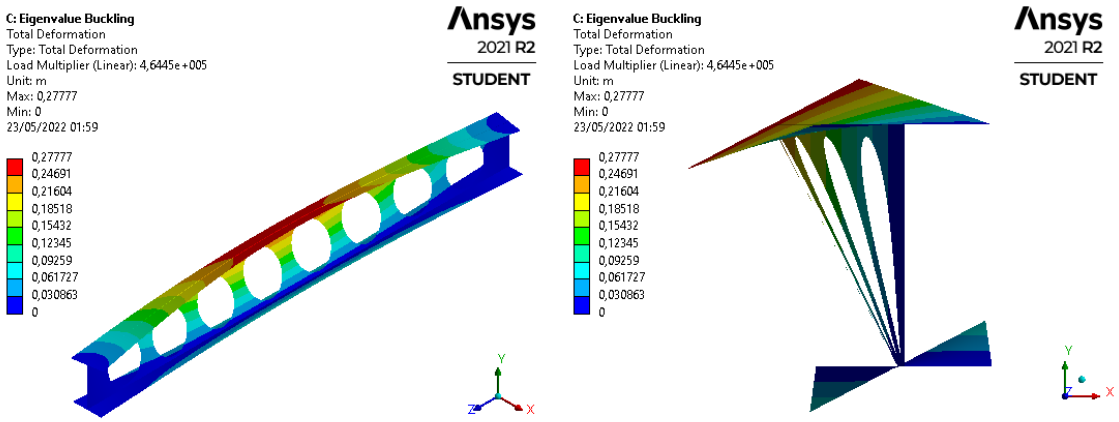

Figure 44. Lateral- torsional buckling of $a_0 = 0.8$h cellular beam case based on RM2 of L=3 [m].

Table 18 shows the relative difference of the critical moment between the numerical and the analytical analyzes, using the torsion constant $I_{t,avg3}$, for the $a_0 = 0.8$h and $a_0 = 1.3$h cellular beam cases based on the RM2.

Table 18. Relative difference of the critical moment between the numerical and the analytical analyzes, using the torsion constant $I_{t,avg3}$, for the $a_0 = 0.8$h, $a_0 = 1.3$h, and RM2 cellular beam cases.

L [m]	Relative difference [%]		
	APDL command		
	$I_{t,avg3}$		
	$a_0 = 0.8$h	$a_0 = 1.3$h	RM2
1	-10.58	-8.34	-11.59
1.5	-3.16	-3.17	-3.02
2	-1.01	-0.97	-0.87
2.5	-0.13	-0.22	-0.17
3	0.30	0.29	0.10
3.5	0.59	0.34	0.37
4	0.81	0.40	0.49
4.5	1.01	0.70	0.66
5	1.14	0.75	0.73
5.5	1.20	0.63	0.74
6	1.32	0.68	0.86
6.5	1.44	0.80	0.89
7	1.53	0.79	0.95
7.5	1.66	0.76	1.48
8	1.73	1.19	1.56
8.5	1.82	1.26	1.50
9	1.85	0.83	1.54
9.5	1.86	0.88	1.87
10	1.94	1.16	1.76

These relative differences also increase with increasing beam length and are less than 2 % in most cases. The LTB was not the first mode for the first length of these cases and the closest mode found has some local deformations in the web, which justifies the higher relative difference in this length of the beam. Figure 45 shows the analytical critical moment divided by the numerical critical moment in the function of the beam length.

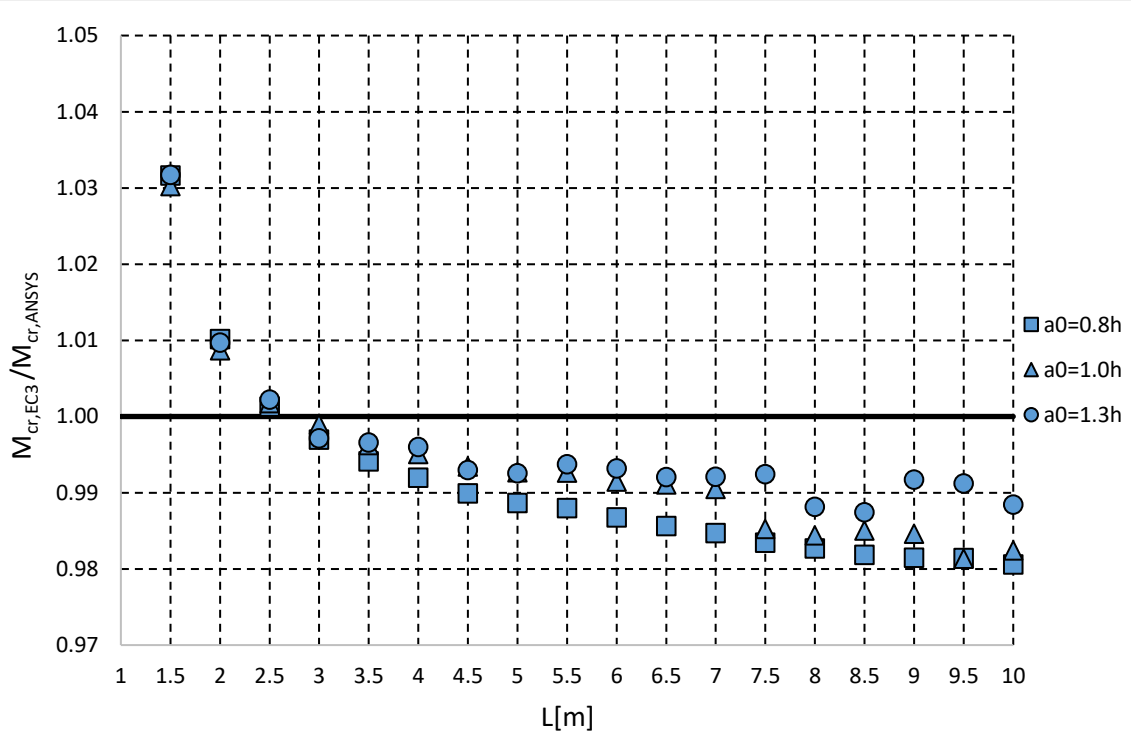

Figure 45. Analytical critical moment, using the torsion constant $I_{t,avg3}$, divided by the ANSYS critical moment of the $a_0 = 0.8$h, $a_0 = 1.3$h, and RM2 cellular beam cases.

The results of the first beam length do not appear in the range of the graph axis for better visualization of the relative difference between the variation of geometric parameters. In most cases, the larger the hole diameter, the smaller the relative difference. Moreover, the variation of the increase of the number of holes causes this illustrated behavior, which is not constant, overlapping some points of results.

5.4.4. Variation of the spacing between the holes

The spacing between the holes S is the second geometric parameter evaluated. Table 19 shows the results of the critical moment for LTB o $S = 1.1a_0$f and $S = 1.7a_0$ cellular beam cases based on the RM1 and compares the Eurocode analytical method, using the torsion constant $I_{t,avg3}$, with the ANSYS numerical method.

Table 19. Comparison of critical moment between EC3 method, with the torsion constant $I_{t,avg3}$, and numerical analysis for the $S = 1.1a_0$, $S = 1.7a_0$, and RM1 cellular beam cases.

L [m]	M_{cr} [kN.m]					
	Analytical EC3			Numerical ANSYS		
	$I_{t,avg3}$			APDL command		
	$S = 1.1a_0$	$S = 1.7a_0$	RM1	$S = 1.1a_0$	$S = 1.7a_0$	RM1
1	441.91	443.08	442.50	441.06	442.96	442.11
1.5	203.75	204.79	204.10	205.13	206.39	205.64
2	120.16	120.88	120.64	121.24	122.27	121.85
2.5	81.06	81.95	81.60	81.83	83.04	82.55
3	59.75	60.45	60.17	60.37	61.42	60.95
3.5	46.73	47.40	47.06	47.26	48.21	47.73
4	38.04	38.67	38.40	38.46	39.43	38.99
4.5	32.02	32.63	32.40	32.40	33.30	32.92
5	27.62	28.13	27.94	27.96	28.76	28.41
5.5	24.26	24.75	24.54	24.58	25.32	24.97
6	21.59	22.06	21.87	21.86	22.61	22.27
6.5	19.49	19.94	19.78	19.74	20.44	20.14
7	17.76	18.16	18.02	18.01	18.64	18.36
7.5	16.29	16.71	16.55	16.51	17.15	16.87
8	15.08	15.45	15.31	15.28	15.88	15.61
8.5	14.04	14.39	14.24	14.23	14.79	14.53
9	13.14	13.46	13.34	13.32	13.84	13.61
9.5	12.32	12.65	12.53	12.49	13.02	12.79
10	11.63	11.93	11.82	11.79	12.28	12.06

The results show that the critical moment decreases with the length increase of the beam and the analytical critical moment is greater than the numerical just in the case of L=1[m]. Figure 46 and Figure 47 illustrate the LTB of $S = 1.1a_0$ and $S = 1.7a_0$ cellular beam cases based on the RM1 of length L=3 [m]. Annexes F and G present the LTB of all lengths of RM1 and RM2 cases.

Table 20 shows the relative differences of the critical moment between the numerical and the analytical analyzes, using the torsion constant $I_{t,avg3}$, for the $S = 1.1a_0$ and $S = 1.7a_0$ cellular beam cases based on the RM1.

These relative differences increase with increasing beam length and are less than 3 % in all cases. Figure 48 shows the analytical critical moment divided by the numerical critical moment in the function of the beam length.

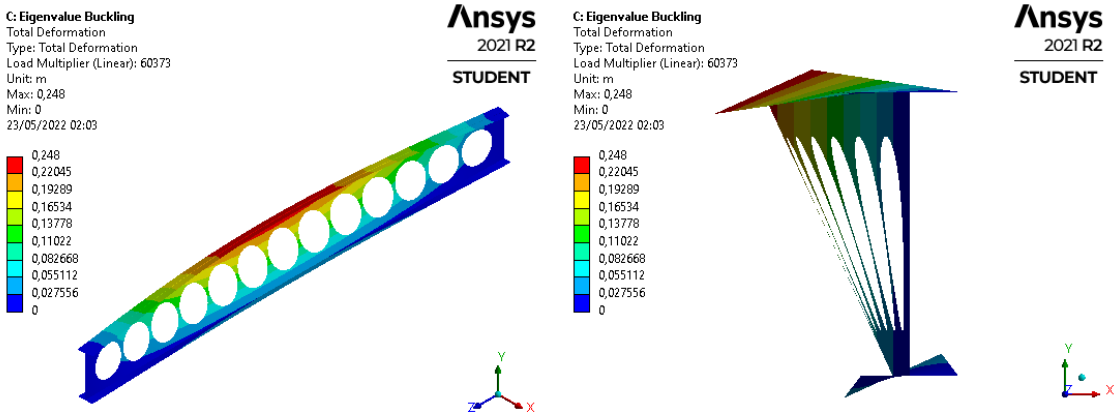

Figure 46. Lateral-torsional buckling of $S = 1.1a_0$ cellular beam case based on RM1 of L=3 [m].

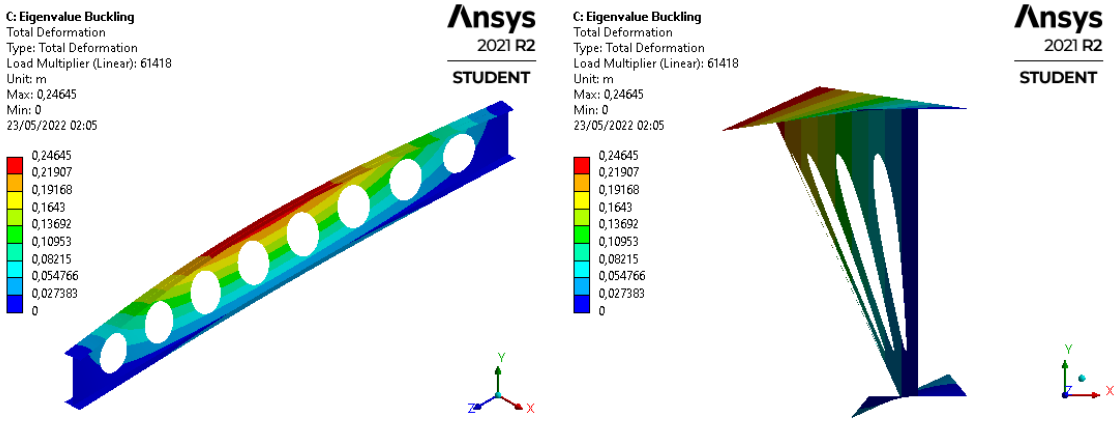

Figure 47. Lateral-torsional buckling of $S = 1.7a_0$ cellular beam case based on RM1 of L=3 [m].

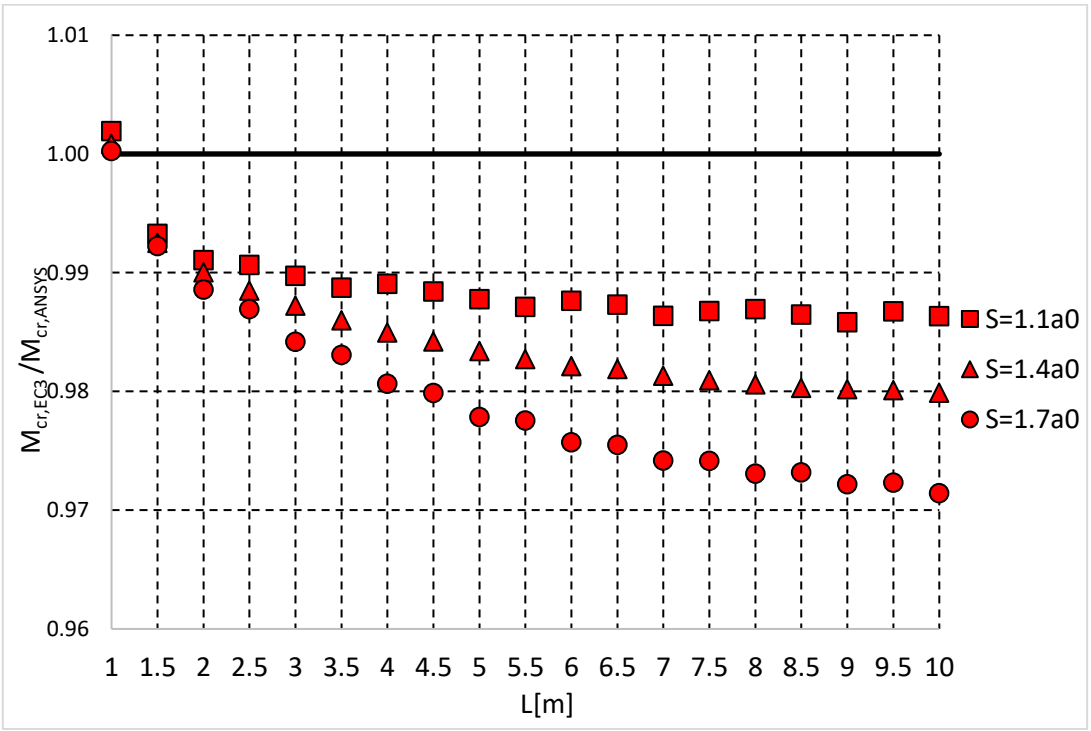

Figure 48. Analytical critical moment, using the torsion constant $I_{t,avg3}$, divided by the ANSYS critical moment of the $S = 1.1a_0$, $S = 1.7a_0$, and RM1 cellular beam cases.

Table 20.Relative difference of the critical moment between the numerical and the analytical analyzes, using the torsion constant $I_{t,avg3}$, for the $S = 1.1a_0$, $S = 1.7a_0$, and RM1 cellular beam cases.

L [m]	Relative difference [%]		
	APDL command		
	$I_{t,avg3}$		
	$S = 1.1a_0$	$S = 1.7a_0$	RM1
1	-0.19	-0.03	-0.09
1.5	0.67	0.77	0.75
2	0.89	1.14	1.00
2.5	0.93	1.31	1.15
3	1.03	1.58	1.28
3.5	1.12	1.69	1.40
4	1.09	1.93	1.50
4.5	1.16	2.01	1.58
5	1.22	2.22	1.66
5.5	1.29	2.24	1.73
6	1.24	2.43	1.79
6.5	1.27	2.45	1.81
7	1.36	2.58	1.87
7.5	1.32	2.58	1.91
8	1.30	2.69	1.94
8.5	1.35	2.68	1.97
9	1.42	2.78	1.98
9.5	1.33	2.77	1.99
10	1.37	2.86	2.01

Note that the larger the spacing between the holes, the higher the relative difference between the analytical and numerical methods.

Table 21 shows the results of the critical moment for LTB of $S = 1.1a_0$ and $S = 1.7a_0$ cellular beam cases based on the RM2 and compares the Eurocode analytical method, using the torsion constant $I_{t,avg3}$, with the ANSYS numerical method.

The results also show that the critical moment decreases with the length increase of the beam and the analytical critical moment is greater than the numerical just in the four-first beam lengths of these cases. Figure 49 and Figure 50 illustrate the LTB of $S = 1.1a_0$ and $S = 1.7a_0$ cellular beam cases based on the RM2 of length L=3 [m]. Annexes F and G present the LTB of all lengths of RM1 and RM2 cases.

Table 22 shows the relative difference of the critical moment between the numerical and the analytical analyzes, using the torsion constant $I_{t,avg3}$, for the $S = 1.1a_0$ and $S = 1.7a_0$ cellular beam cases based on the RM2.

Table 21. Comparison of critical moment between EC3 method, with the torsion constant $I_{t,avg3}$, and numerical analysis for the $S = 1.1a_0$, $S = 1.7a_0$, and RM2 cellular beam cases.

L [m]	M_{cr} [kN.m]					
	Analytical EC3			Numerical ANSYS		
	$I_{t,avg3}$			APDL command		
	$S = 1.1a_0$	$S = 1.7a_0$	RM2	$S = 1.1a_0$	$S = 1.7a_0$	RM2
1	3843.19	3844.93	3844.06	3518.26	3516.97	3444.69
1.5	1731.14	1732.74	1732.21	1674.88	1679.73	1681.39
2	991.97	993.49	992.73	981.27	984.23	984.19
2.5	649.54	650.71	650.13	647.39	649.47	649.00
3	463.00	464.42	463.94	464.14	465.36	464.41
3.5	350.41	351.59	351.20	351.89	354.59	352.52
4	276.91	278.23	277.73	277.61	280.14	279.11
4.5	226.39	227.53	227.10	227.34	229.55	228.60
5	190.03	191.01	190.65	190.97	192.87	192.05
5.5	162.81	163.88	163.45	163.77	166.04	164.67
6	142.00	142.95	142.57	142.94	144.97	143.80
6.5	125.55	126.56	126.14	126.15	128.21	127.27
7	112.41	113.32	112.94	113.09	114.78	114.02
7.5	101.67	102.55	102.22	102.34	104.10	103.75
8	92.70	93.55	93.25	93.63	95.06	94.72
8.5	85.20	86.03	85.70	86.03	87.34	87.00
9	78.81	79.56	79.26	79.65	80.76	80.50
9.5	73.26	74.00	73.72	73.75	75.22	75.12
10	68.48	69.20	68.91	68.94	70.67	70.14

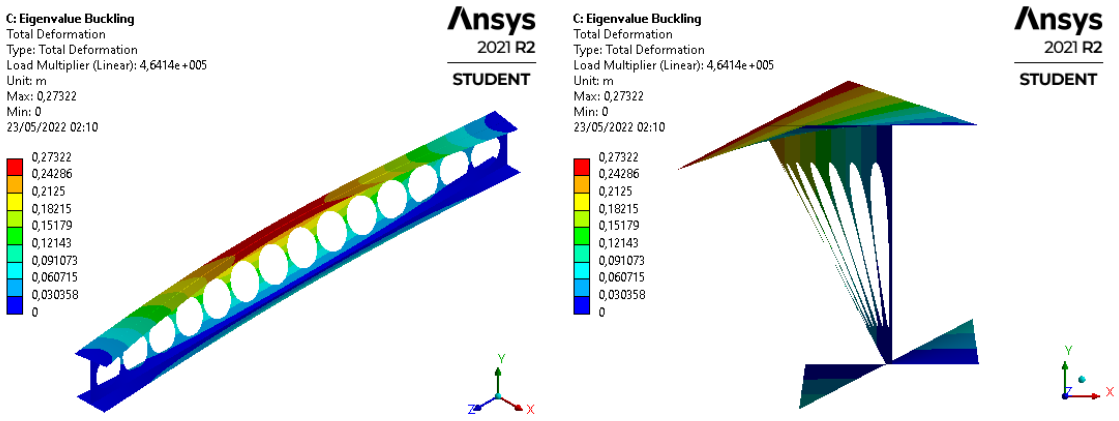

Figure 49. Lateral- torsional buckling of $S = 1.1a_0$ cellular beam case based on RM2 of L=3 [m].

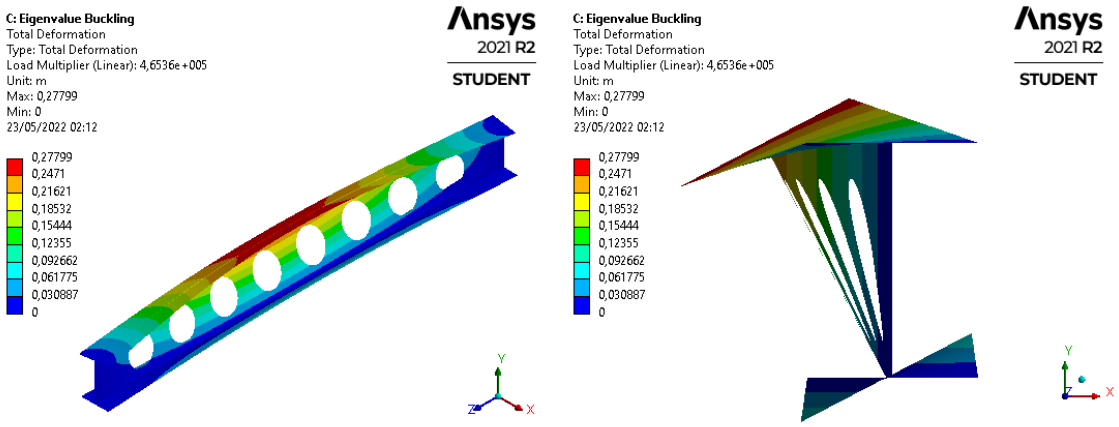

Figure 50. Lateral- torsional buckling of $S = 1.7a_0$ cellular beam case based on RM2 of L=3 [m].

Table 22. Relative difference of the critical moment between the numerical and the analytical analyzes, using the torsion constant $I_{t,avg3}$, for the $S = 1.1a_0$, $S = 1.7a_0$, and RM2 cellular beam cases.

L [m]	Relative difference [%]		
	APDL command		
	$I_{t,avg3}$		
	$S = 1.1a_0$	$S = 1.7a_0$	RM2
1	-9.24	-9.33	-11.59
1.5	-3.36	-3.16	-3.02
2	-1.09	-0.94	-0.87
2.5	-0.33	-0.19	-0.17
3	0.25	0.20	0.10
3.5	0.42	0.85	0.37
4	0.25	0.68	0.49
4.5	0.42	0.88	0.66
5	0.49	0.96	0.73
5.5	0.59	1.30	0.74
6	0.66	1.39	0.86
6.5	0.47	1.28	0.89
7	0.60	1.27	0.95
7.5	0.65	1.49	1.48
8	1.00	1.59	1.56
8.5	0.97	1.51	1.50
9	1.05	1.49	1.54
9.5	0.67	1.62	1.87
10	0.66	2.08	1.76

These relative differences also increase with increasing beam length and are less than 2 % in most cases. Which justifies the higher relative difference in the first length of the beam is the LTB was not the first mode for this length of these cases and the closest mode found has some local deformations in the web. Figure 51 shows the analytical

critical moment divided by the numerical critical moment in the function of the beam length.

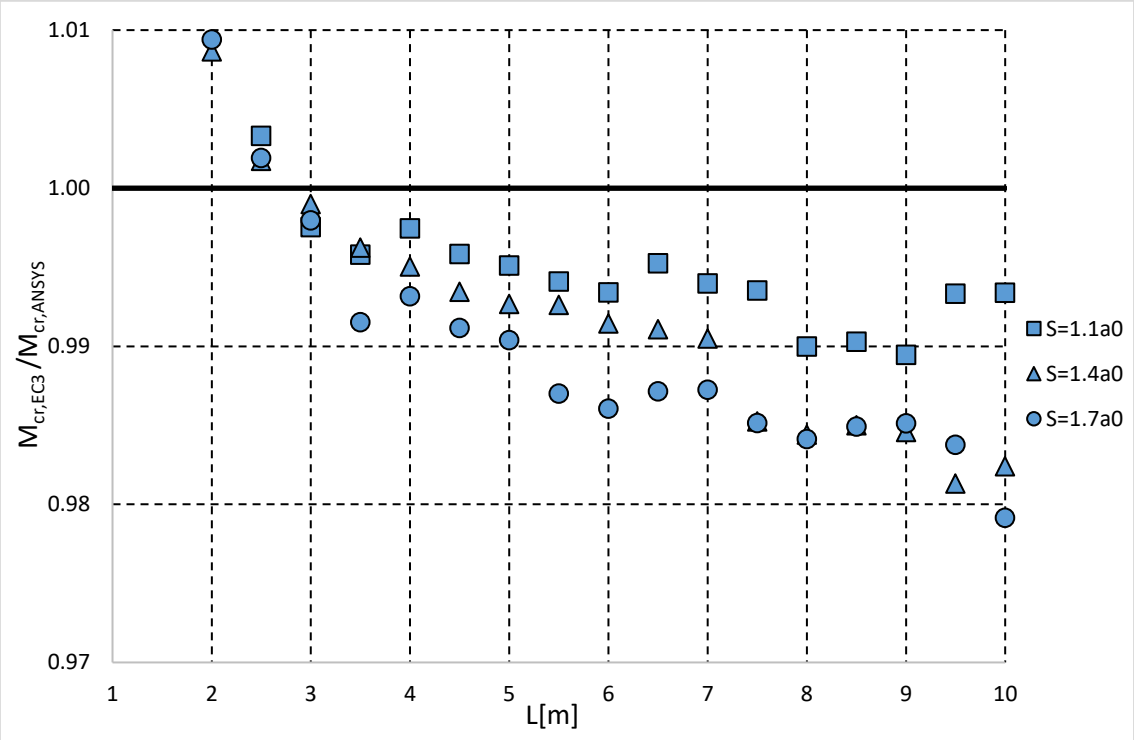

Figure 51. Analytical critical moment, using the torsion constant $I_{t,avg3}$, divided by the ANSYS critical moment of the $S = 1.1a_0$, $S = 1.7a_0$, and RM2 cellular beam cases.

The results of the first beam lengths do not appear in the range of the graph axis for better visualization of the relative difference between the variation of geometric parameters. Although the variation of the increase of the number of holes causes this illustrated behavior, which is not constant, overlaps some points of results, the larger the spacing between the holes, the higher the relative difference between the analytical and numerical methods in most length cases. The presented behavior is different in lengths from L=1.5[m] to L=3[m]: the larger the spacing between the holes, the smaller the relative difference.

5.4.5. Variation of the final height of the cellular beam

Finally, the final height H is the third geometric parameter evaluated. Table 23 shows the results of the critical moment for LTB of $H = 1.3$h and $H = 1.6$h cellular beam cases based on the RM1 and compares the Eurocode analytical method, using the torsion constant $I_{t,avg3}$, with the ANSYS numerical method.

Table 23. Comparison of critical moment between EC3 method, with the torsion constant $I_{t,avg3}$, and numerical analysis for the $H = 1.3$h, $H = 1.6$h, and RM1 cellular beam cases.

L [m]	M_{cr} [kN.m]					
	Analytical EC3			Numerical ANSYS		
	$I_{t,avg3}$			APDL command		
	$H = 1.3$h	$H = 1.6$h	RM1	$H = 1.3$h	$H = 1.6$h	RM1
1	385.09	471.34	442.50	385.15	470.70	442.11
1.5	179.26	216.64	204.10	180.55	218.32	205.64
2	107.14	127.49	120.64	108.15	128.82	121.85
2.5	73.26	85.85	81.60	74.00	86.92	82.55
3	54.58	63.04	60.17	55.15	63.94	60.95
3.5	43.09	49.11	47.06	43.55	49.90	47.73
4	35.44	39.92	38.40	35.83	40.63	38.99
4.5	30.13	33.58	32.40	30.49	34.19	32.92
5	26.13	28.87	27.94	26.44	29.44	28.41
5.5	23.07	25.30	24.54	23.34	25.82	24.97
6	20.66	22.50	21.87	20.90	22.99	22.27
6.5	18.75	20.31	19.78	18.98	20.75	20.14
7	17.13	18.47	18.02	17.35	18.89	18.36
7.5	15.78	16.94	16.55	15.98	17.34	16.87
8	14.63	15.65	15.31	14.81	16.03	15.61
8.5	13.64	14.55	14.24	13.81	14.91	14.53
9	12.80	13.62	13.34	12.97	13.95	13.61
9.5	12.04	12.78	12.53	12.20	13.10	12.79
10	11.37	12.04	11.82	11.52	12.35	12.06

The results show that the critical moment decreases with the length increase of the beam and the analytical critical moment is greater than the numerical just in the case of L=1[m]. Figure 52 and Figure 53 illustrate the LTB of $H = 1.3$h and $H = 1.3$h cellular beam cases based on the RM1 of length L=3 [m]. Annexes F and G present the LTB of all lengths of RM1 and RM2 cases.

Table 24 shows the relative difference of the critical moment between the numerical and the analytical analyzes, using the torsion constant $I_{t,avg3}$, for the $H = 1.3$h and $H = 1.6$h cellular beam cases based on the RM1.

These relative differences increase with increasing beam length and are less than 2.5% in all cases. Figure 54 shows the analytical critical moment divided by the numerical critical moment in the function of the beam length.

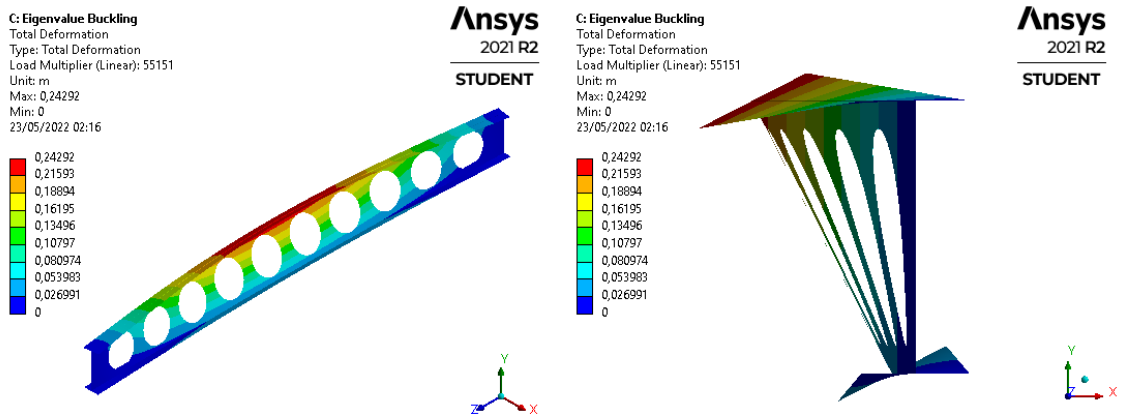

Figure 52. Lateral-torsional buckling of $H = 1.3$h cellular beam case based on RM1 of L=3 [m].

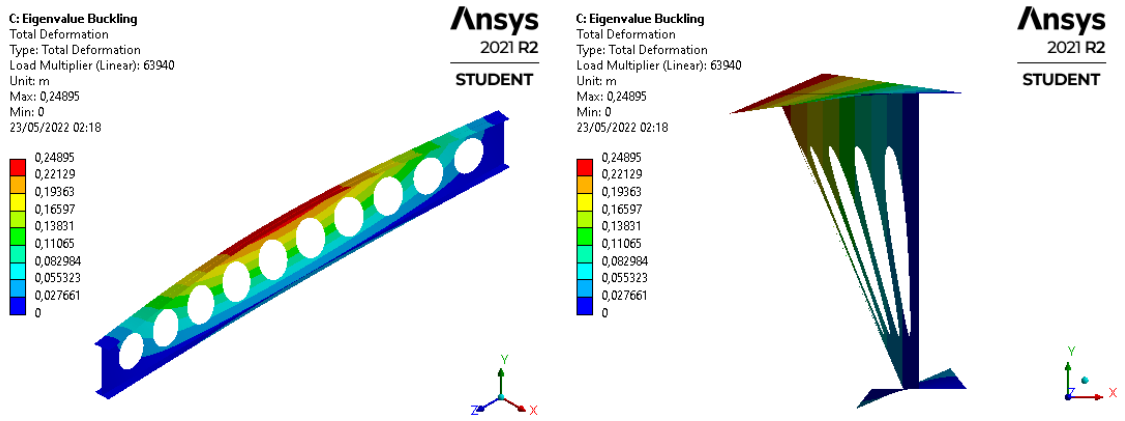

Figure 53. Lateral-torsional buckling of $H = 1.6$h cellular beam case based on RM1 of L=3 [m].

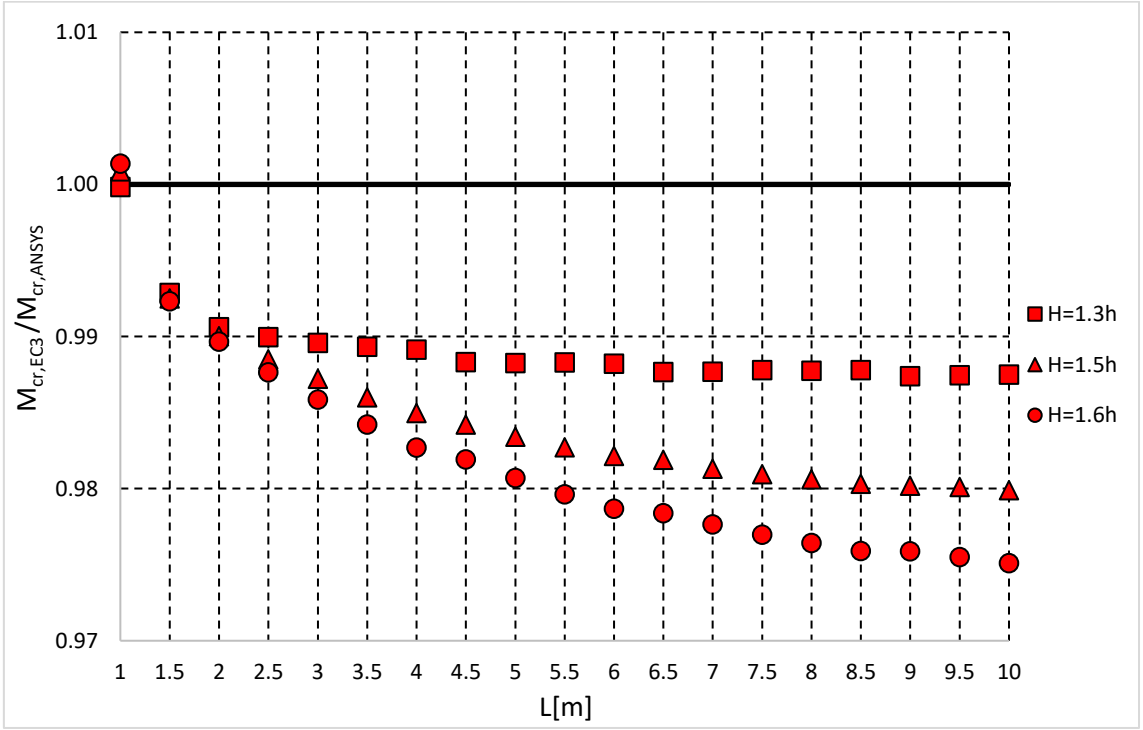

Figure 54. Analytical critical moment, using the torsion constant $I_{t,avg3}$, divided by the ANSYS critical moment of the $H = 1.3$h, $H = 1.3$h, and RM1 cellular beam cases.

Table 24. Relative difference of the critical moment between the numerical and the analytical analyzes, using the torsion constant $I_{t,avg3}$, for the $H = 1.3$h, $H = 1.6$h, and RM1 cellular beam cases.

L [m]	Relative difference [%]		
	APDL command		
	$I_{t,avg3}$		
	$H = 1.3$h	$H = 1.6$h	RM1
1	0.02	-0.14	-0.09
1.5	0.71	0.77	0.75
2	0.94	1.03	1.00
2.5	1.00	1.23	1.15
3	1.04	1.41	1.28
3.5	1.07	1.58	1.40
4	1.09	1.73	1.50
4.5	1.17	1.81	1.58
5	1.17	1.93	1.66
5.5	1.17	2.04	1.73
6	1.18	2.13	1.79
6.5	1.23	2.16	1.81
7	1.23	2.24	1.87
7.5	1.22	2.30	1.91
8	1.22	2.36	1.94
8.5	1.22	2.41	1.97
9	1.26	2.41	1.98
9.5	1.25	2.45	1.99
10	1.25	2.49	2.01

Note that greater the height of the cellular beam, the higher the relative difference between the analytical and numerical methods.

Table 25 shows the results of the critical moment for LTB of $H = 1.3$h and $H = 1.6$h cellular beam cases based on the RM2 and compares the Eurocode analytical method, using the torsion constant $I_{t,avg3}$, with the ANSYS numerical method.

The results also show that the critical moment decreases with the length increase of the beam and the analytical critical moment is greater than the numerical just in the four-first beam lengths of these cases. Figure 55 and Figure 56 illustrate the LTB of $H = 1.3$h and $H = 1.6$h cellular beam cases based on the RM2 of length L=3 [m]. Annexes F and G present the LTB of all lengths of RM1 and RM2 cases.

Table 25. Comparison of critical moment between EC3 method, with the torsion constant $I_{t,avg3}$, and numerical analysis for the $H = 1.3$h, $H = 1.6$h, and RM2 cellular beam cases.

L [m]	M_{cr} [kN.m]					
	Analytical EC3			Numerical ANSYS		
	$I_{t,avg3}$			APDL command		
	$H = 1.3$h	$H = 1.6$h	RM2	$H = 1.3$h	$H = 1.6$h	RM2
1	3324.57	4104.37	3844.06	3007.89	3653.66	3444.69
1.5	1504.33	1846.67	1732.21	1462.61	1791.31	1681.39
2	866.78	1056.20	992.73	860.41	1046.70	984.19
2.5	571.22	690.04	650.13	570.84	688.65	649.00
3	410.49	491.09	463.94	411.11	491.50	464.41
3.5	312.95	370.70	351.20	314.29	372.06	352.52
4	249.26	292.31	277.73	250.58	293.75	279.11
4.5	205.25	238.34	227.10	206.66	239.91	228.60
5	173.46	199.51	190.65	174.74	201.00	192.05
5.5	149.66	170.59	163.45	150.75	171.91	164.67
6	131.31	148.42	142.57	132.42	149.75	143.80
6.5	116.81	131.00	126.14	117.82	132.23	127.27
7	105.12	117.03	112.94	106.07	118.20	114.02
7.5	95.58	105.69	102.22	97.04	107.31	103.75
8	87.56	96.23	93.25	88.96	97.79	94.72
8.5	80.77	88.28	85.70	81.97	89.66	87.00
9	74.97	81.52	79.26	76.12	82.84	80.50
9.5	69.95	75.71	73.72	71.27	77.19	75.12
10	65.56	70.66	68.91	66.71	71.98	70.14

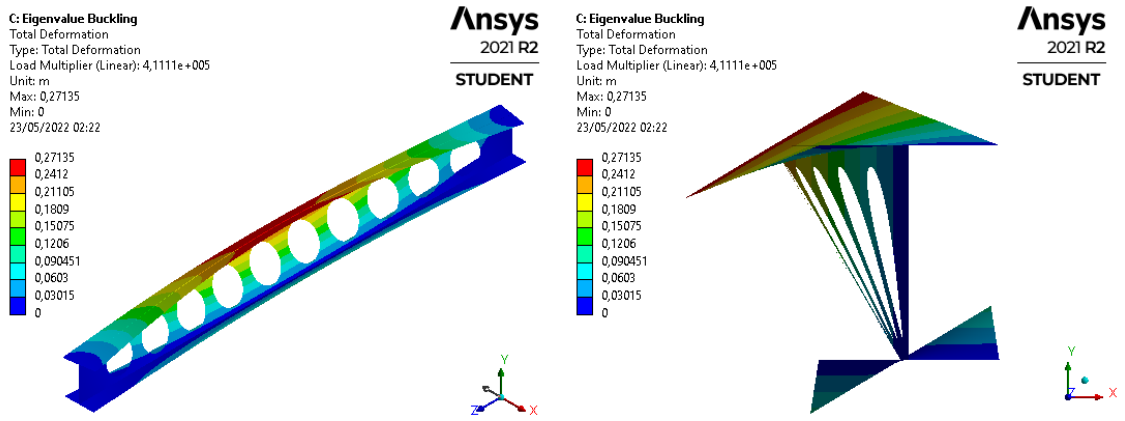

Figure 55. Lateral- torsional buckling of $H = 1.3$h cellular beam case based on RM2 of L=3 [m].

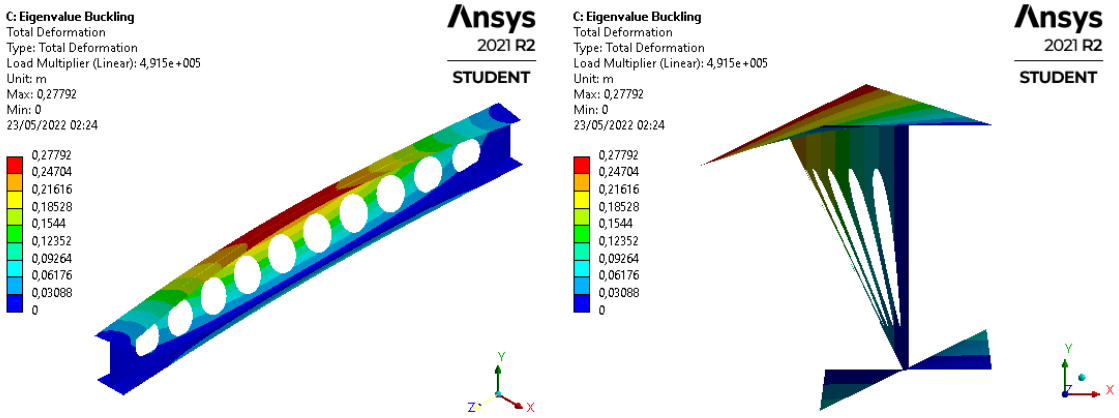

Figure 56. Lateral- torsional buckling of $H = 1.6$h cellular beam case based on RM2 of L=3 [m].

Table 26 shows the relative difference of the critical moment between the numerical and the analytical analyzes, using the torsion constant $I_{t,avg3}$, for the $H = 1.3$h and $H = 1.6$h cellular beam cases based on the RM2.

Table 26. Relative difference of the critical moment between the numerical and the analytical analyzes, using the torsion constant $I_{t,avg3}$, for the $H = 1.3$h, $H = 1.6$h, and RM2 cellular beam cases.

L [m]	Relative difference [%]		
	APDL command		
	$I_{t,avg3}$		
	$H = 1.3$h	$H = 1.6$h	RM2
1	-10.53	-12.34	-11.59
1.5	-2.85	-3.09	-3.02
2	-0.74	-0.91	-0.87
2.5	-0.07	-0.20	-0.17
3	0.15	0.08	0.10
3.5	0.43	0.37	0.37
4	0.52	0.49	0.49
4.5	0.68	0.65	0.66
5	0.73	0.74	0.73
5.5	0.73	0.77	0.74
6	0.83	0.89	0.86
6.5	0.85	0.94	0.89
7	0.90	0.99	0.95
7.5	1.51	1.51	1.48
8	1.58	1.60	1.56
8.5	1.46	1.54	1.50
9	1.52	1.60	1.54
9.5	1.86	1.92	1.87
10	1.71	1.83	1.76

These relative differences also increase with increasing beam length and are less than 2 % in most cases. Which justifies the higher relative difference in the first length of the beam is the LTB was not the first mode for this length of these cases and the closest mode found has some local deformations in the web. Figure 57 shows the analytical critical moment divided by the numerical critical moment in the function of the beam length.

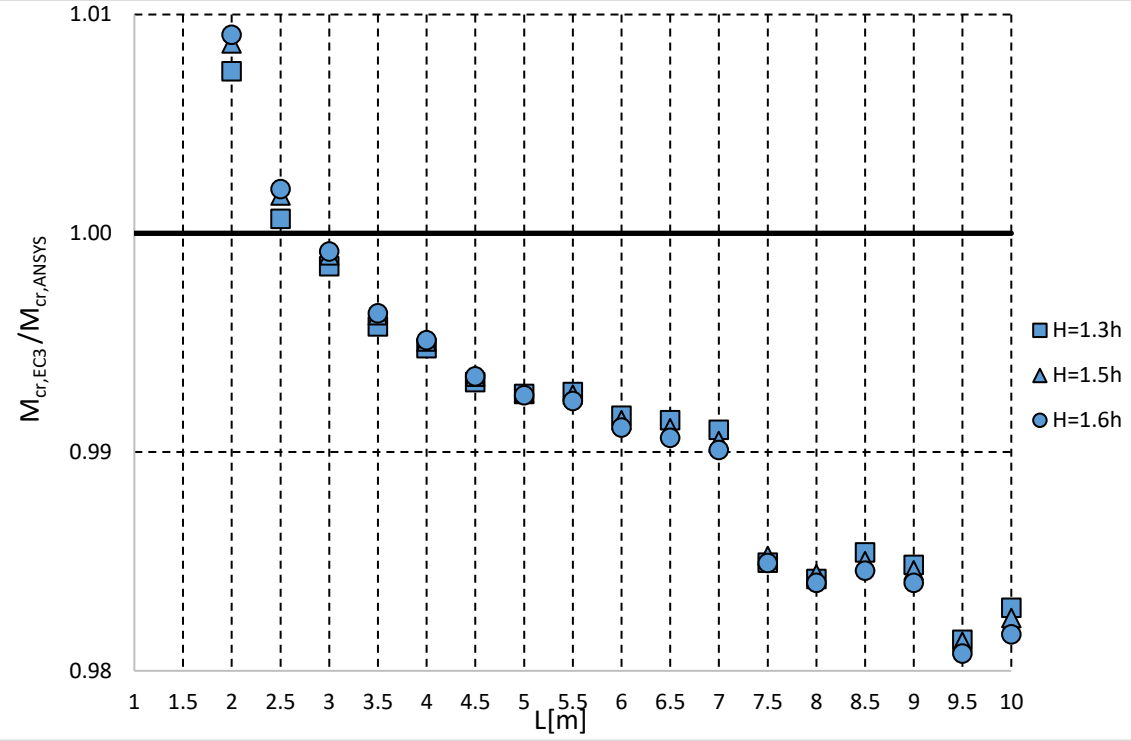

Figure 57. Analytical critical moment, using the torsion constant $I_{t,avg3}$, divided by the ANSYS critical moment of the $H = 1.3$h, $H = 1.3$h, and RM2 cellular beam cases.

The results of the first beam lengths do not appear in the range of the graph axis for better visualization of the relative difference between the variation of geometric parameters. In lengths from L=3[m] to L=4.5[m], the bigger the height, the smaller the relative difference. In the other length cases of the cellular beam, the presented behavior is the opposite: the bigger the height, the higher the relative difference. Note that the variation of the increase in the number of holes causes this illustrated behavior, which is not constant, to overlap some result points.

Annex E presents the graphs with the analytical critical moment divided by the numerical critical moment in the function of the beam length, considering the other three constants of torsion $I_{t,2T}$, $I_{t,avg1}$ and $I_{t,avg2}$.

5.4.6. Non-uniform angle of torsion of solid beam cases

The non-uniform angle of the numerical model (Equation 37) was calculated from the directional deformation (D_d) at a distance z along the length of the beam.

$$\phi = \text{asin}\left[D_d / \left(\left(H - t_f\right)/2\right)\right] \times 180/\pi \tag{37}$$

The solid beam cases are compared between the SCI P385 guide analytical method and the ANSYS numerical method. Table 27 shows the results of the non-uniform angle of torsion along the distance z[m] of the length L=10[m]. Annex C presents the tables with the non-uniform angle of torsion of the other two study cases with L=5[m] and L=1[m].

Table 27. Comparison between the non-uniform angle of torsion of the analytical and numerical methods for the solid beam cases RM1 and RM2 with L=10 [m].

z [m]	Φ [º] solid cases			
	Analytical SCI		Numerical ANSYS	
	RM1	RM2	RM1	RM2
1	0.59	0.14	0.59	0.14
1.5	1.12	0.28	1.14	0.28
2	1.73	0.45	1.76	0.46
2.5	2.37	0.64	2.41	0.65
3	3.04	0.85	3.09	0.86
3.5	3.71	1.06	3.78	1.08
4	4.39	1.29	4.47	1.30
4.5	5.07	1.51	5.17	1.53
5	5.76	1.75	5.87	1.77
5.5	6.44	1.98	6.57	2.00
6	7.13	2.21	7.27	2.24
6.5	7.82	2.45	7.98	2.48
7	8.50	2.68	8.68	2.72
7.5	9.19	2.92	9.39	2.97
8	9.88	3.16	10.10	3.21
8.5	10.56	3.40	10.82	3.46
9	11.25	3.63	11.54	3.71
9.5	11.94	3.87	12.26	3.96
10	12.62	4.11	13.00	4.22

The results between the methods are closest and show that the angle increases with the length increase of the beam. Figure 58 and Figure 59 illustrate the non-uniform torsion of RM1 and RM2 solid beam cases of length L=1 [m]. Annexes H and I present the numerical mode of the non-uniform torsion of the other two lengths of study cases.

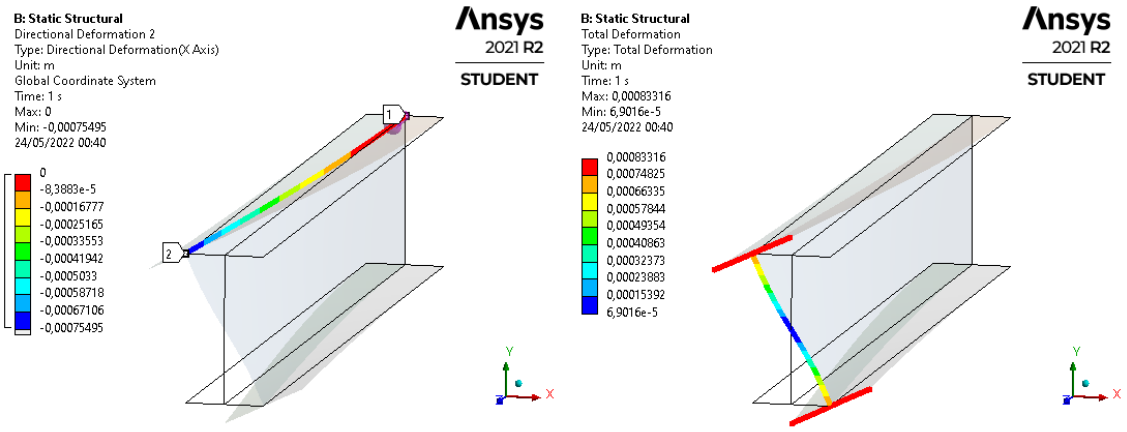

Figure 58. Non-uniform torsion of RM1 solid beam case of L=1 [m].

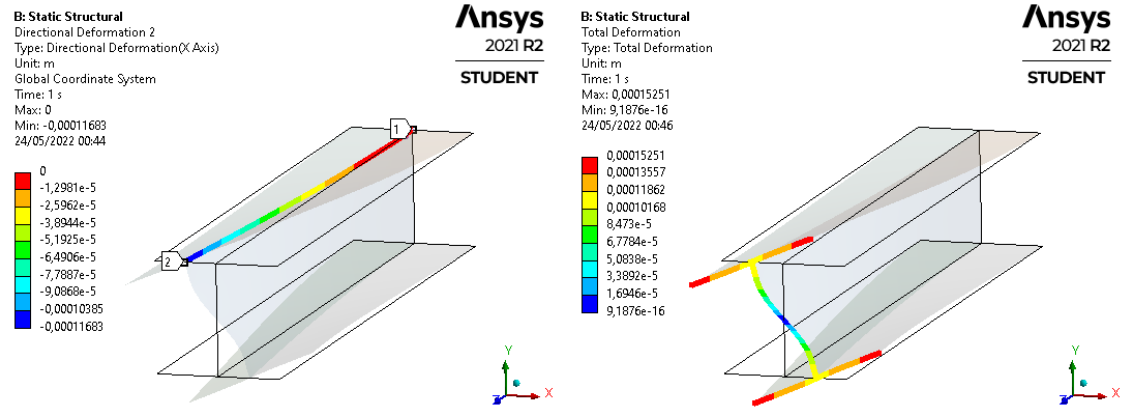

Figure 59. Non-uniform torsion of RM2 solid beam case of L=1 [m].

The relative differences between the analytical and numerical methods are shown in Table 28 and are less than 3 % in most cases, except for the case with L=1[m]. This great relative difference occurs in the first distances z of the length L=1[m] because the angle of torsion is zero at the end of the beam with the torsional and warping restraint. So, at the beginning of this length, the variation of the torsional angle between the numerical and analytical methods is higher than at the end of the length.

Figures 59 to 61 illustrate the analytical divided by the numerical value of the non-uniform angle of torsion in the function of the distance along the beam of RM1 and RM2 study cases.

Table 28. Relative difference between the non-uniform angle of torsion of the analytical and numerical methods for the solid beam cases RM1 and RM2.

Relative difference [%]								
L=10 [m]			L=5 [m]			L=1 [m]		
z [m]	RM1	RM2	z [m]	RM1	RM2	z [m]	RM1	RM2
1	-1.62	-1.67	1	-1.65	-2.19	0.1	-4.95	-14.25
1.5	-1.64	-1.47	1.5	-1.68	-2.09	0.2	-4.07	-11.12
2	-1.66	-1.39	2	-1.72	-2.12	0.3	-3.68	-9.22
2.5	-1.69	-1.35	2.5	-1.77	-2.23	0.4	-3.53	-8.19
3	-1.73	-1.32	3	-1.85	-2.41	0.5	-3.49	-7.60
3.5	-1.76	-1.31	3.5	-1.95	-2.67	0.6	-3.52	-7.26
4	-1.80	-1.32	4	-2.11	-3.01	0.7	-3.57	-7.07
4.5	-1.84	-1.32	4.5	-2.34	-3.47	0.8	-3.65	-6.98
5	-1.89	-1.34	5	-2.66	-4.04	0.9	-3.73	-6.95
5.5	-1.94	-1.36				1	-3.72	-7.01
6	-2.00	-1.40						
6.5	-2.06	-1.44						
7	-2.13	-1.50						
7.5	-2.21	-1.58						
8	-2.30	-1.69						
8.5	-2.41	-1.83						
9	-2.54	-2.02						
9.5	-2.73	-2.29						
10	-2.97	-2.62						

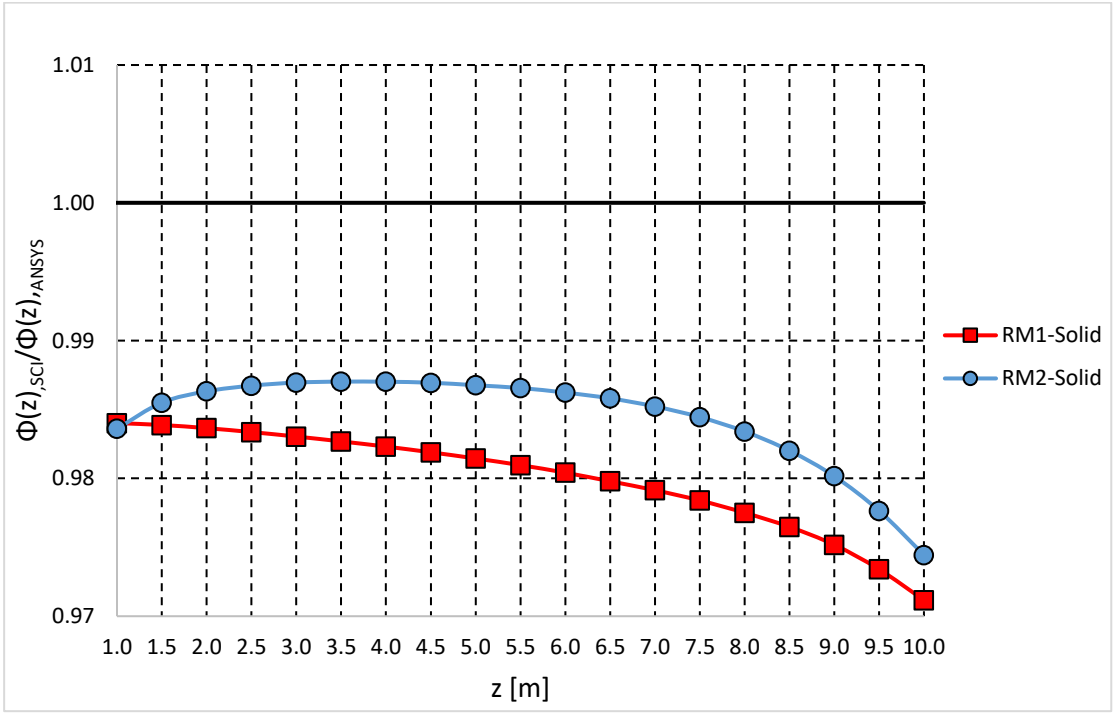

Figure 60. Analytical angle of torsion $\Phi(z)_{,SCI}$ divided by the ANSYS angle of torsion $\Phi(z)_{,ANSYS}$ of solid beam study cases with L=10[m].

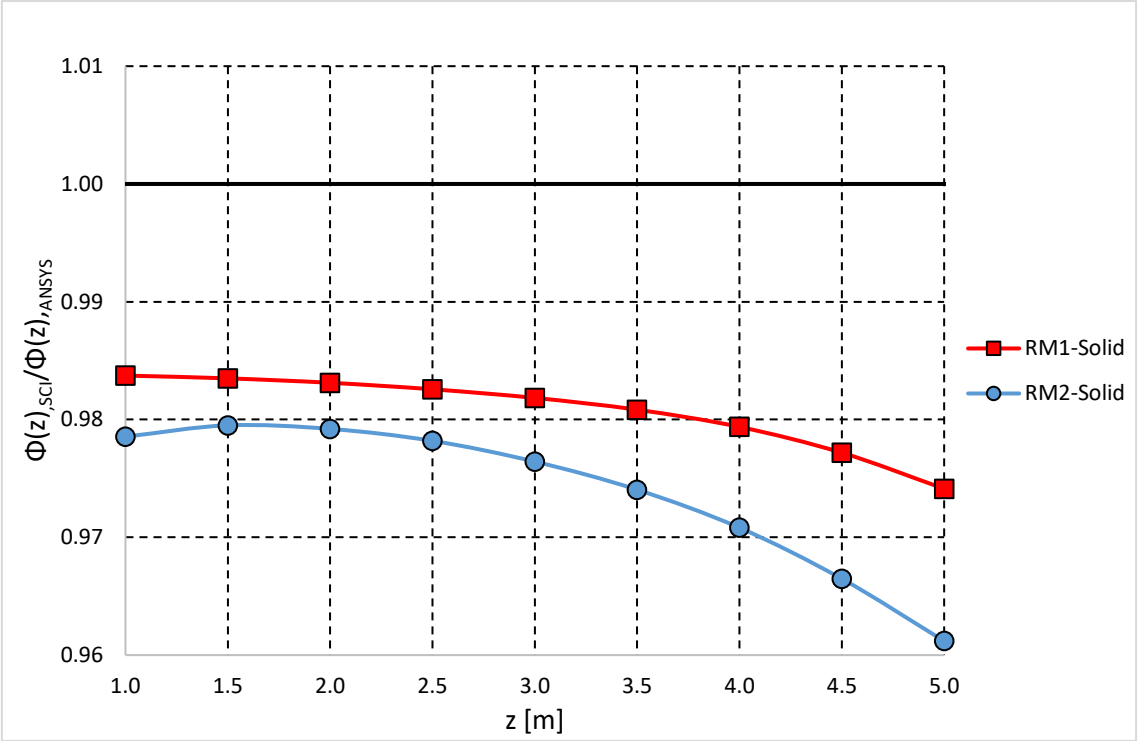

Figure 61. Analytical angle of torsion $\Phi(z)_{,SCI}$ divided by the ANSYS angle of torsion $\Phi(z)_{,ANSYS}$ of solid beam study cases with L=5[m].

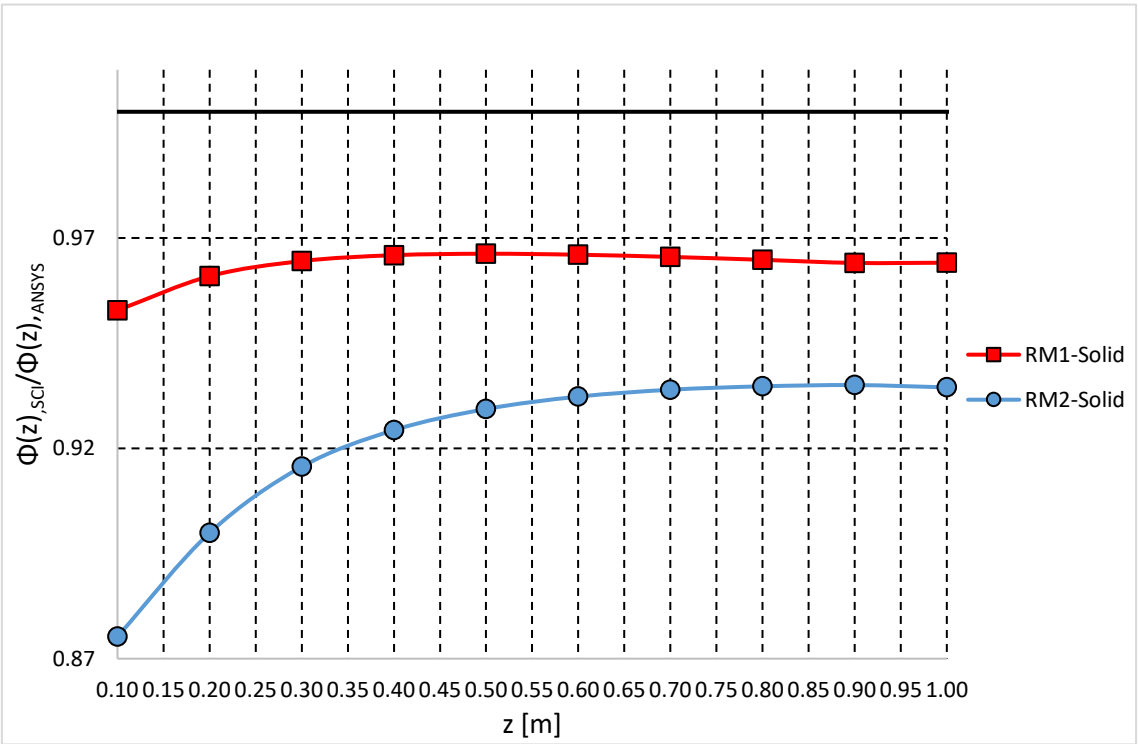

Figure 62. Analytical angle of torsion $\Phi(z)_{,SCI}$ divided by the ANSYS angle of torsion $\Phi(z)_{,ANSYS}$ of solid beam study cases with L=1[m].

Figure 61 shows that, only in the study case of L=10[m], the RM2 have a smaller relative difference than the RM1. In all cases, the results of the analytical method are smaller than the numerical, falling below the reference value line 1. Furthermore, the relative difference of the angle of torsion increases along the distance z of the beam, except for the case of L=1 [m]. The results for the L=1[m] in Figure 62, confirm the behavior of the angle of torsion at the beginning of the beam.

5.4.7. Non-uniform angle of torsion of cellular beam cases

The cellular beam cases are compared between the SCI P385 guide analytical method and the ANSYS numerical method, varying the torsion constant. Table 29 and Table 30 show the results of the non-uniform angle of torsion along the distance z[m] of the length L=10[m] of RM1 and RM2 study cases. Annex C presents the tables with the non-uniform angle of torsion of the other two study cases with L=5[m] and L=1[m].

Table 29. Comparison between the non-uniform angle of torsion of the analytical and numerical methods for the cellular beam case RM1 with L=10 [m].

z [m]	Φ [º] RM1 cellular case L=10 [m]			
	Analytical SCI			Numerical ANSYS
	$I_{t,avg1}$	$I_{t,avg2}$	$I_{t,avg3}$	
1	0.45	0.44	0.44	0.45
1.5	0.90	0.89	0.88	0.90
2	1.44	1.42	1.40	1.44
2.5	2.03	2.01	1.98	2.04
3	2.67	2.64	2.60	2.68
3.5	3.34	3.29	3.24	3.34
4	4.02	3.96	3.90	4.03
4.5	4.71	4.65	4.58	4.73
5	5.41	5.34	5.26	5.43
5.5	6.12	6.04	5.94	6.14
6	6.83	6.74	6.63	6.86
6.5	7.55	7.44	7.32	7.58
7	8.26	8.14	8.01	8.30
7.5	8.98	8.85	8.70	9.03
8	9.70	9.56	9.40	9.76
8.5	10.42	10.26	10.09	10.49
9	11.14	10.97	10.78	11.22
9.5	11.85	11.68	11.48	11.96
10	12.57	12.38	12.17	12.70

Table 30. Comparison between the non-uniform angle of torsion of the analytical and numerical methods for the cellular beam case RM2 with L=10 [m].

z [m]	Φ [º] RM2 cellular case L=10 [m]			
	Analytical SCI			Numerical ANSYS
	$I_{t,avg1}$	$I_{t,avg2}$	$I_{t,avg3}$	
1	0.10	0.10	0.10	0.10
1.5	0.21	0.21	0.21	0.21
2	0.34	0.34	0.34	0.35
2.5	0.50	0.50	0.50	0.51
3	0.68	0.68	0.67	0.69
3.5	0.87	0.87	0.86	0.88
4	1.07	1.07	1.06	1.08
4.5	1.28	1.28	1.27	1.30
5	1.50	1.49	1.48	1.52
5.5	1.73	1.72	1.70	1.75
6	1.95	1.94	1.92	1.97
6.5	2.18	2.17	2.15	2.21
7	2.42	2.40	2.38	2.45
7.5	2.65	2.64	2.62	2.69
8	2.89	2.87	2.85	2.94
8.5	3.13	3.11	3.08	3.18
9	3.37	3.34	3.32	3.43
9.5	3.61	3.58	3.55	3.68
10	3.84	3.82	3.78	3.93

The results between the methods are closest and show that the angle increases with the length increase of the beam. Figure 63 and Figure 64 illustrate the non-uniform torsion of RM1 and RM2 cellular beam cases of length L=1 [m]. Annexes H and I present the numerical mode of the non-uniform torsion of the other two lengths of study cases.

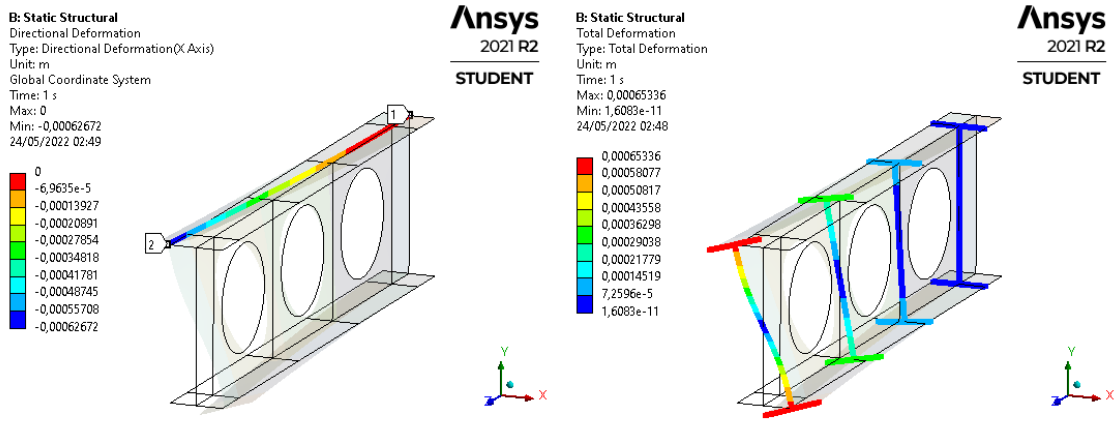

Figure 63. Non-uniform torsion of RM1 cellular beam case of L=1 [m].

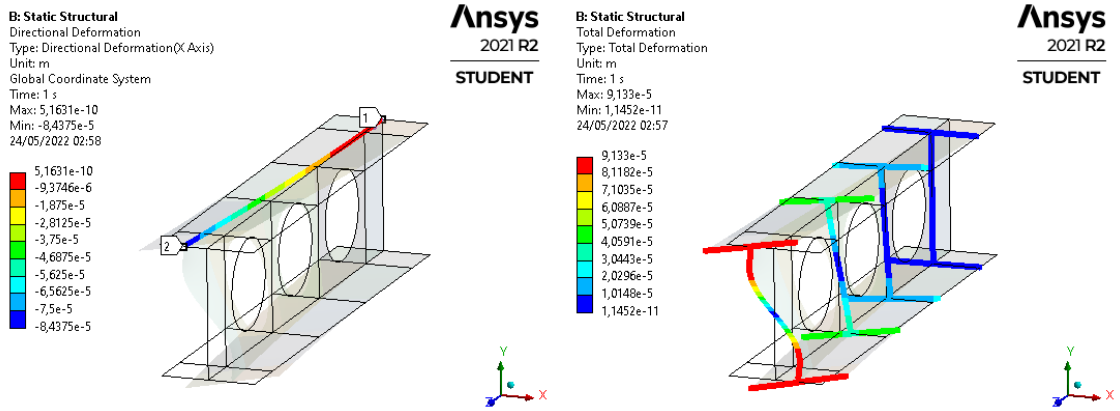

Figure 64. Non-uniform torsion of RM2 cellular beam case of L=1 [m].

The relative difference between the analytical and numerical methods of L=10[m] and L=5[m] is shown in Table 31 and Table 32.

Table 31. Relative difference between the non-uniform angle of torsion of the analytical and numerical methods for the cellular beam cases RM1 and RM2 with L=10[m].

z [m]	Relative difference [%] L=10 [m]					
	RM1			RM2		
	$I_{t,avg1}$	$I_{t,avg2}$	$I_{t,avg3}$	$I_{t,avg1}$	$I_{t,avg2}$	$I_{t,avg3}$
1	0.28	1.28	2.41	0.90	1.37	1.91
1.5	0.31	1.40	2.61	0.89	1.39	1.96
2	0.31	1.46	2.74	0.89	1.41	2.01
2.5	0.30	1.51	2.85	0.89	1.43	2.05
3	0.29	1.54	2.94	0.91	1.47	2.11
3.5	0.28	1.58	3.02	0.92	1.51	2.17
4	0.28	1.61	3.09	0.94	1.54	2.22
4.5	0.30	1.66	3.17	0.96	1.58	2.28
5	0.31	1.69	3.23	1.00	1.63	2.34
5.5	0.34	1.74	3.31	1.04	1.68	2.41
6	0.37	1.80	3.38	1.09	1.75	2.49
6.5	0.41	1.85	3.45	1.16	1.82	2.57
7	0.47	1.92	3.54	1.24	1.92	2.68
7.5	0.53	2.00	3.62	1.34	2.03	2.79
8	0.60	2.08	3.72	1.47	2.16	2.93
8.5	0.69	2.17	3.82	1.62	2.31	3.09
9	0.79	2.28	3.94	1.79	2.49	3.28
9.5	0.91	2.41	4.07	2.01	2.71	3.50
10	1.03	2.53	4.20	2.24	2.94	3.74

Table 32. Relative difference between the non-uniform angle of torsion of the analytical and numerical methods for the cellular beam cases RM1 and RM2 with L=5[m].

z [m]	Relative difference [%] L=5 [m]					
	RM1			RM2		
	$I_{t,avg1}$	$I_{t,avg2}$	$I_{t,avg3}$	$I_{t,avg1}$	$I_{t,avg2}$	$I_{t,avg3}$
1	0.62	1.58	2.66	2.07	2.49	2.96
1.5	0.69	1.73	2.89	2.16	2.60	3.09
2	0.73	1.83	3.05	2.29	2.75	3.27
2.5	0.75	1.90	3.19	2.44	2.92	3.46
3	0.78	1.98	3.31	2.63	3.12	3.67
3.5	0.82	2.05	3.43	2.85	3.35	3.92
4	0.88	2.14	3.55	3.11	3.62	4.20
4.5	0.96	2.25	3.68	3.41	3.93	4.52
5	1.02	2.32	3.78	3.72	4.24	4.84

In all these cases of L=10[m] and L=5[m], the relative differences are less than 5%. However, the results were not expected, because the torsion constant $I_{t,avg3}$ has a greater relative difference than the other two constants

Table 33 shows the relative difference between the analytical and numerical methods with L=1[m] The relative differences are less than 4% in this RM1 case, but the RM2 has a greater relative difference in torsion angle than RM1. Moreover, the torsion constant $I_{t,avg3}$ also has a greater relative difference than the other two constants.

Table 33. Relative difference between the non-uniform angle of torsion of the analytical and numerical methods for the cellular beam cases RM1 and RM2 with L=1[m].

z [m]	Relative difference [%] L=1 [m]					
	RM1			RM2		
	$I_{t,avg1}$	$I_{t,avg2}$	$I_{t,avg3}$	$I_{t,avg1}$	$I_{t,avg2}$	$I_{t,avg3}$
0.1	3.42	3.65	3.91	11.82	11.86	11.91
0.2	2.95	3.19	3.46	9.58	9.62	9.67
0.3	2.72	2.97	3.25	8.09	8.14	8.19
0.4	2.61	2.86	3.15	7.22	7.27	7.32
0.5	2.57	2.83	3.12	6.66	6.71	6.76
0.6	2.56	2.82	3.12	6.34	6.39	6.45
0.7	2.56	2.82	3.13	6.13	6.18	6.24
0.8	2.56	2.83	3.14	5.99	6.05	6.10
0.9	2.54	2.81	3.12	5.89	5.94	6.00
1	2.44	2.72	3.03	5.86	5.91	5.97

As in all cases of solid beams, the angle of torsion of the analytical method presented values smaller than the angle of torsion of the numerical method (values below

the reference value line 1), the results of the next graphs will be normalized by the division of the angle of torsion of the solid beam, allowing a better comparison between the constant of torsion.

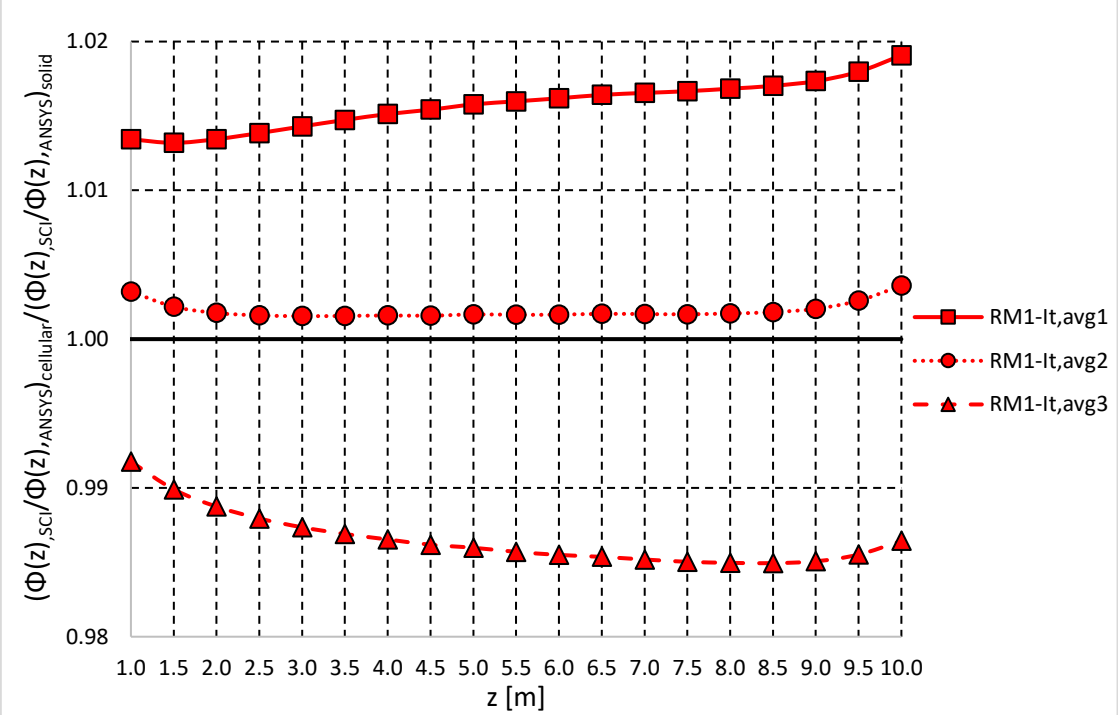

Figure 65. Analytical angle of torsion $\Phi(z)_{,SCI}$ divided by the ANSYS angle of torsion $\Phi(z)_{,ANSYS}$ of cellular RM1 study case with L=10[m], normalized by the values of the same case of solid beam

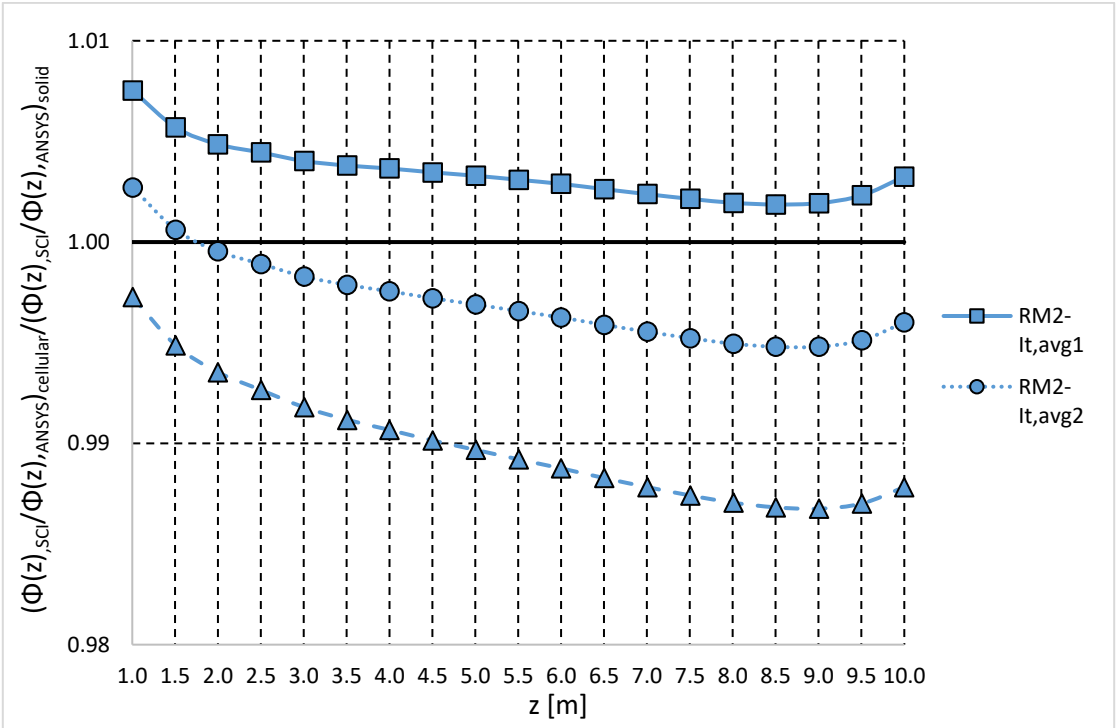

Figure 66. Analytical angle of torsion $\Phi(z)_{,SCI}$ divided by the ANSYS angle of torsion $\Phi(z)_{,ANSYS}$ of cellular RM2 study case with L=10[m], normalized by the values of the same case of solid beam

Figure 65 and Figure 66 illustrate the graph of the non-uniform analytical angle of torsion divided by the numerical as a function of the distance along the beam of the cellular beam case studies RM1 and RM2 with L=10[m], normalized by the same division between the methods for the solid beam cases.

In both cases of RM1 and RM2 with L=10[m], the constant $I_{t,avg3}$ did not present good results, which remain below the reference value line 1. In the case of RM1, constant $I_{t,avg2}$ presented the best results and in the case of RM2, the constant$I_{t,avg1}$ had a better performance, getting closer to the reference value line 1.

Figure 67 Figure 68 illustrate the graph of the non-uniform analytical angle of torsion divided by the numerical as a function of the distance along the beam of the cellular beam case studies RM1 and RM2 with L=5[m], normalized by the same division between the methods for the solid beam cases.

The cases of RM1 and RM2 with L=5[m] presented a behavior similar to the cases with L=10[m] and the results of the constant $I_{t,avg3}$ remained below the reference value line 1.

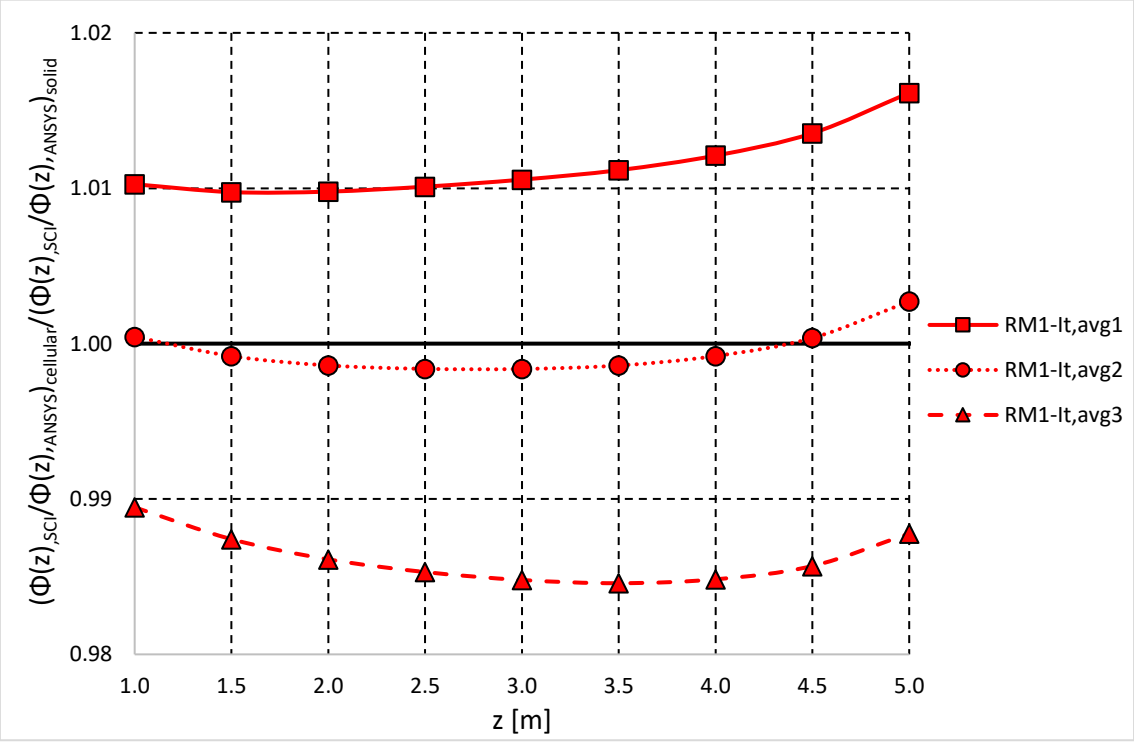

Figure 67. Analytical angle of torsion $\Phi(z)_{,SCI}$ divided by the ANSYS angle of torsion $\Phi(z)_{,ANSYS}$ of cellular RM1 study case with L=5[m], normalized by the values of the same case of solid beam

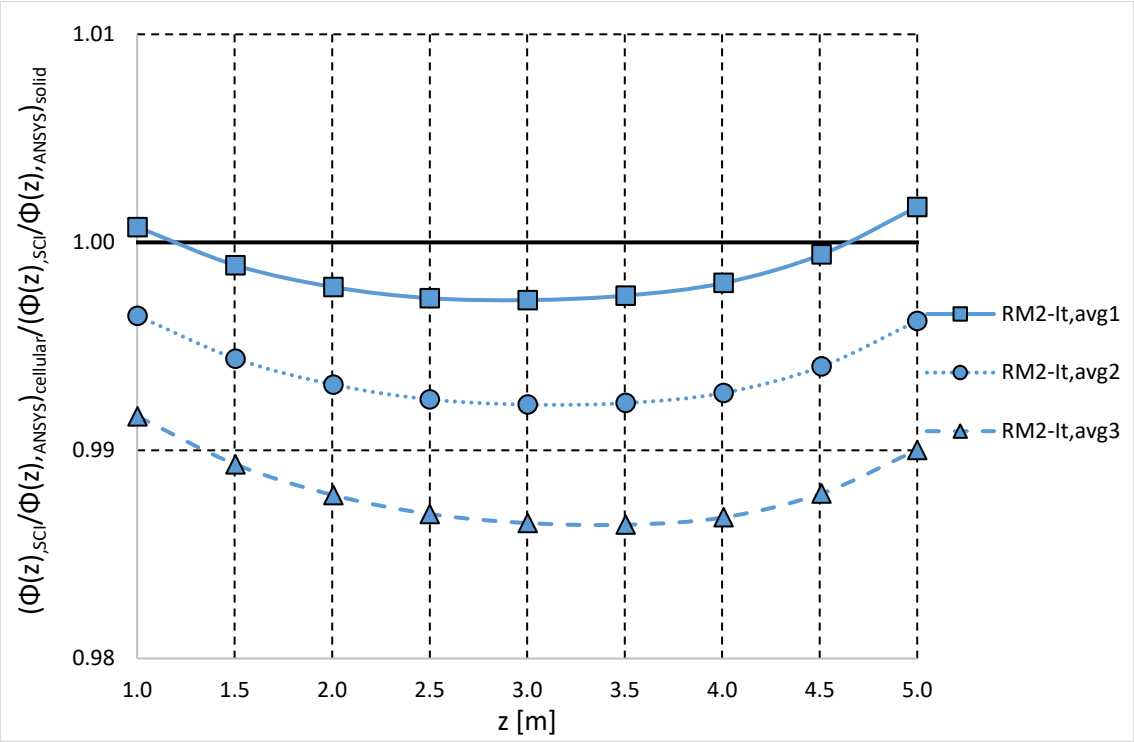

Figure 68. Analytical angle of torsion $\Phi(z)_{,SCI}$ divided by the ANSYS angle of torsion $\Phi(z)_{,ANSYS}$ of cellular RM2 study case with L=5[m], normalized by the values of the same case of solid beam

Finally, Figure 69 and Figure 70 illustrate the graph of the non-uniform analytical angle of torsion divided by the numerical as a function of the distance along the beam of the cellular beam case studies RM1 and RM2 with L=1[m], normalized by the same division between the methods for the solid beam cases.

In the cases of RM1 and RM2 with L=1[m], the results of all constants are illustrated above the reference value line 1, with the constant $I_{t,avg3}$ being the closest. Even though the beam of L=1[m] presented good results for the constant $I_{t,avg3}$, the same behavior was expected in all beam lengths analyzed.

Note carefully that even for solid beams, the values of the torsion angle of the analytical method are smaller than the numerical one, so this behavior tends to be maintained in cellular beams. It is not possible to say why the constant $I_{t,avg3}$ only brought good results for the case of L=1[m]. More studies with other beam lengths and variations of geometric parameters should be analyzed for a better understanding.

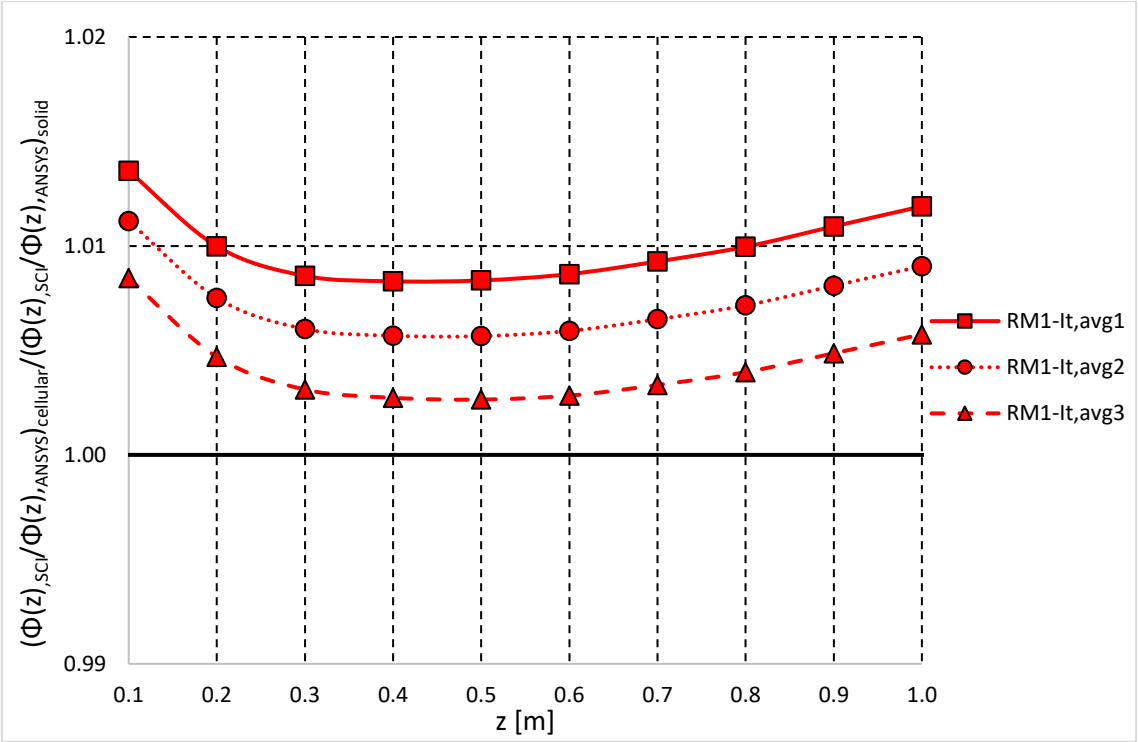

Figure 69. Analytical angle of torsion $\Phi(z)_{,SCI}$ divided by the ANSYS angle of torsion $\Phi(z)_{,ANSYS}$ of cellular RM1 study case with L=1[m], normalized by the values of the same case of solid beam

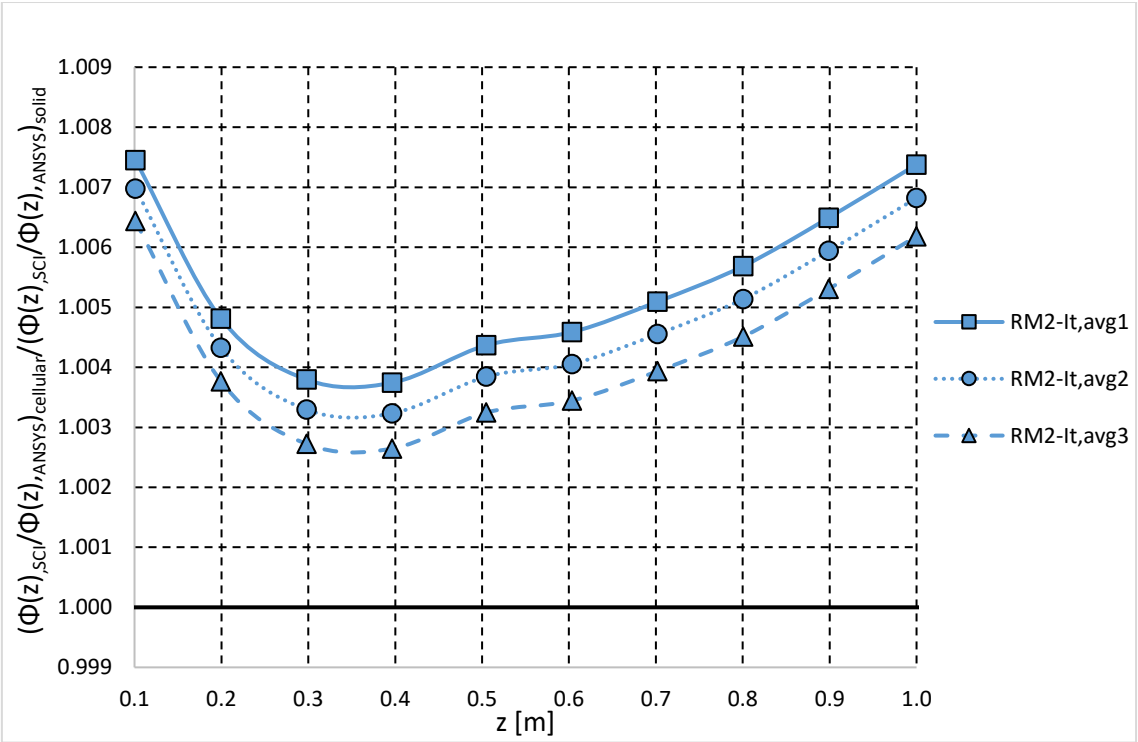

Figure 70. Analytical angle of torsion $\Phi(z)_{,SCI}$ divided by the ANSYS angle of torsion $\Phi(z)_{,ANSYS}$ of cellular RM2 study case with L=1[m], normalized by the values of the same case of solid beam

6. CONCLUSIONS

6.1. Main conclusions

A numerical analysis of solid and cellular beams using the ANSYS software was carried out in the development of this study and its results were compared with the results obtained through the simplified methods of Eurocode 3 part 1-1 and the SCI P385 guide.

Different calculation methods of the torsion constant of cellular beams, including a new one (method 3), were approached in this study. The comparison between the analytical and numerical methods aimed to analyze the behavior and influence of the new torsion constant in the values of the critical moment for LTB and the values of the non-uniform angle of torsion.

The type of steel chosen was S355, and the reference model profiles for the solid and cellular beams were IPE 200 (RM1) and HE 200 A (RM2). In total, 316 numerical simulations were performed, varying the beam length and the geometric parameters of the cellular beam (diameter of the hole, spacing between the holes, and height of the beam).

In the analysis of the critical moment for LTB of RM1 and RM2, the new torsion constant approached by method 3 presented the best result among all the methods approached in all case studies. The relative difference between the analytical and numerical methods is slightly greater in beams with longer lengths, except for the first lengths of RM2 where some local deformities in the beam web are visualized together with LTB. It is also noted that case studies based on RM1 have a slightly greater relative difference than RM2. Also except for these cases of the first lengths of RM2, the relative

difference between the analytical and numerical methods is less than 10% in all approached weighted average calculation methods for the torsion constant.

After concluding that the new torsion constant $I_{t,avg3}$ is efficient and presented the best results in the comparison between the values of the analytical and numerical critical moments, the influence of the variation of the geometric parameters was analyzed using this constant in the calculation of the analytical method.

The hole diameter has little influence on the critical moment for LTB. The larger the hole diameter, the smaller the relative difference between most cases based on the HE 200 A profile. In the cases based on the IPE 200 profile, the reference model with the average value of the hole diameter was the one that presented the smallest relative difference.

The variation of the spacing between the holes and the final height of the beam also did not cause a great variation between the relative differences in the values of the analytical and numerical moments. The greater the spacing between the holes and the height of the beam, the greater the relative difference between most cases based on the two different profiles. And the variation of the beam height in the cases based on the profile HE 200 A causes a very small variation between the relative differences.

In the analysis of the non-uniform torsion angle, the relative difference between the analytical and numerical methods is smaller for the RM1 cases than the RM2 cases. When analyzing the influence of the beam length, the relative difference is greater for the case of L=1[m], mainly for the RM2. In all cases, the new torsion constant $I_{t,avg3}$ showed the greatest relative difference.

This behavior was not expected since calculation method 3 is the closest to the real model of the cellular beam. This behavior may be due to a difference between the development of the numerical model and the analytical one, and the relative difference can also be observed in the results of the solid beam cases. By normalizing the division of the angle of torsion between the two methods by the values of the solid beam, the results were more acceptable. However, only for the beam of L=1[m] is that the constant $I_{t,avg3}$ presents the best results with a smaller relative difference. Therefore, more studies should be done for a better understanding of these cases.

6.2. Future lines of investigation

This investigation of LTB of cellular beams provided the following suggestions for future work:

1. Analyze other types of beam profiles to be used as a reference model for the cellular beam;
2. Study other variations of the geometric parameters in the cellular beam, different from those used in this work;
3. Analyze the effectiveness of the new torsion constant $I_{t,avg3}$ in the calculations of the critical moment for LTB in a fire situation;
4. Deepen the study of non-uniform torsion angle, analyzing other beam lengths and different geometric parameters;
5. Carry out experimental studies and compare the results with analytical and numerical methods.

REFERENCES

[1] S. S. Fares, J. Coulson, and D. W. Dinehart, *Design Guide 31: Castellated and Cellular Beam Design*. Chicago, IL, USA: American Institute of Steel Construction, 2016.

[2] F. Erdal and M. P. Saka, "Ultimate load carrying capacity of optimally designed steel cellular beams," *Journal of Constructional Steel Research*, vol. 80, pp. 355–368, Jan. 2013, doi: 10.1016/j.jcsr.2012.10.007.

[3] ArcelorMittal Commercial Sections S.A., *ACB ® and Angelina ™ beams - A new generation of castellated beams*. ArcelorMittal, 2015.

[4] D. Sonck, R. van Impe, and J. Belis, "Experimental investigation of residual stresses in steel cellular and castellated members," *Construction and Building Materials*, vol. 54, pp. 512–519, Mar. 2014, doi: 10.1016/j.conbuildmat.2013.12.045.

[5] CEN, *Draft of EN 1993-1-13 - Steel beams with large web openings*. European Committee for Standardization, 2017.

[6] CEN, "Anexo N: Aberturas nas almas," in *ENV 1993-1-1, Eurocódigo 3: Projecto de estruturas de aço - Parte 1-1: Regras gerais e regras para edifícios*, Bruxelas, Bélgica: Comitê Europeu de Normalização, 1992.

[7] A. M. I. Sweedan, "Elastic lateral stability of I-shaped cellular steel beams," *Journal of Constructional Steel Research*, vol. 67, no. 2, pp. 151–163, Feb. 2011, doi: 10.1016/j.jcsr.2010.08.009.

[8] E. Ellobody, "Nonlinear analysis of cellular steel beams under combined buckling modes," *Thin-Walled Structures*, vol. 52, pp. 66–79, 2012, doi: 10.1016/j.tws.2011.12.009.

[9] D. Sonck and J. Belis, "Lateral-torsional buckling resistance of cellular beams," *Journal of Constructional Steel Research*, vol. 105, pp. 119–128, 2015, doi: 10.1016/j.jcsr.2014.11.003.

[10] J. A. Silva, "Estudo numérico da estabilidade de vigas alveolares em situação de incêndio," Master theis, Instituto Plitécnico de Bragança, Bragança, 2019.

[11] P. Panedpojaman, W. Sae-Long, and T. Chub-Uppakarn, "Cellular beam design for resistance to inelastic lateral-torsional buckling," *Thin-Walled Structures*, vol. 99, pp. 182–194, Feb. 2016, doi: 10.1016/j.tws.2015.08.026.

[12] F. P. V. Ferreira, A. Rossi, and C. H. Martins, “Lateral-torsional buckling of cellular beams according to the possible updating of EC3,” *Journal of Constructional Steel Research*, vol. 153, pp. 222–242, Feb. 2019, doi: 10.1016/j.jcsr.2018.10.011.

[13] D. Sonck, “Global Buckling of Castellated and Cellular Steel Beams and Columns,” Ph.D. dissertation, Faculty of Engineering and Architecture - Ghent University, Belgium, 2014.

[14] K. M. El-Sawy, A. M. I. Sweedan, and M. I. Martini, “Moment gradient factor of cellular steel beams under inelastic flexure,” *Journal of Constructional Steel Research*, vol. 98, pp. 20–34, 2014, doi: 10.1016/j.jcsr.2014.02.007.

[15] D. Sonck, W. Vanlaere, and R. van Impe, “Elastic lateral-torsional buckling of cellular beams.” International Symposium - Steel Structures: Culture & Sustainability 2010, Istanbul, Turkey, 2010.

[16] L. Kang, S. Hong, and X. Liu, “Shear behaviour and strength design of cellular beams with circular or elongated openings,” *Thin-Walled Structures*, vol. 160, Mar. 2021, doi: 10.1016/j.tws.2020.107353.

[17] D. A. Nethercot, P. R. Salter, and A. S. Malik, *Design of members subject to combined bending and torsion*. Silwood Park, Ascot, Berkshire: SCI (P057), 1989.

[18] A. F. Hughes, D. C. Iles, and A. S. Malik, *Design of steel beams in torsion*. Silwood Park, Ascot, Berkshire: SCI (P385), 2011.

[19] A. C. Ugural, *Mecânica dos Materiais*. Rio de Janeiro: LTC, 2009.

[20] D. V. Hutton, *Fundamentals of finite element analysis*. New York, NY: McGraw-Hill, 2004.

[21] D. E.-D. Kerdal, “Lateral-torsinal buckling strength of castellated beams,” Ph.D. thesis, University of Sheffield, Sheffield, 1982.

[22] D. Kerdal and D. A. Nethercott, “Failure modes for castellated beams,” *Journal of Constructional Steel Research*, vol. 4, pp. 295–315, 1984.

[23] P. Piloto, L. M. R. Mesquita, P. J. M. M. Vila Real, and M. A. P. Vaz, “Análise experimental da encurvadura lateral torsional de vigas com reforços transversais.” 3º Congresso Luso-Moçambicano de Engenharia, Maputo, Moçambique, pp. 403–412, 2003.

[24] A. Mohebkhah, “The moment-gradient factor in lateral-torsional buckling on inelastic castellated beams,” *Journal of Constructional Steel Research*, vol. 60, no. 10, pp. 1481–1494, Oct. 2004, doi: 10.1016/j.jcsr.2004.02.002.

[25] P. M. M. Vila Real, R. Cazeli, L. Simoes da Silva, A. Santiago, and P. Piloto, "The effect of residual stresses in the lateral-torsional buckling of steel I-beams at elevated temperature," *Journal of Constructional Steel Research*, vol. 60, no. 3–5, pp. 783–793, 2004, doi: 10.1016/S0143-974X(03)00143-3.

[26] P. M. M. Vila Real, N. Lopes, L. Simões da Silva, and J. M. Franssen, "Parametric analysis of the lateral-torsional buckling resistance of steel beams in case of fire," *Fire Safety Journal*, vol. 42, no. 6–7, pp. 416–424, Sep. 2007, doi: 10.1016/j.firesaf.2006.11.010.

[27] A. Nadjai, O. Vassart, F. Ali, D. Talamona, A. Allam, and M. Hawes, "Performance of cellular composite floor beams at elevated temperatures," *Fire Safety Journal*, vol. 42, no. 6–7, pp. 489–497, Sep. 2007, doi: 10.1016/j.firesaf.2007.05.001.

[28] L. Simões da Silva, C. Rebelo, D. Nethercot, L. Marques, R. Simões, and P. M. M. Vila Real, "Statistical evaluation of the lateral-torsional buckling resistance of steel I-beams, Part 2: Variability of steel properties," *Journal of Constructional Steel Research*, vol. 65, no. 4, pp. 832–849, Apr. 2009, doi: 10.1016/j.jcsr.2008.07.017.

[29] E. Ellobody, "Interaction of buckling modes in castellated steel beams," *Journal of Constructional Steel Research*, vol. 67, no. 5, pp. 814–825, May 2011, doi: 10.1016/j.jcsr.2010.12.012.

[30] A. M. I. Sweedan, "Elastic lateral stability of I-shaped cellular steel beams," *Journal of Constructional Steel Research*, vol. 67, no. 2, pp. 151–163, Feb. 2011, doi: 10.1016/j.jcsr.2010.08.009.

[31] J. Nseir, M. Lo, D. Sonck, H. Somja, O. Vassart, and N. Boissonnade, "Lateral torsional buckling of cellular steel beams," Apr. 2012.

[32] P. Panedpojaman, "Investigation on lateral torsional buckling resistance of EC3 for cellular beam," *International Journal of Advances in Mechanical and Civil Engineering*, vol. 2, no. 4, pp. 30–34, Aug. 2015.

[33] D. Manal, "Thermomechanical behaviour of cellular beams," Master thesis, Polytechnic Institute of Bragança, Bragança, 2017.

[34] F. De'nan, F. M. Nazri, and N. S. Hashim, "Finite element analysis on lateral torsional buckling behaviour of i-beam with web opening," *Engineering Heritage Journal*, vol. 1, no. 2, pp. 19–22, Nov. 2017, doi: 10.26480/gwk.02.2017.19.22.

[35] S. A. Elsawaf and M. M. Hassan, "Behaviour of structural sub-assemblies of steel beams with openings in fire conditions," *Journal of Constructional Steel Research*, vol. 148, pp. 627–638, Sep. 2018, doi: 10.1016/j.jcsr.2018.06.023.

[36] O. F. Zaher, N. M. Yossef, M. H. El-Boghdadi, and M. A. Dabaon, "Structural behaviour of arched steel beams with cellular openings," *Journal of Constructional Steel Research*, vol. 148, pp. 756–767, Sep. 2018, doi: 10.1016/j.jcsr.2018.06.029.

[37] CEN, *EN 1993-1-1, Eurocódigo 3-Projecto de estruturas de aço - Parte 1-1: Regras gerais e regras para edifícios*. Bruxelas, Bélgica: Comitê Europeu de Normalização, 2010.

[38] CEN, *EN 1993-1-2, Eurocódigo 3: Projecto de estruturas de aço - Parte 1-2: Regras gerais - Verificação da resistência ao fogo*. Bruxelas, Bélgica: Comitê Europeu de Normalização, 2010.

[39] R. M. Lawson and S. J. Hicks, *Design of composite beams with large web openings: In accordance with Eurocodes and the UK National Annexes*. Silwood Park, Ascot, Berkshire: SCI (P355), 2011.

[40] D. Braz Costa, "Encurvadura global de vigas alveolares em situação de incêndio," Master thesis, Instituto Politécnico de Bragança, Bragança, 2020.

[41] C. Correa de Faria, H. Carvalho, R. Hallal Fakury, and L. Figueiredo Grilo, "Lateral-torsional buckling resistance of cellular steel beams at room temperature and fire situation," *Engineering Structures*, vol. 237, Jun. 2021, doi: 10.1016/j.engstruct.2021.112046.

[42] T. Tankova, F. Rodrigues, C. Leitão, C. Martins, and L. Simões da Silva, "Lateral-torsional buckling of high strength steel beams: Experimental resistance," *Thin-Walled Structures*, vol. 164, Jul. 2021, doi: 10.1016/j.tws.2021.107913.

[43] A. P. Khatri, S. R. Katikala, and V. K. Kotapati, "Effect of load height on elastic buckling behavior of I-shaped cellular beams," *Structures*, vol. 33, pp. 1923–1935, Oct. 2021, doi: 10.1016/j.istruc.2021.05.047.

[44] N. Boissonnade, R. Greiner, J. P. Jaspart, and J. Lindner, *Rules for member stability in EN 1993-1-1. Background documentation and design guidelines*, Nº119. Brussels, Belgium: ECCS, 2006.

[45] ANSYS®, "Theory Reference." 2022.

[46] ANSYS®, "Mechanical User's Guide." 2021.

[47] ANSYS®, "Element Reference." 2022.

ANNEXES

ANNEX A – Structure of the APDL command applied in the static structural analysis in ANSYS

ANNEX B – Table of the analytical and numerical critical moments

ANNEX C – Table of the non-uniform angle of torsion

ANNEX D – Graphs of the analytical critical moment divided by the ANSYS critical moment, varying the torsion of constant

ANNEX E – Graphs of the analytical critical moment divided by the ANSYS critical moment, varying the geometric parameters of the cellular beam

ANNEX F – Lateral-torsional buckling of solid and cellular beam cases based on RM1

ANNEX G – Lateral-torsional buckling of solid and cellular beam cases based on RM2

ANNEX H – Non-uniform torsion of solid and cellular beam cases based on RM1

ANNEX I– Non-uniform torsion of solid and cellular beam cases based on RM2

ANNEX A – Structure of the APDL command applied in the static structural analysis in ANSYS

```
L=arg1
Le=0.01
ne=1
ncoup=(L/Le)/ne
*DO,conta,0,ncoup,1
zcoord=conta*Le*ne
nsel,s,loc,z,zcoord-0.01/2,zcoord+0.01/2
no_centro=node(0,0,zcoord)
cerig,no_centro,all,rotz
allsel,all
*ENDDO
```

ANNEX B – Table of the analytical and numerical critical moments

Solid beams				
L [m]	M_{cr} [kN.m]			
	Analytical EC3		Numerical ANSYS APDL command	
	RM1	RM2	RM1	RM2
1	302.43	2553.45	289.41	473.18
1.5	145.25	1170.47	142.54	466.42
2	89.54	685.45	88.02	463.60
2.5	63.17	459.99	62.12	435.16
3	48.39	336.64	47.52	325.69
3.5	39.11	261.48	38.40	255.09
4	32.81	212.01	32.21	207.62
4.5	28.27	177.50	27.79	174.15
5	24.85	152.31	24.44	149.56
5.5	22.19	133.24	21.81	130.90
6	20.05	118.36	19.70	116.33
6.5	18.30	106.46	17.98	104.66
7	16.84	96.76	16.55	95.13
7.5	15.60	88.69	15.33	87.22
8	14.53	81.88	14.29	80.54
8.5	13.60	76.07	13.39	74.84
9	12.79	71.04	12.60	69.91
9.5	12.07	66.66	11.90	65.61
10	11.43	62.79	11.27	61.81

Cellular beams

L [m]	M_{cr} [kN.m] Numerical ANSYS APDL command						
	$a_0 = 0.8$h	$a_0 = 1.3$h	$S = 1.1a_0$	$S = 1.7a_0$	$H = 1.3$h	$H = 1.6$h	RM1
1	442.18	442.63	441.06	442.96	385.15	470.70	442.11
1.5	206.53	206.08	205.13	206.39	180.55	218.32	205.64
2	122.71	121.39	121.24	122.27	108.15	128.82	121.85
2.5	83.27	82.27	81.83	83.04	74.00	86.92	82.55
3	61.74	60.88	60.37	61.42	55.15	63.94	60.95
3.5	48.46	47.59	47.26	48.21	43.55	49.90	47.73
4	39.75	38.79	38.46	39.43	35.83	40.63	38.99
4.5	33.62	32.63	32.40	33.30	30.49	34.19	32.92
5	29.03	28.21	27.96	28.76	26.44	29.44	28.41
5.5	25.59	24.85	24.58	25.32	23.34	25.82	24.97
6	22.82	22.05	21.86	22.61	20.90	22.99	22.27
6.5	20.87	19.95	19.74	20.44	18.98	20.75	20.14
7	18.82	18.21	18.01	18.64	17.35	18.89	18.36
7.5	17.47	16.67	16.51	17.15	15.98	17.34	16.87
8	16.05	15.45	15.28	15.88	14.81	16.03	15.61
8.5	14.97	14.37	14.23	14.79	13.81	14.91	14.53
9	14.03	13.47	13.32	13.84	12.97	13.95	13.61
9.5	13.17	12.63	12.49	13.02	12.20	13.10	12.79
10	12.52	11.91	11.79	12.28	11.52	12.35	12.06

L [m]	M_{cr} [kN.m]						
	Numerical ANSYS APDL command						
	$a_0 = 0.8$h	$a_0 = 1.3$h	$S = 1.1a_0$	$S = 1.7a_0$	$H = 1.3$h	$H = 1.6$h	RM2
1	3476.57	3547.77	3518.26	3516.97	3007.89	3653.66	3444.69
1.5	1679.68	1678.04	1674.88	1679.73	1462.61	1791.31	1681.39
2	983.22	982.65	981.27	984.23	860.41	1046.70	984.19
2.5	649.86	648.35	647.39	649.47	570.84	688.65	649.00
3	465.75	464.45	464.14	465.36	411.11	491.50	464.41
3.5	353.63	351.78	351.89	354.59	314.29	372.06	352.52
4	280.40	278.09	277.61	280.14	250.58	293.75	279.11
4.5	229.88	228.10	227.34	229.55	206.66	239.91	228.60
5	193.24	191.38	190.97	192.87	174.74	201.00	192.05
5.5	165.87	163.91	163.77	166.04	150.75	171.91	164.67
6	144.94	142.91	142.94	144.97	132.42	149.75	143.80
6.5	128.39	126.61	126.15	128.21	117.82	132.23	127.27
7	115.12	113.38	113.09	114.78	106.07	118.20	114.02
7.5	104.30	102.42	102.34	104.10	97.04	107.31	103.75
8	95.22	93.86	93.63	95.06	88.96	97.79	94.72
8.5	87.62	86.25	86.03	87.34	81.97	89.66	87.00
9	81.07	79.45	79.65	80.76	76.12	82.84	80.50
9.5	75.44	73.88	73.75	75.22	71.27	77.19	75.12
10	70.60	69.27	68.94	70.67	66.71	71.98	70.14

L [m]	M_{cr} [kN.m]											
	Analytical EC3											
	$I_{t,2T}$			$I_{t,avg1}$			$I_{t,avg2}$			$I_{t,avg3}$		
	$a_0 = 0.8$h	$a_0 = 1.3$h	RM1	$a_0 = 0.8$h	$a_0 = 1.3$h	RM1	$a_0 = 0.8$h	$a_0 = 1.3$h	RM1	$a_0 = 0.8$h	$a_0 = 1.3$h	RM1
1.0	441.37	439.57	440.65	442.41	441.82	442.09	442.59	442.06	442.31	442.75	442.27	442.50
1.5	203.23	201.60	202.58	204.17	203.63	203.66	204.33	203.85	203.88	204.50	204.07	204.10
2.0	119.66	118.14	119.05	120.53	119.53	120.27	120.68	119.78	120.45	120.85	120.05	120.64
2.5	80.77	79.34	80.20	81.58	80.74	81.22	81.73	80.97	81.40	81.88	81.21	81.60
3.0	59.45	58.10	58.91	60.10	59.48	59.80	60.24	59.69	59.98	60.40	59.92	60.17
3.5	46.42	45.16	45.92	47.05	46.25	46.71	47.18	46.47	46.88	47.33	46.71	47.06
4.0	37.83	36.64	37.36	38.42	37.72	38.06	38.54	37.92	38.22	38.68	38.14	38.40
4.5	31.81	30.69	31.37	32.37	31.58	32.10	32.49	31.78	32.24	32.62	32.00	32.40
5.0	27.40	26.35	26.98	27.88	27.24	27.64	28.00	27.42	27.78	28.12	27.62	27.94
5.5	24.05	23.06	23.66	24.51	23.93	24.26	24.62	24.10	24.39	24.73	24.28	24.54
6.0	21.43	20.49	21.06	21.87	21.24	21.61	21.97	21.40	21.73	22.08	21.59	21.87
6.5	19.32	18.44	18.97	19.74	19.18	19.53	19.84	19.33	19.65	19.94	19.50	19.78
7.0	17.60	16.76	17.27	18.00	17.48	17.78	18.09	17.63	17.89	18.19	17.78	18.02
7.5	16.16	15.37	15.85	16.52	16.00	16.33	16.61	16.14	16.43	16.70	16.30	16.55
8.0	14.95	14.19	14.65	15.29	14.82	15.09	15.37	14.95	15.19	15.46	15.09	15.31
8.5	13.91	13.19	13.62	14.24	13.74	14.04	14.32	13.87	14.13	14.40	14.02	14.24
9.0	13.00	12.32	12.73	13.33	12.87	13.15	13.40	12.99	13.24	13.48	13.12	13.34
9.5	12.21	11.56	11.96	12.51	12.10	12.35	12.58	12.21	12.43	12.66	12.34	12.53
10.0	11.52	10.89	11.27	11.80	11.38	11.64	11.87	11.49	11.72	11.94	11.62	11.82

L [m]	M_{cr} [kN.m]											
	Analytical EC3											
	$I_{t,2T}$			$I_{t,avg1}$			$I_{t,avg2}$			$I_{t,avg3}$		
	$a_0 = 0.8$h	$a_0 = 1.3$h	RM2	$a_0 = 0.8$h	$a_0 = 1.3$h	RM2	$a_0 = 0.8$h	$a_0 = 1.3$h	RM2	$a_0 = 0.8$h	$a_0 = 1.3$h	RM2
1.0	3842.14	3839.30	3841.00	3843.92	3843.03	3843.44	3844.19	3843.40	3843.77	3844.45	3843.73	3844.06
1.5	1730.65	1728.02	1729.60	1732.30	1730.35	1731.53	1732.56	1730.81	1731.86	1732.82	1731.27	1732.21
2.0	991.35	988.82	990.33	992.62	991.33	992.03	992.90	991.74	992.37	993.20	992.18	992.73
2.5	648.86	646.41	647.88	650.15	649.00	649.43	650.42	649.38	649.76	650.70	649.79	650.13
3.0	462.52	460.15	461.57	463.81	462.26	463.31	464.06	462.66	463.61	464.34	463.11	463.94
3.5	349.88	347.58	348.97	351.00	349.77	350.57	351.26	350.15	350.86	351.54	350.57	351.20
4.0	276.51	274.29	275.62	277.63	276.14	277.11	277.87	276.53	277.40	278.14	276.97	277.73
4.5	225.96	223.81	225.10	227.07	225.72	226.49	227.30	226.08	226.78	227.56	226.50	227.10
5.0	189.57	187.49	188.74	190.56	189.16	190.05	190.79	189.53	190.33	191.05	189.95	190.65
5.5	162.44	160.43	161.64	163.42	162.13	162.87	163.63	162.48	163.14	163.88	162.88	163.45
6.0	141.61	139.68	140.84	142.57	141.19	142.00	142.78	141.54	142.27	143.02	141.93	142.57
6.5	125.23	123.37	124.49	126.11	124.90	125.59	126.31	125.23	125.85	126.54	125.60	126.14
7.0	112.07	110.28	111.36	112.94	111.82	112.41	113.13	112.13	112.66	113.36	112.48	112.94
7.5	101.32	99.60	100.64	102.17	100.98	101.72	102.36	101.29	101.95	102.57	101.64	102.22
8.0	92.40	90.73	91.74	93.18	92.12	92.76	93.36	92.42	92.99	93.57	92.75	93.25
8.5	84.89	83.28	84.25	85.65	84.55	85.23	85.83	84.84	85.45	86.03	85.16	85.70
9.0	78.49	76.94	77.88	79.20	78.21	78.81	79.37	78.48	79.02	79.57	78.79	79.26
9.5	72.99	71.49	72.39	73.68	72.65	73.28	73.85	72.92	73.49	74.04	73.23	73.72
10.0	68.20	66.76	67.63	68.89	67.92	68.48	69.05	68.18	68.68	69.23	68.47	68.91

L [m]	M_{cr} [kN.m]											
	Analytical EC3											
	$I_{t,2T}$			$I_{t,avg1}$			$I_{t,avg2}$			$I_{t,avg3}$		
	$S = 1.1a_0$	$S = 1.7a_0$	RM1	$S = 1.1a_0$	$S = 1.7a_0$	RM1	$S = 1.1a_0$	$S = 1.7a_0$	RM1	$S = 1.1a_0$	$S = 1.7a_0$	RM1
1.0	440.65	440.65	440.65	441.37	442.81	442.09	441.66	442.95	442.31	441.91	443.08	442.50
1.5	202.58	202.58	202.58	203.23	204.53	203.66	203.49	204.66	203.88	203.75	204.79	204.10
2.0	119.05	119.05	119.05	119.66	120.57	120.27	119.90	120.72	120.45	120.16	120.88	120.64
2.5	80.20	80.20	80.20	80.54	81.67	81.22	80.79	81.81	81.40	81.06	81.95	81.60
3.0	58.91	58.91	58.91	59.27	60.15	59.80	59.50	60.29	59.98	59.75	60.45	60.17
3.5	45.92	45.92	45.92	46.28	47.13	46.71	46.50	47.26	46.88	46.73	47.40	47.06
4.0	37.36	37.36	37.36	37.59	38.41	38.06	37.80	38.53	38.22	38.04	38.67	38.40
4.5	31.37	31.37	31.37	31.61	32.39	32.10	31.81	32.50	32.24	32.02	32.63	32.40
5.0	26.98	26.98	26.98	27.23	27.89	27.64	27.41	28.00	27.78	27.62	28.13	27.94
5.5	23.66	23.66	23.66	23.91	24.54	24.26	24.08	24.64	24.39	24.26	24.75	24.54
6.0	21.06	21.06	21.06	21.24	21.85	21.61	21.41	21.95	21.73	21.59	22.06	21.87
6.5	18.97	18.97	18.97	19.16	19.74	19.53	19.32	19.83	19.65	19.49	19.94	19.78
7.0	17.27	17.27	17.27	17.46	17.97	17.78	17.60	18.06	17.89	17.76	18.16	18.02
7.5	15.85	15.85	15.85	16.00	16.53	16.33	16.14	16.61	16.43	16.29	16.71	16.55
8.0	14.65	14.65	14.65	14.80	15.27	15.09	14.93	15.36	15.19	15.08	15.45	15.31
8.5	13.62	13.62	13.62	13.77	14.23	14.04	13.90	14.31	14.13	14.04	14.39	14.24
9.0	12.73	12.73	12.73	12.88	13.30	13.15	13.00	13.37	13.24	13.14	13.46	13.34
9.5	11.96	11.96	11.96	12.08	12.51	12.35	12.20	12.58	12.43	12.32	12.65	12.53
10.0	11.27	11.27	11.27	11.40	11.78	11.64	11.51	11.85	11.72	11.63	11.93	11.82

L [m]	M_{cr} [kN.m]											
	Analytical EC3											
	$I_{t,2T}$			$I_{t,avg1}$			$I_{t,avg2}$			$I_{t,avg3}$		
	$S = 1.1a_0$	$S = 1.7a_0$	RM2	$S = 1.1a_0$	$S = 1.7a_0$	RM2	$S = 1.1a_0$	$S = 1.7a_0$	RM2	$S = 1.1a_0$	$S = 1.7a_0$	RM2
1.0	3841.00	3841.00	3841.00	3842.36	3844.52	3843.44	3842.80	3844.74	3843.77	3843.19	3844.93	3844.06
1.5	1729.60	1729.60	1729.60	1730.19	1732.20	1731.53	1730.66	1732.46	1731.86	1731.14	1732.74	1732.21
2.0	990.33	990.33	990.33	991.07	992.99	992.03	991.50	993.23	992.37	991.97	993.49	992.73
2.5	647.88	647.88	647.88	648.68	650.17	649.43	649.09	650.43	649.76	649.54	650.71	650.13
3.0	461.57	461.57	461.57	462.11	463.91	463.31	462.53	464.15	463.61	463.00	464.42	463.94
3.5	348.97	348.97	348.97	349.57	351.06	350.57	349.97	351.31	350.86	350.41	351.59	351.20
4.0	275.62	275.62	275.62	276.06	277.74	277.11	276.46	277.97	277.40	276.91	278.23	277.73
4.5	225.10	225.10	225.10	225.59	227.03	226.49	225.97	227.26	226.78	226.39	227.53	227.10
5.0	188.74	188.74	188.74	189.26	190.52	190.05	189.62	190.75	190.33	190.03	191.01	190.65
5.5	161.64	161.64	161.64	162.04	163.42	162.87	162.40	163.63	163.14	162.81	163.88	163.45
6.0	140.84	140.84	140.84	141.28	142.49	142.00	141.62	142.70	142.27	142.00	142.95	142.57
6.5	124.49	124.49	124.49	124.84	126.13	125.59	125.17	126.33	125.85	125.55	126.56	126.14
7.0	111.36	111.36	111.36	111.73	112.89	112.41	112.05	113.09	112.66	112.41	113.32	112.94
7.5	100.64	100.64	100.64	101.03	102.15	101.72	101.33	102.34	101.95	101.67	102.55	102.22
8.0	91.74	91.74	91.74	92.06	93.15	92.76	92.36	93.34	92.99	92.70	93.55	93.25
8.5	84.25	84.25	84.25	84.59	85.65	85.23	84.87	85.83	85.45	85.20	86.03	85.70
9.0	77.88	77.88	77.88	78.23	79.19	78.81	78.50	79.37	79.02	78.81	79.56	79.26
9.5	72.39	72.39	72.39	72.69	73.64	73.28	72.96	73.81	73.49	73.26	74.00	73.72
10.0	67.63	67.63	67.63	67.94	68.86	68.48	68.19	69.02	68.68	68.48	69.20	68.91

L [m]	M_{cr} [kN.m]											
	Analytical EC3											
	$I_{t,2T}$			$I_{t,avg1}$			$I_{t,avg2}$			$I_{t,avg3}$		
	$H = 1.3h$	$H = 1.6h$	RM1	$H = 1.3h$	$H = 1.6h$	RM1	$H = 1.3h$	$H = 1.6h$	RM1	$H = 1.3h$	$H = 1.6h$	RM1
1.0	383.02	469.59	440.65	384.62	470.96	442.09	384.86	471.17	442.31	385.09	471.34	442.50
1.5	177.55	215.20	202.58	178.77	216.23	203.66	179.01	216.43	203.88	179.26	216.64	204.10
2.0	105.37	125.99	119.05	106.72	127.14	120.27	106.92	127.31	120.45	107.14	127.49	120.64
2.5	71.70	84.52	80.20	72.84	85.49	81.22	73.04	85.67	81.40	73.26	85.85	81.60
3.0	53.19	61.84	58.91	54.17	62.68	59.80	54.36	62.85	59.98	54.58	63.04	60.17
3.5	41.84	48.02	45.92	42.70	48.77	46.71	42.88	48.93	46.88	43.09	49.11	47.06
4.0	34.31	38.92	37.36	35.07	39.60	38.06	35.25	39.75	38.22	35.44	39.92	38.40
4.5	29.01	32.58	31.37	29.80	33.28	32.10	29.96	33.42	32.24	30.13	33.58	32.40
5.0	25.11	27.95	26.98	25.82	28.59	27.64	25.97	28.72	27.78	26.13	28.87	27.94
5.5	22.13	24.44	23.66	22.77	25.02	24.26	22.91	25.15	24.39	23.07	25.30	24.54
6.0	19.79	21.71	21.06	20.37	22.24	21.61	20.51	22.37	21.73	20.66	22.50	21.87
6.5	17.90	19.52	18.97	18.49	20.07	19.53	18.61	20.18	19.65	18.75	20.31	19.78
7.0	16.35	17.74	17.27	16.89	18.24	17.78	17.00	18.35	17.89	17.13	18.47	18.02
7.5	15.05	16.26	15.85	15.55	16.73	16.33	15.66	16.83	16.43	15.78	16.94	16.55
8.0	13.94	15.01	14.65	14.41	15.44	15.09	14.51	15.54	15.19	14.63	15.65	15.31
8.5	12.99	13.94	13.62	13.43	14.35	14.04	13.53	14.44	14.13	13.64	14.55	14.24
9.0	12.17	13.02	12.73	12.60	13.43	13.15	12.70	13.52	13.24	12.80	13.62	13.34
9.5	11.45	12.22	11.96	11.85	12.60	12.35	11.94	12.69	12.43	12.04	12.78	12.53
10.0	10.81	11.51	11.27	11.19	11.87	11.64	11.27	11.95	11.72	11.37	12.04	11.82

L [m]	M_{cr} [kN.m]											
	Analytical EC3											
	$I_{t,2T}$			$I_{t,avg1}$			$I_{t,avg2}$			$I_{t,avg3}$		
	$H = 1.3h$	$H = 1.6h$	RM2	$H = 1.3h$	$H = 1.6h$	RM2	$H = 1.3h$	$H = 1.6h$	RM2	$H = 1.3h$	$H = 1.6h$	RM2
1.0	3321.11	4101.47	3841.00	3321.11	4103.79	3843.44	3321.11	4104.10	3843.77	3324.57	4104.37	3844.06
1.5	1501.36	1844.21	1729.60	1501.36	1846.04	1731.53	1501.36	1846.35	1731.86	1504.33	1846.67	1732.21
2.0	864.05	1053.94	990.33	864.05	1055.54	992.03	864.05	1055.86	992.37	866.78	1056.20	992.73
2.5	568.66	687.92	647.88	568.66	689.38	649.43	568.66	689.69	649.76	571.22	690.04	650.13
3.0	407.81	488.85	461.57	407.81	490.50	463.31	407.81	490.78	463.61	410.49	491.09	463.94
3.5	310.45	368.59	348.97	310.45	370.10	350.57	310.45	370.38	350.86	312.95	370.70	351.20
4.0	246.91	290.31	275.62	246.91	291.72	277.11	246.91	292.00	277.40	249.26	292.31	277.73
4.5	203.04	236.43	225.10	203.04	237.75	226.49	203.04	238.03	226.78	205.25	238.34	227.10
5.0	171.37	197.69	188.74	171.37	198.94	190.05	171.37	199.21	190.33	173.46	199.51	190.65
5.5	147.68	168.86	161.64	147.68	170.03	162.87	147.68	170.30	163.14	149.66	170.59	163.45
6.0	129.43	146.76	140.84	129.43	147.87	142.00	129.43	148.13	142.27	131.31	148.42	142.57
6.5	115.03	129.41	124.49	115.03	130.47	125.59	115.03	130.72	125.85	116.81	131.00	126.14
7.0	103.42	115.50	111.36	103.42	116.51	112.41	103.42	116.75	112.66	105.12	117.03	112.94
7.5	93.89	104.16	100.64	93.89	105.21	101.72	93.89	105.43	101.95	95.58	105.69	102.22
8.0	85.95	94.77	91.74	85.95	95.76	92.76	85.95	95.98	92.99	87.56	96.23	93.25
8.5	79.24	86.88	84.25	79.24	87.83	85.23	79.24	88.04	85.45	80.77	88.28	85.70
9.0	73.50	80.17	77.88	73.50	81.08	78.81	73.50	81.28	79.02	74.97	81.52	79.26
9.5	68.54	74.41	72.39	68.54	75.28	73.28	68.54	75.48	73.49	69.95	75.71	73.72
10.0	64.22	69.42	67.63	64.22	70.25	68.48	64.22	70.44	68.68	65.56	70.66	68.91

ANNEX C – Table of the non-uniform angle of torsion

Φ [º] solid cases														
L=10 [m]					L=5 [m]					L=1 [m]				
z [m]	Analytical SCI		Numerical ANSYS		z [m]	Analytical SCI		Numerical ANSYS		z [m]	Analytical SCI		Numerical ANSYS	
	RM1	RM2	RM1	RM2		RM1	RM2	RM1	RM2		RM1	RM2	RM1	RM2
1	0.59	0.14	0.59	0.14	1	0.585	0.138	0.595	0.141	0.1	0.0068	0.0010	0.0072	0.0012
1.5	1.12	0.28	1.14	0.28	1.5	1.123	0.279	1.142	0.285	0.2	0.0260	0.0040	0.0271	0.0044
2	1.73	0.45	1.76	0.46	2	1.730	0.450	1.759	0.460	0.3	0.0558	0.0086	0.0578	0.0094
2.5	2.37	0.64	2.41	0.65	2.5	2.373	0.641	2.415	0.655	0.4	0.0944	0.0147	0.0978	0.0159
3	3.04	0.85	3.09	0.86	3	3.037	0.845	3.093	0.866	0.5	0.1405	0.0220	0.1454	0.0236
3.5	3.71	1.06	3.78	1.08	3.5	3.711	1.059	3.783	1.088	0.6	0.1925	0.0303	0.1993	0.0325
4	4.39	1.29	4.47	1.30	4	4.390	1.280	4.483	1.318	0.7	0.2493	0.0394	0.2582	0.0422
4.5	5.07	1.51	5.17	1.53	4.5	5.073	1.503	5.191	1.555	0.8	0.3095	0.0491	0.3208	0.0525
5	5.76	1.75	5.87	1.77	5	5.756	1.729	5.909	1.799	0.9	0.3719	0.0592	0.3858	0.0633
5.5	6.44	1.98	6.57	2.00						1	0.4355	0.0695	0.4518	0.0744
6	7.13	2.21	7.27	2.24										
6.5	7.82	2.45	7.98	2.48										
7	8.50	2.68	8.68	2.72										
7.5	9.19	2.92	9.39	2.97										
8	9.88	3.16	10.10	3.21										
8.5	10.56	3.40	10.82	3.46										
9	11.25	3.63	11.54	3.71										
9.5	11.94	3.87	12.26	3.96										
10	12.62	4.11	13.00	4.22										

Φ [º] RM1 cellular cases

L=10 [m]					L=5 [m]					L=1 [m]				
z	Analytical SCI			Numerical	z	Analytical SCI			Numerical	z	Analytical SCI			Numerical
[m]	$I_{t,avg1}$	$I_{t,avg2}$	$I_{t,avg3}$	ANSYS	[m]	$I_{t,avg1}$	$I_{t,avg2}$	$I_{t,avg3}$	ANSYS	[m]	$I_{t,avg1}$	$I_{t,avg2}$	$I_{t,avg3}$	ANSYS
1	0.45	0.44	0.44	0.45	1	0.444	0.440	0.435	0.447	0.1	0.00361	0.00360	0.00359	0.00374
1.5	0.90	0.89	0.88	0.90	1.5	0.893	0.883	0.873	0.899	0.2	0.01385	0.01382	0.01378	0.01427
2	1.44	1.42	1.40	1.44	2	1.429	1.413	1.395	1.439	0.3	0.02989	0.02982	0.02973	0.03073
2.5	2.03	2.01	1.98	2.04	2.5	2.023	1.999	1.973	2.038	0.4	0.05092	0.05079	0.05064	0.05228
3	2.67	2.64	2.60	2.68	3	2.656	2.624	2.588	2.677	0.5	0.07617	0.07597	0.07574	0.07818
3.5	3.34	3.29	3.24	3.34	3.5	3.314	3.273	3.227	3.341	0.6	0.10489	0.10461	0.10429	0.10765
4	4.02	3.96	3.90	4.03	4	3.988	3.938	3.881	4.024	0.7	0.13637	0.13600	0.13557	0.13995
4.5	4.71	4.65	4.58	4.73	4.5	4.672	4.612	4.544	4.718	0.8	0.16990	0.16943	0.16889	0.17436
5	5.41	5.34	5.26	5.43	5	5.361	5.290	5.211	5.416	0.9	0.20479	0.20422	0.20356	0.21013
5.5	6.12	6.04	5.94	6.14						1.0	0.24036	0.23968	0.23890	0.24637
6	6.83	6.74	6.63	6.86										
6.5	7.55	7.44	7.32	7.58										
7	8.26	8.14	8.01	8.30										
7.5	8.98	8.85	8.70	9.03										
8	9.70	9.56	9.40	9.76										
8.5	10.42	10.26	10.09	10.49										
9	11.14	10.97	10.78	11.22										
9.5	11.85	11.68	11.48	11.96										
10	12.57	12.38	12.17	12.70										

Φ [º] RM2 cellular cases

L=10 [m]					L=5 [m]					L=1 [m]				
z [m]	Analytical SCI			Numerical ANSYS	z [m]	Analytical SCI			Numerical ANSYS	z [m]	Analytical SCI			Numerical ANSYS
	$I_{t,avg1}$	$I_{t,avg2}$	$I_{t,avg3}$			$I_{t,avg1}$	$I_{t,avg2}$	$I_{t,avg3}$			$I_{t,avg1}$	$I_{t,avg2}$	$I_{t,avg3}$	
1	0.10	0.10	0.10	0.10	1	0.097	0.097	0.096	0.099	0.1	0.0004955	0.0004953	0.0004950	0.0005620
1.5	0.21	0.21	0.21	0.21	1.5	0.203	0.202	0.201	0.208	0.2	0.0018640	0.0018631	0.0018621	0.0020614
2	0.34	0.34	0.34	0.35	2	0.337	0.335	0.333	0.345	0.3	0.0040053	0.0040033	0.0040010	0.0043578
2.5	0.50	0.50	0.50	0.51	2.5	0.488	0.486	0.483	0.500	0.4	0.0068204	0.0068170	0.0068130	0.0073514
3	0.68	0.68	0.67	0.69	3	0.658	0.655	0.651	0.676	0.5	0.0105793	0.0105738	0.0105675	0.0113341
3.5	0.87	0.87	0.86	0.88	3.5	0.840	0.836	0.831	0.865	0.6	0.0144939	0.0144862	0.0144774	0.0154757
4	1.07	1.07	1.06	1.08	4	1.031	1.025	1.019	1.064	0.7	0.0187848	0.0187747	0.0187632	0.0200119
4.5	1.28	1.28	1.27	1.30	4.5	1.227	1.220	1.213	1.270	0.8	0.0233576	0.0233449	0.0233304	0.0248472
5	1.50	1.49	1.48	1.52	5	1.420	1.412	1.404	1.475	0.9	0.0281187	0.0281033	0.0280856	0.0298784
5.5	1.73	1.72	1.70	1.75						1	0.0330978	0.0330794	0.0330585	0.0351588
6	1.95	1.94	1.92	1.97										
6.5	2.18	2.17	2.15	2.21										
7	2.42	2.40	2.38	2.45										
7.5	2.65	2.64	2.62	2.69										
8	2.89	2.87	2.85	2.94										
8.5	3.13	3.11	3.08	3.18										
9	3.37	3.34	3.32	3.43										
9.5	3.61	3.58	3.55	3.68										
10	3.84	3.82	3.78	3.93										

ANNEX D – Graphs of the analytical critical moment divided by the ANSYS critical moment, varying the torsion of constant

$a_0 = 1.0h$ - $S = 1.4a_0$ - $H = 1.0h$ - Reference model of cellular beams

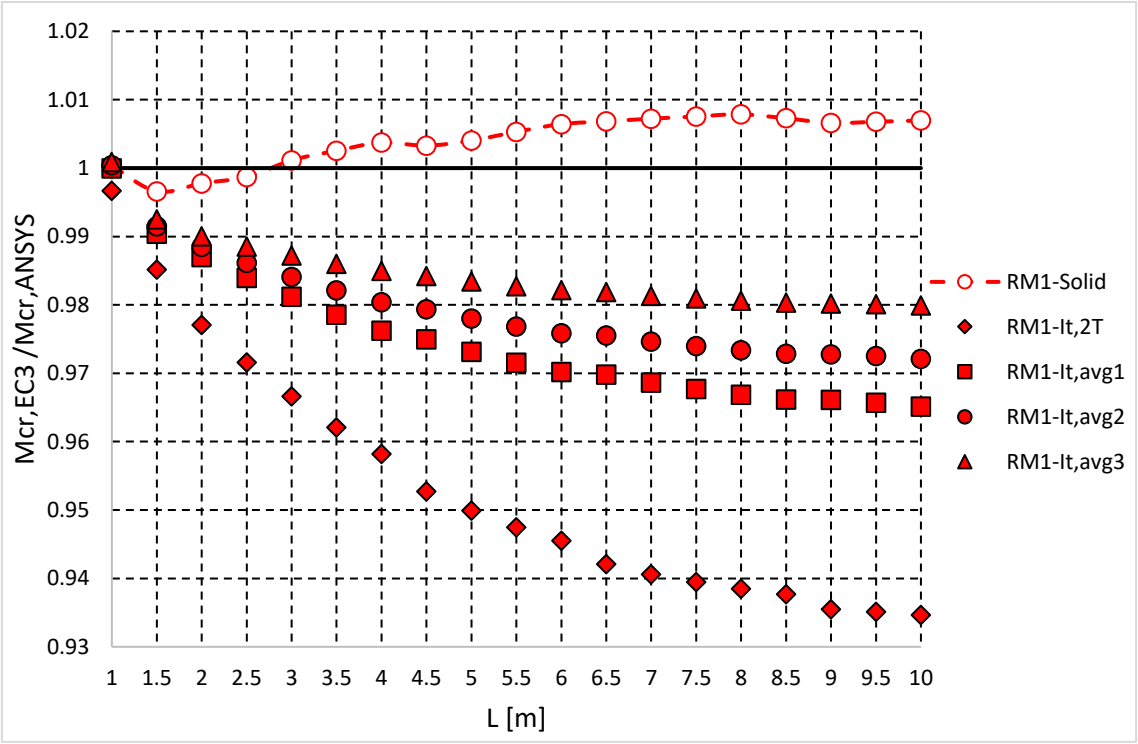

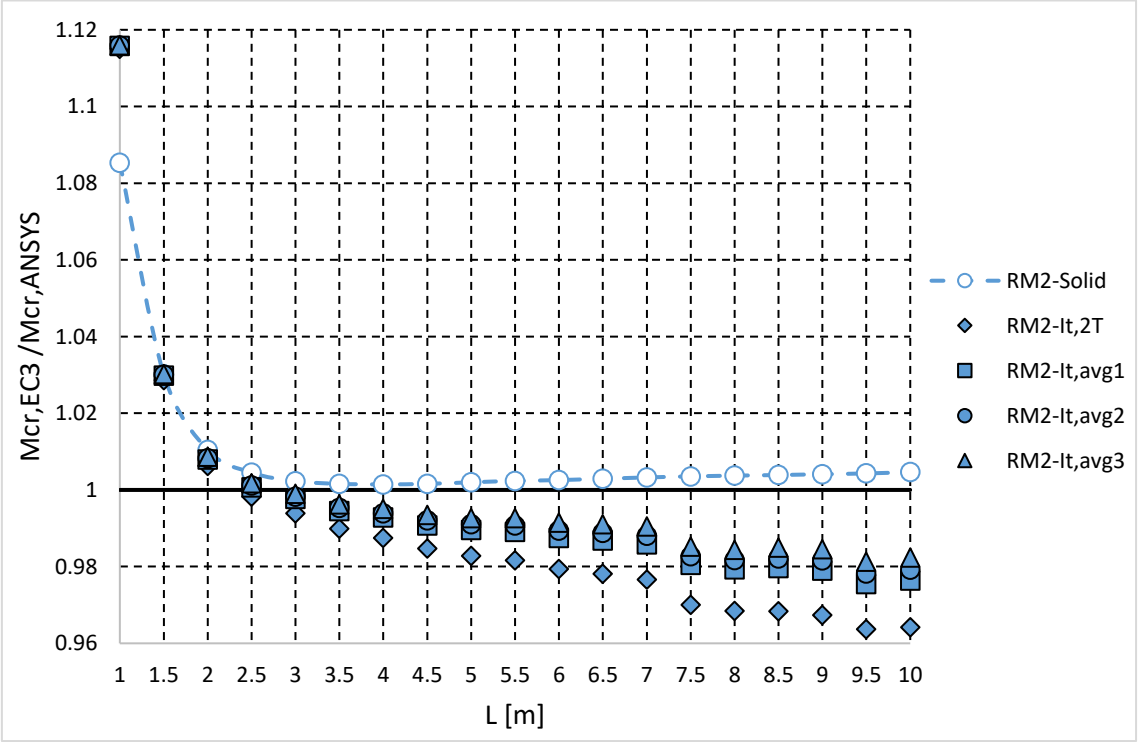

$$a_0 = 0.8h$$

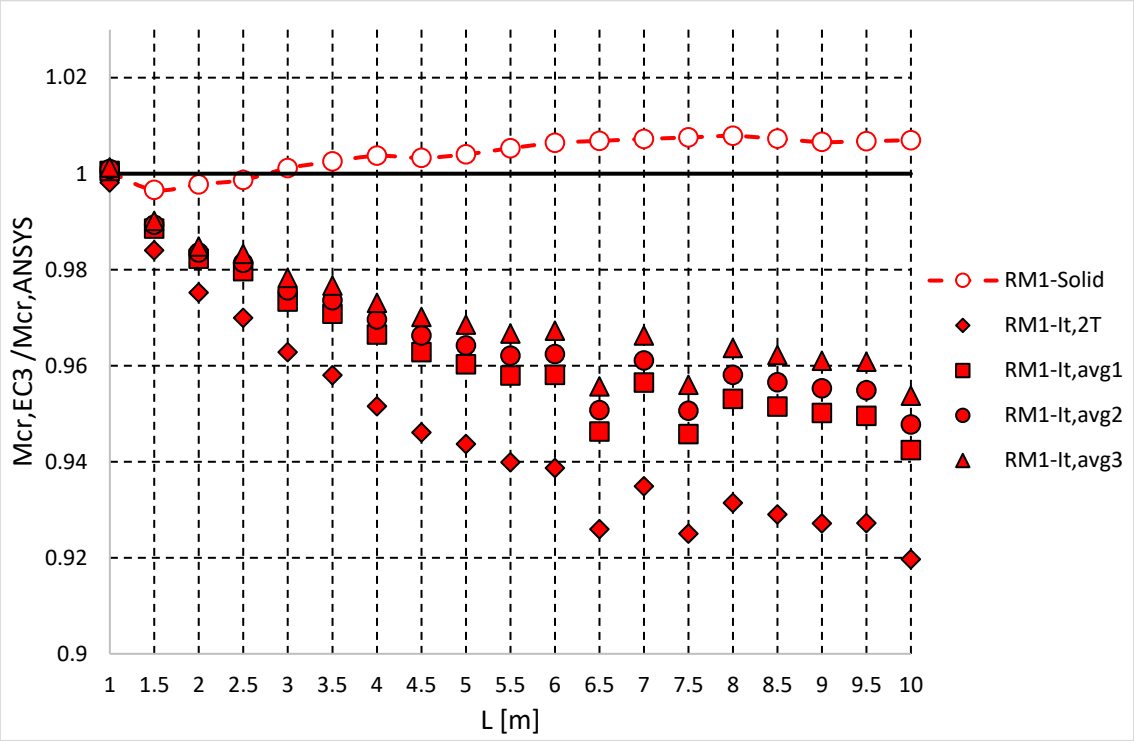
1.02
1
0.98
0.96
0.94
0.92
0.9
Mcr,EC3 /Mcr,ANSYS
1 1.5 2 2.5 3 3.5 4 4.5 5 5.5 6 6.5 7 7.5 8 8.5 9 9.5 10
L [m]
RM1-Solid
RM1-It,2T
RM1-It,avg1
RM1-It,avg2
RM1-It,avg3

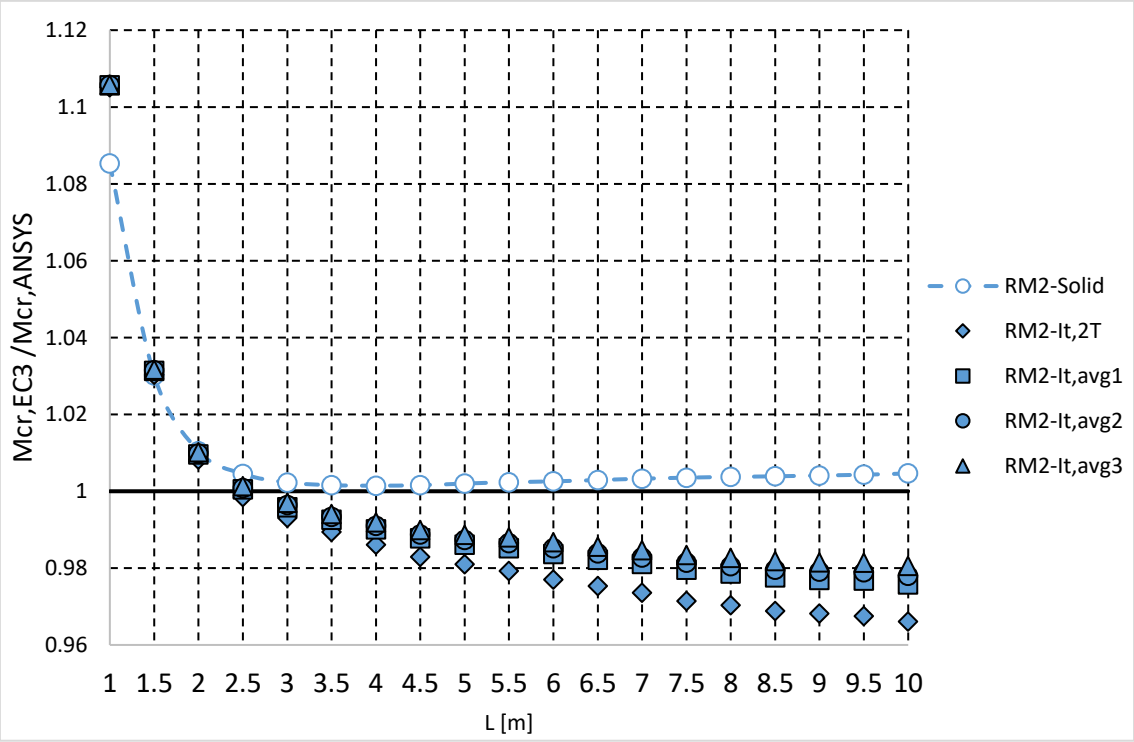
1.12
1.1
1.08
1.06
1.04
1.02
1
0.98
0.96
Mcr,EC3 /Mcr,ANSYS
1 1.5 2 2.5 3 3.5 4 4.5 5 5.5 6 6.5 7 7.5 8 8.5 9 9.5 10
L [m]
RM2-Solid
RM2-It,2T
RM2-It,avg1
RM2-It,avg2
RM2-It,avg3

$$a_0 = 1.3h$$

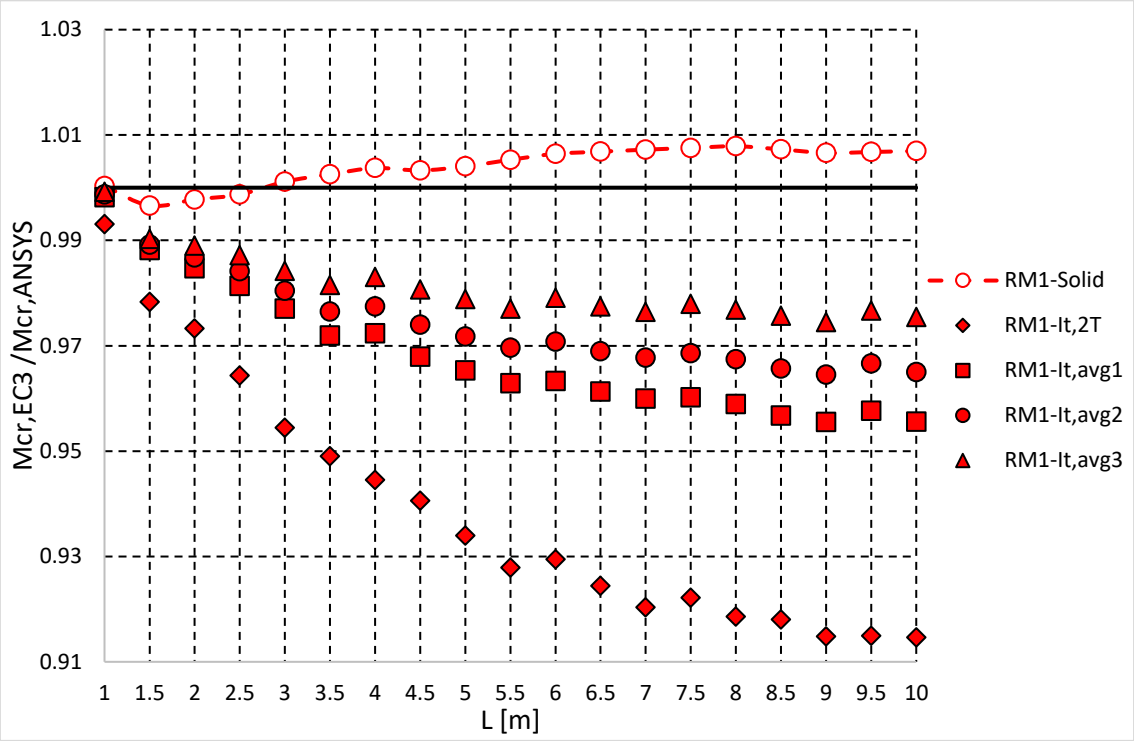
1.03
1.01
0.99
0.97
0.95
0.93
0.91
Mcr,EC3 /Mcr,ANSYS
1 1.5 2 2.5 3 3.5 4 4.5 5 5.5 6 6.5 7 7.5 8 8.5 9 9.5 10
L [m]
RM1-Solid
RM1-It,2T
RM1-It,avg1
RM1-It,avg2
RM1-It,avg3

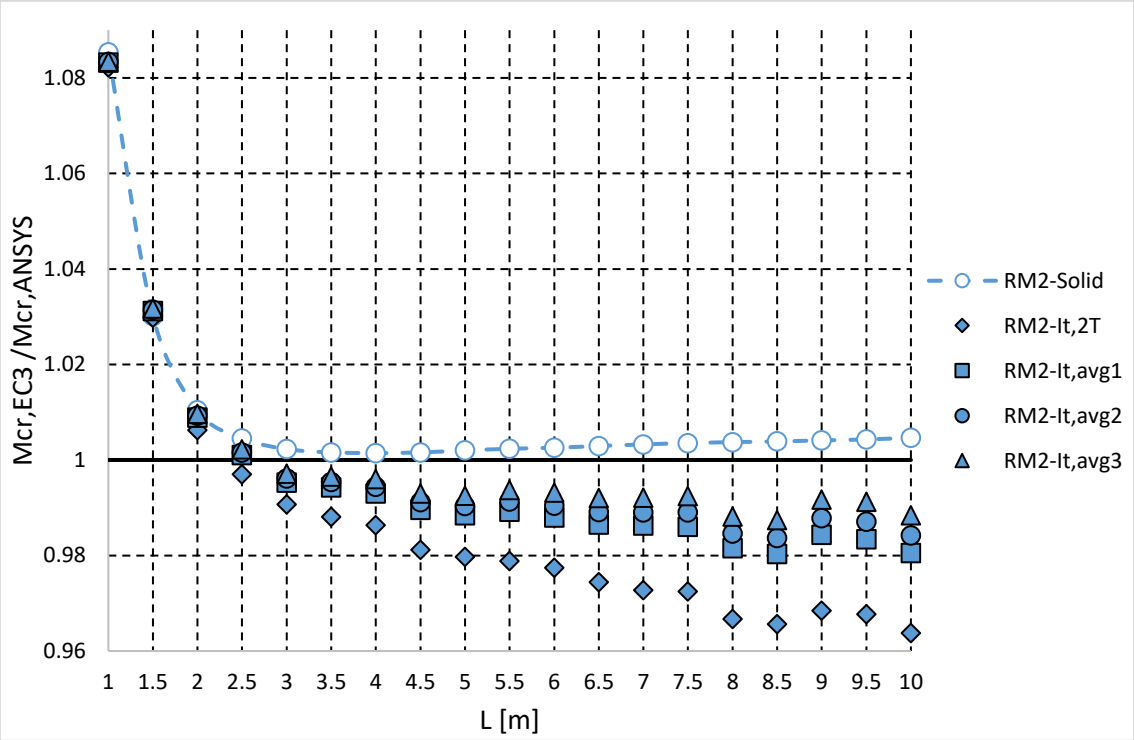
1.08
1.06
1.04
1.02
1
0.98
0.96
Mcr,EC3 /Mcr,ANSYS
1 1.5 2 2.5 3 3.5 4 4.5 5 5.5 6 6.5 7 7.5 8 8.5 9 9.5 10
L [m]
RM2-Solid
RM2-It,2T
RM2-It,avg1
RM2-It,avg2
RM2-It,avg3

$$S = 1.1a_0$$

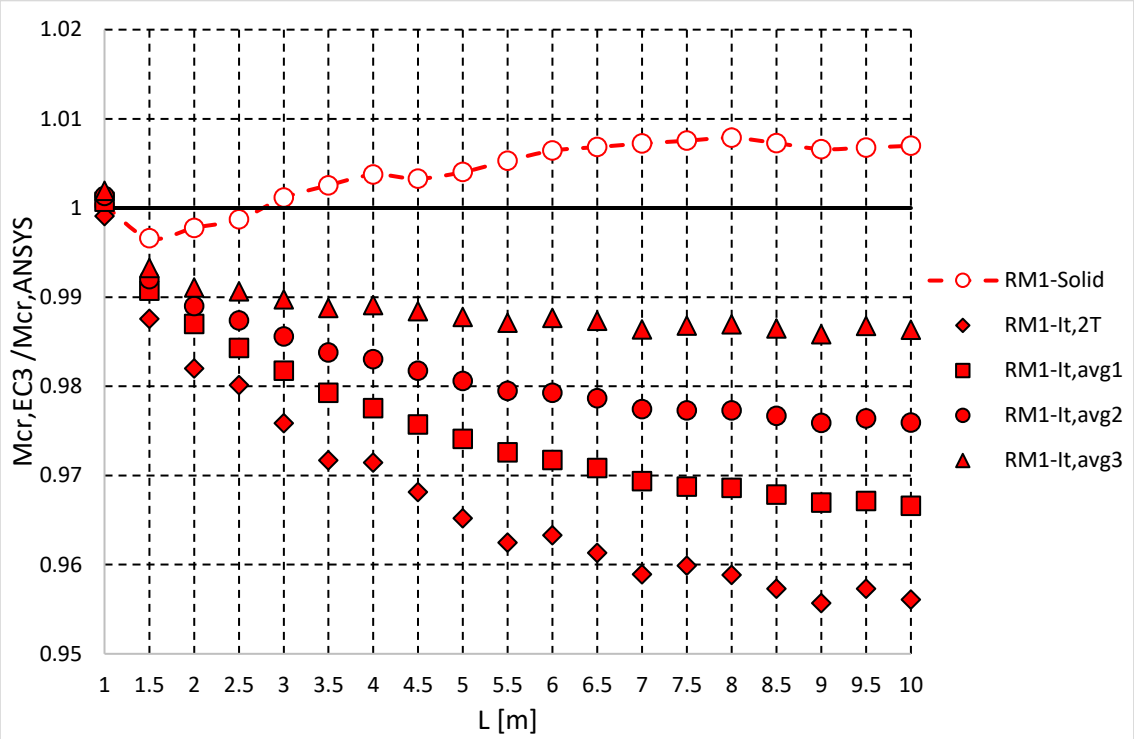
1.02
1.01
1
0.99
0.98
0.97
0.96
0.95
Mcr,EC3 /Mcr,ANSYS
1 1.5 2 2.5 3 3.5 4 4.5 5 5.5 6 6.5 7 7.5 8 8.5 9 9.5 10
L [m]
RM1-Solid
RM1-It,2T
RM1-It,avg1
RM1-It,avg2
RM1-It,avg3

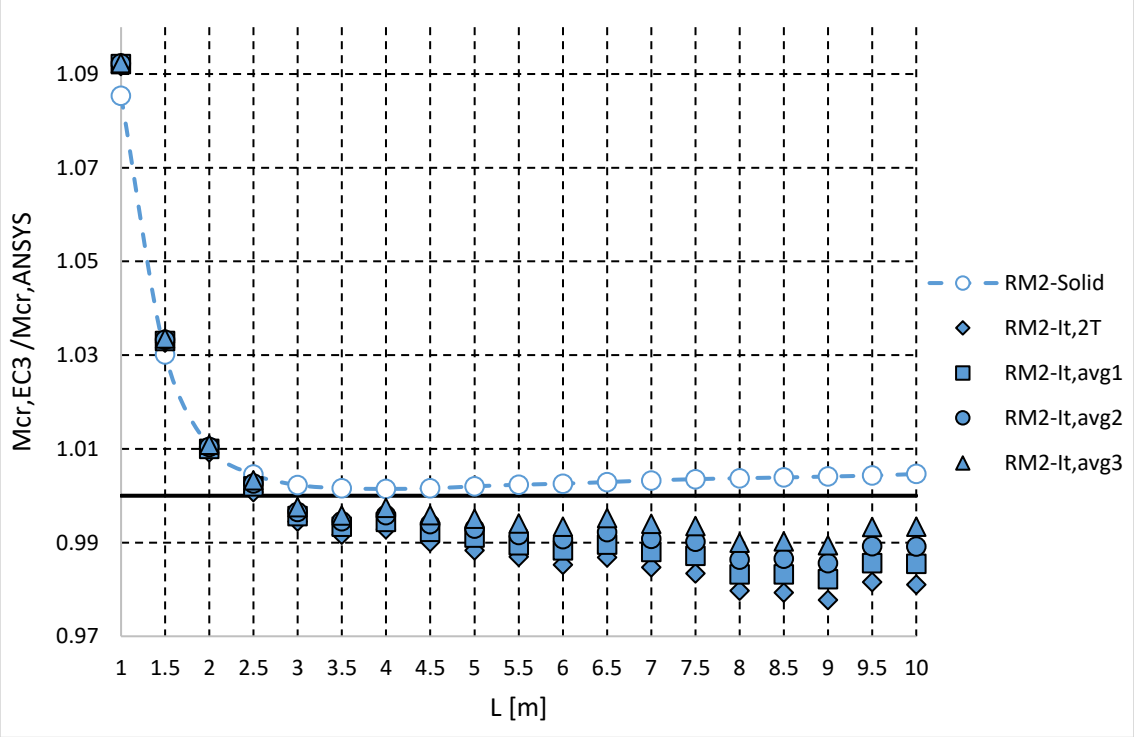
1.09
1.07
1.05
1.03
1.01
0.99
0.97
Mcr,EC3 /Mcr,ANSYS
1 1.5 2 2.5 3 3.5 4 4.5 5 5.5 6 6.5 7 7.5 8 8.5 9 9.5 10
L [m]
RM2-Solid
RM2-It,2T
RM2-It,avg1
RM2-It,avg2
RM2-It,avg3

$$S = 1.7a_0$$

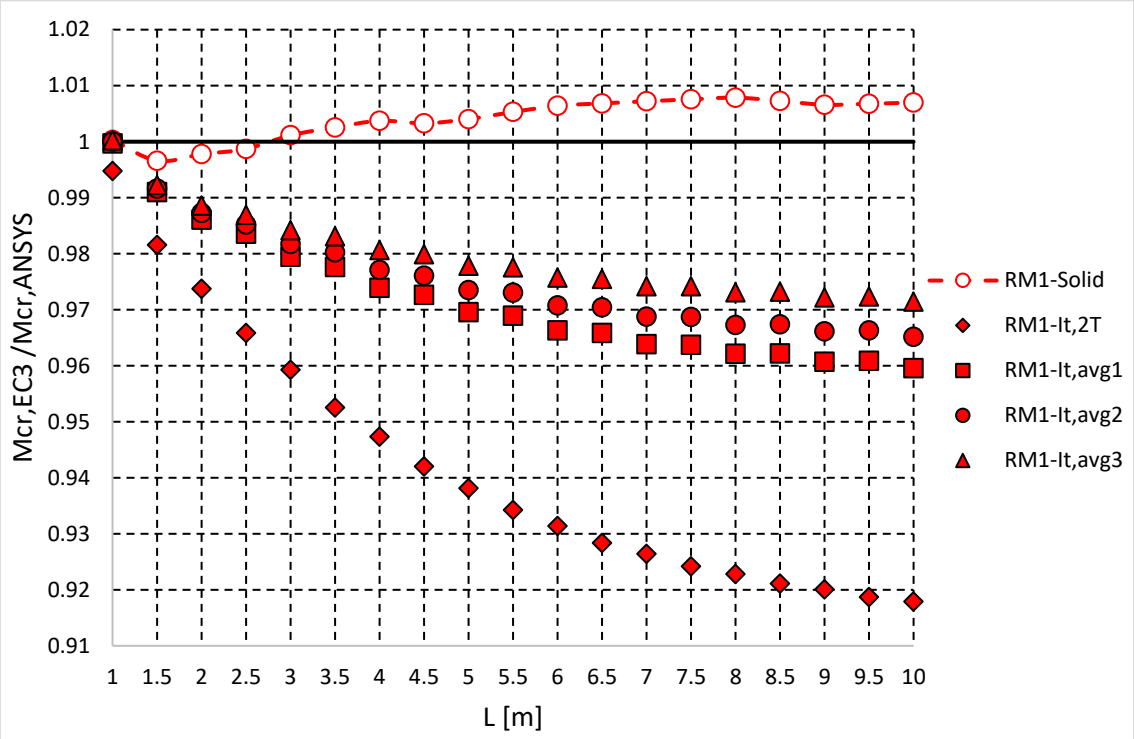
1.02
1.01
1
0.99
0.98
0.97
0.96
0.95
0.94
0.93
0.92
0.91
Mcr,EC3 /Mcr,ANSYS
1 1.5 2 2.5 3 3.5 4 4.5 5 5.5 6 6.5 7 7.5 8 8.5 9 9.5 10
L [m]
RM1-Solid
RM1-It,2T
RM1-It,avg1
RM1-It,avg2
RM1-It,avg3

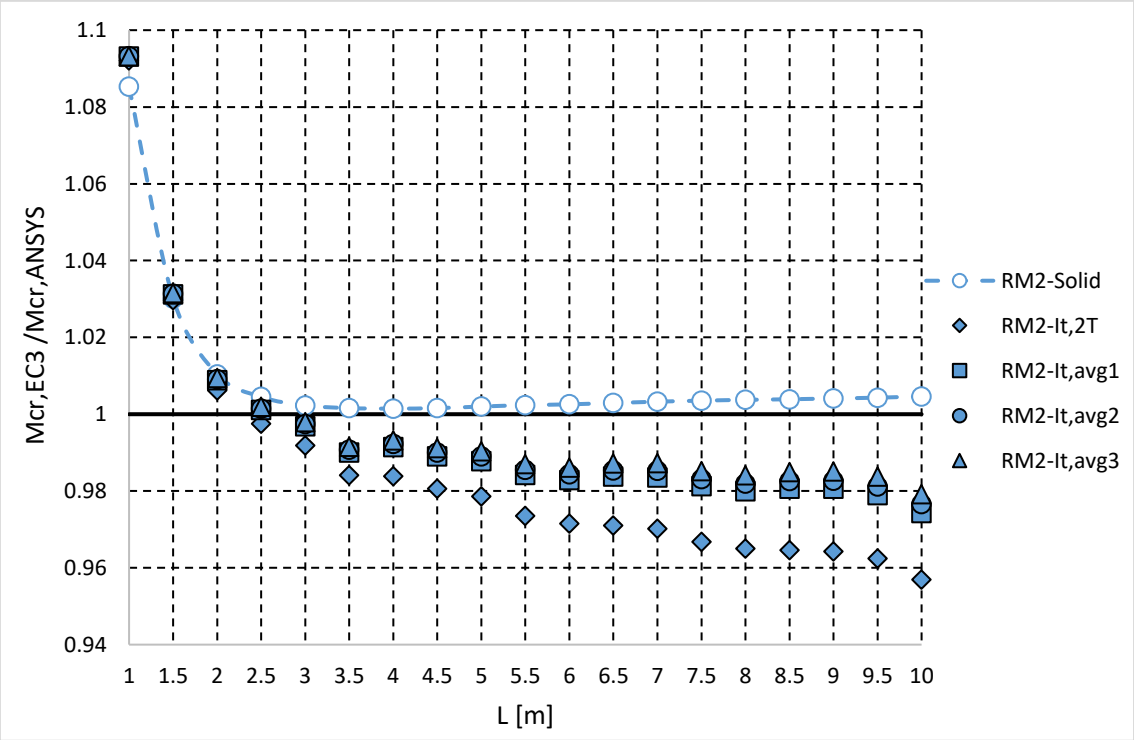
1.1
1.08
1.06
1.04
1.02
1
0.98
0.96
0.94
Mcr,EC3 /Mcr,ANSYS
1 1.5 2 2.5 3 3.5 4 4.5 5 5.5 6 6.5 7 7.5 8 8.5 9 9.5 10
L [m]
RM2-Solid
RM2-It,2T
RM2-It,avg1
RM2-It,avg2
RM2-It,avg3

$$H = 1.3h$$

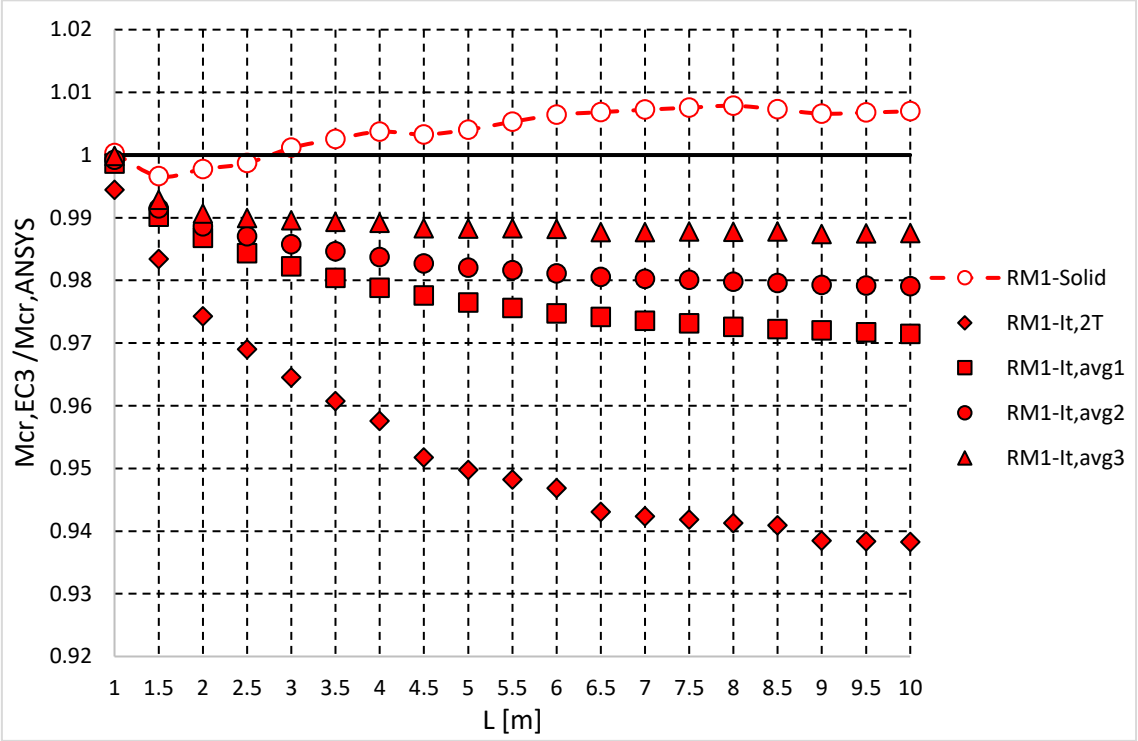
1.02
1.01
1
0.99
0.98
0.97
0.96
0.95
0.94
0.93
0.92
Mcr,EC3 /Mcr,ANSYS
1 1.5 2 2.5 3 3.5 4 4.5 5 5.5 6 6.5 7 7.5 8 8.5 9 9.5 10
L [m]
RM1-Solid
RM1-It,2T
RM1-It,avg1
RM1-It,avg2
RM1-It,avg3

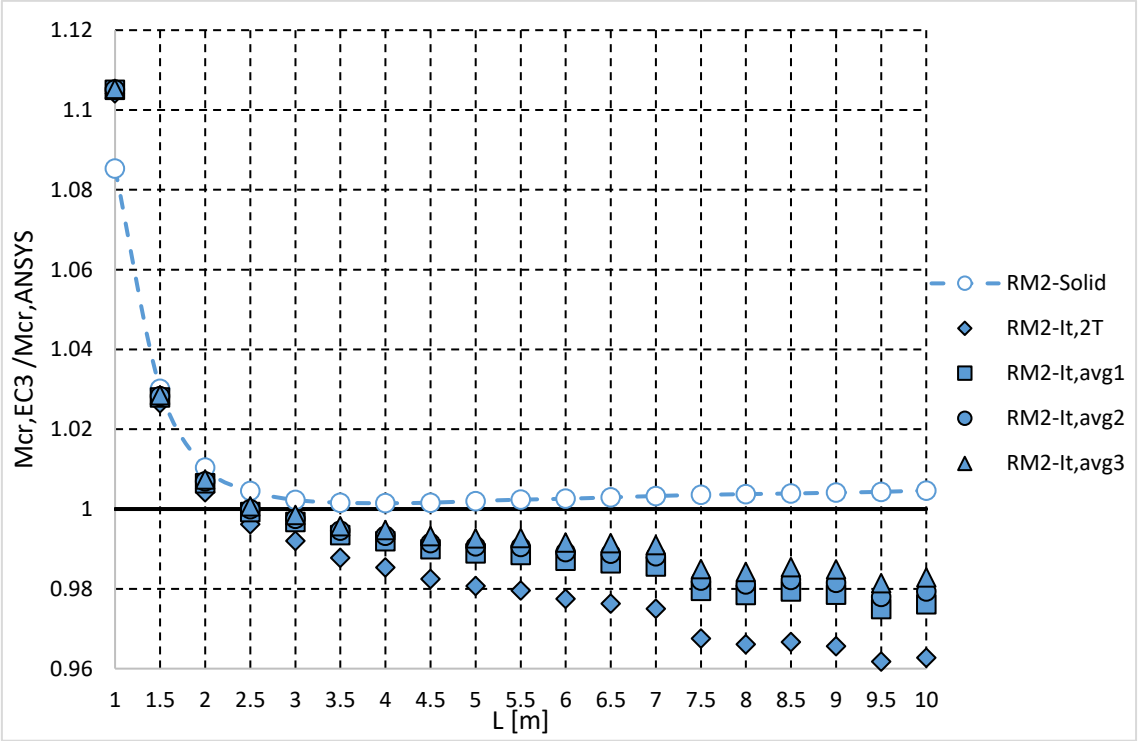
1.12
1.1
1.08
1.06
1.04
1.02
1
0.98
0.96
Mcr,EC3 /Mcr,ANSYS
1 1.5 2 2.5 3 3.5 4 4.5 5 5.5 6 6.5 7 7.5 8 8.5 9 9.5 10
L [m]
RM2-Solid
RM2-It,2T
RM2-It,avg1
RM2-It,avg2
RM2-It,avg3

$$H = 1.6h$$

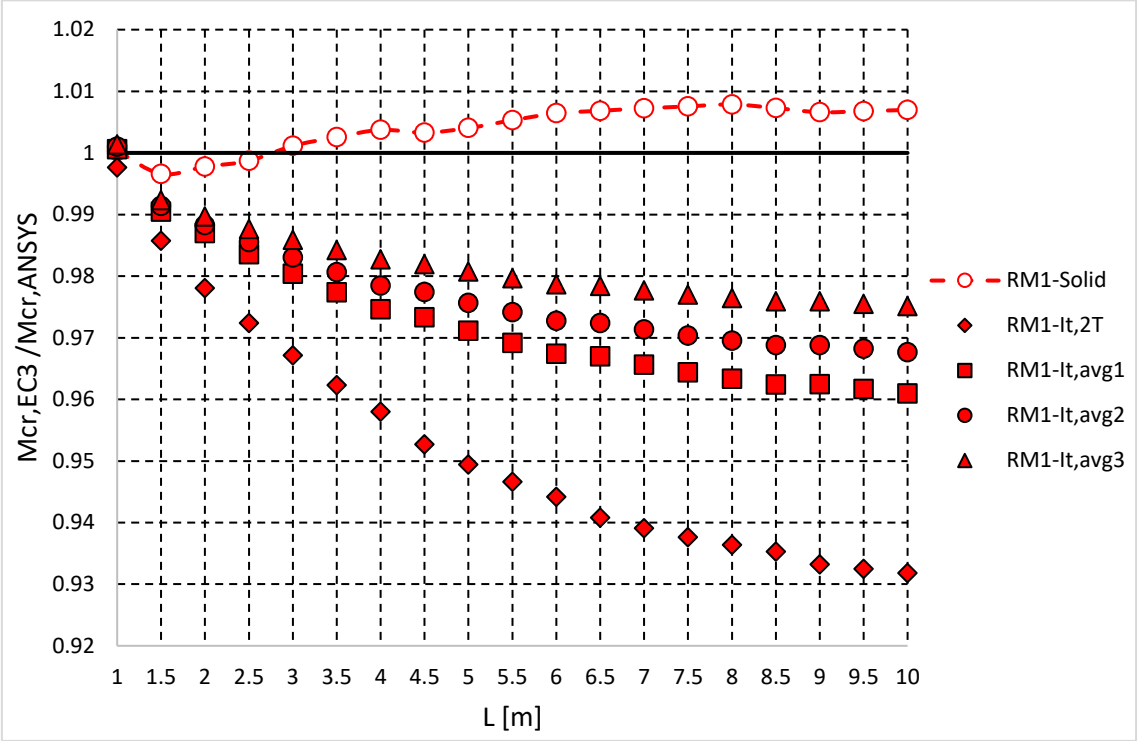
1.02
1.01
1
0.99
0.98
0.97
0.96
0.95
0.94
0.93
0.92
Mcr,EC3 /Mcr,ANSYS
1 1.5 2 2.5 3 3.5 4 4.5 5 5.5 6 6.5 7 7.5 8 8.5 9 9.5 10
L [m]
RM1-Solid
RM1-It,2T
RM1-It,avg1
RM1-It,avg2
RM1-It,avg3

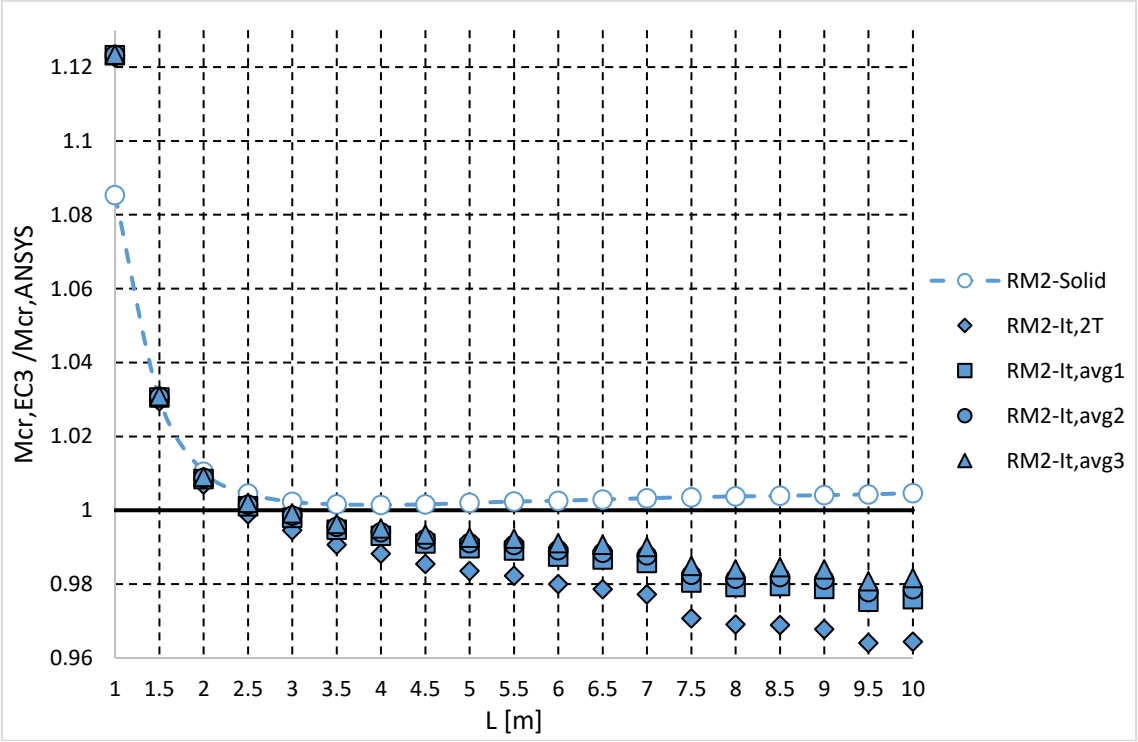
1.12
1.1
1.08
1.06
1.04
1.02
1
0.98
0.96
Mcr,EC3 /Mcr,ANSYS
1 1.5 2 2.5 3 3.5 4 4.5 5 5.5 6 6.5 7 7.5 8 8.5 9 9.5 10
L [m]
RM2-Solid
RM2-It,2T
RM2-It,avg1
RM2-It,avg2
RM2-It,avg3

ANNEX E – Graphs of the analytical critical moment divided by the ANSYS critical moment, varying the geometric parameters of the cellular beam

RM1-$I_{t,2T}$

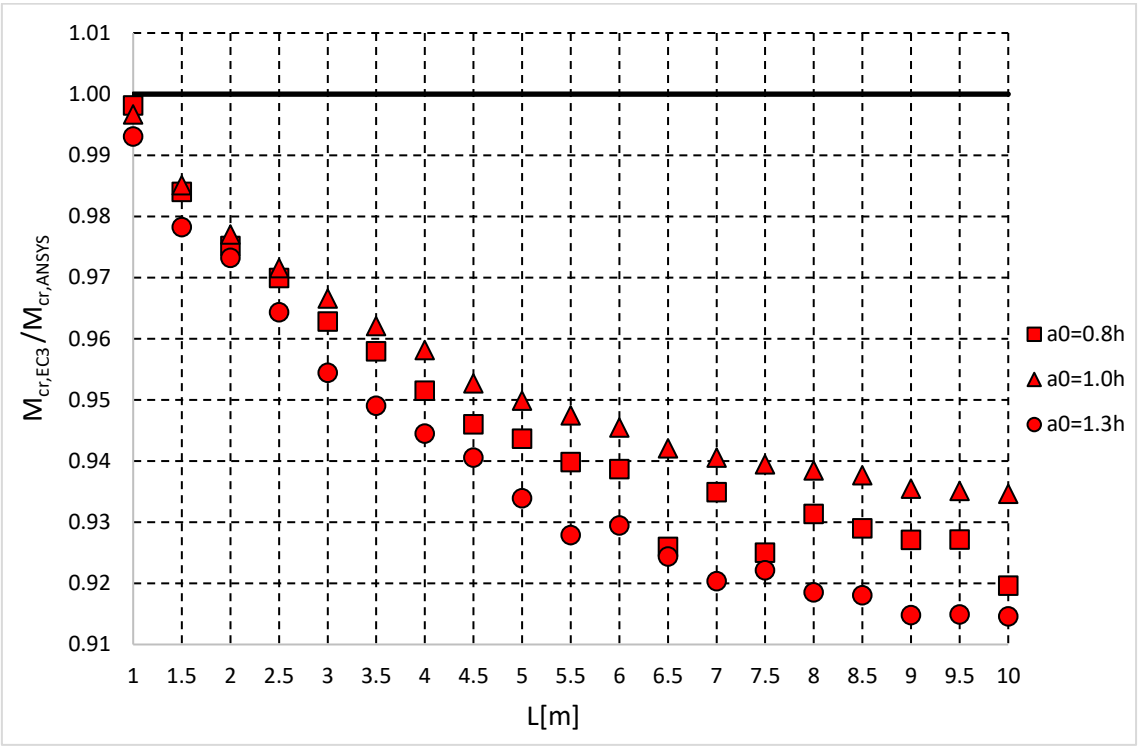

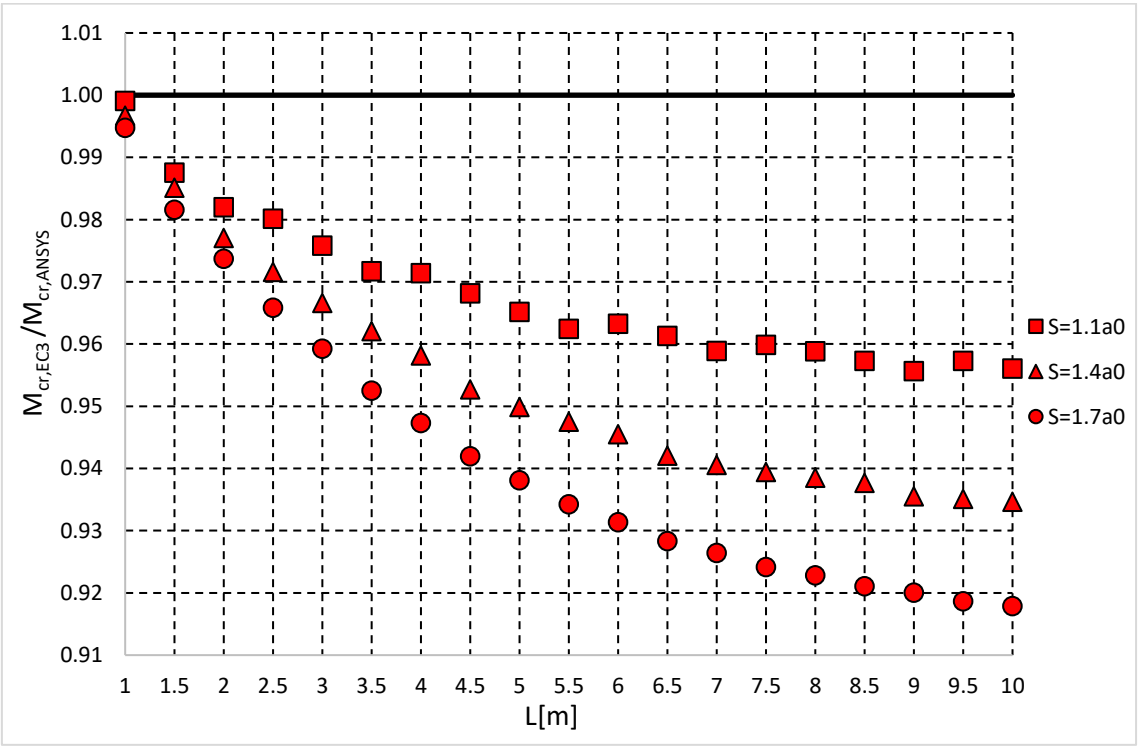

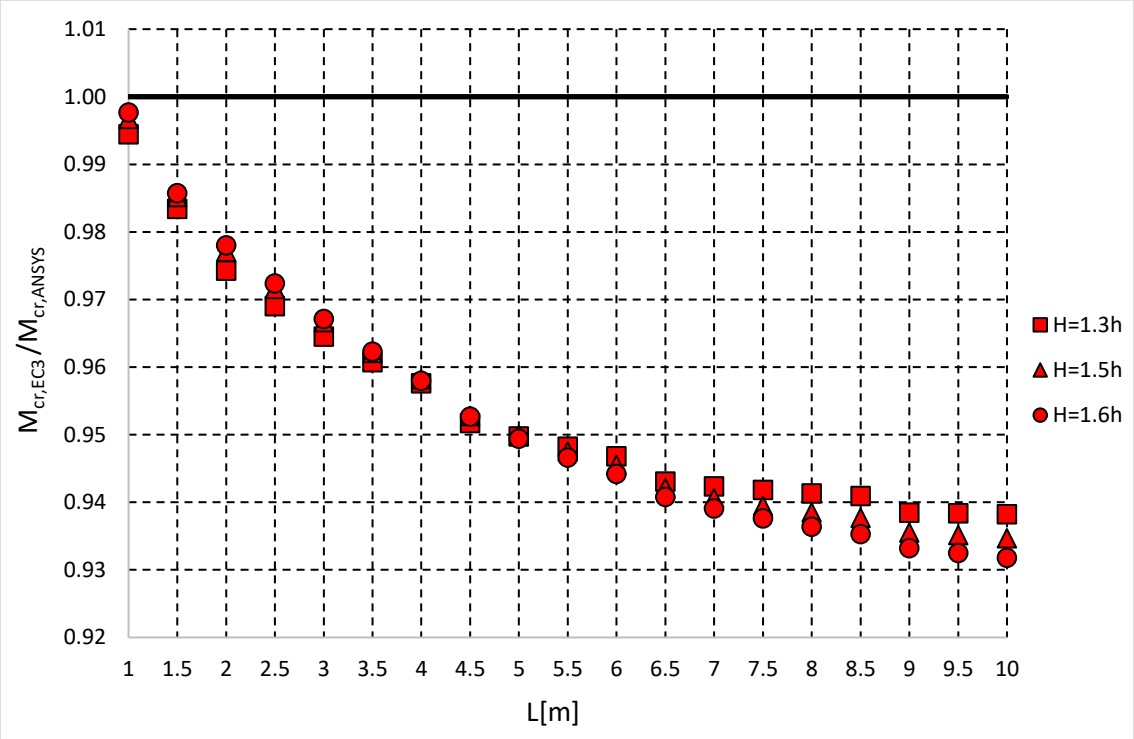
1.01
1.00
0.99
0.98
0.97
0.96
0.95
0.94
0.93
0.92
$M_{cr,EC3}/M_{cr,ANSYS}$
1
1.5
2
2.5
3
3.5
4
4.5
5
5.5
6
6.5
7
7.5
8
8.5
9
9.5
10
L[m]
H=1.3h
H=1.5h
H=1.6h

RM2-$I_{t,2T}$

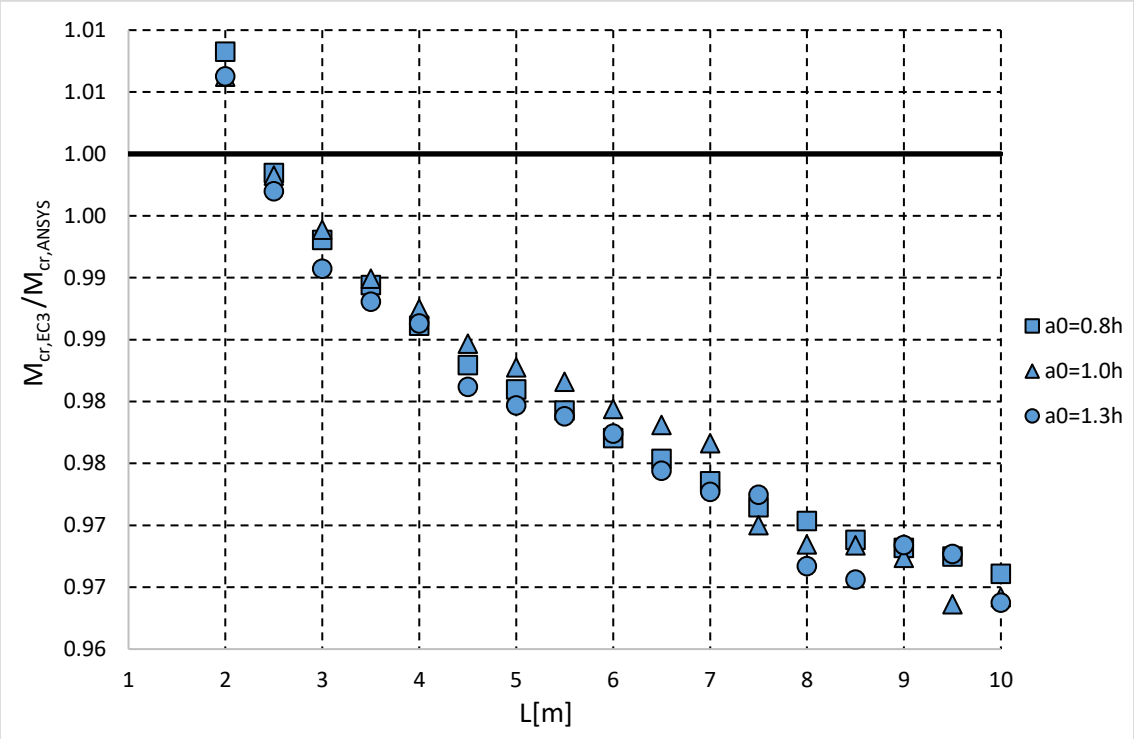
1.01
1.01
1.00
1.00
0.99
0.99
0.98
0.98
0.97
0.97
0.96
1
2
3
4
5
6
7
8
9
10
L[m]
M_cr,EC3 /M_cr,ANSYS
a0=0.8h
a0=1.0h
a0=1.3h

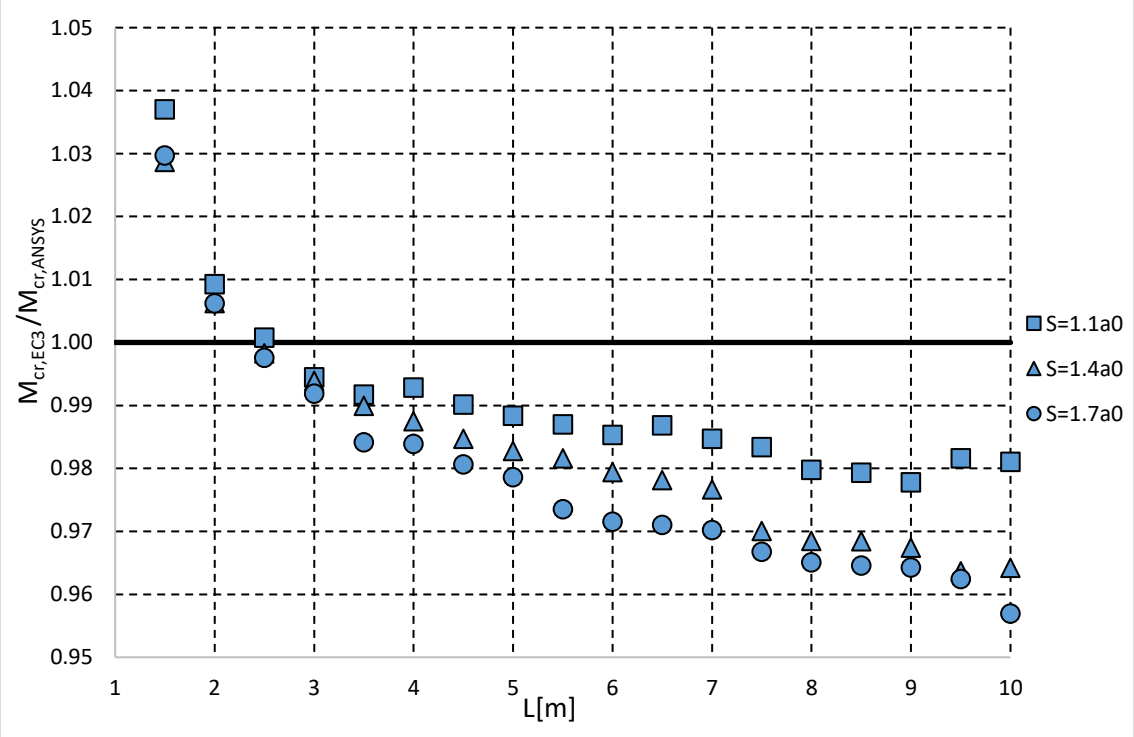
1.05
1.04
1.03
1.02
1.01
1.00
0.99
0.98
0.97
0.96
0.95
1
2
3
4
5
6
7
8
9
10
L[m]
M_cr,EC3 /M_cr,ANSYS
S=1.1a0
S=1.4a0
S=1.7a0

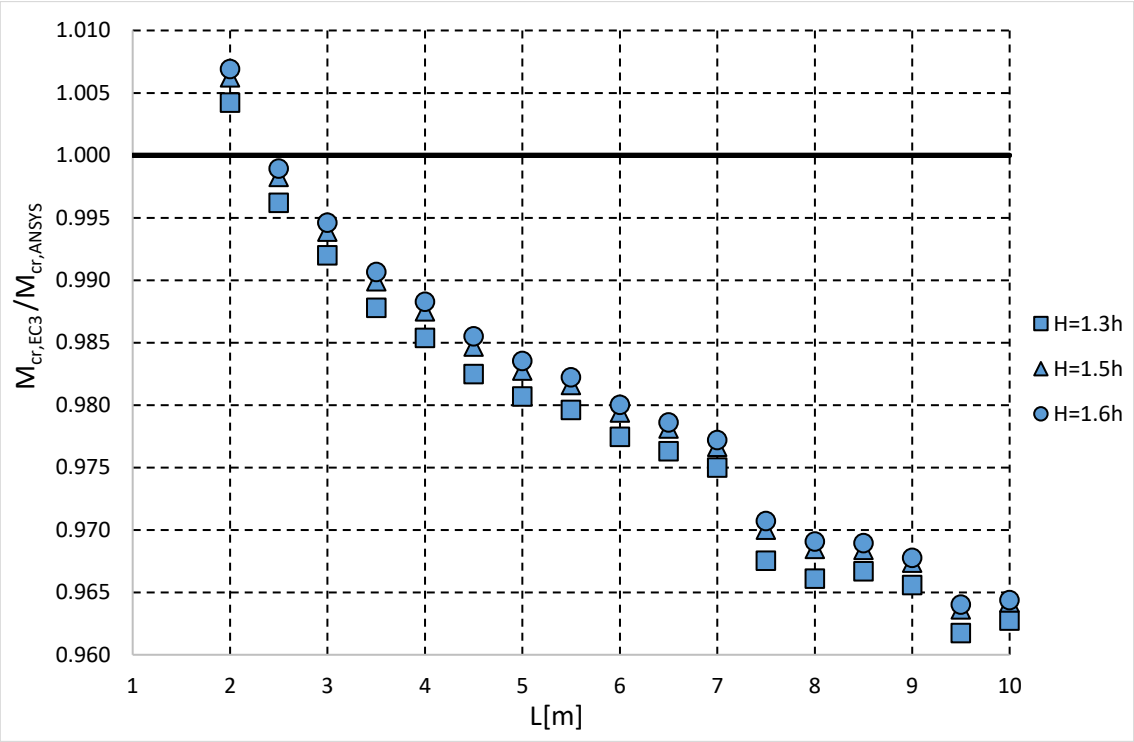
1.010
1.005
1.000
0.995
0.990
0.985
0.980
0.975
0.970
0.965
0.960
$M_{cr,EC3}/M_{cr,ANSYS}$
1
2
3
4
5
6
7
8
9
10
L[m]
H=1.3h
H=1.5h
H=1.6h

RM1-$I_{t,avg1}$

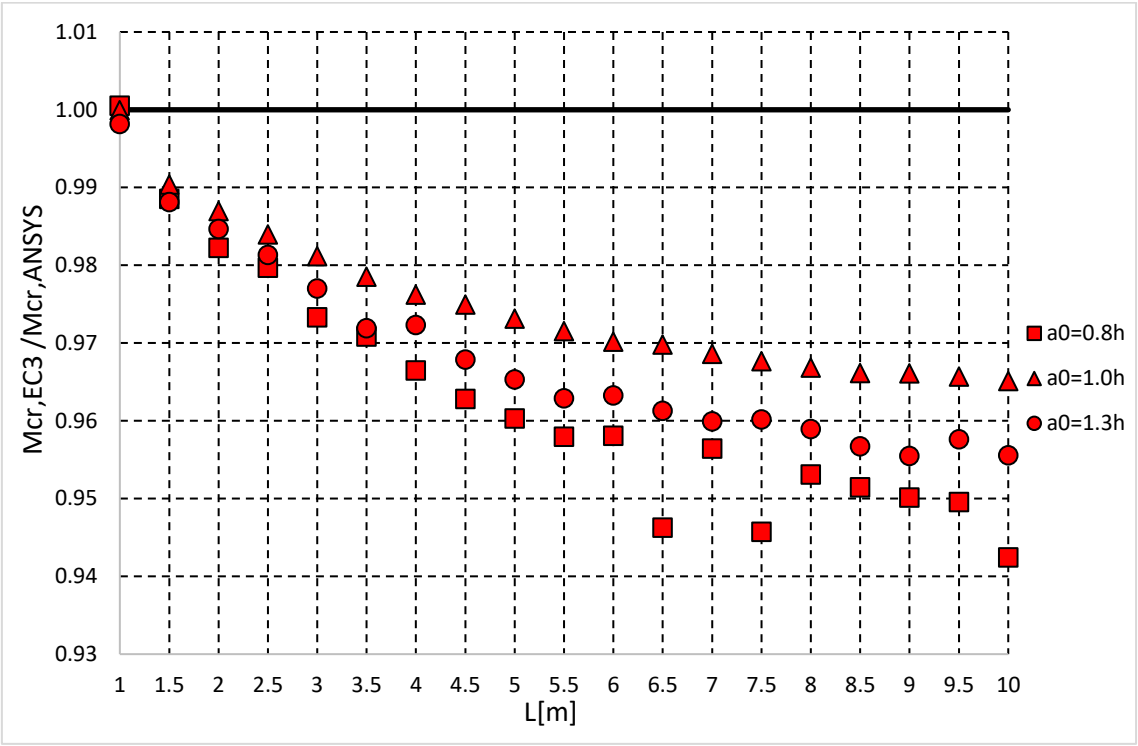
1.01
1.00
0.99
0.98
0.97
0.96
0.95
0.94
0.93
Mcr,EC3 /Mcr,ANSYS
1 1.5 2 2.5 3 3.5 4 4.5 5 5.5 6 6.5 7 7.5 8 8.5 9 9.5 10
L[m]
a0=0.8h
a0=1.0h
a0=1.3h

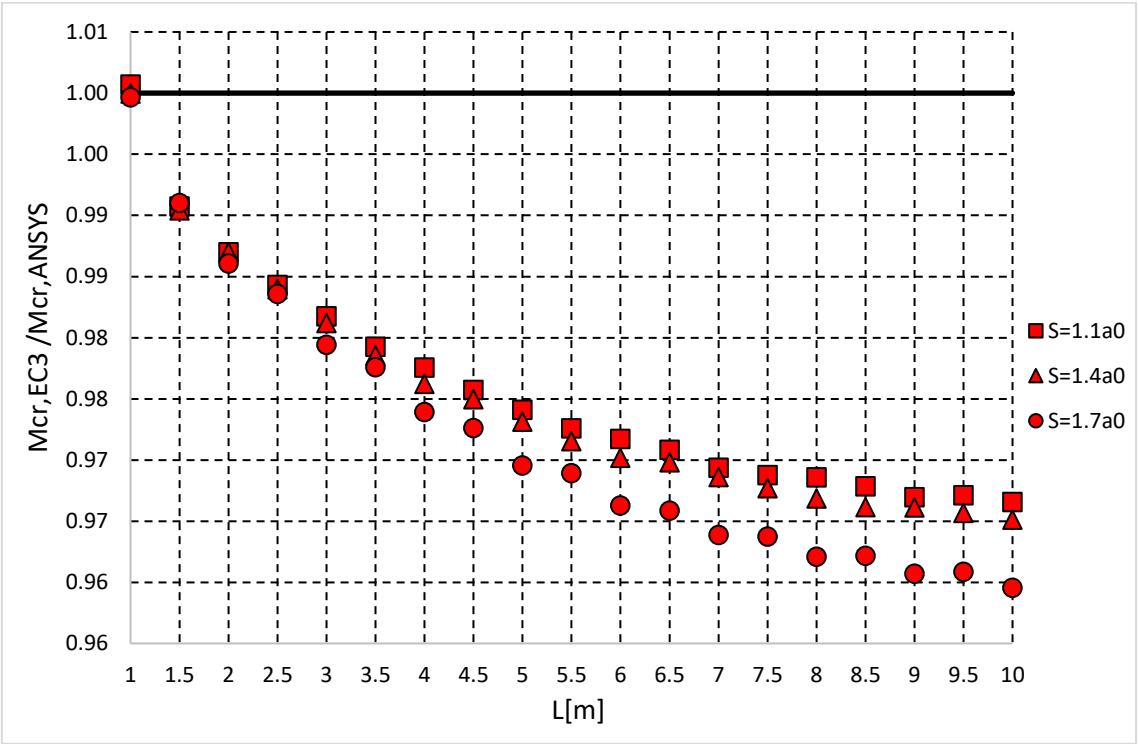
1.01
1.00
1.00
0.99
0.99
0.98
0.98
0.97
0.97
0.96
0.96
Mcr,EC3 /Mcr,ANSYS
1 1.5 2 2.5 3 3.5 4 4.5 5 5.5 6 6.5 7 7.5 8 8.5 9 9.5 10
L[m]
S=1.1a0
S=1.4a0
S=1.7a0

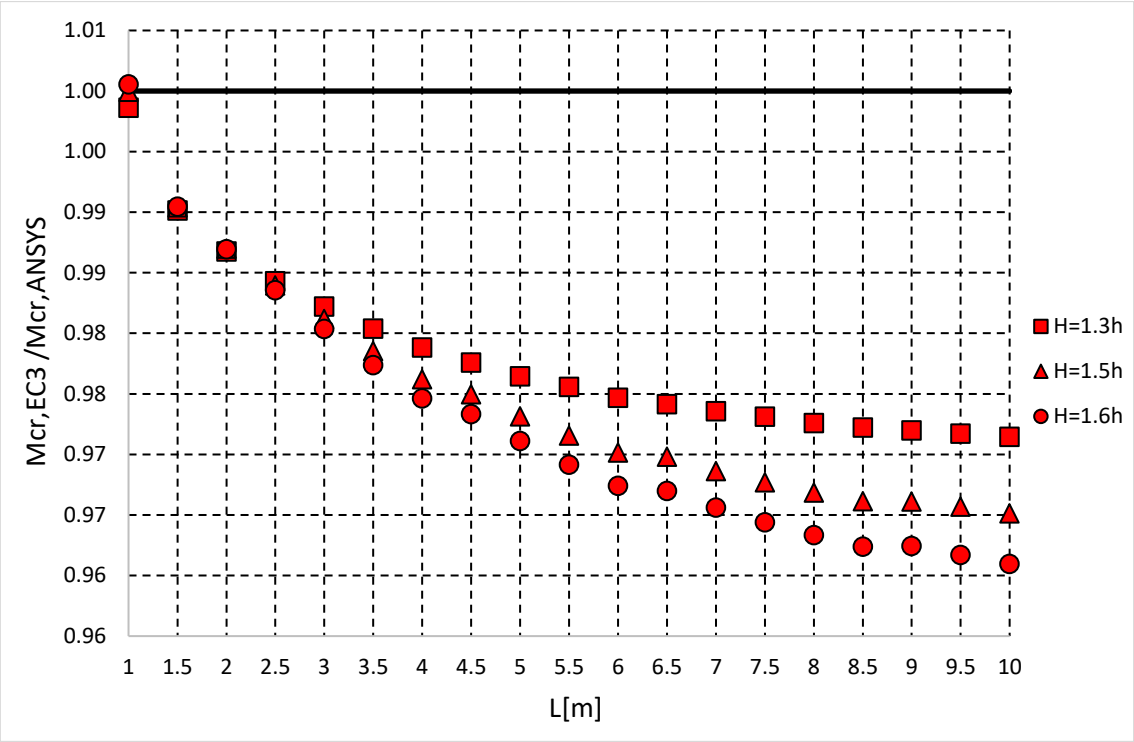
1.01
1.00
1.00
0.99
0.99
0.98
0.98
0.97
0.97
0.96
0.96
Mcr,EC3 /Mcr,ANSYS
1
1.5
2
2.5
3
3.5
4
4.5
5
5.5
6
6.5
7
7.5
8
8.5
9
9.5
10
L[m]
H=1.3h
H=1.5h
H=1.6h

RM2-$I_{t,avg1}$

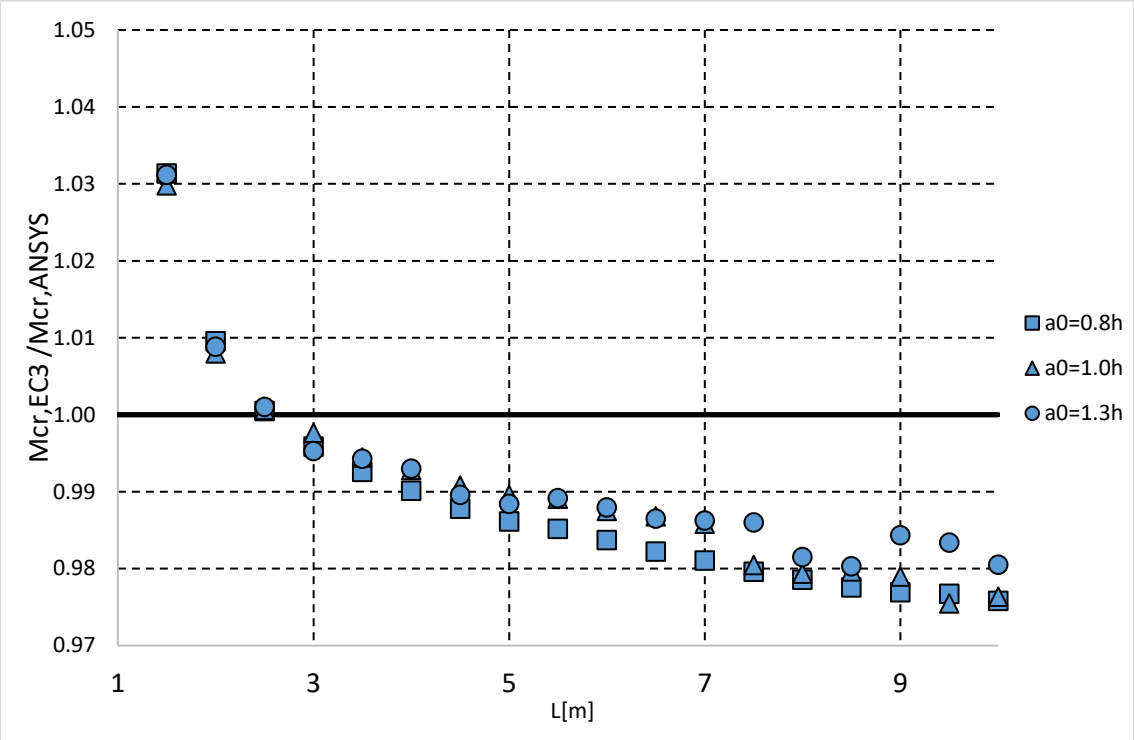
1.05
1.04
1.03
1.02
1.01
1.00
0.99
0.98
0.97
Mcr,EC3 /Mcr,ANSYS
1
3
5
7
9
L[m]
a0=0.8h
a0=1.0h
a0=1.3h

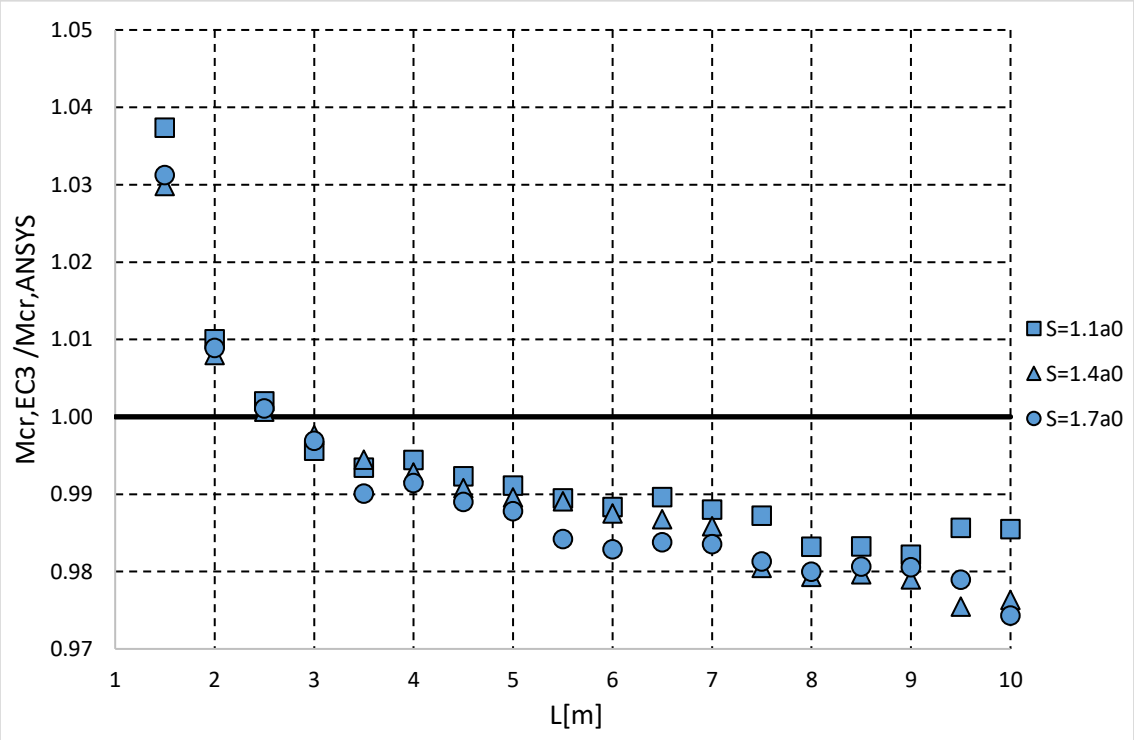
1.05
1.04
1.03
1.02
1.01
1.00
0.99
0.98
0.97
Mcr,EC3 /Mcr,ANSYS
1
2
3
4
5
6
7
8
9
10
L[m]
S=1.1a0
S=1.4a0
S=1.7a0

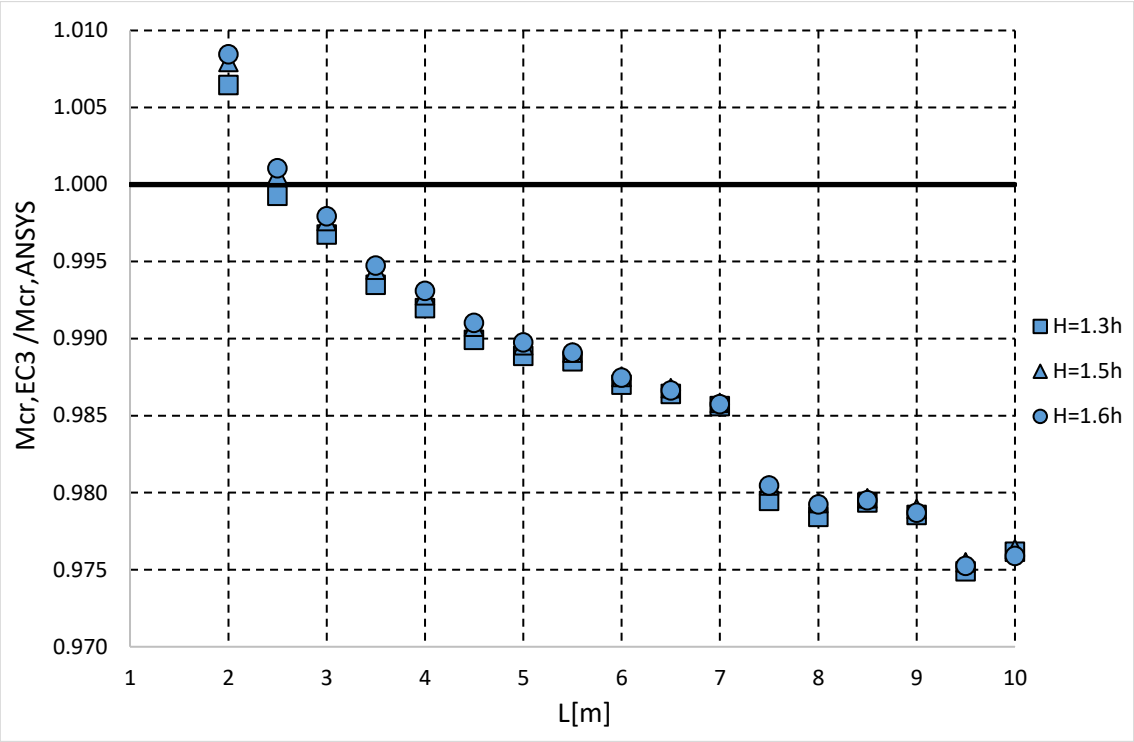
1.010
1.005
1.000
0.995
0.990
0.985
0.980
0.975
0.970
Mcr,EC3 /Mcr,ANSYS
1
2
3
4
5
6
7
8
9
10
L[m]
H=1.3h
H=1.5h
H=1.6h

RM1-$I_{t,avg2}$

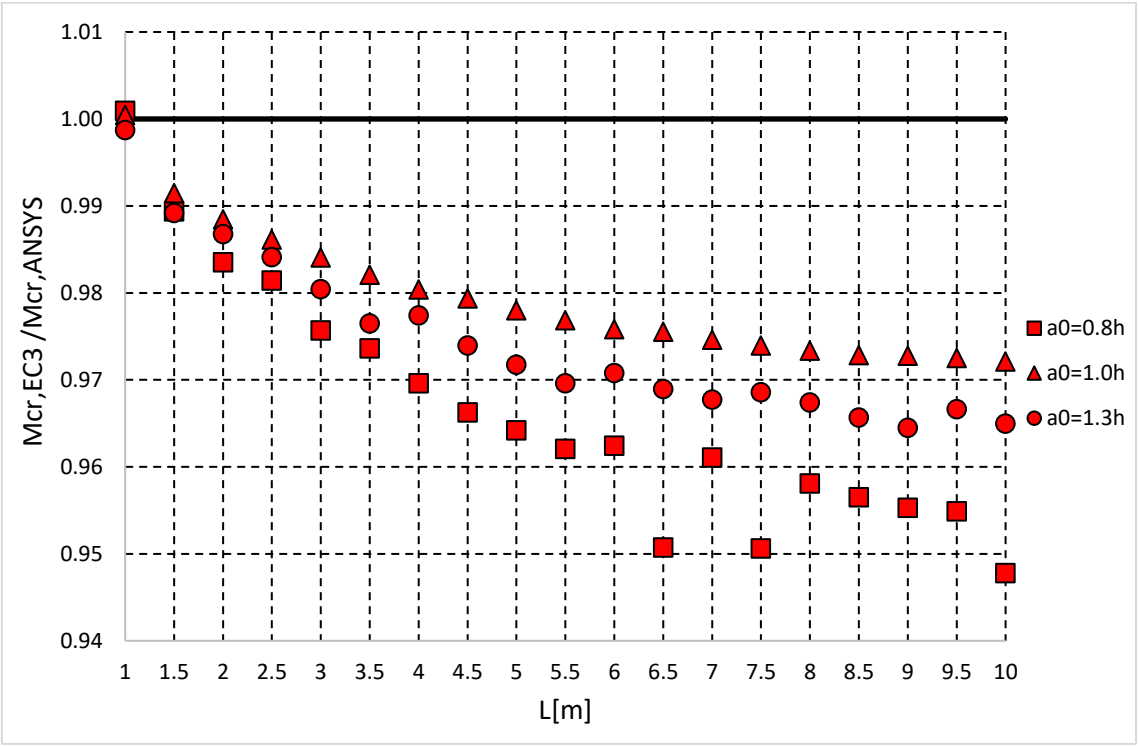
1.01
1.00
0.99
0.98
0.97
0.96
0.95
0.94
Mcr,EC3 /Mcr,ANSYS
1
1.5
2
2.5
3
3.5
4
4.5
5
5.5
6
6.5
7
7.5
8
8.5
9
9.5
10
L[m]
a0=0.8h
a0=1.0h
a0=1.3h

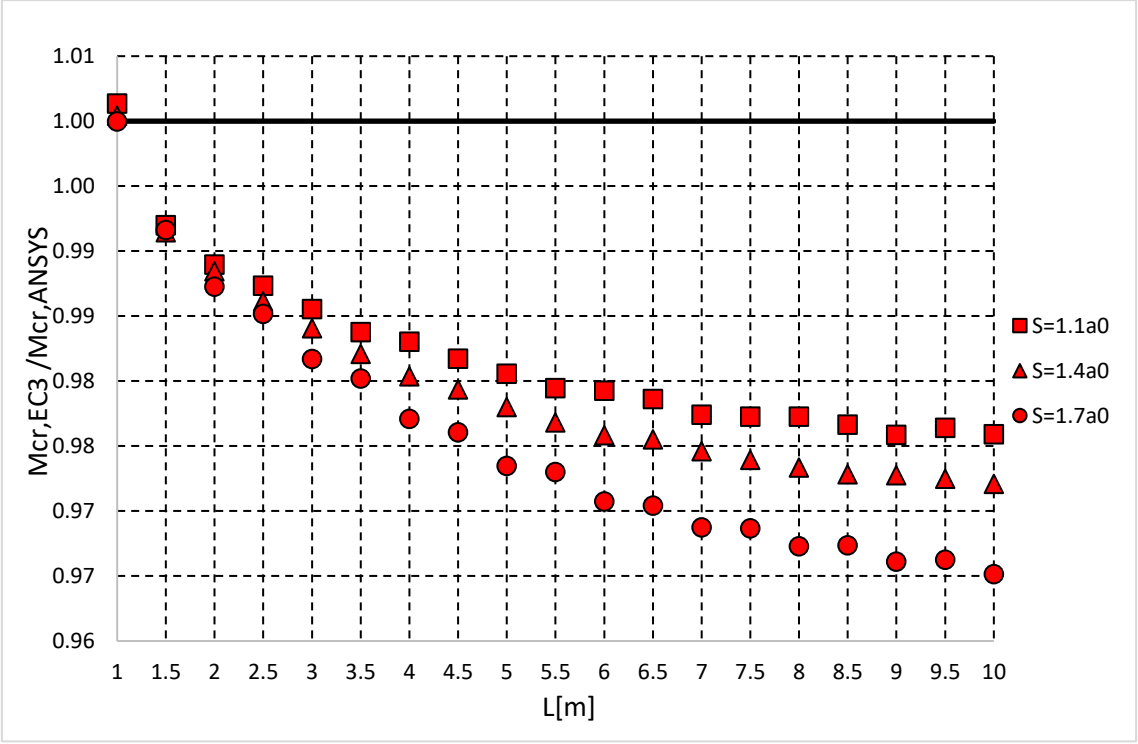
1.01
1.00
1.00
0.99
0.99
0.98
0.98
0.97
0.97
0.96
Mcr,EC3 /Mcr,ANSYS
1
1.5
2
2.5
3
3.5
4
4.5
5
5.5
6
6.5
7
7.5
8
8.5
9
9.5
10
L[m]
S=1.1a0
S=1.4a0
S=1.7a0

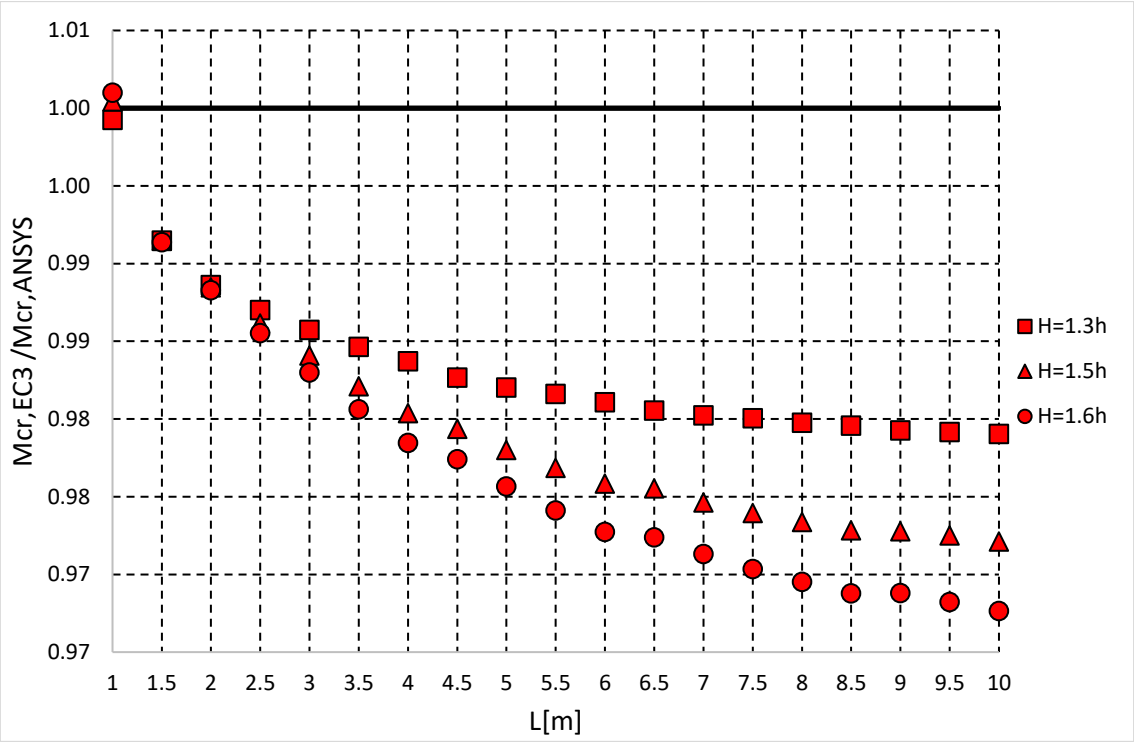
1.01
1.00
1.00
0.99
0.99
0.98
0.98
0.97
0.97
Mcr,EC3 /Mcr,ANSYS
1
1.5
2
2.5
3
3.5
4
4.5
5
5.5
6
6.5
7
7.5
8
8.5
9
9.5
10
L[m]
H=1.3h
H=1.5h
H=1.6h

RM2-$I_{t,avg2}$

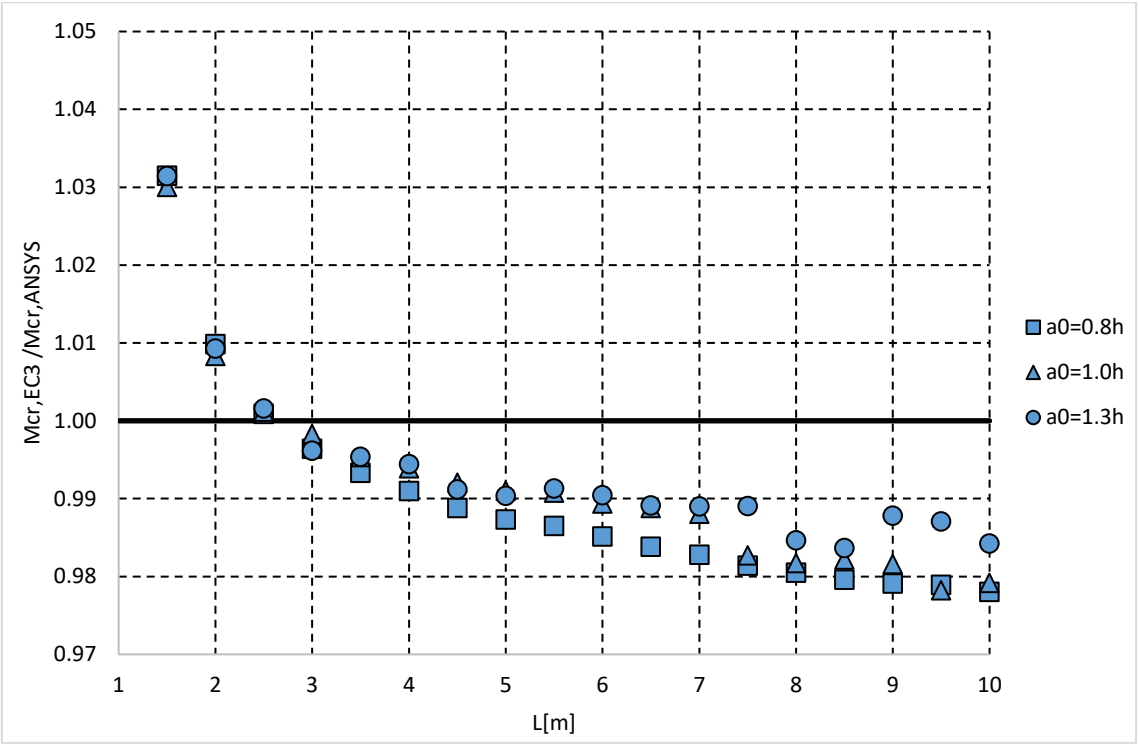
1.05
1.04
1.03
1.02
1.01
1.00
0.99
0.98
0.97
Mcr,EC3 /Mcr,ANSYS
1
2
3
4
5
6
7
8
9
10
L[m]
a0=0.8h
a0=1.0h
a0=1.3h

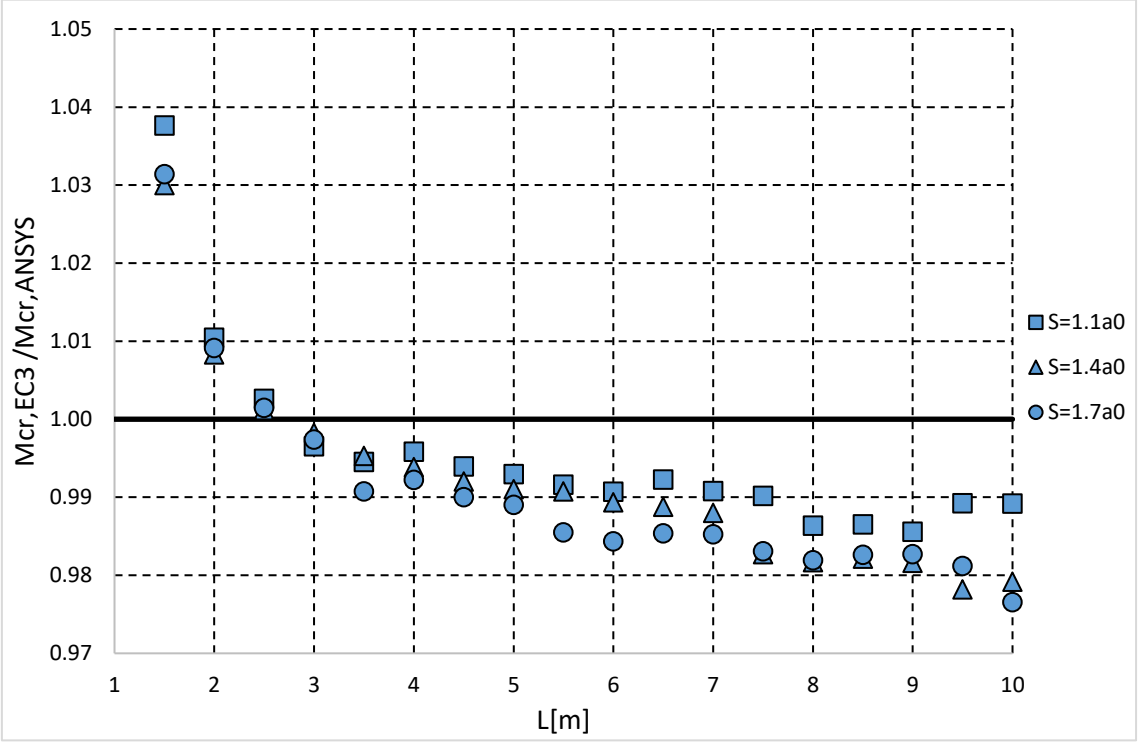
1.05
1.04
1.03
1.02
1.01
1.00
0.99
0.98
0.97
Mcr,EC3 /Mcr,ANSYS
1
2
3
4
5
6
7
8
9
10
L[m]
S=1.1a0
S=1.4a0
S=1.7a0

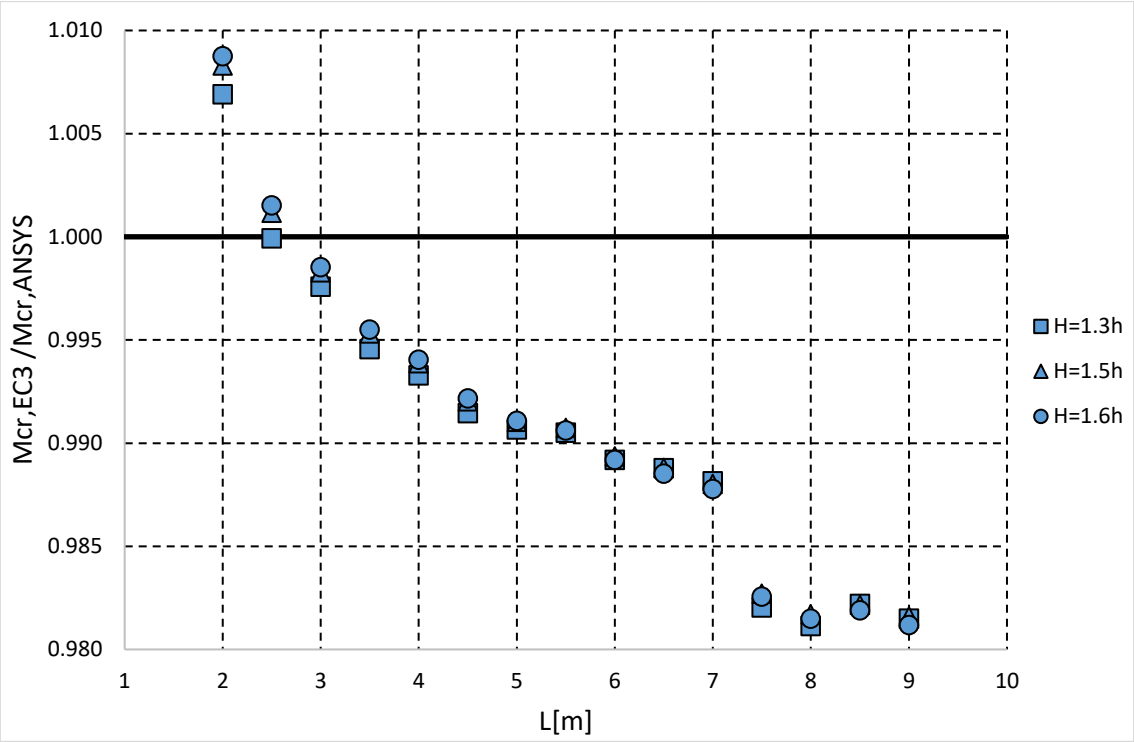
1.010
1.005
1.000
0.995
0.990
0.985
0.980
Mcr,EC3 /Mcr,ANSYS
1
2
3
4
5
6
7
8
9
10
L[m]
H=1.3h
H=1.5h
H=1.6h

RM1-$I_{t,avg3}$

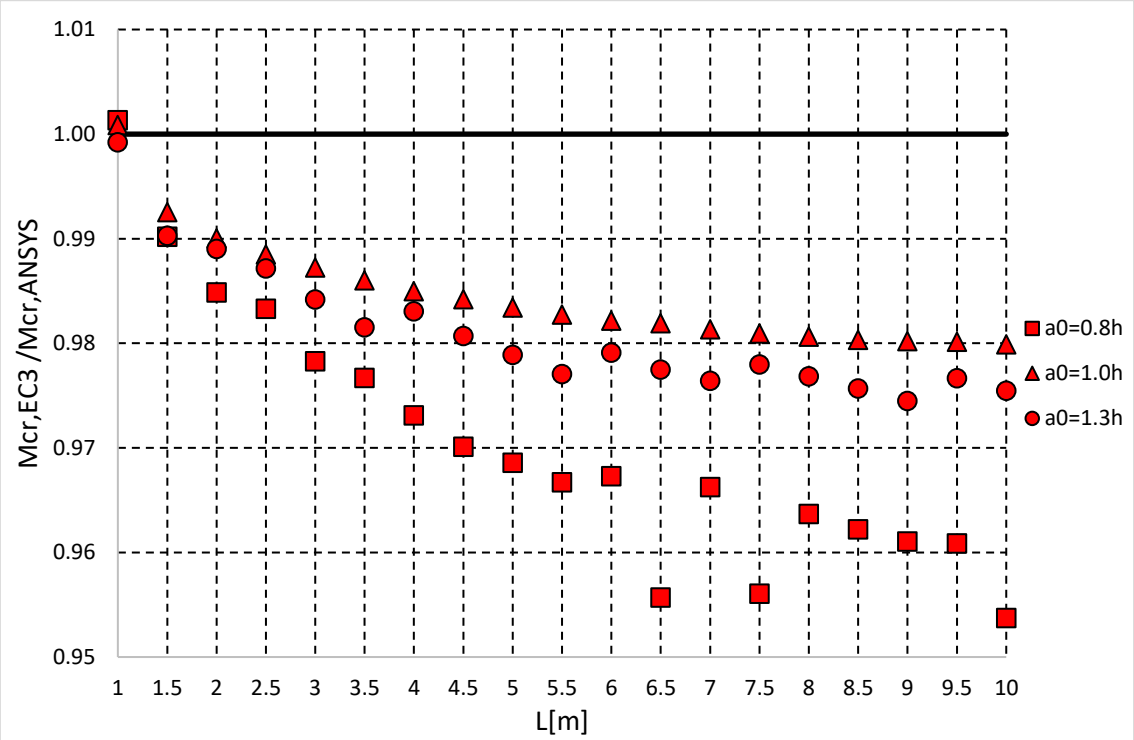
1.01
1.00
0.99
0.98
0.97
0.96
0.95
Mcr,EC3 /Mcr,ANSYS
1 1.5 2 2.5 3 3.5 4 4.5 5 5.5 6 6.5 7 7.5 8 8.5 9 9.5 10
L[m]
a0=0.8h
a0=1.0h
a0=1.3h

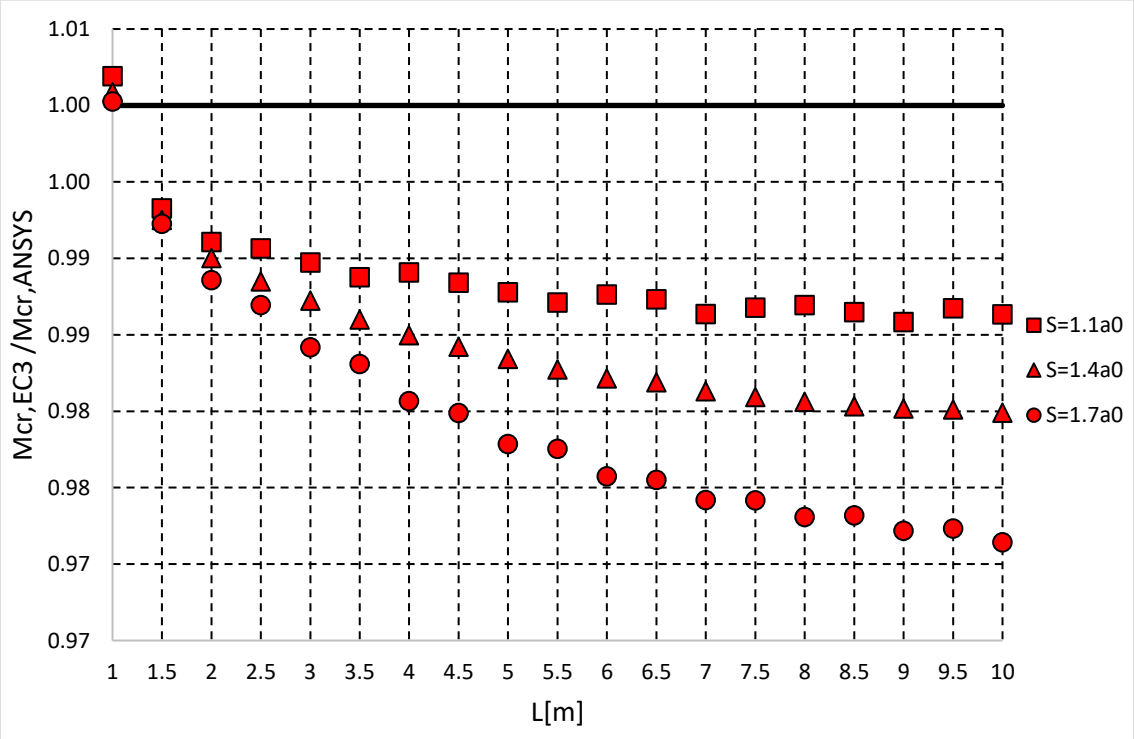
1.01
1.00
1.00
0.99
0.99
0.98
0.98
0.97
0.97
Mcr,EC3 /Mcr,ANSYS
1 1.5 2 2.5 3 3.5 4 4.5 5 5.5 6 6.5 7 7.5 8 8.5 9 9.5 10
L[m]
S=1.1a0
S=1.4a0
S=1.7a0

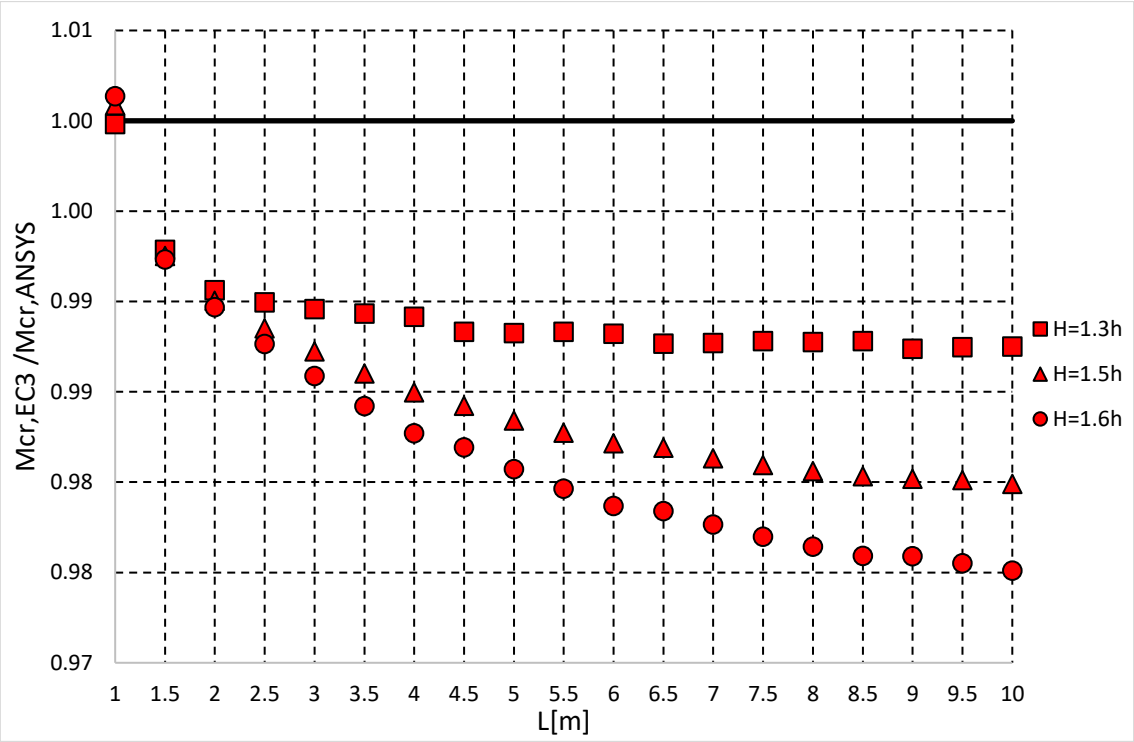
1.01
1.00
1.00
0.99
0.99
0.98
0.98
0.97
Mcr,EC3 /Mcr,ANSYS
1
1.5
2
2.5
3
3.5
4
4.5
5
5.5
6
6.5
7
7.5
8
8.5
9
9.5
10
L[m]
H=1.3h
H=1.5h
H=1.6h

RM2-$I_{t,avg3}$

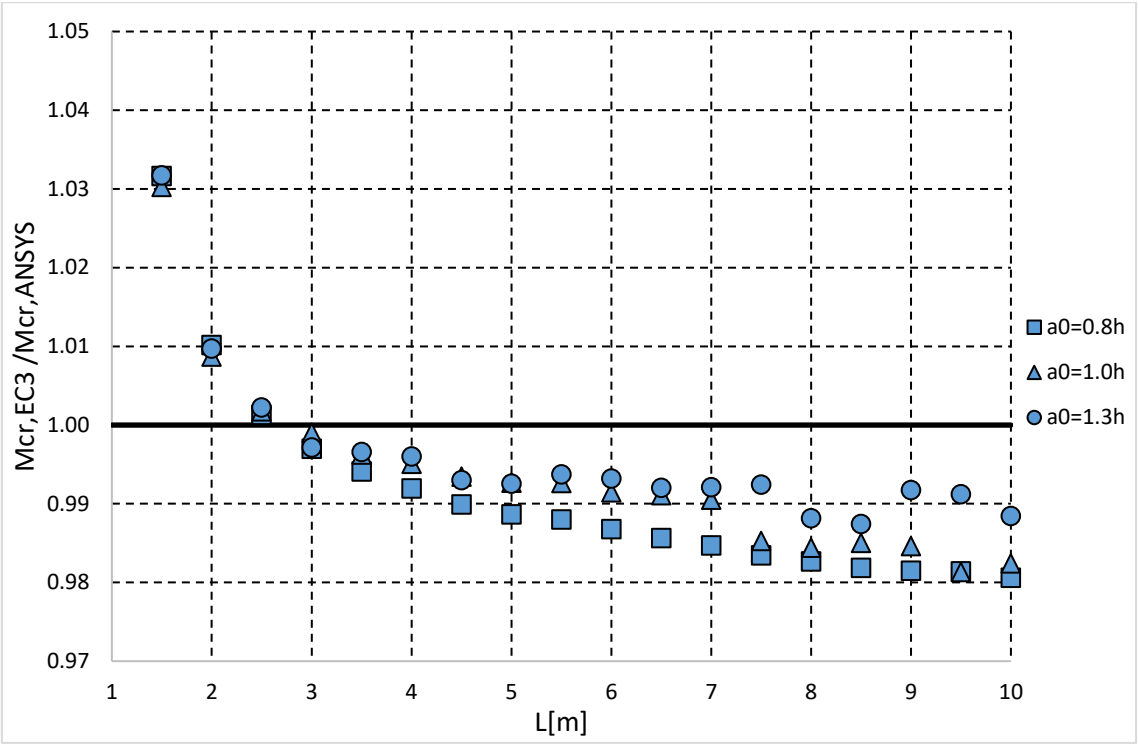
1.05
1.04
1.03
1.02
1.01
1.00
0.99
0.98
0.97
Mcr,EC3 /Mcr,ANSYS
1
2
3
4
5
6
7
8
9
10
L[m]
a0=0.8h
a0=1.0h
a0=1.3h

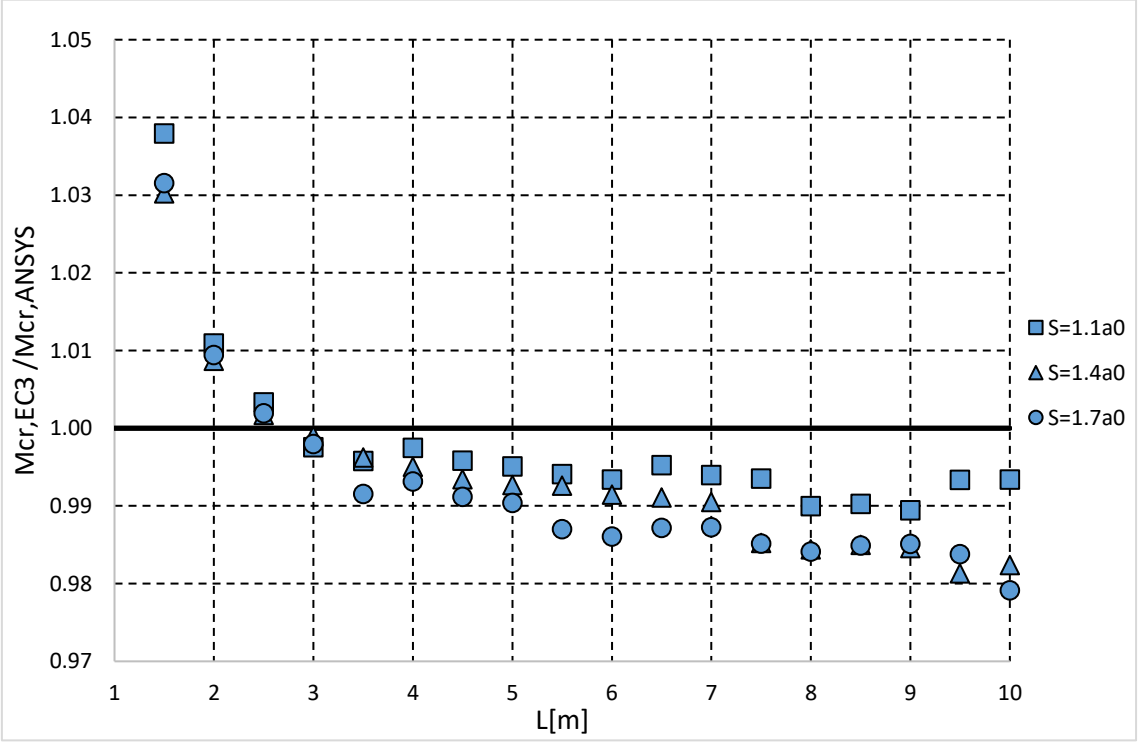
1.05
1.04
1.03
1.02
1.01
1.00
0.99
0.98
0.97
Mcr,EC3 /Mcr,ANSYS
1
2
3
4
5
6
7
8
9
10
L[m]
S=1.1a0
S=1.4a0
S=1.7a0

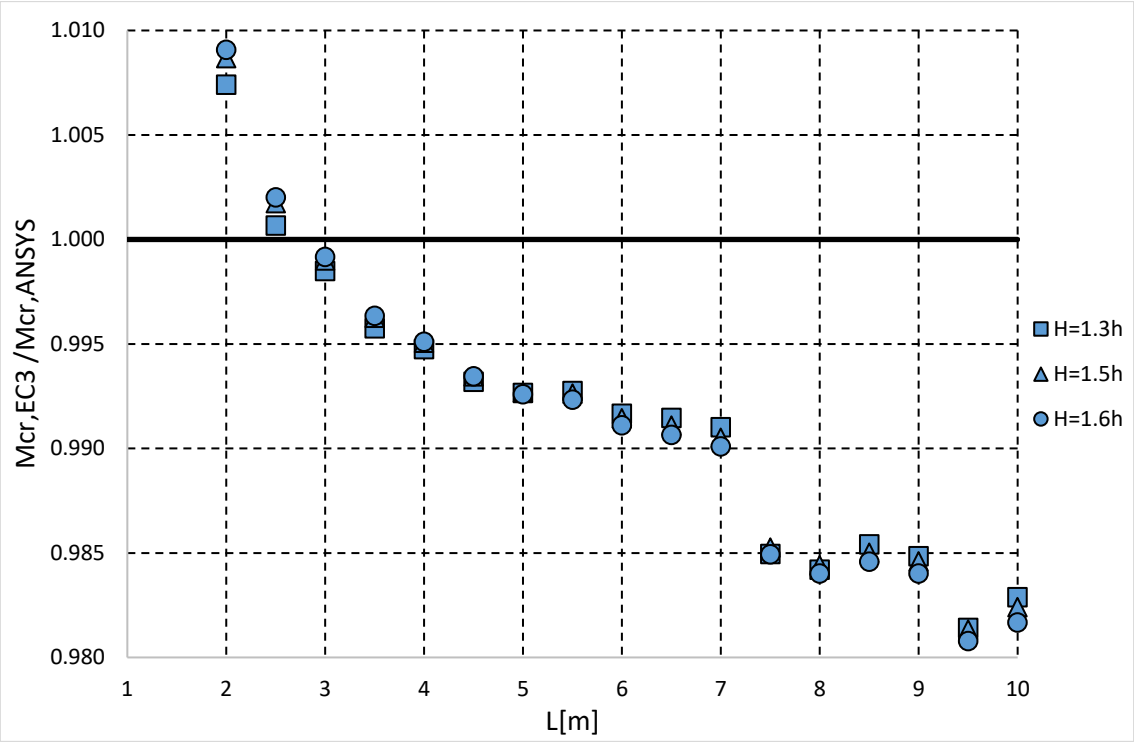
1.010
1.005
1.000
0.995
0.990
0.985
0.980
Mcr,EC3 /Mcr,ANSYS
1
2
3
4
5
6
7
8
9
10
L[m]
H=1.3h
H=1.5h
H=1.6h

ANNEX F – Lateral-torsional buckling of solid and cellular beam cases based on RM1

Solid beams

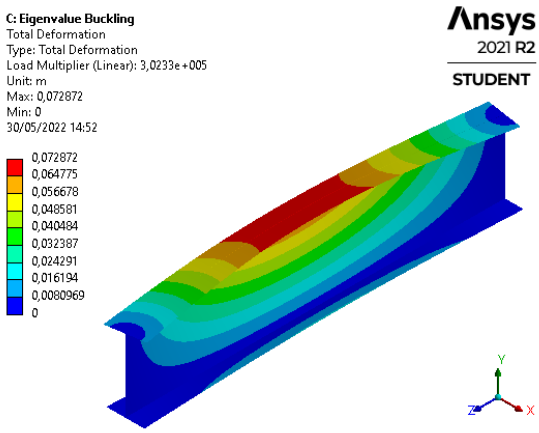

L=1 [m]

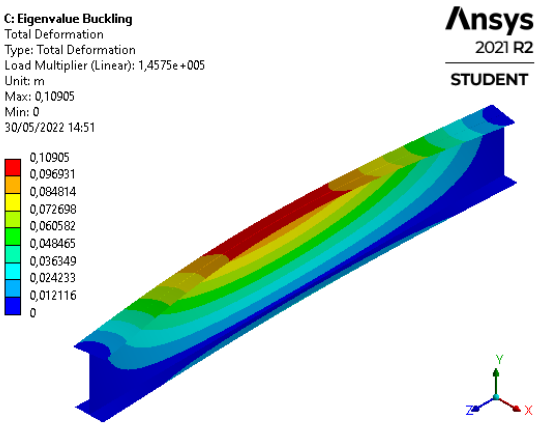

L=1.5 [m]

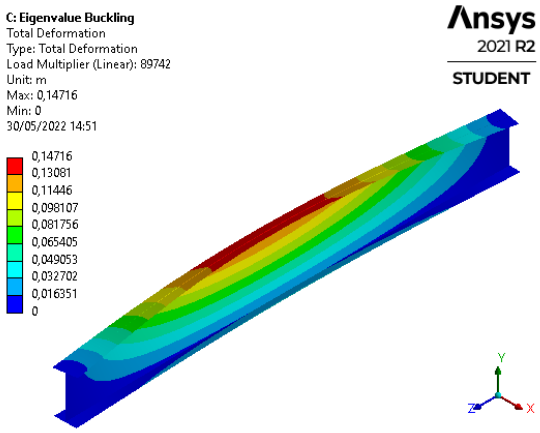

L=2 [m]

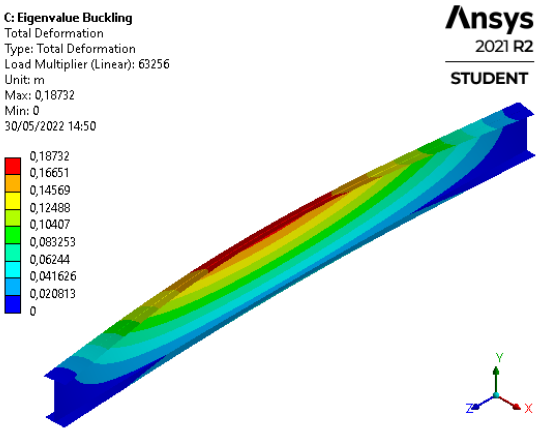

L=2.5 [m]

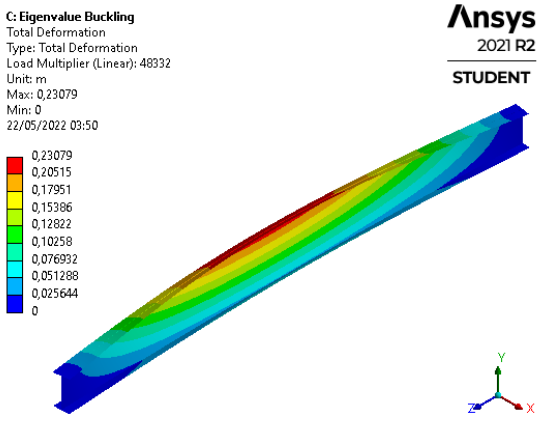

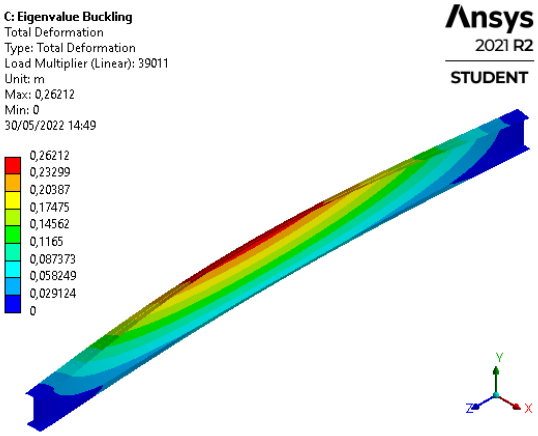

L=3 [m]

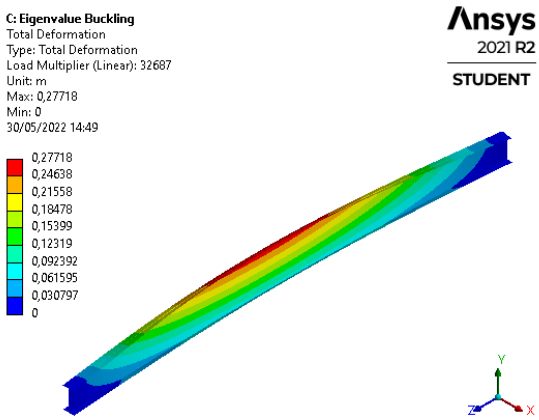

L=3.5 [m]

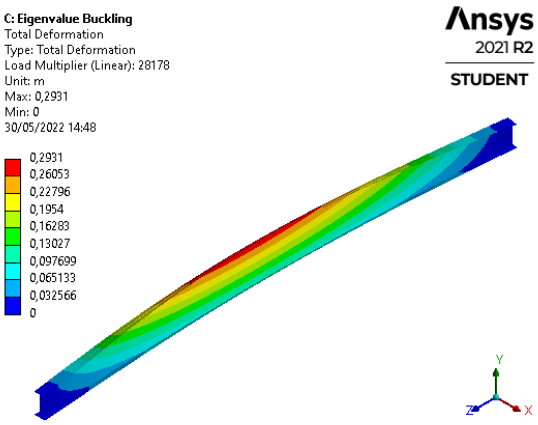

L=4 [m]

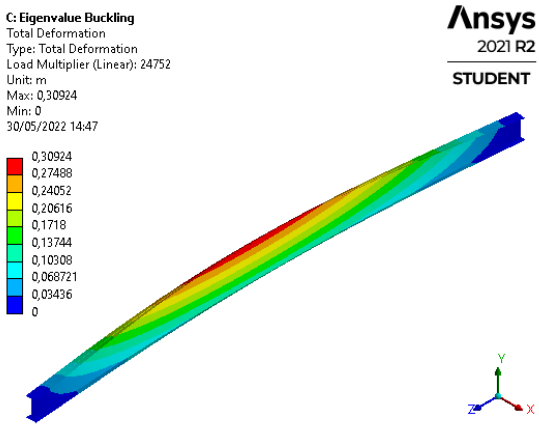

L=4.5 [m]

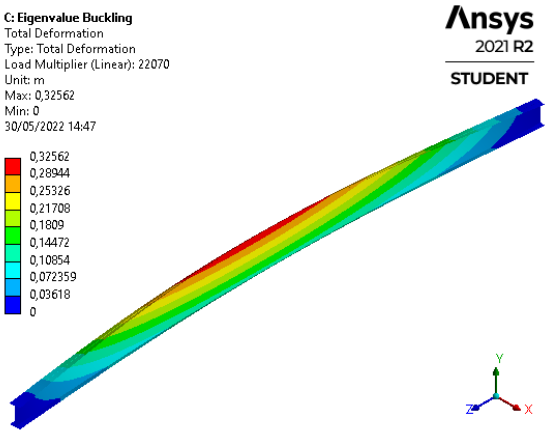

L=5 [m]

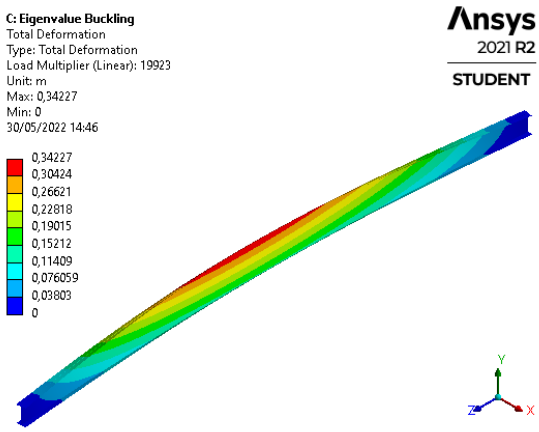

L=5.5 [m]

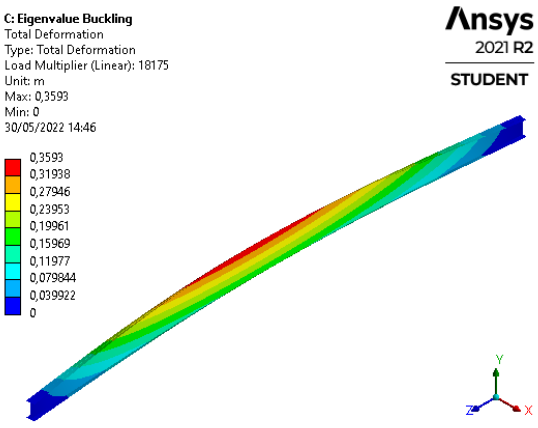

L=6 [m]

L=6.5 [m]

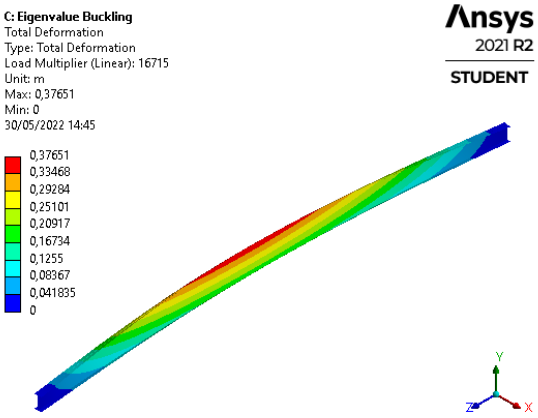

L=7 [m]

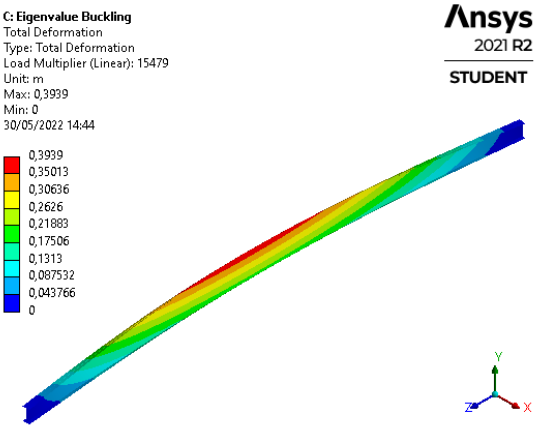

L=7.5 [m]

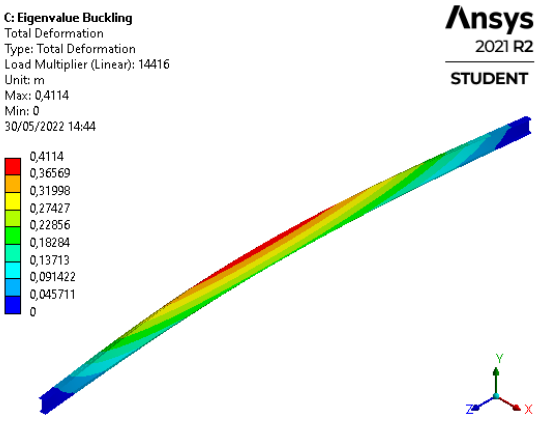

L=8 [m]

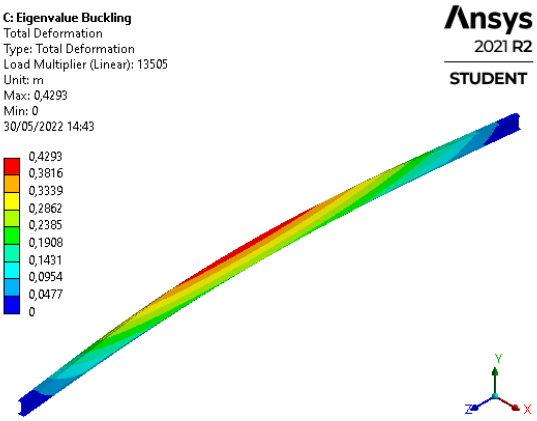

L=8.5 [m]

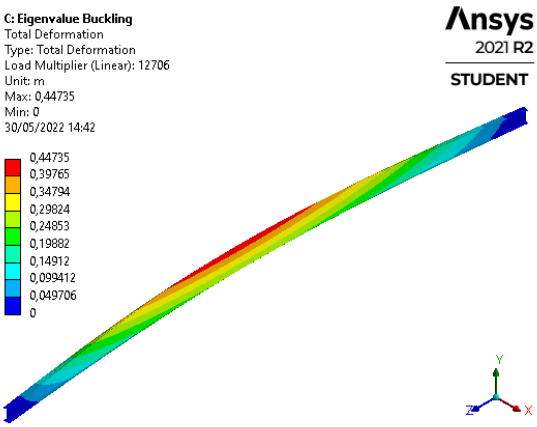

L=9 [m]

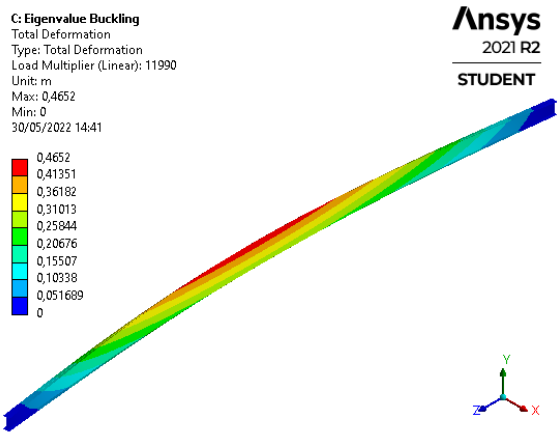

L=9.5 [m]

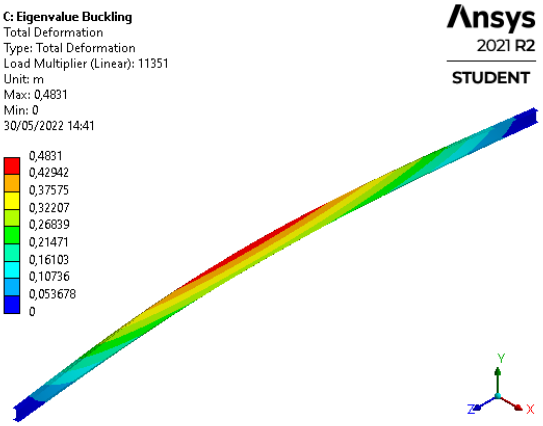
C: Eigenvalue Buckling
Total Deformation
Type: Total Deformation
Load Multiplier (Linear): 11351
Unit: m
Max: 0,4831
Min: 0
30/05/2022 14:41
0,4831
0,42942
0,37575
0,32207
0,26839
0,21471
0,16103
0,10736
0,053678
0
Ansys
2021 R2
STUDENT
Y
Z
X

L=10 [m]

$a_0 = 1.0h$ - $S = 1.4a_0$ - $H = 1.0h$ - RM1

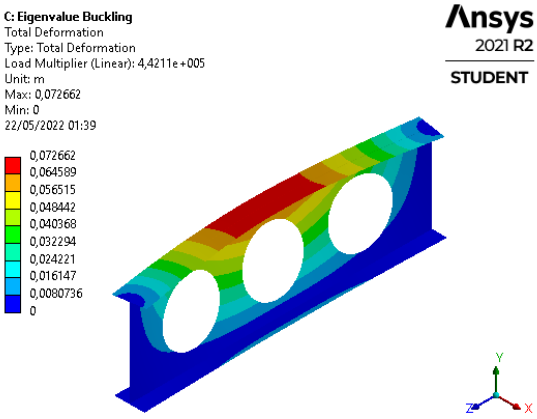

L=1 [m]

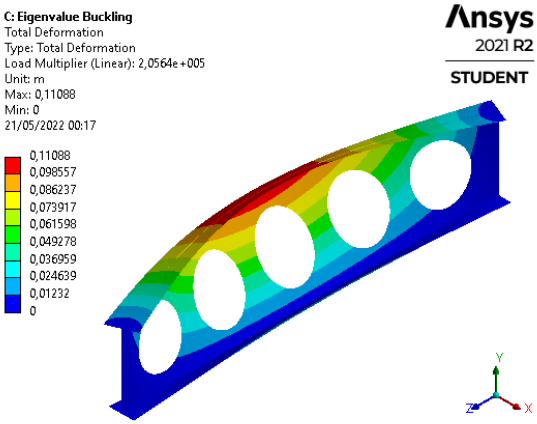

L=1.5 [m]

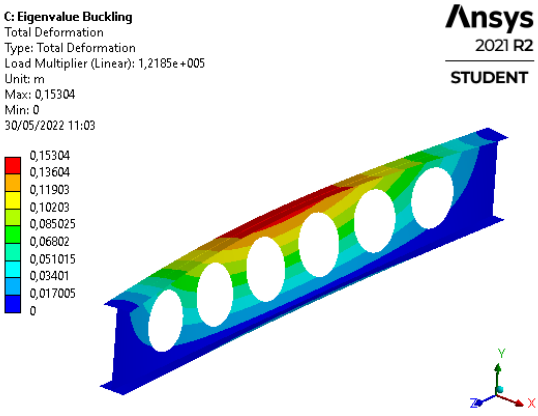

L=2 [m]

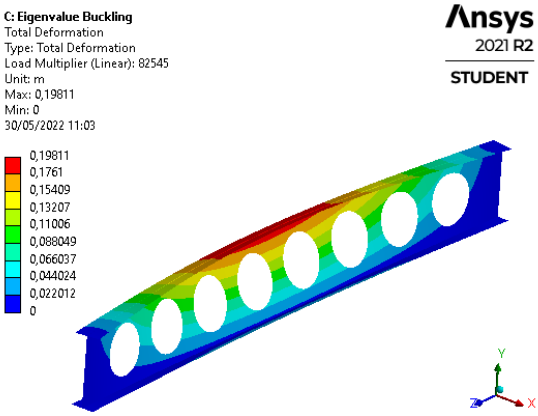

L=2.5 [m]

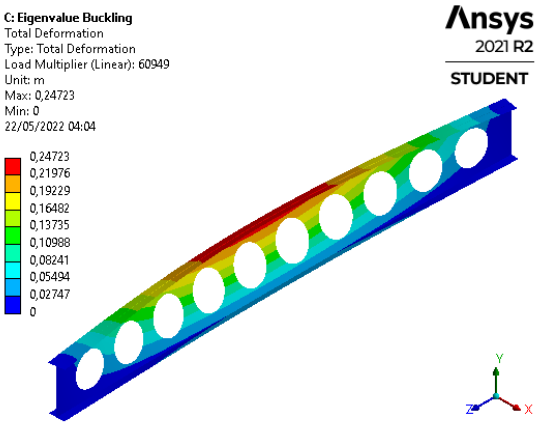

L=3 [m]

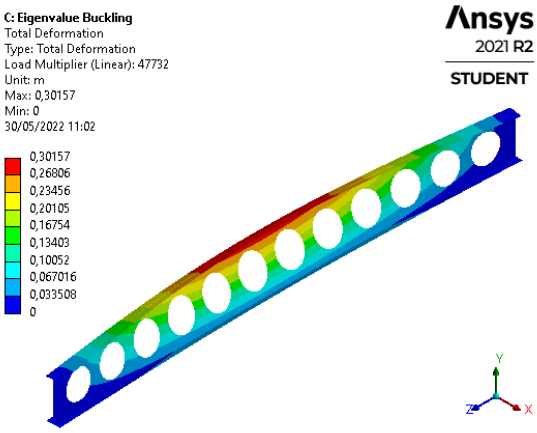

L=3.5 [m]

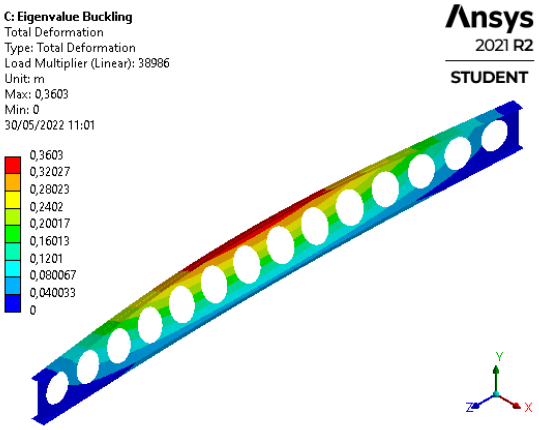

L=4 [m]

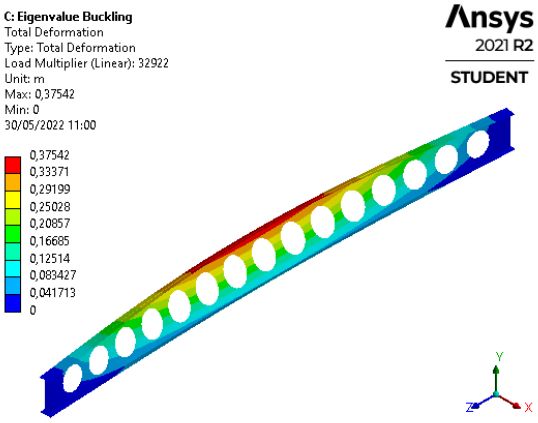

L=4.5 [m]

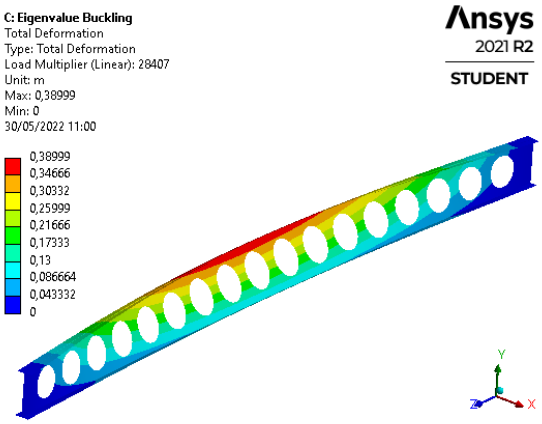

L=5 [m]

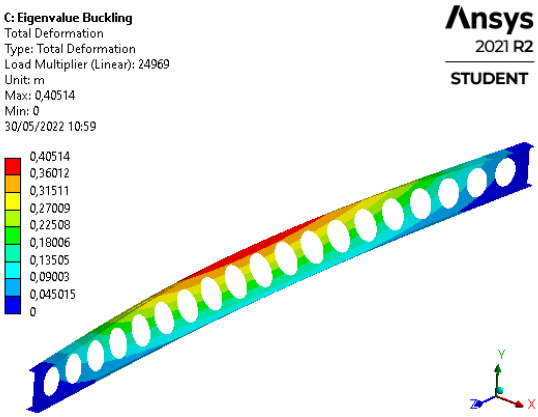

L=5.5 [m]

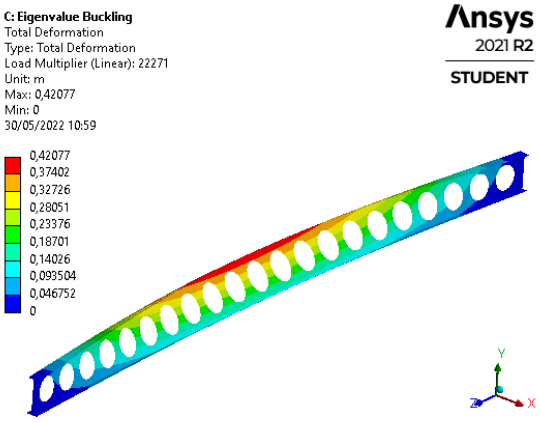

L=6 [m]

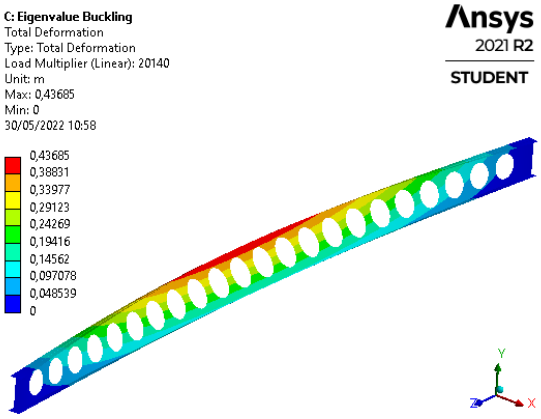

L=6.5 [m]

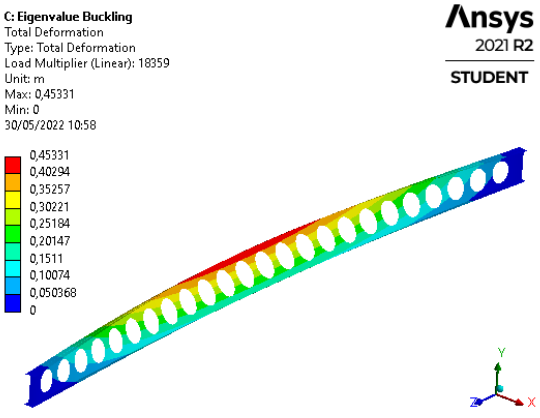

L=7 [m]

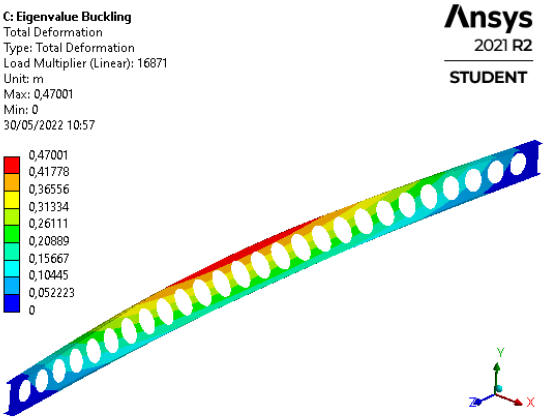

L=7.5 [m]

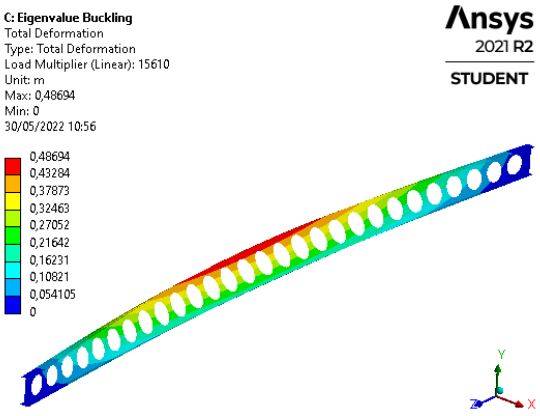

L=8 [m]

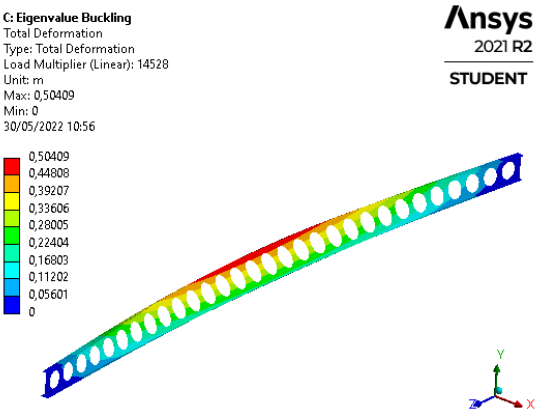

L=8.5 [m]

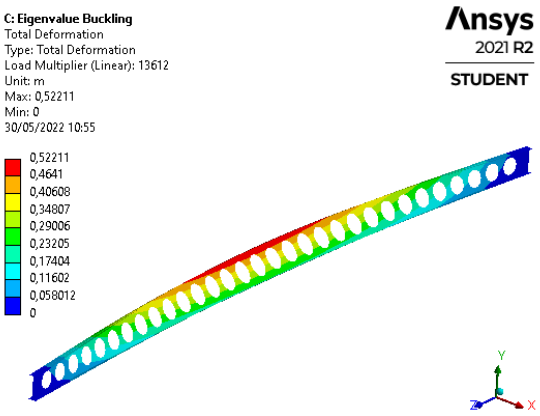

L=9 [m]

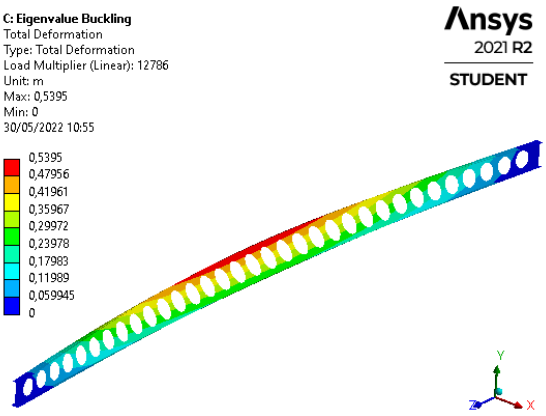

L=9.5 [m]

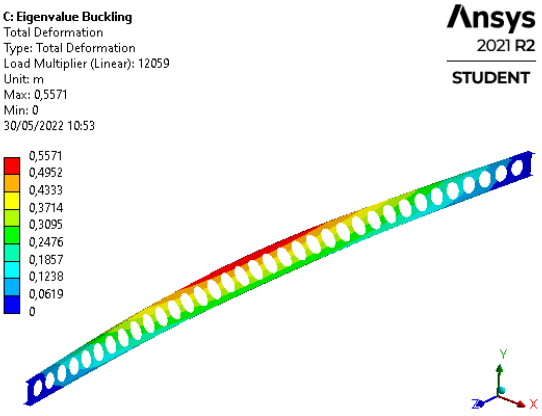
C: Eigenvalue Buckling
Total Deformation
Type: Total Deformation
Load Multiplier (Linear): 12059
Unit: m
Max: 0,5571
Min: 0
30/05/2022 10:53
0,5571
0,4952
0,4333
0,3714
0,3095
0,2476
0,1857
0,1238
0,0619
0
Ansys
2021 R2
STUDENT
Y
Z
X

L=10 [m]

$$a_0 = 0.8h$$

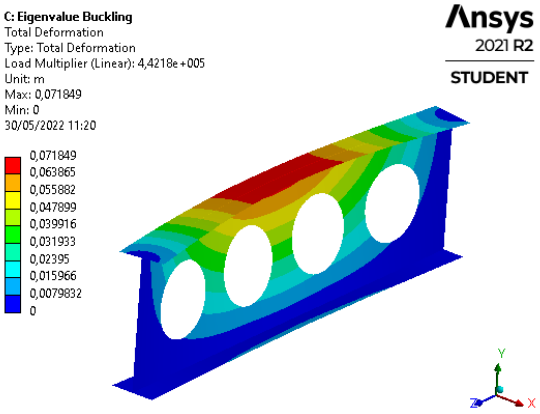

L=1 [m]

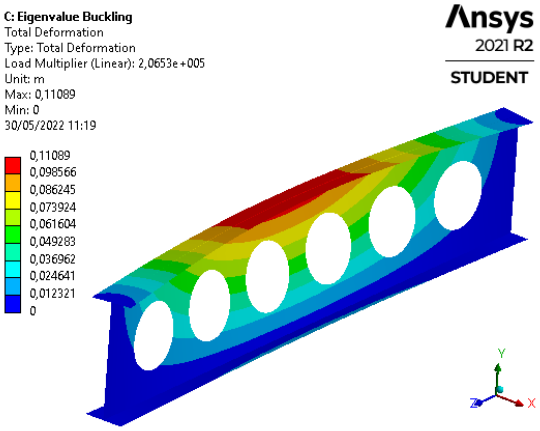

L=1.5 [m]

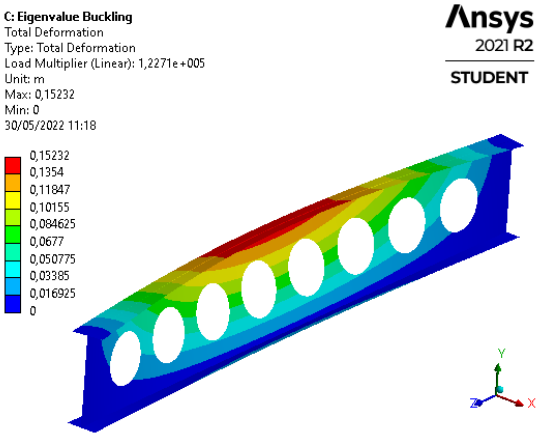

L=2 [m]

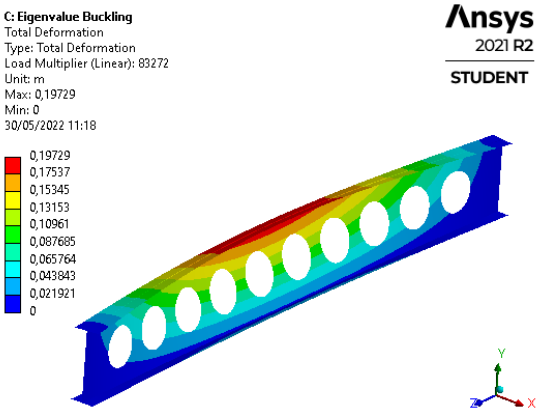

L=2.5 [m]

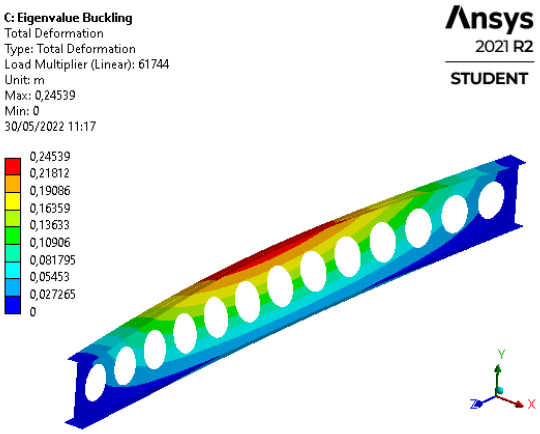

L=3 [m]

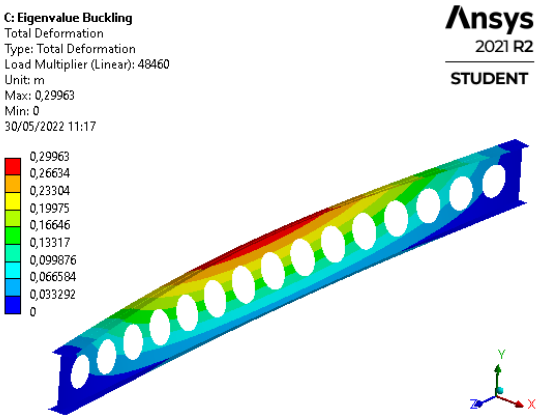

L=3.5 [m]

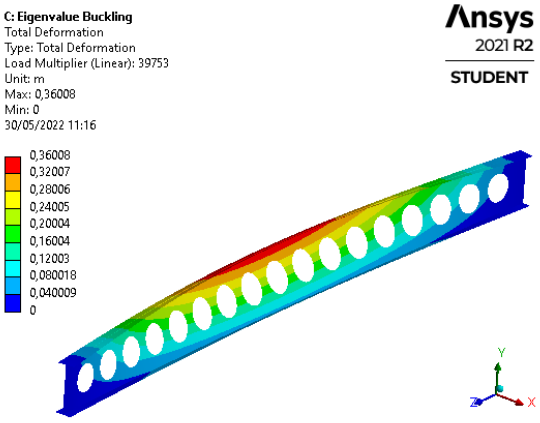

L=4 [m]

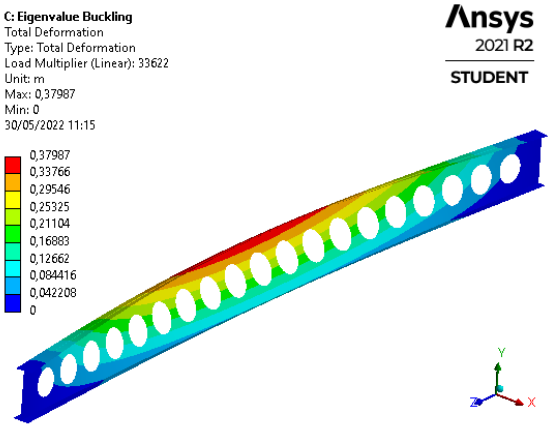

L=4.5 [m]

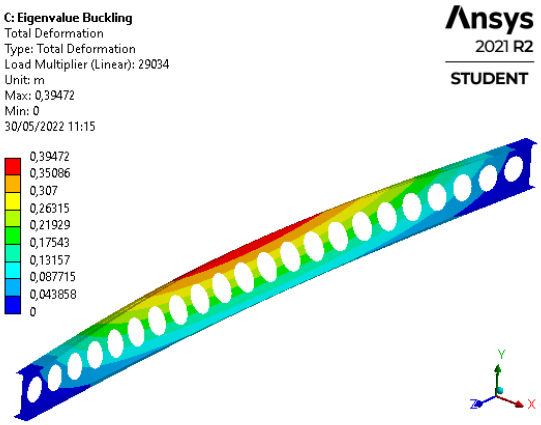

L=5 [m]

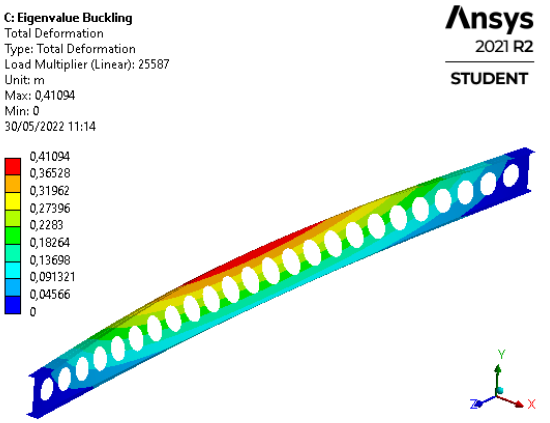

L=5.5 [m]

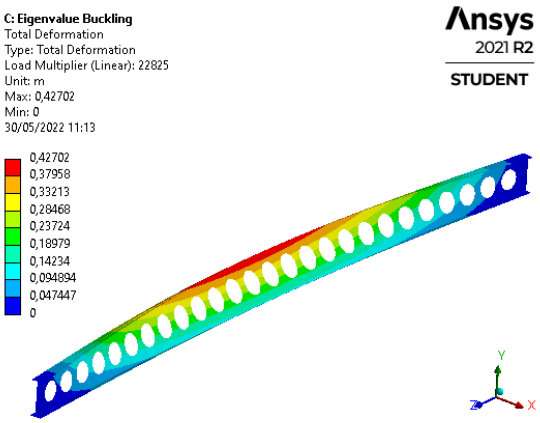

L=6 [m]

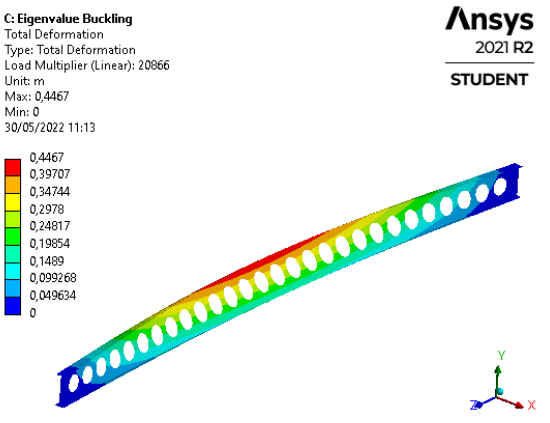

L=6.5 [m]

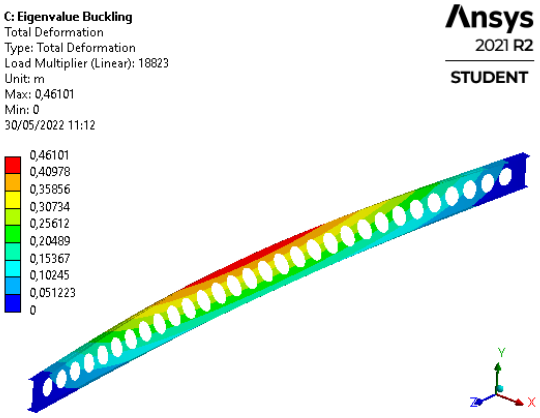

L=7 [m]

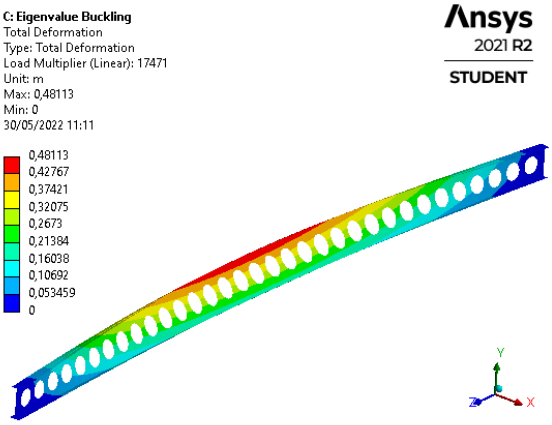

L=7.5 [m]

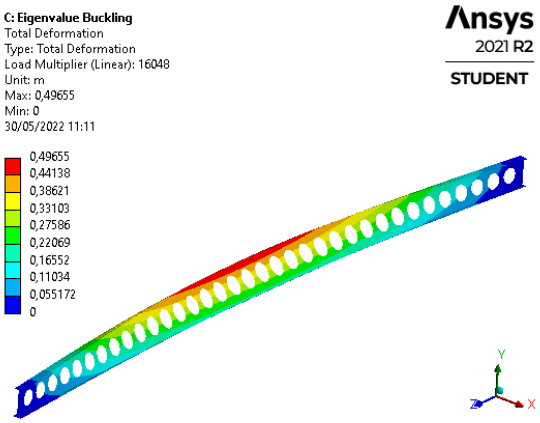

L=8 [m]

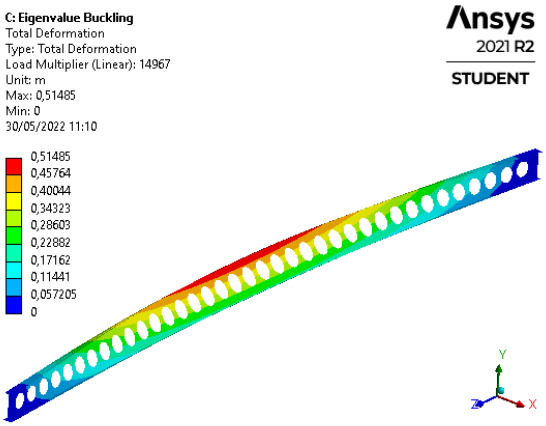

L=8.5 [m]

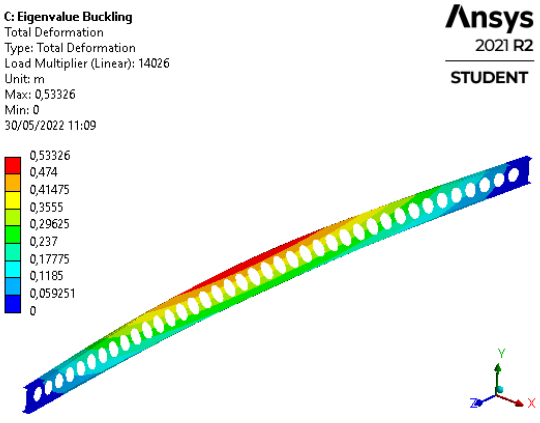

L=9 [m]

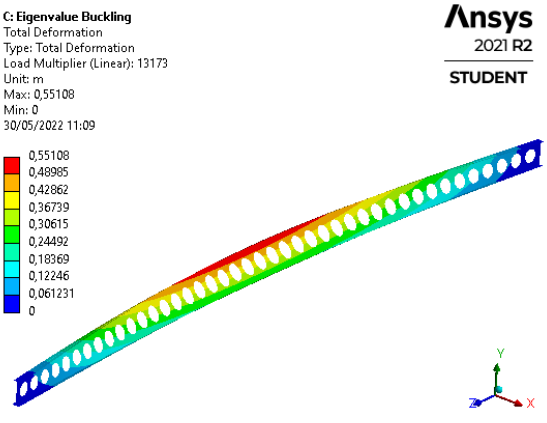

L=9.5 [m]

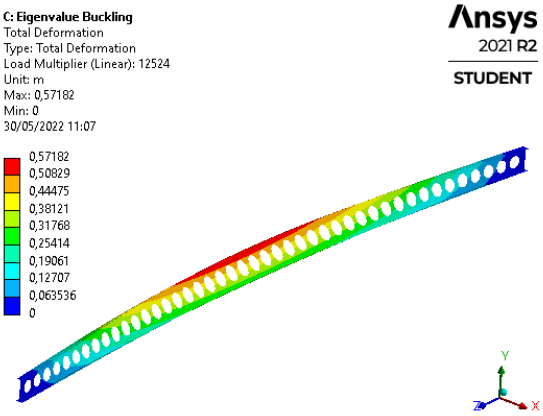
C: Eigenvalue Buckling
Total Deformation
Type: Total Deformation
Load Multiplier (Linear): 12524
Unit: m
Max: 0,57182
Min: 0
30/05/2022 11:07
0,57182
0,50829
0,44475
0,38121
0,31768
0,25414
0,19061
0,12707
0,063536
0
Ansys
2021 R2
STUDENT
Y
Z
X

L=10 [m]

$$a_0 = 1.3h$$

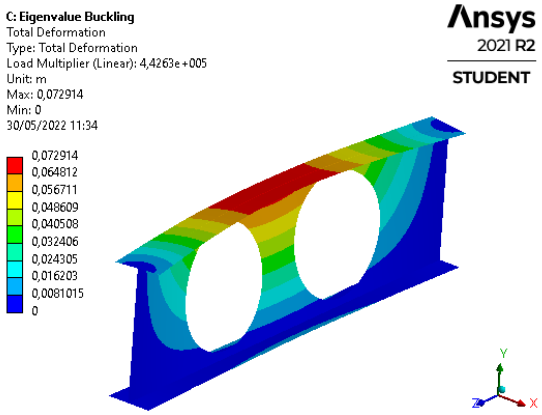

L=1 [m]

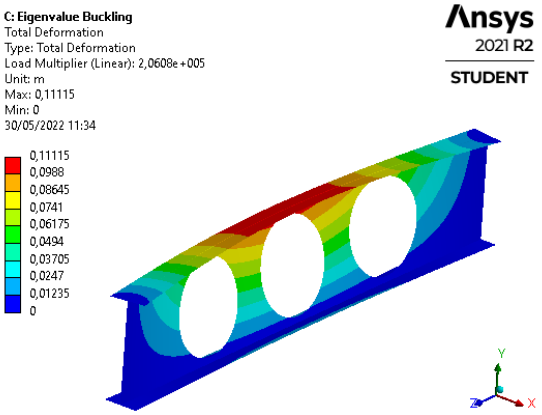

L=1.5 [m]

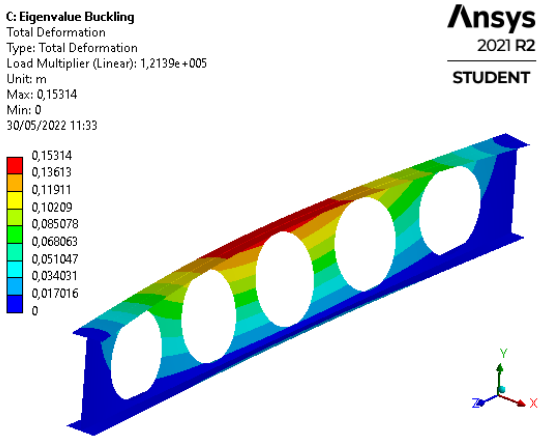

L=2 [m]

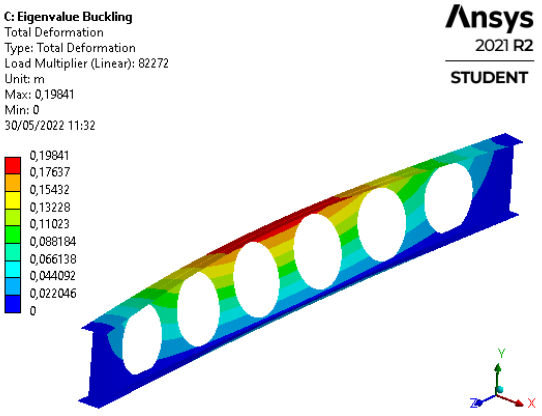

L=2.5 [m]

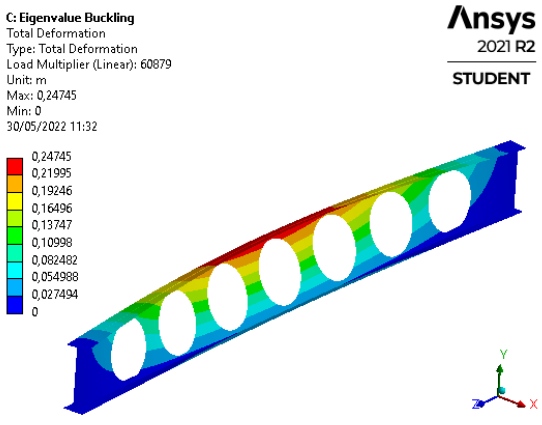

L=3 [m]

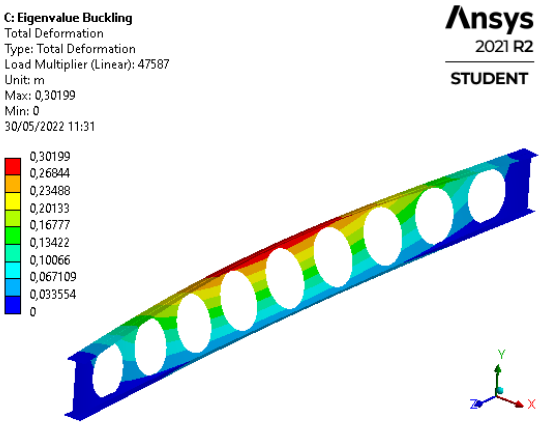

L=3.5 [m]

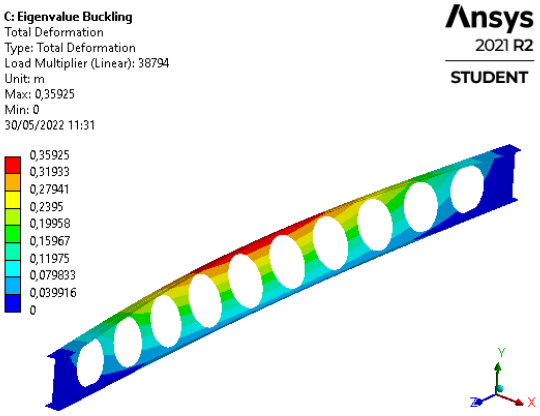

L=4 [m]

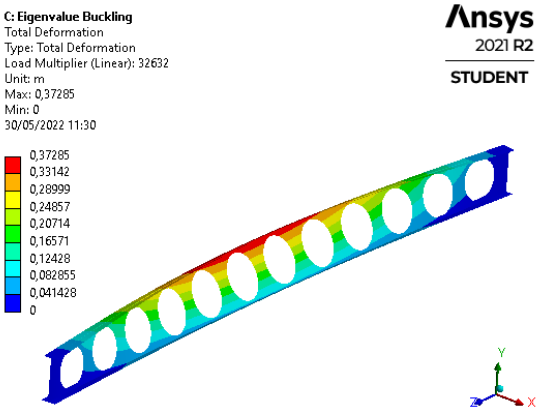

L=4.5 [m]

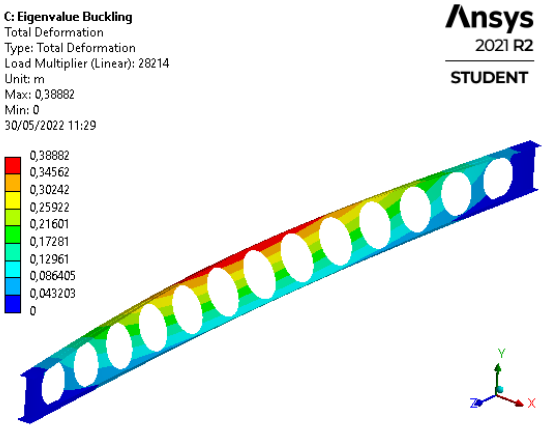

L=5 [m]

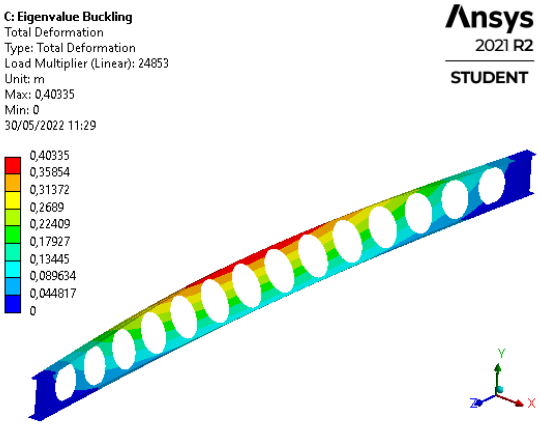

L=5.5 [m]

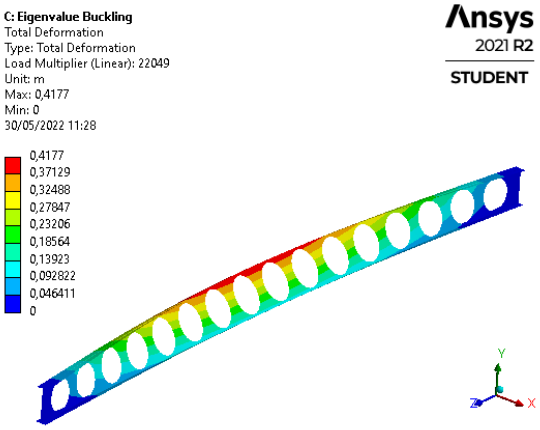

L=6 [m]

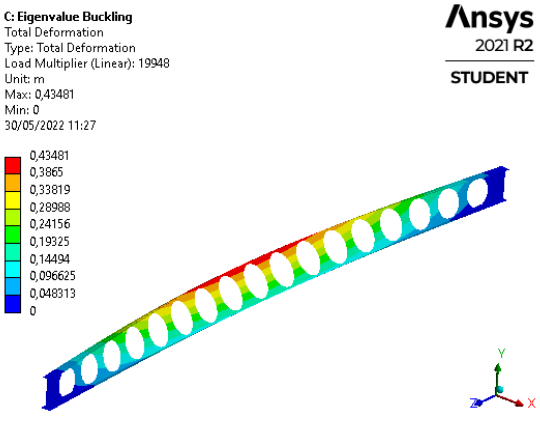

L=6.5 [m]

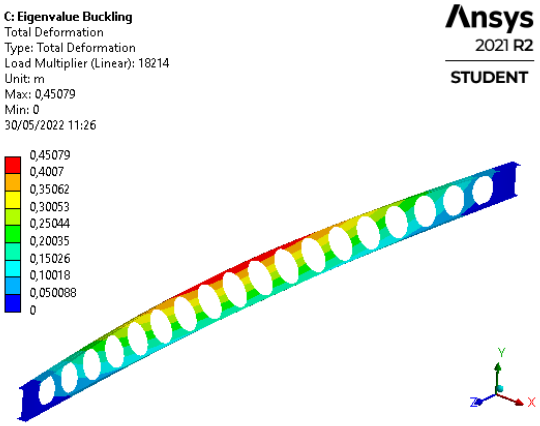

L=7 [m]

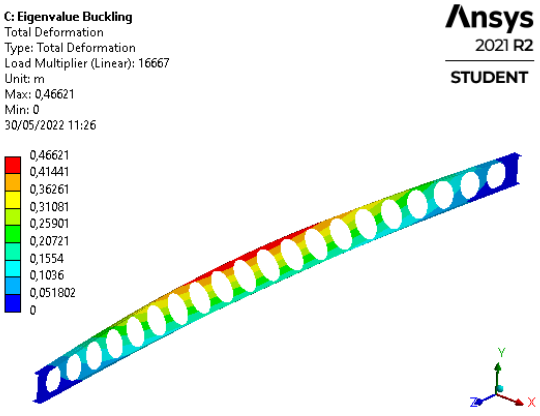

L=7.5 [m]

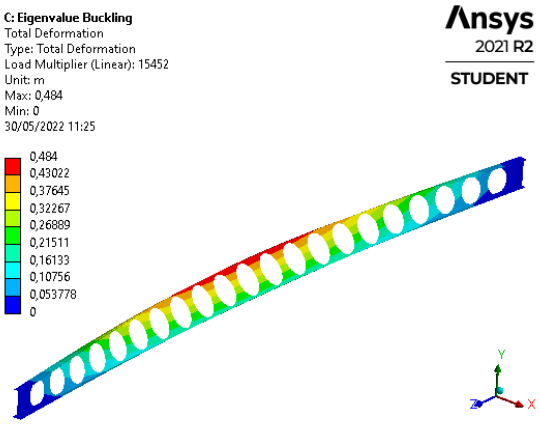

L=8 [m]

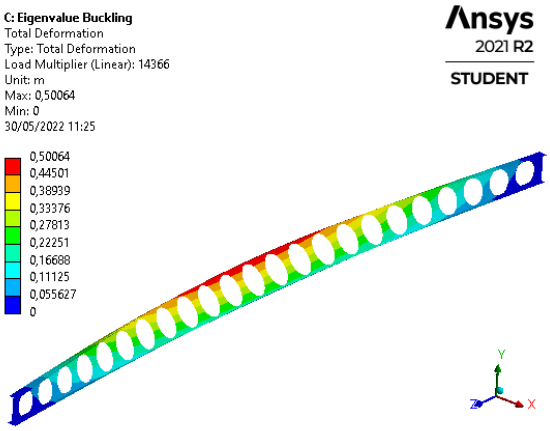

L=8.5 [m]

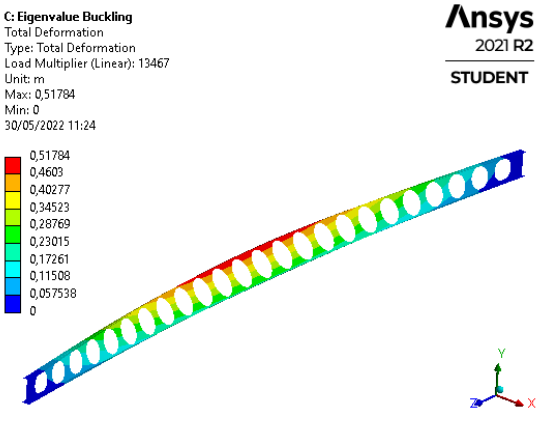

L=9 [m]

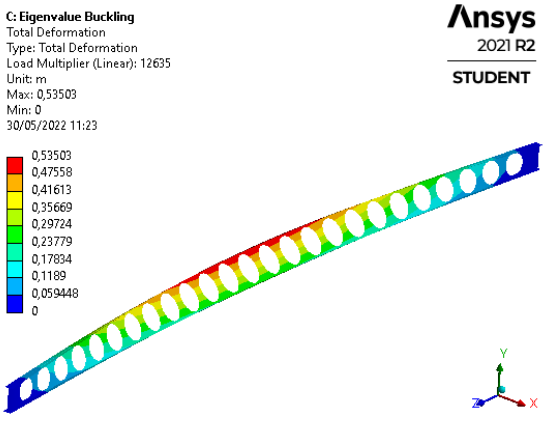

L=9.5 [m]

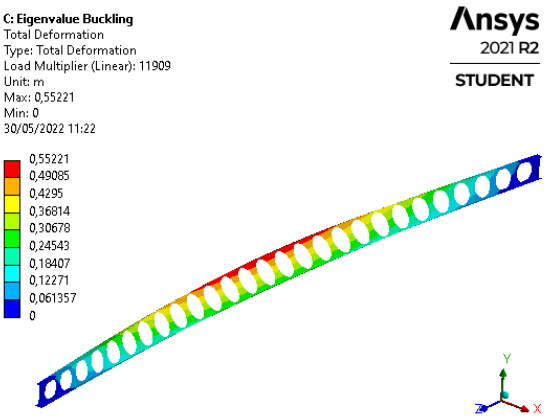
C: Eigenvalue Buckling
Total Deformation
Type: Total Deformation
Load Multiplier (Linear): 11909
Unit: m
Max: 0,55221
Min: 0
30/05/2022 11:22
0,55221
0,49085
0,4295
0,36814
0,30678
0,24543
0,18407
0,12271
0,061357
0
Ansys
2021 R2
STUDENT
Y
X

L=10 [m]

$$S = 1.1a_0$$

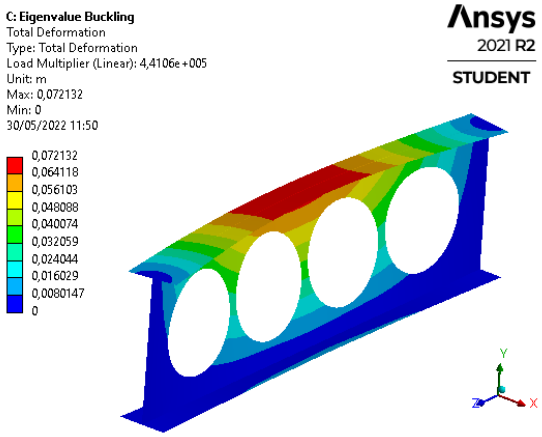

L=1 [m]

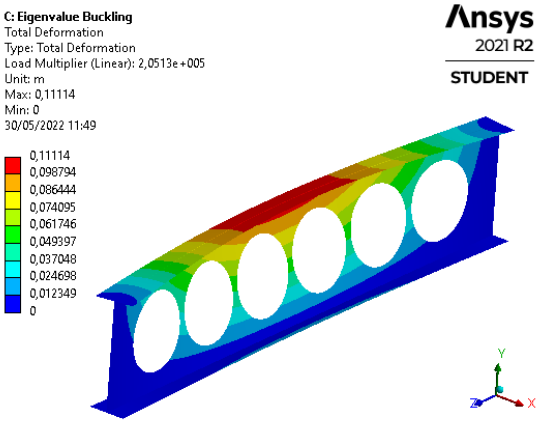

L=1.5 [m]

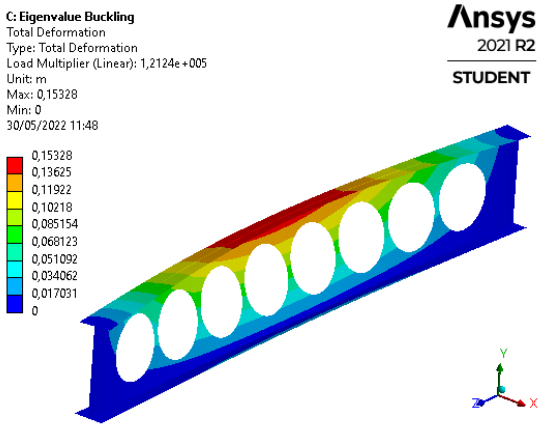

L=2 [m]

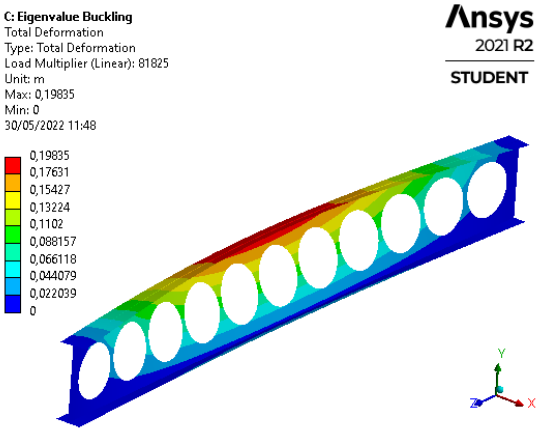

L=2.5 [m]

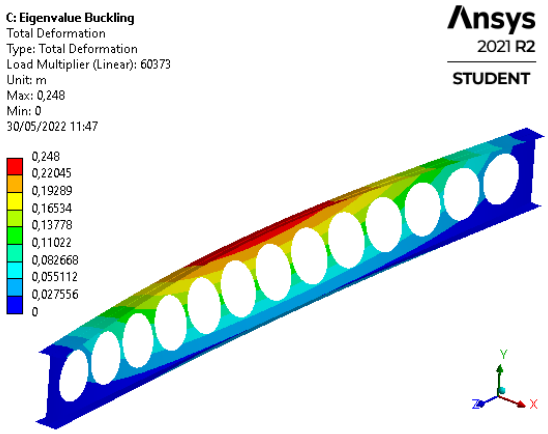

L=3 [m]

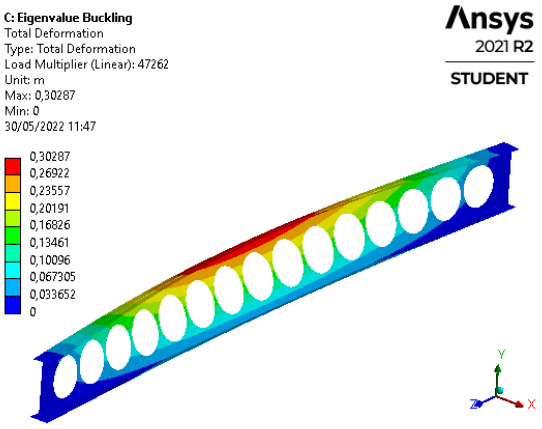

L=3.5 [m]

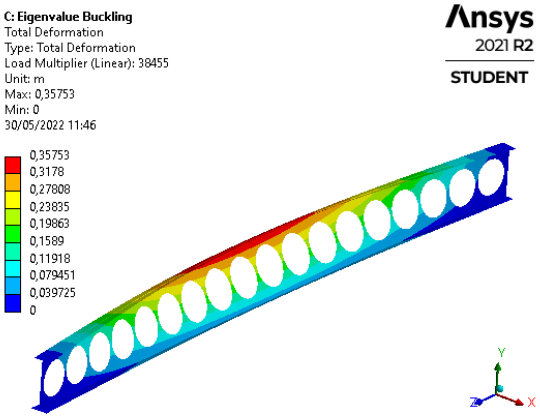

L=4 [m]

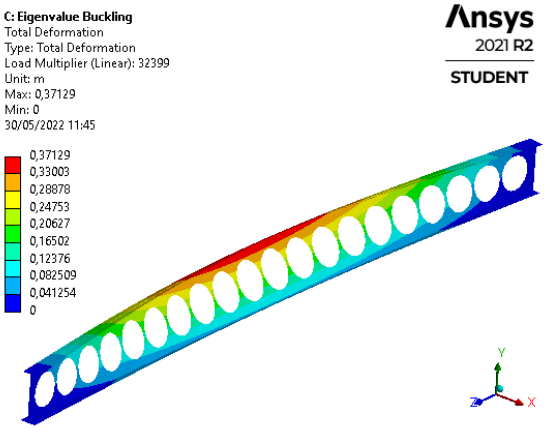

L=4.5 [m]

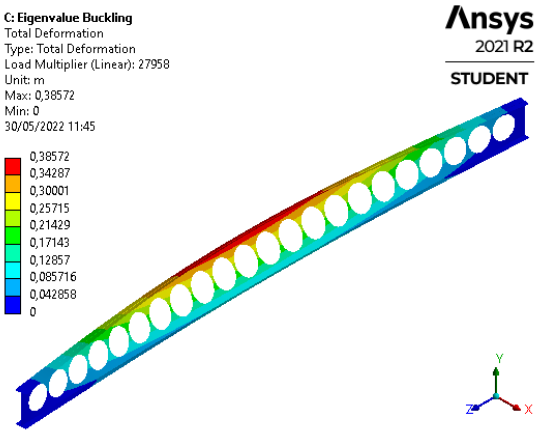

L=5 [m]

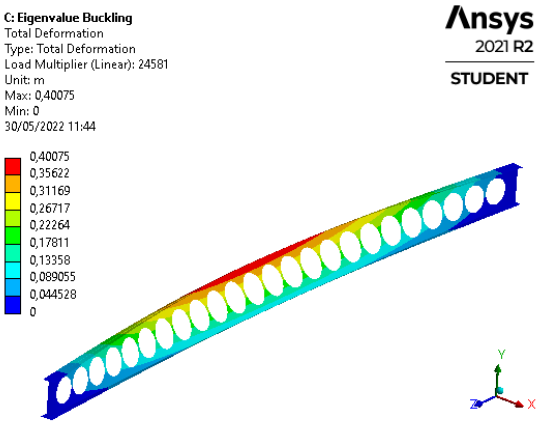

L=5.5 [m]

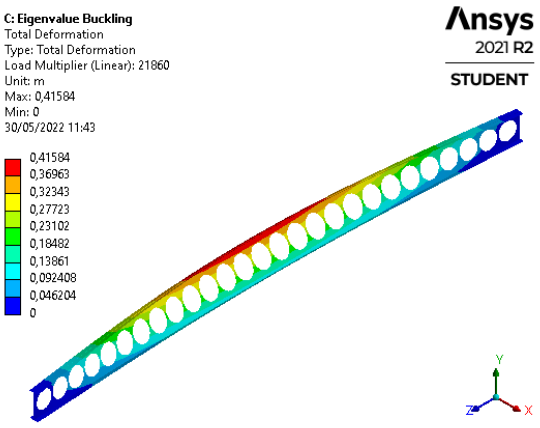

L=6 [m]

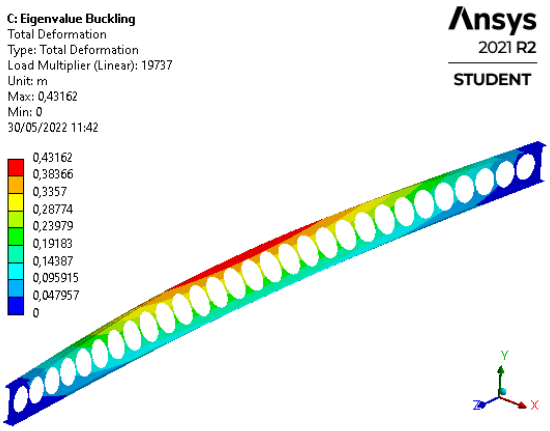

L=6.5 [m]

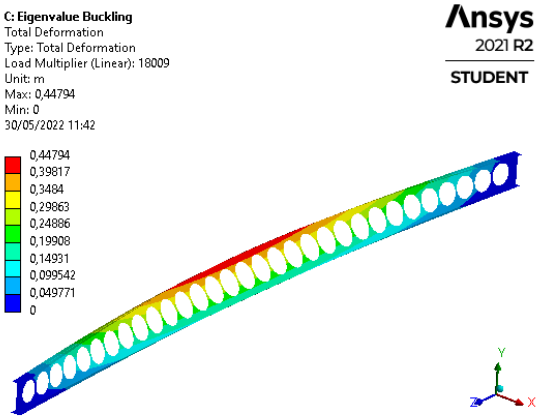

L=7 [m]

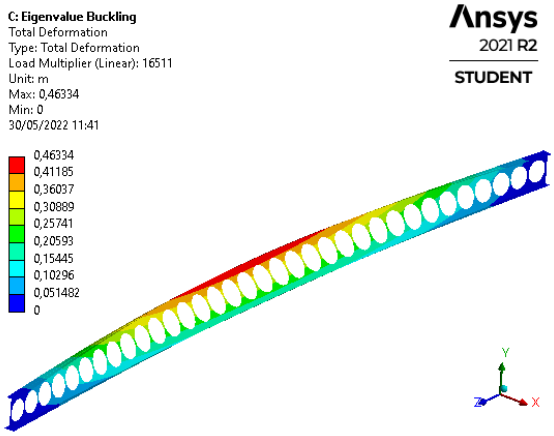

L=7.5 [m]

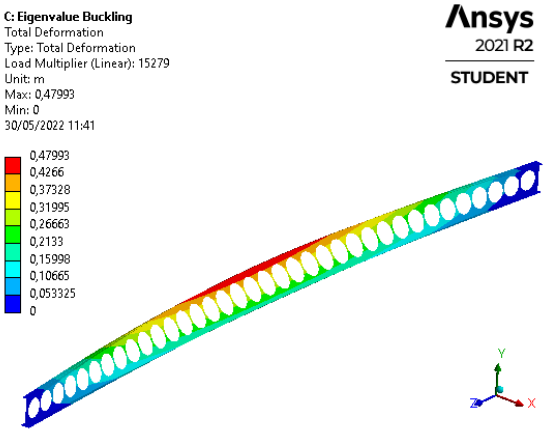

L=8 [m]

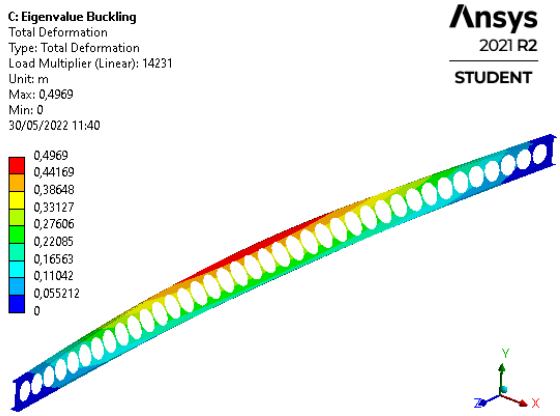

L=8.5 [m]

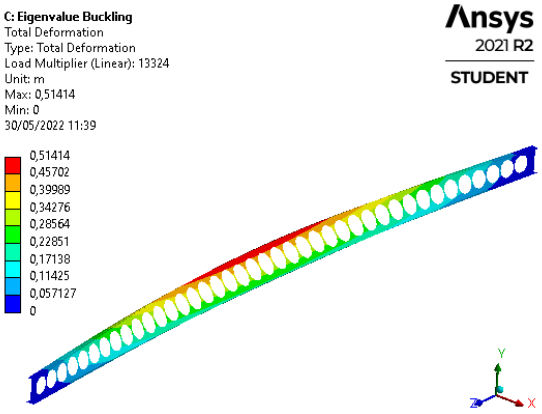

L=9 [m]

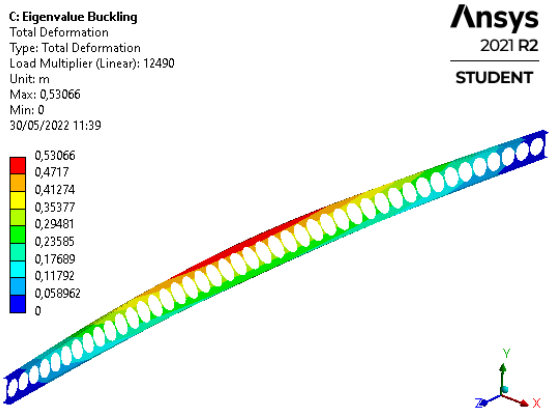

L=9.5 [m]

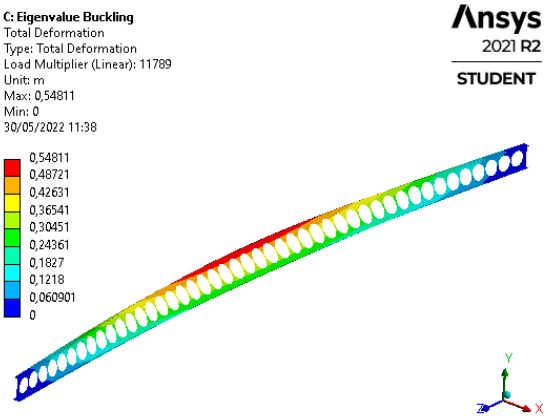
C: Eigenvalue Buckling
Total Deformation
Type: Total Deformation
Load Multiplier (Linear): 11789
Unit: m
Max: 0,54811
Min: 0
30/05/2022 11:38
0,54811
0,48721
0,42631
0,36541
0,30451
0,24361
0,1827
0,1218
0,060901
0
Ansys
2021 R2
STUDENT
Y
Z
X

L=10 [m]

$$S = 1.7a_0$$

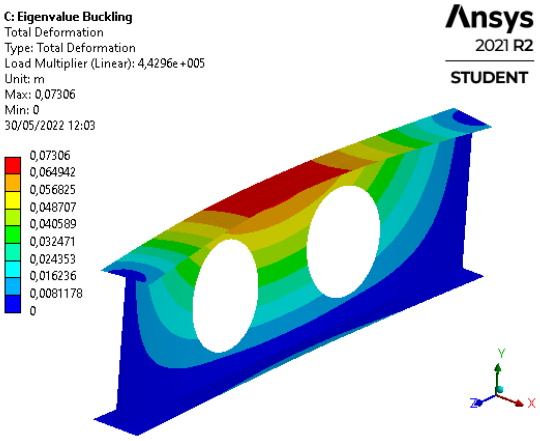

L=1 [m]

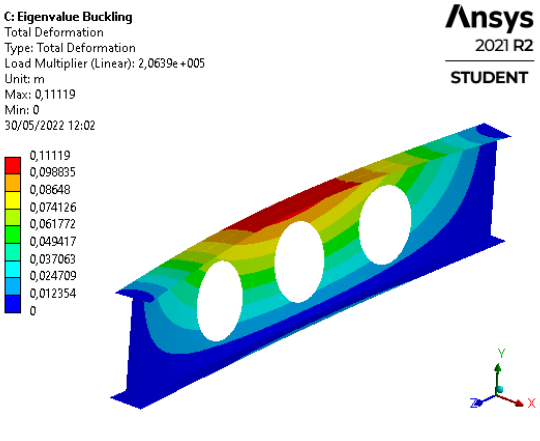

L=1.5 [m]

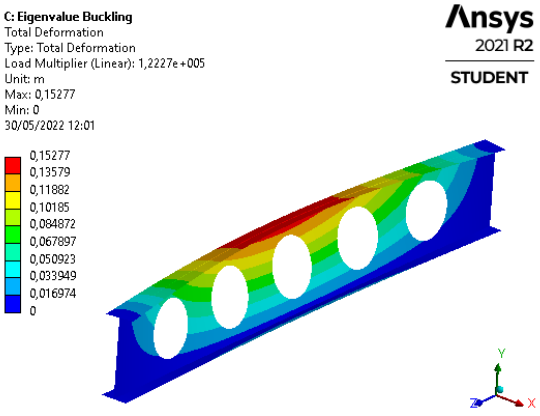

L=2 [m]

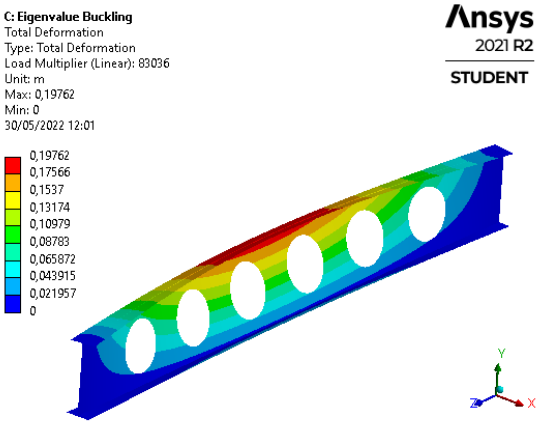

L=2.5 [m]

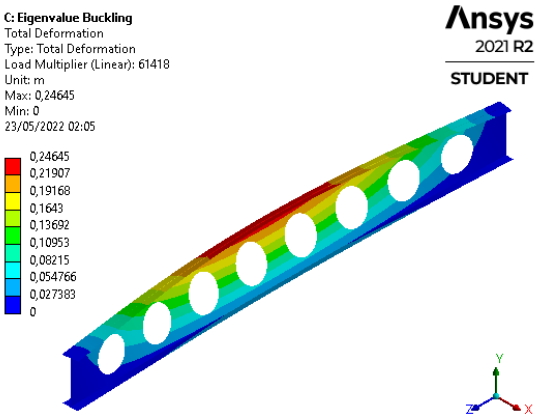

L=3 [m]

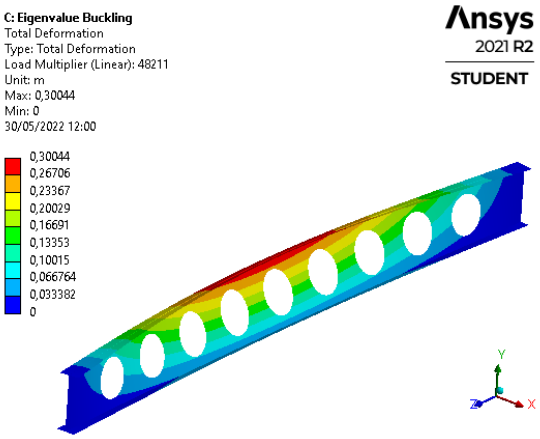

L=3.5 [m]

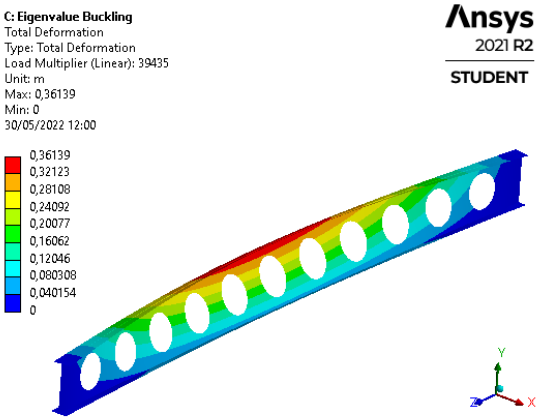

L=4 [m]

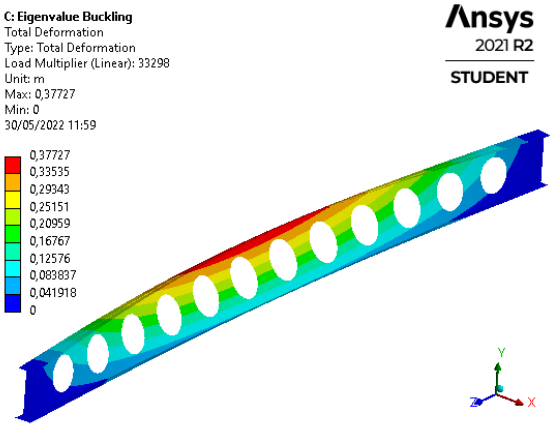

L=4.5 [m]

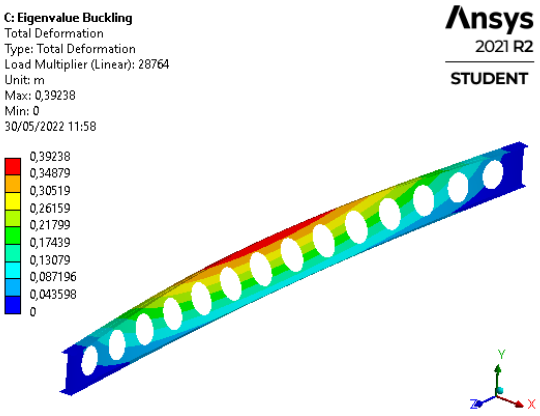

L=5 [m]

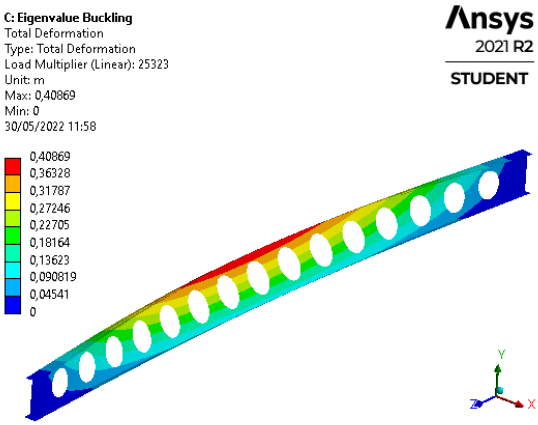

L=5.5 [m]

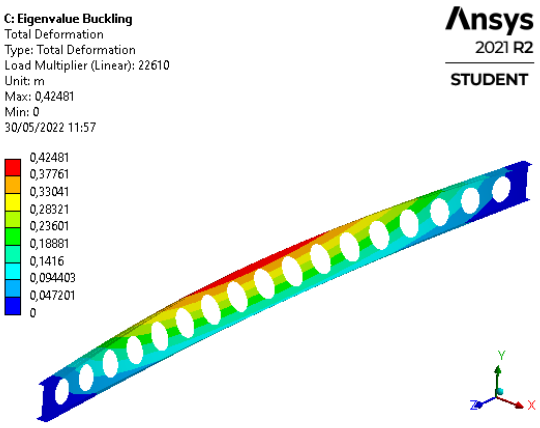

L=6 [m]

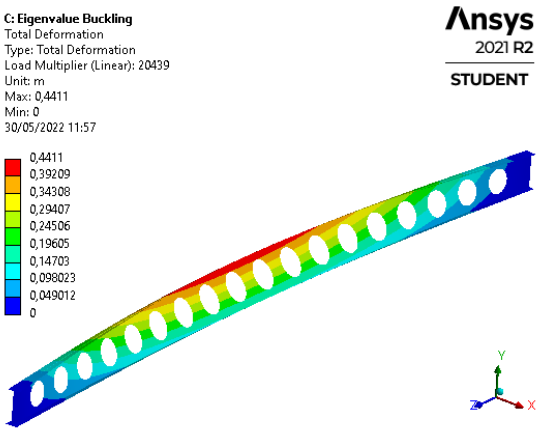

L=6.5 [m]

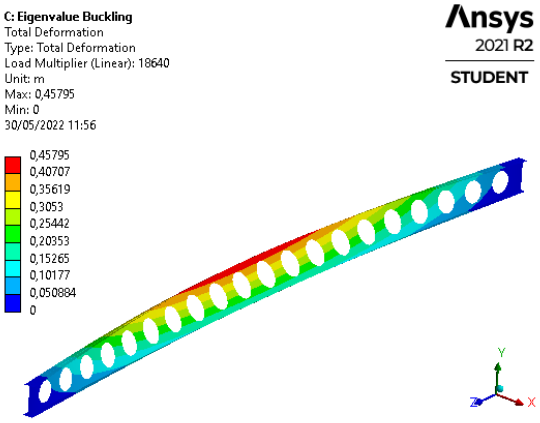

L=7 [m]

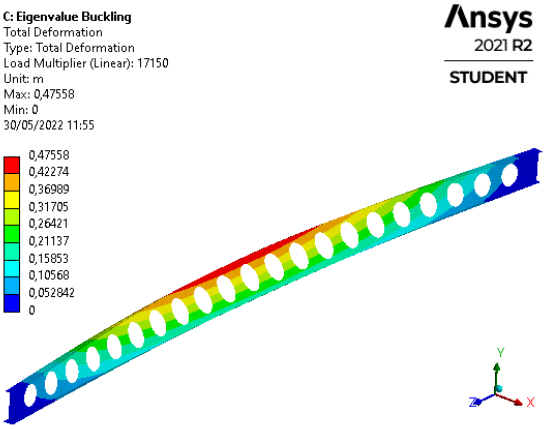

L=7.5 [m]

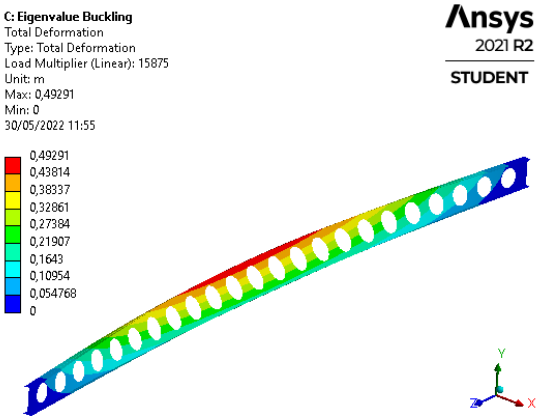

L=8 [m]

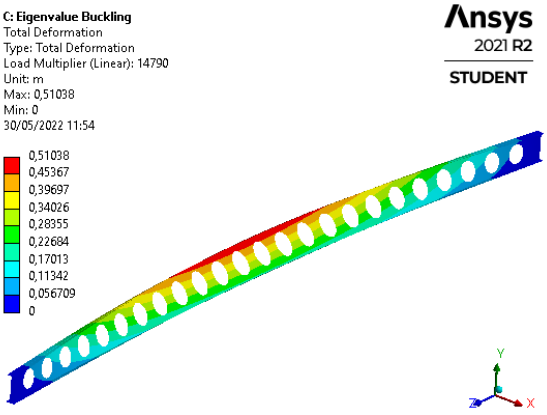

L=8.5 [m]

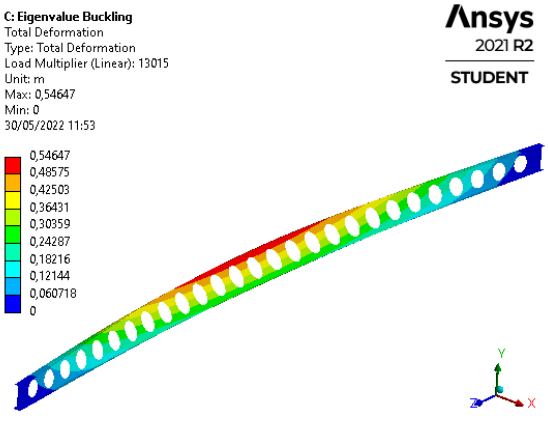

L=9 [m]

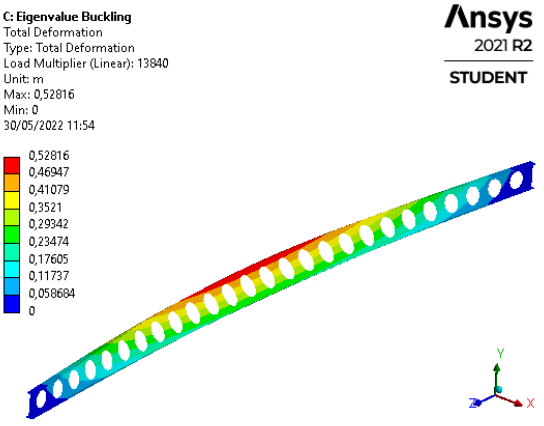

L=9.5 [m]

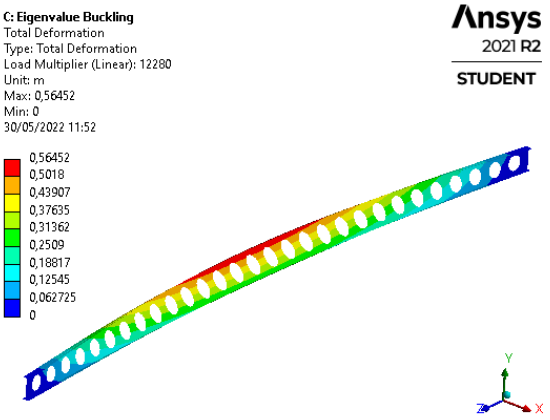
C: Eigenvalue Buckling
Total Deformation
Type: Total Deformation
Load Multiplier (Linear): 12280
Unit: m
Max: 0,56452
Min: 0
30/05/2022 11:52
0,56452
0,5018
0,43907
0,37635
0,31362
0,2509
0,18817
0,12545
0,062725
0
Ansys
2021 R2
STUDENT
Y
Z
X

L=10 [m]

$$H = 1.3h$$

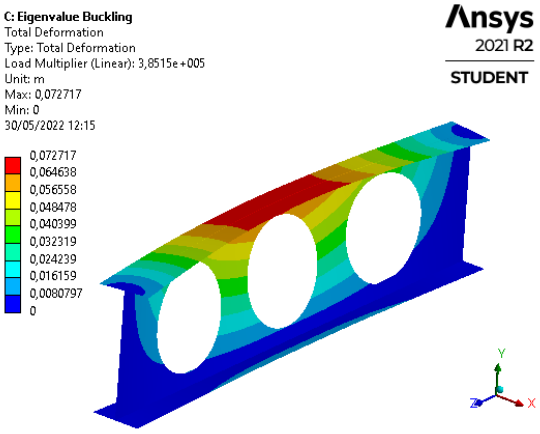

L=1 [m]

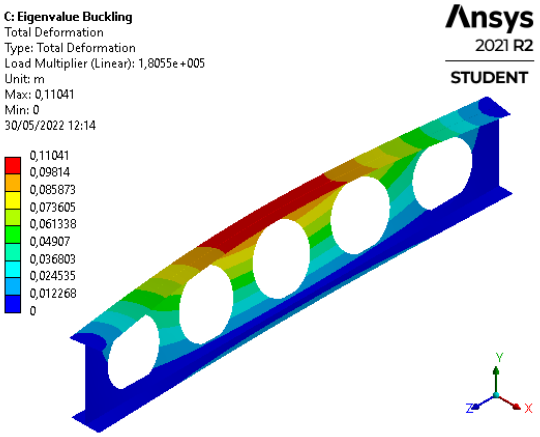

L=1.5 [m]

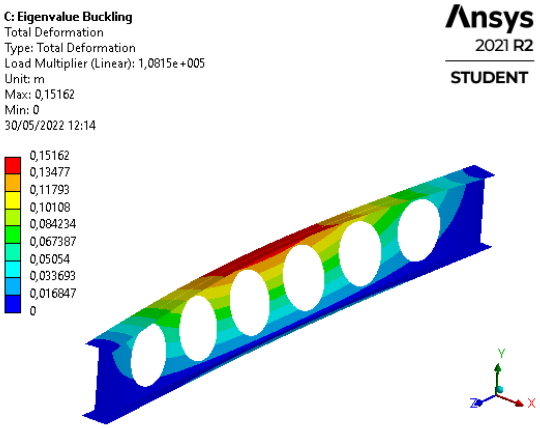

L=2 [m]

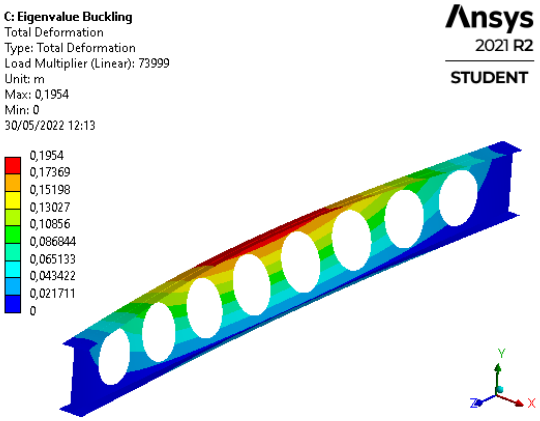

L=2.5 [m]

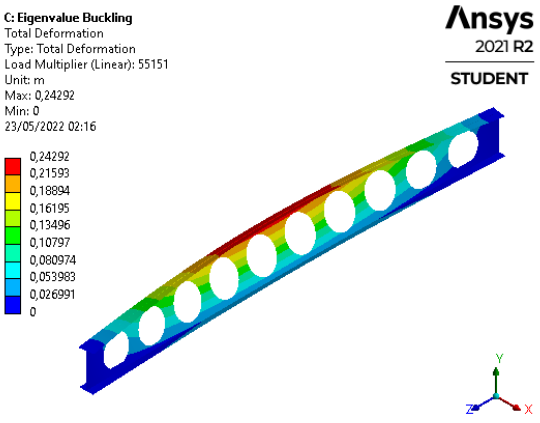

L=3 [m]

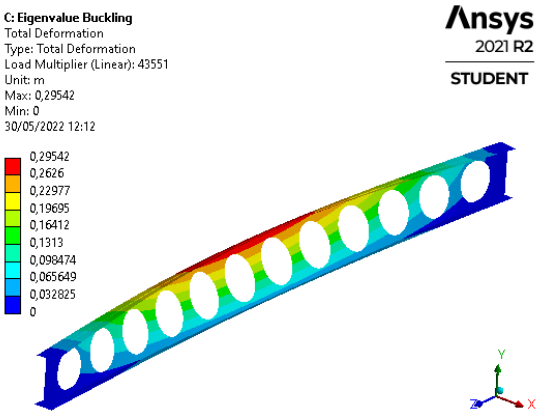

L=3.5 [m]

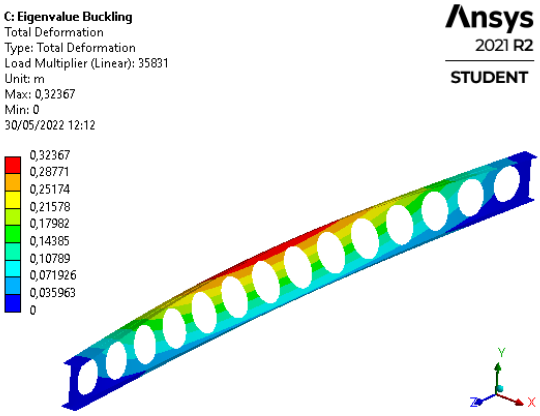

L=4 [m]

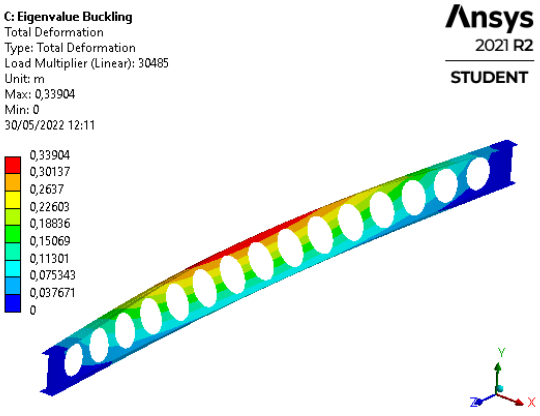

L=4.5 [m]

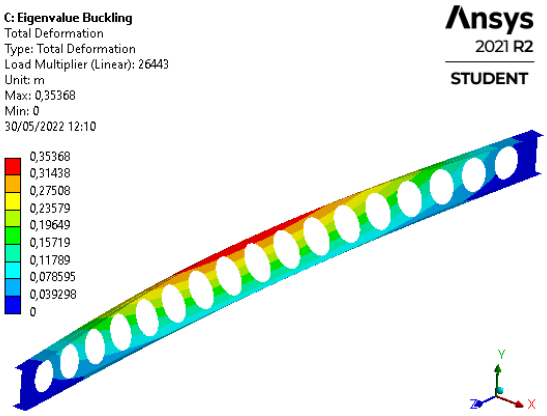

L=5 [m]

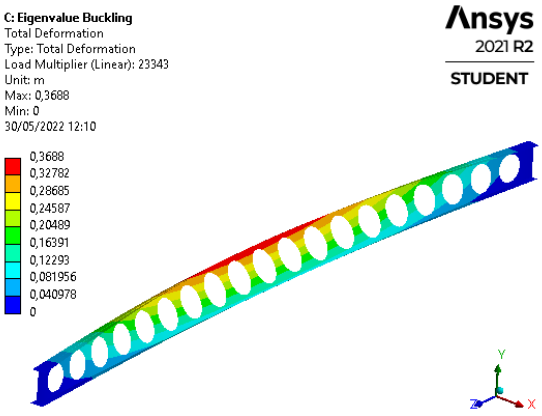

L=5.5 [m]

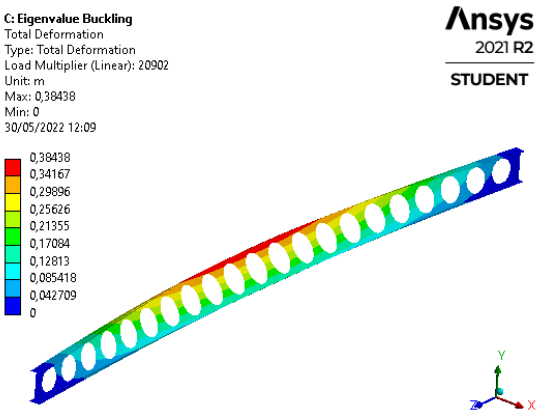

L=6 [m]

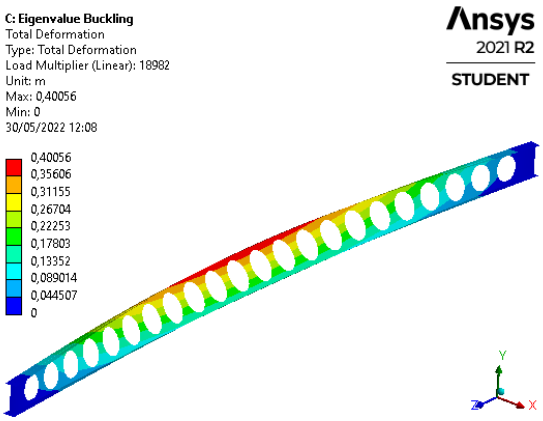

L=6.5 [m]

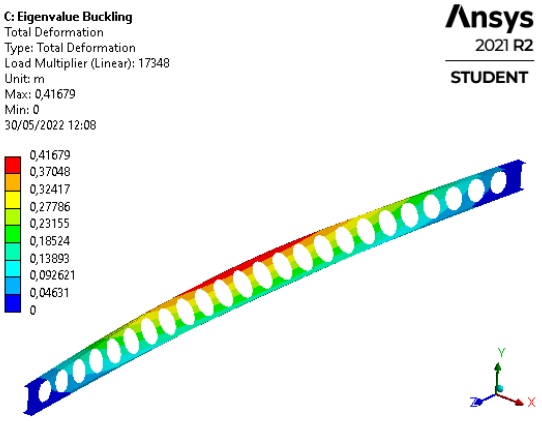

L=7 [m]

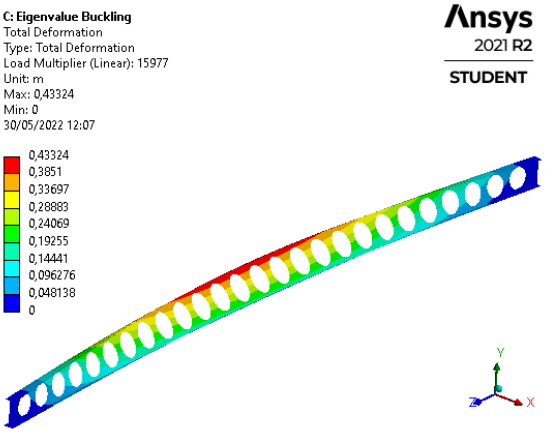

L=7.5 [m]

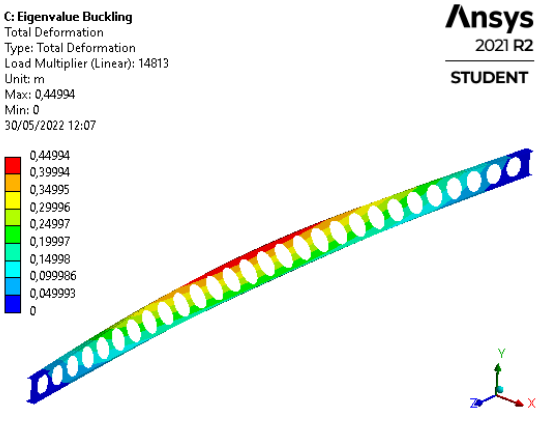

L=8 [m]

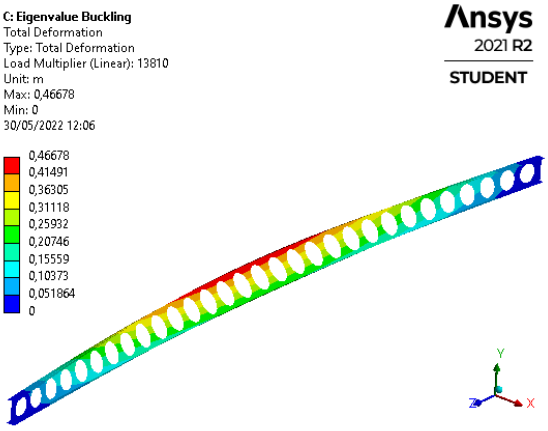

L=8.5 [m]

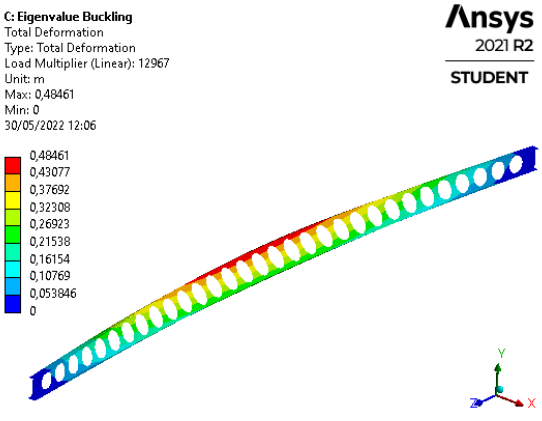

L=9 [m]

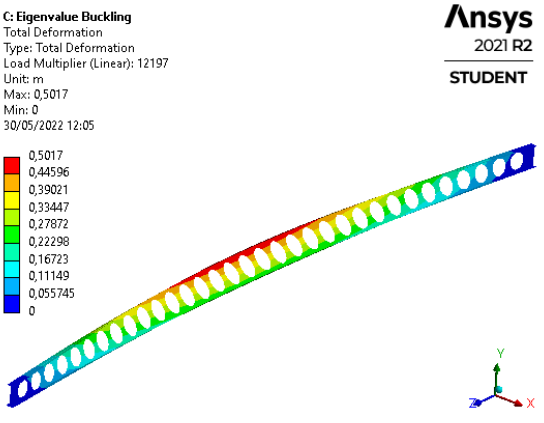

L=9.5 [m]

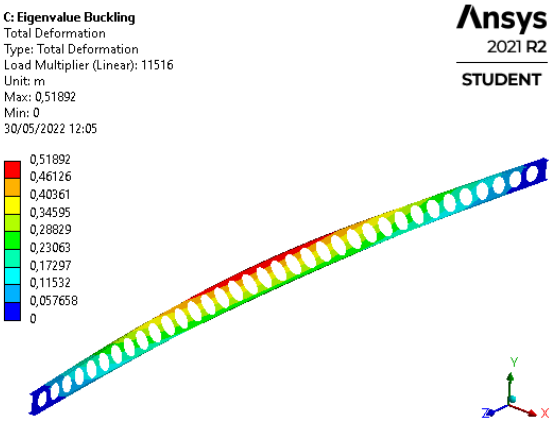
C: Eigenvalue Buckling
Total Deformation
Type: Total Deformation
Load Multiplier (Linear): 11516
Unit: m
Max: 0,51892
Min: 0
30/05/2022 12:05
0,51892
0,46126
0,40361
0,34595
0,28829
0,23063
0,17297
0,11532
0,057658
0
Ansys
2021 R2
STUDENT
Y
Z
X

L=10 [m]

$$H = 1.6h$$

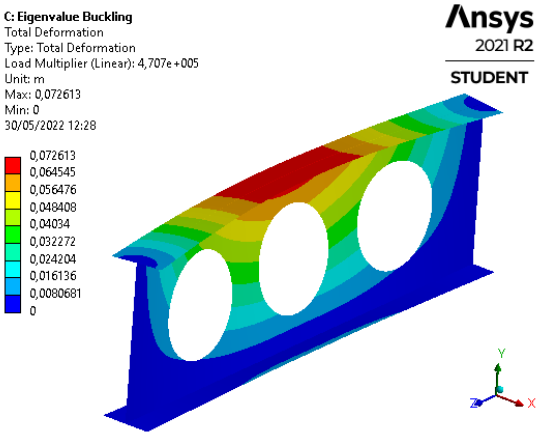

L=1 [m]

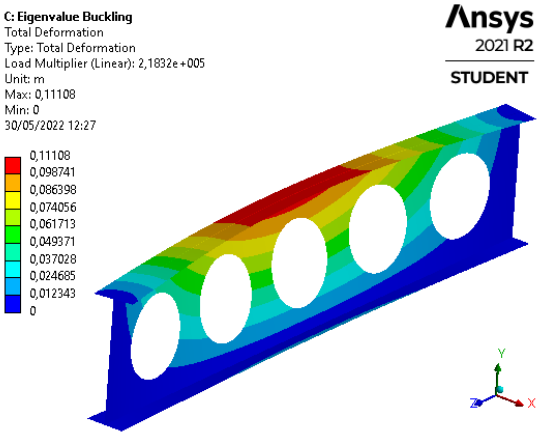

L=1.5 [m]

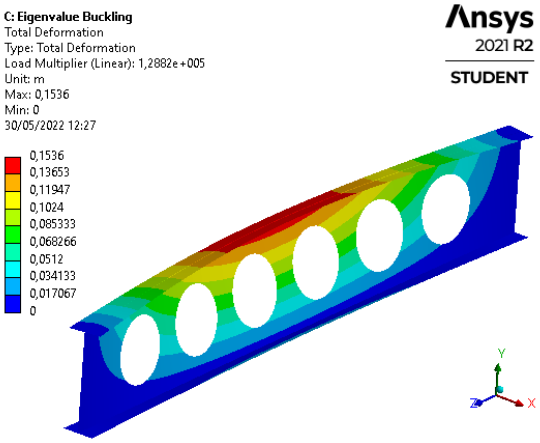

L=2 [m]

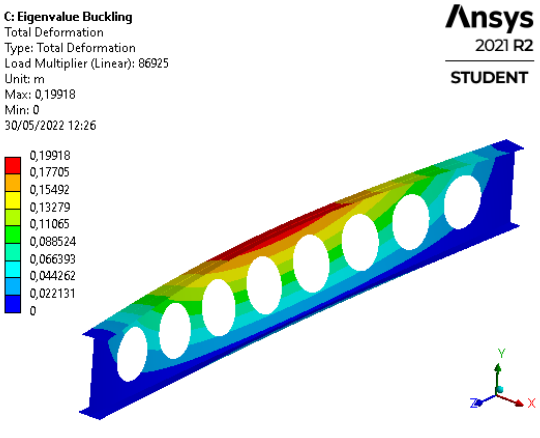

L=2.5 [m]

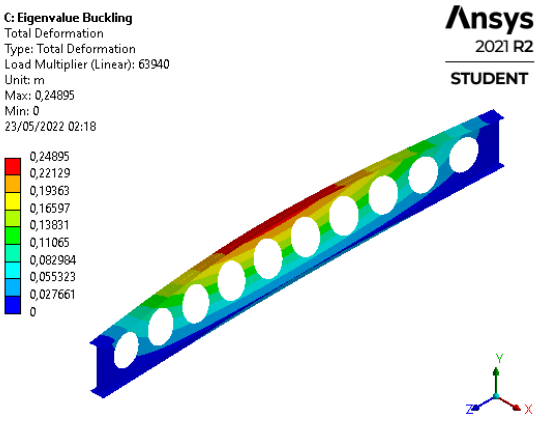

L=3 [m]

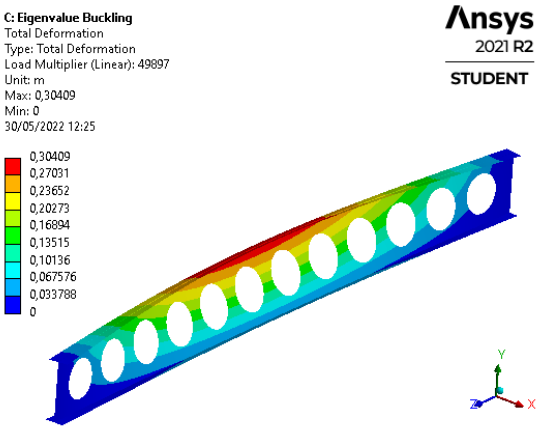

L=3.5 [m]

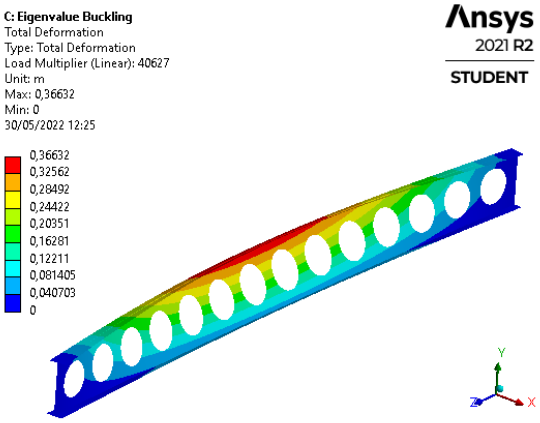

L=4 [m]

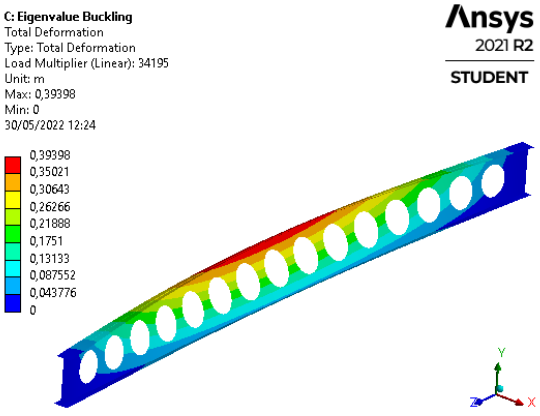

L=4.5 [m]

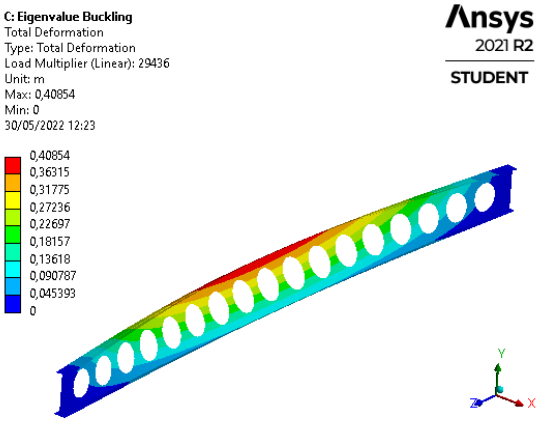

L=5 [m]

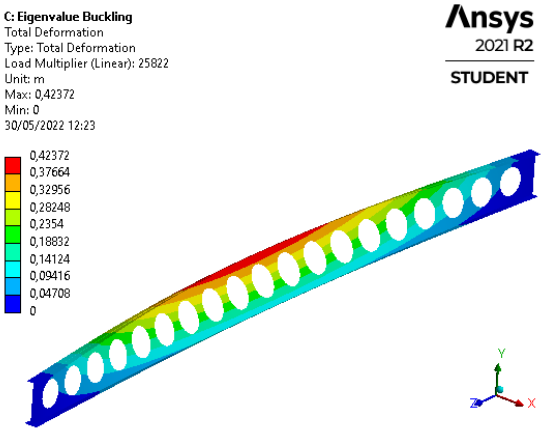

L=5.5 [m]

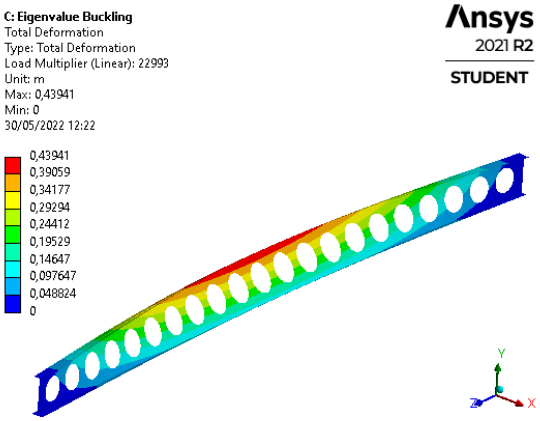

L=6 [m]

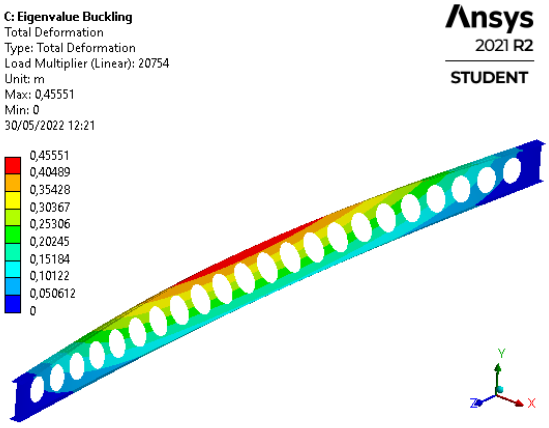

L=6.5 [m]

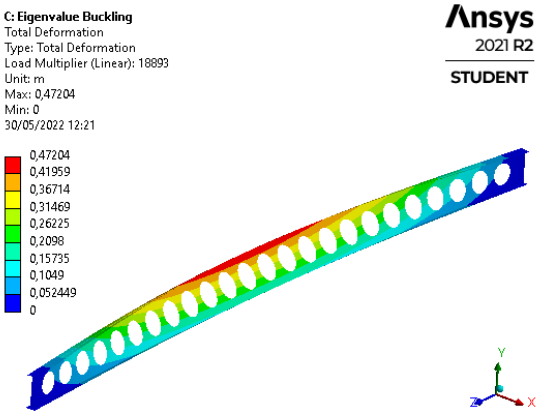

L=7 [m]

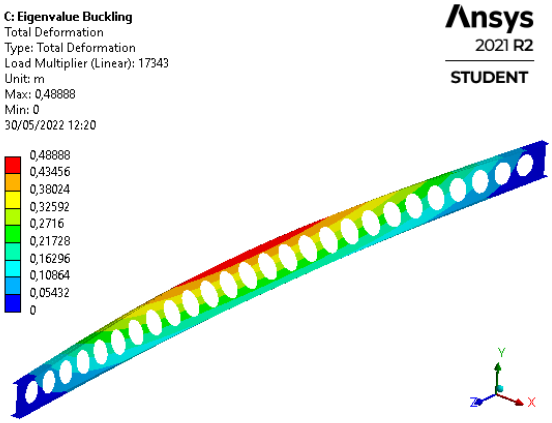

L=7.5 [m]

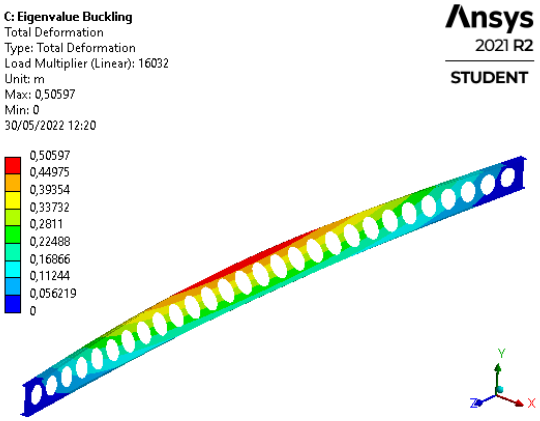

L=8 [m]

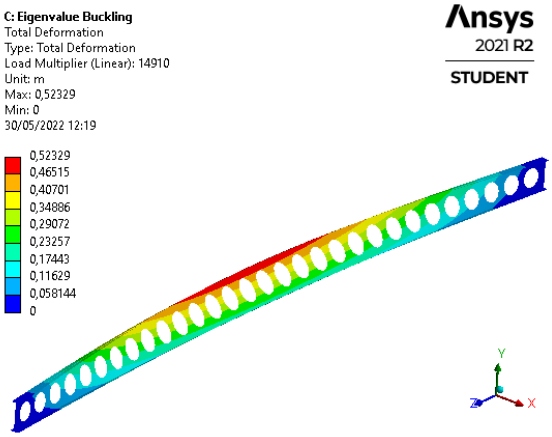

L=8.5 [m]

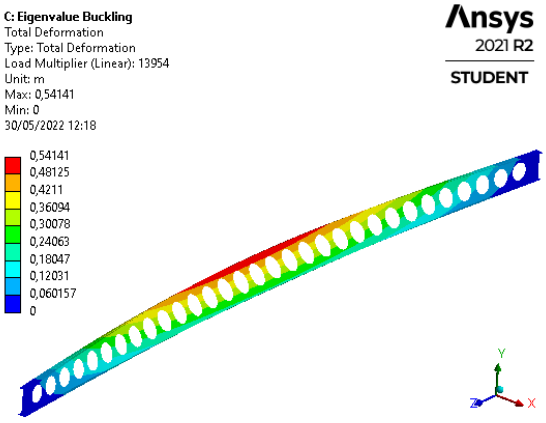

L=9 [m]

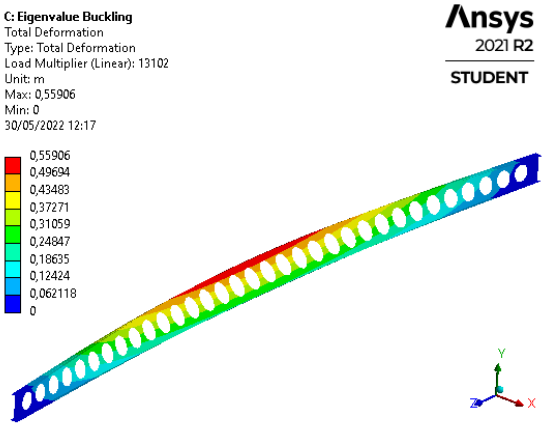

L=9.5 [m]

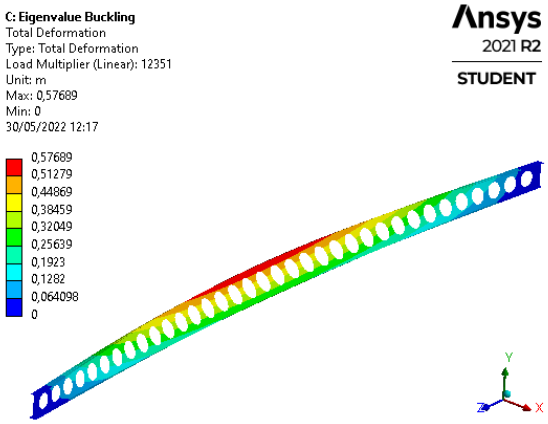
C: Eigenvalue Buckling
Total Deformation
Type: Total Deformation
Load Multiplier (Linear): 12351
Unit: m
Max: 0,57689
Min: 0
30/05/2022 12:17
0,57689
0,51279
0,44869
0,38459
0,32049
0,25639
0,1923
0,1282
0,064098
0
Ansys
2021 R2
STUDENT
Y
Z
X

L=10 [m]

ANNEX G – Lateral-torsional buckling of solid and cellular beam cases based on RM2

Solid beams

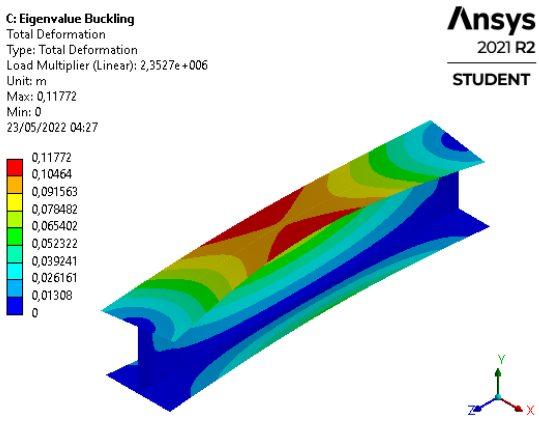

L=1 [m]

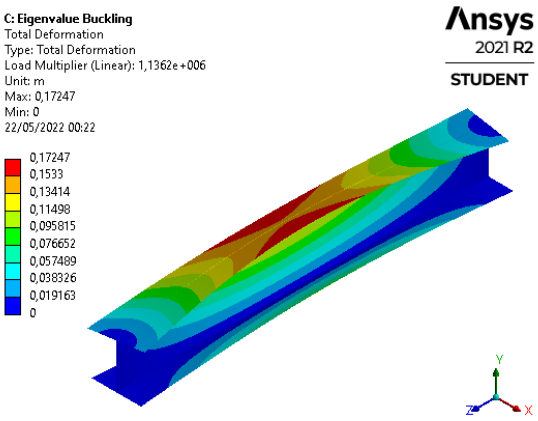

L=1.5 [m]

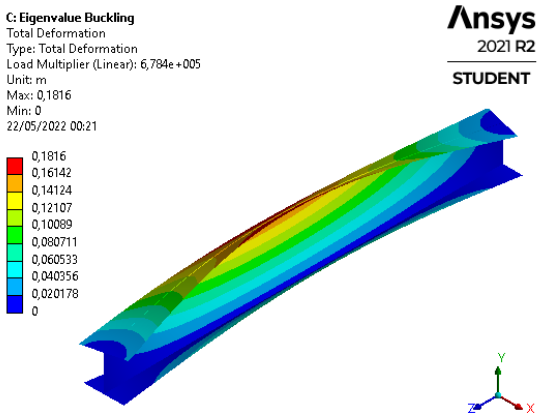

L=2 [m]

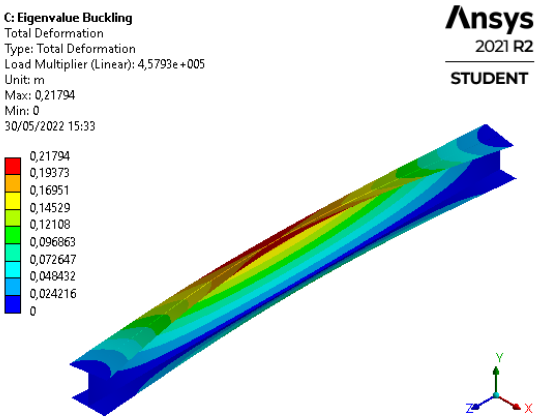

L=2.5 [m]

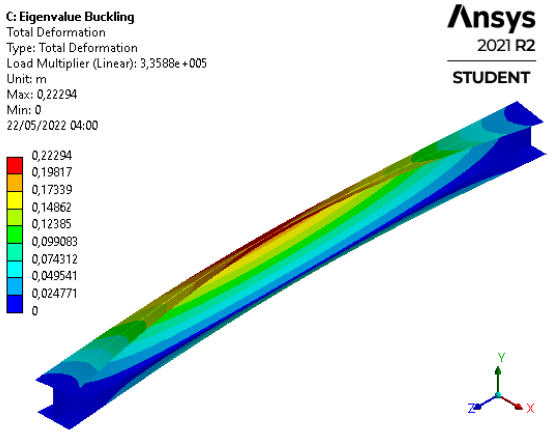

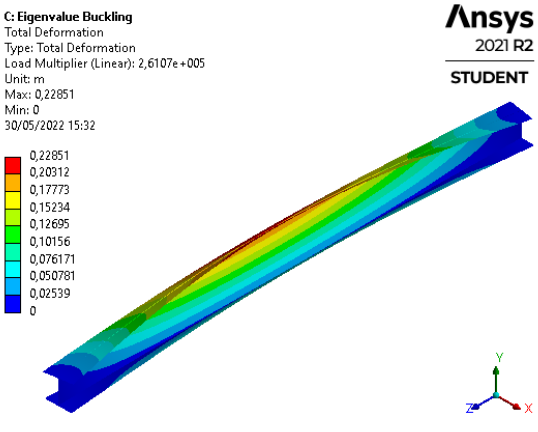

L=3 [m]

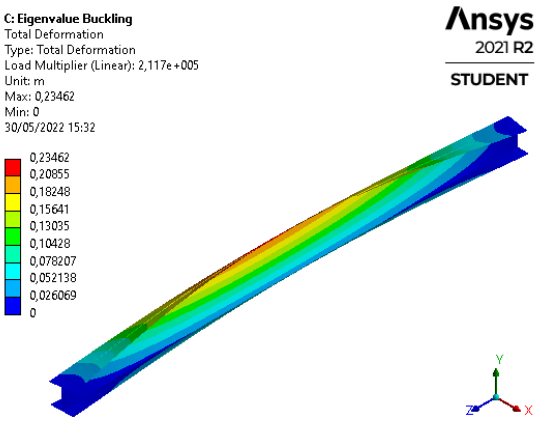

L=3.5 [m]

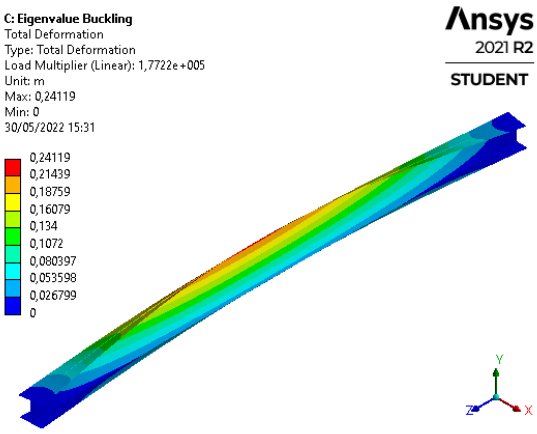

L=4 [m]

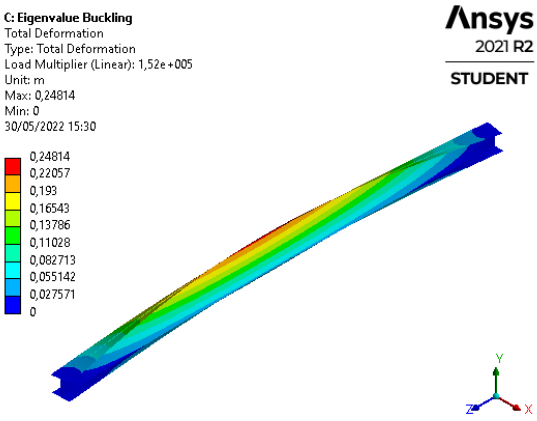

L=4.5 [m]

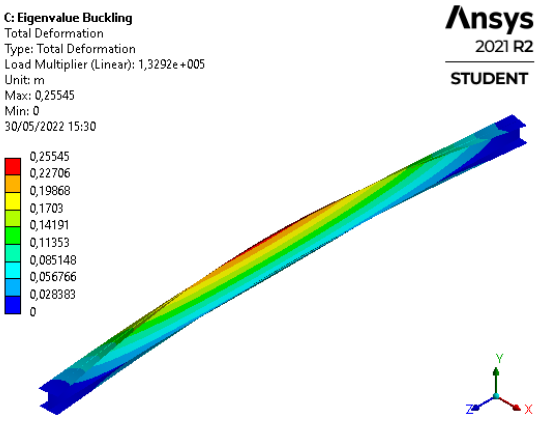

L=5 [m]

L=5.5 [m]

L=6 [m]

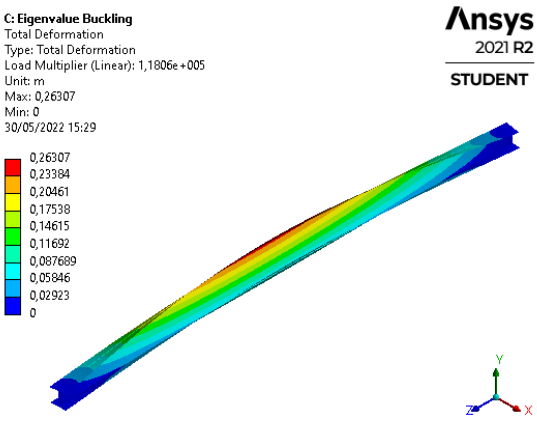

L=6.5 [m]

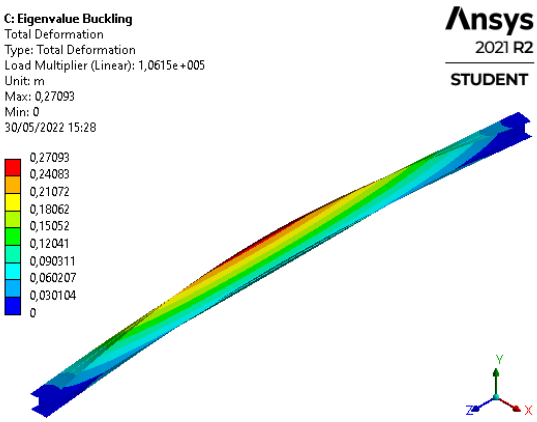

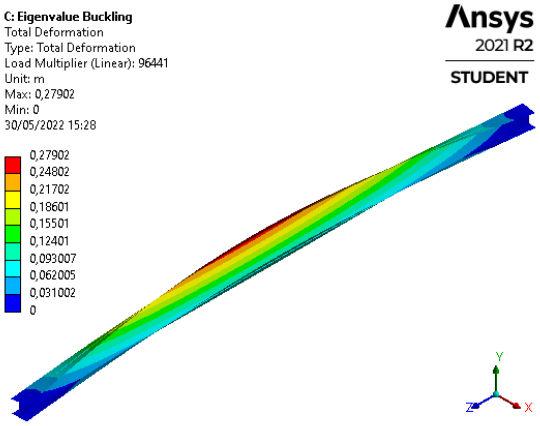

L=7 [m]

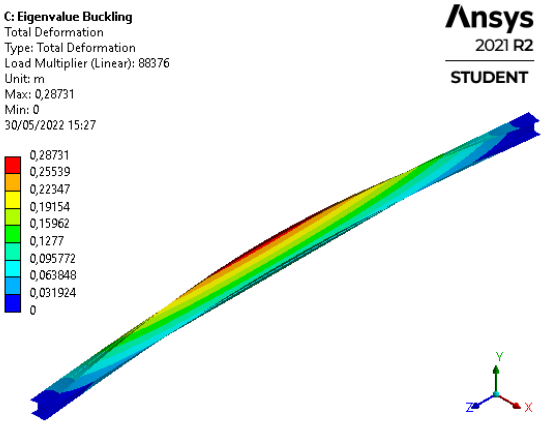

L=7.5 [m]

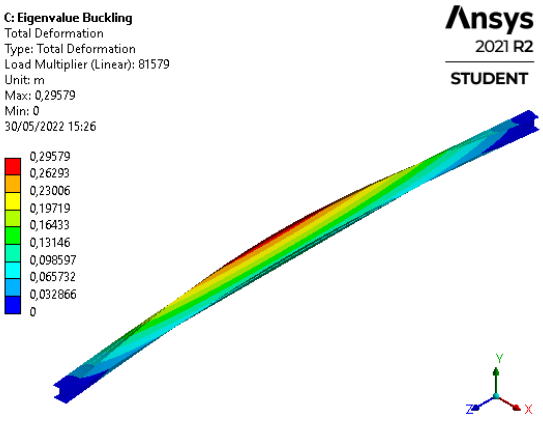

L=8 [m]

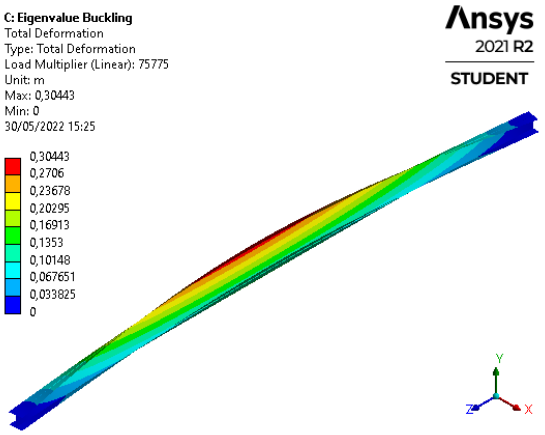

L=8.5 [m]

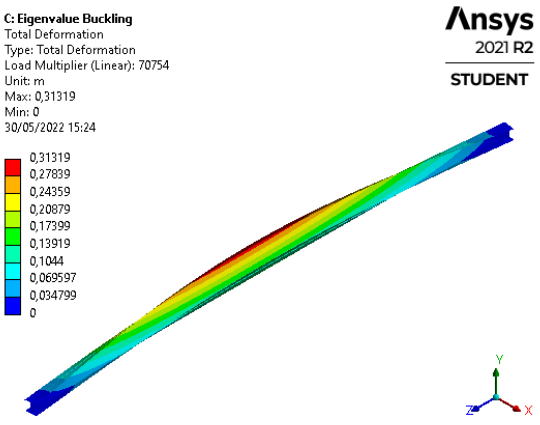

L=9 [m]

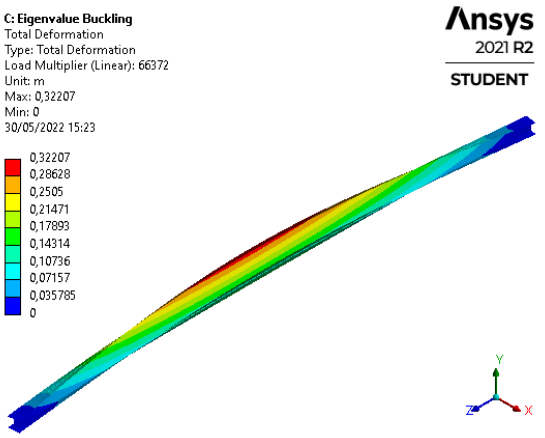

L=9.5 [m]

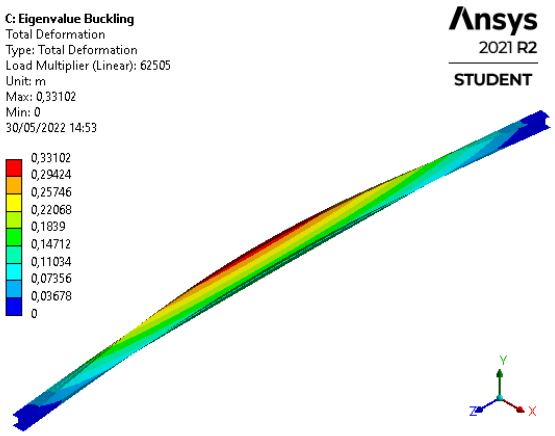
C: Eigenvalue Buckling
Total Deformation
Type: Total Deformation
Load Multiplier (Linear): 62505
Unit: m
Max: 0,33102
Min: 0
30/05/2022 14:53
0,33102
0,29424
0,25746
0,22068
0,1839
0,14712
0,11034
0,07356
0,03678
0
Ansys
2021 R2
STUDENT
Y
Z
X

L=10 [m]

$a_0 = 1.0h$ - $S = 1.4a_0$ - $H = 1.0h$ - RM2

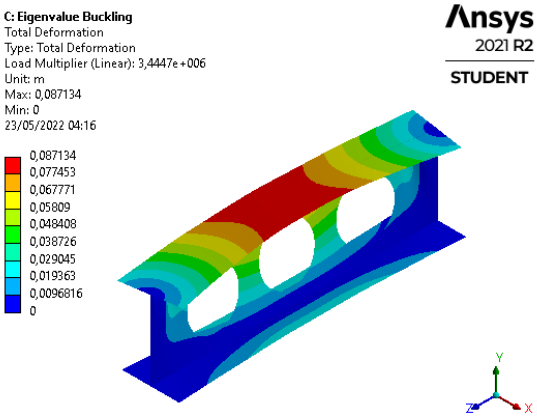

L=1 [m]

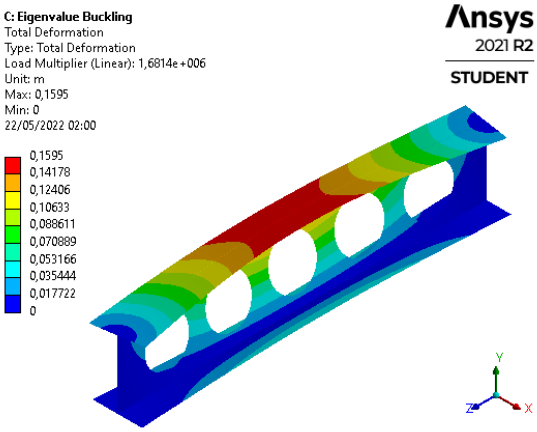

L=1.5 [m]

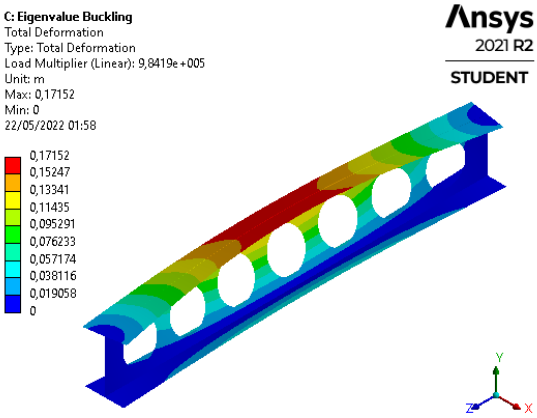

L=2 [m]

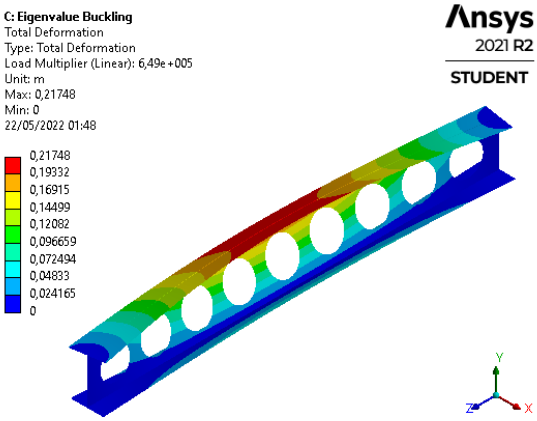

L=2.5 [m]

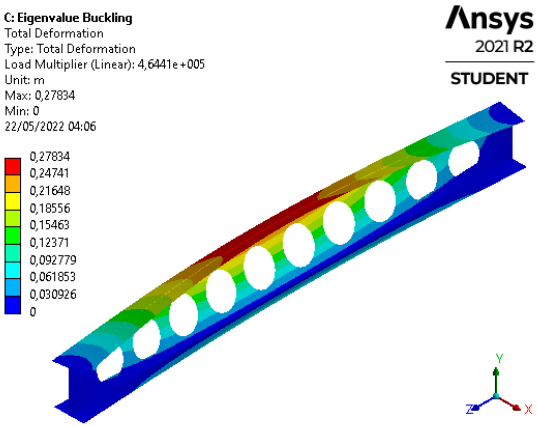

L=3 [m]

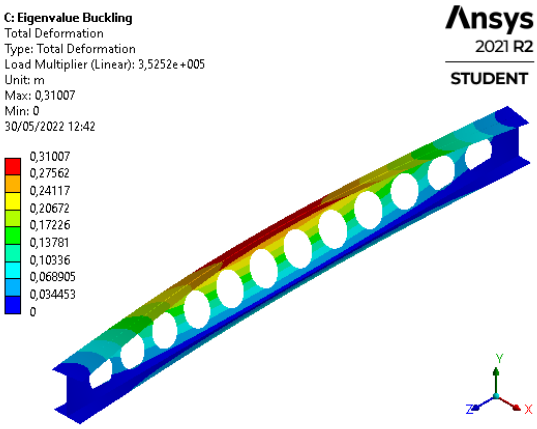

L=3.5 [m]

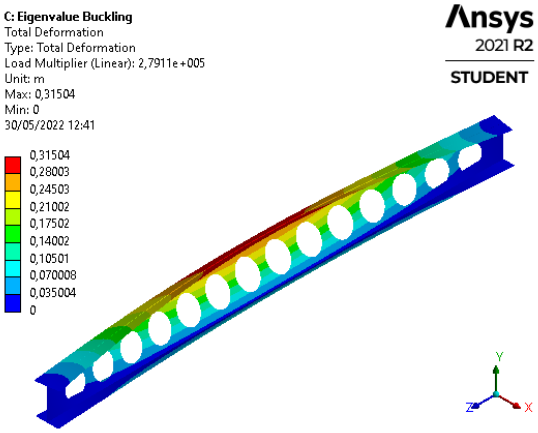

L=4 [m]

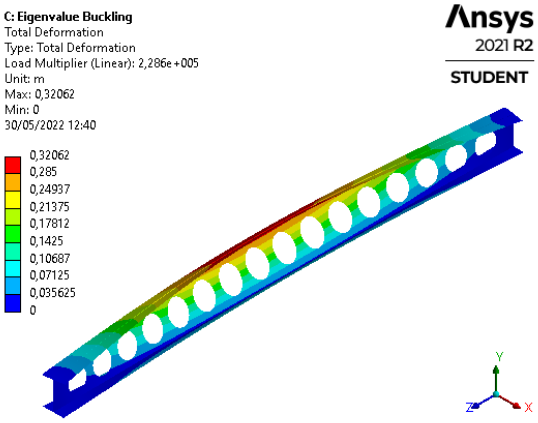

L=4.5 [m]

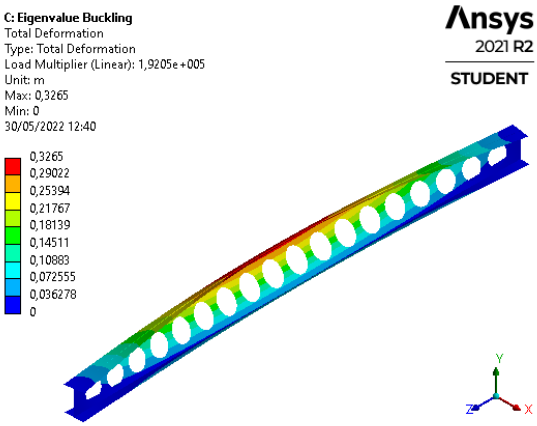

L=5 [m]

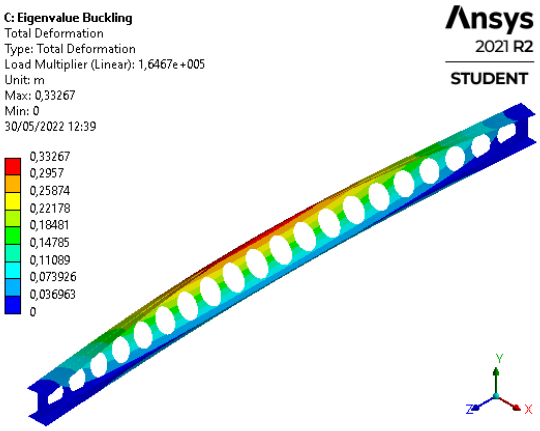

L=5.5 [m]

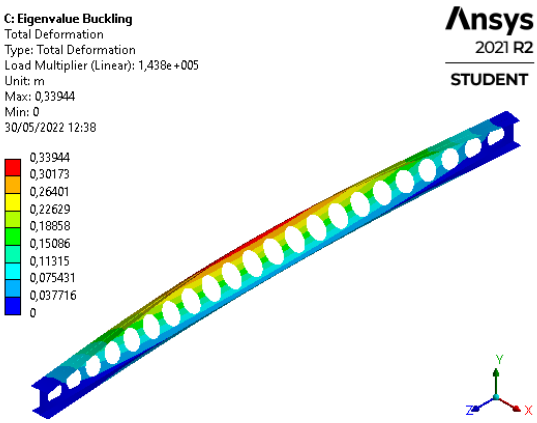

L=6 [m]

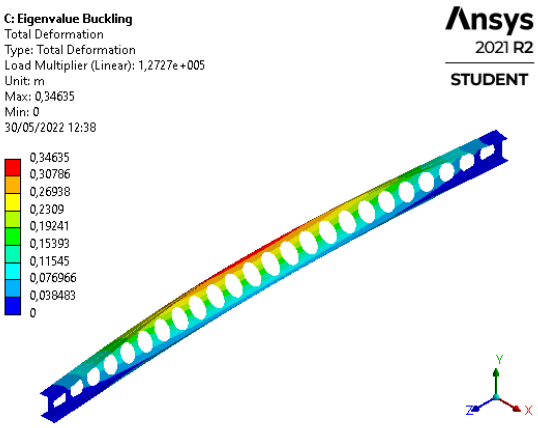

L=6.5 [m]

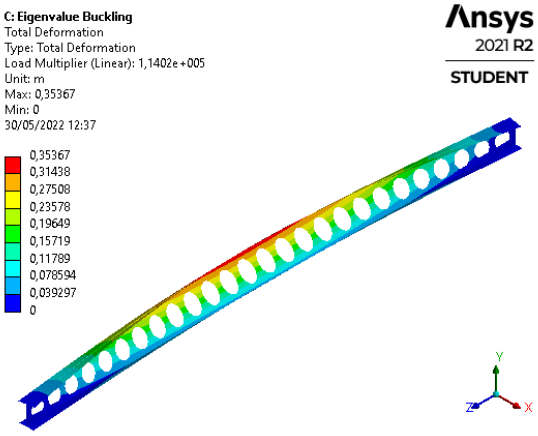

L=7 [m]

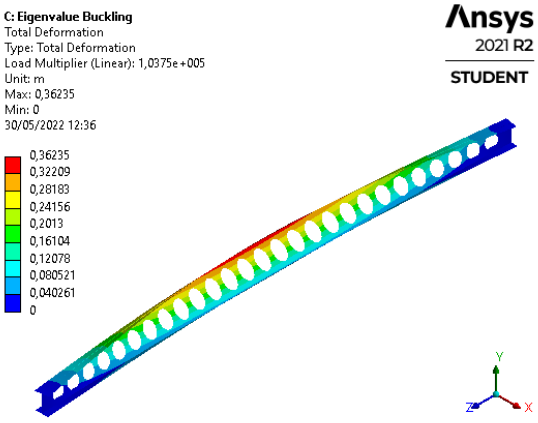

L=7.5 [m]

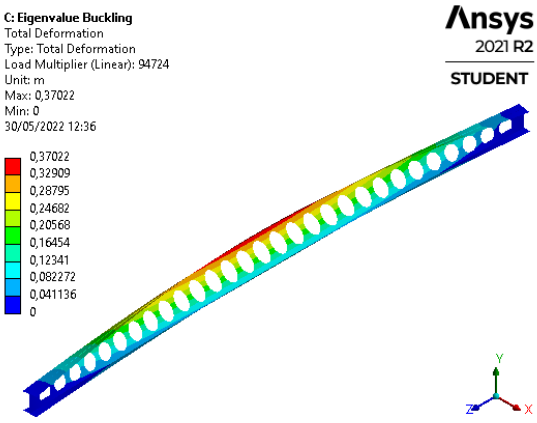

L=8 [m]

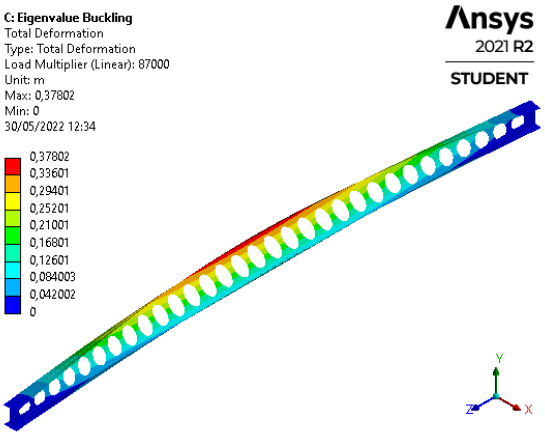

L=8.5 [m]

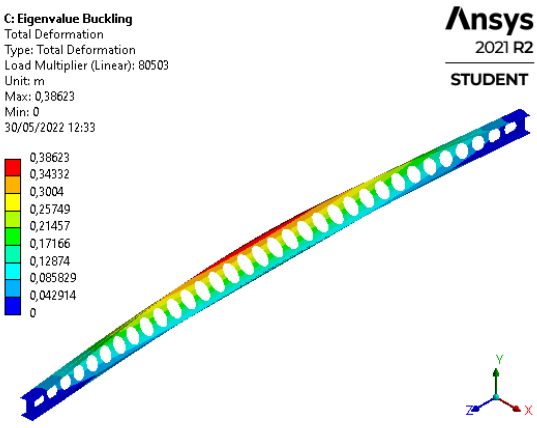

L=9 [m]

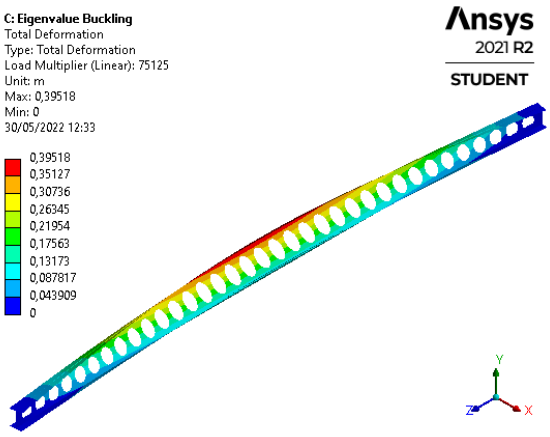

L=9.5 [m]

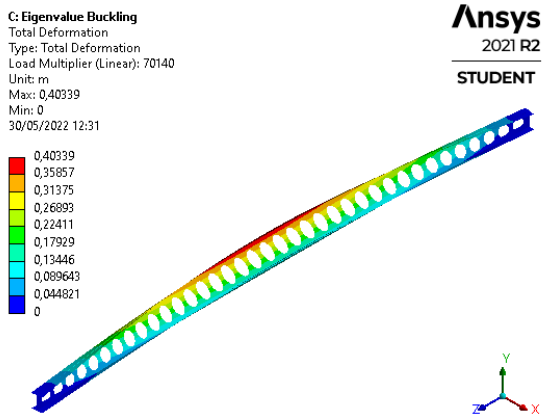
C: Eigenvalue Buckling
Total Deformation
Type: Total Deformation
Load Multiplier (Linear): 70140
Unit: m
Max: 0,40339
Min: 0
30/05/2022 12:31
0,40339
0,35857
0,31375
0,26893
0,22411
0,17929
0,13446
0,089643
0,044821
0
Ansys
2021 R2
STUDENT
Y
Z
X

L=10 [m]

$$a_0 = 0.8h$$

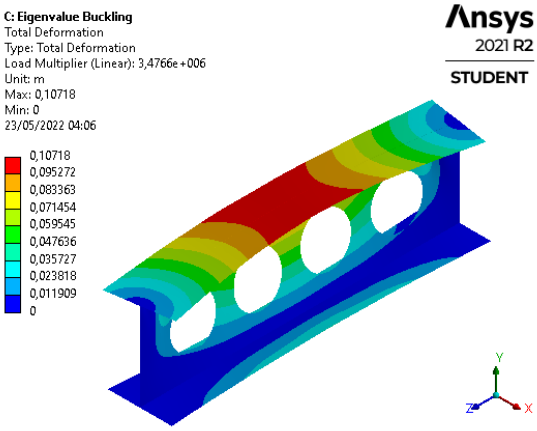

L=1 [m]

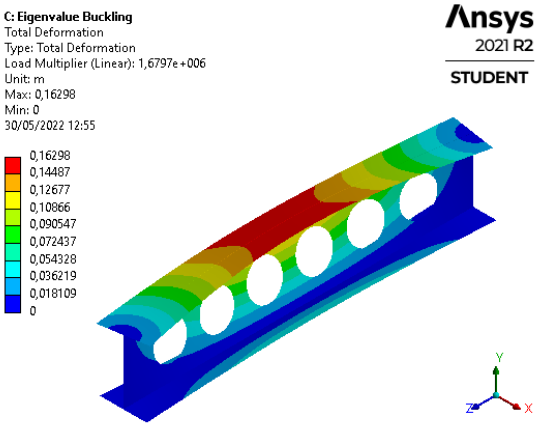

L=1.5 [m]

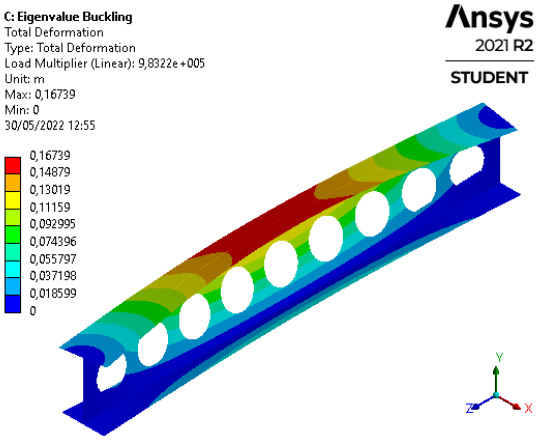

L=2 [m]

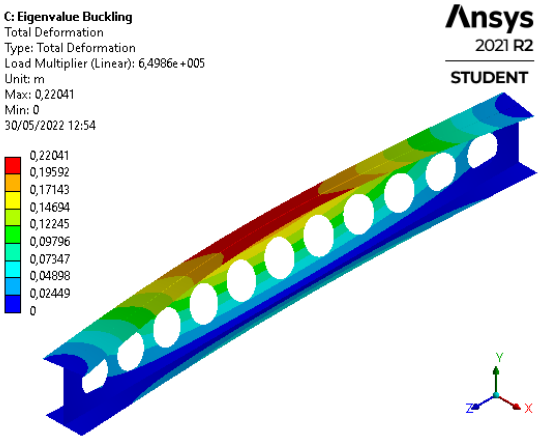

L=2.5 [m]

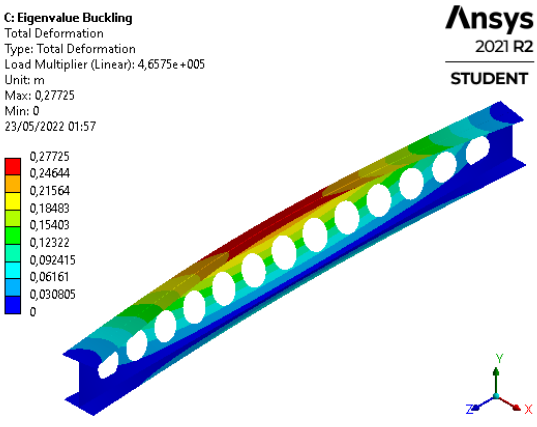

L=3 [m]

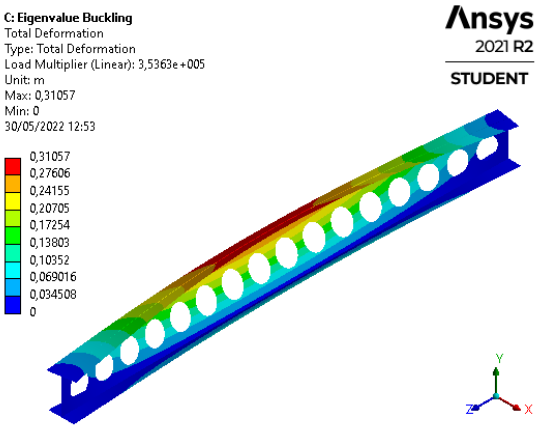

L=3.5 [m]

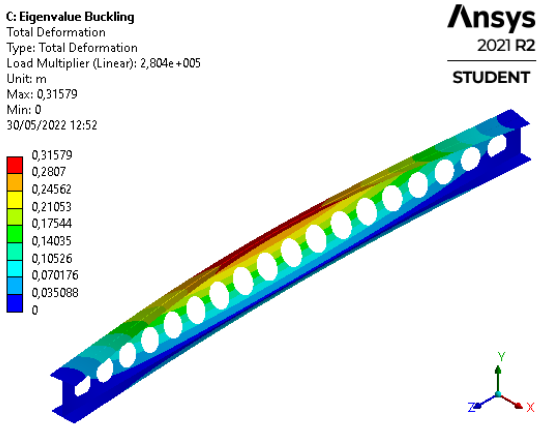

L=4 [m]

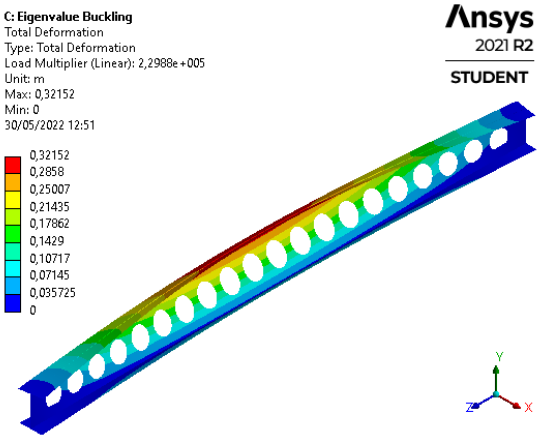

L=4.5 [m]

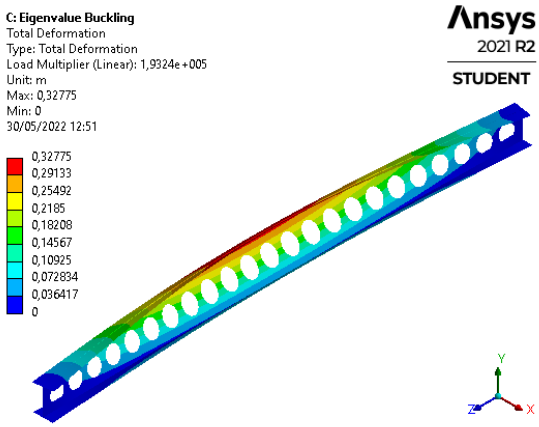

L=5 [m]

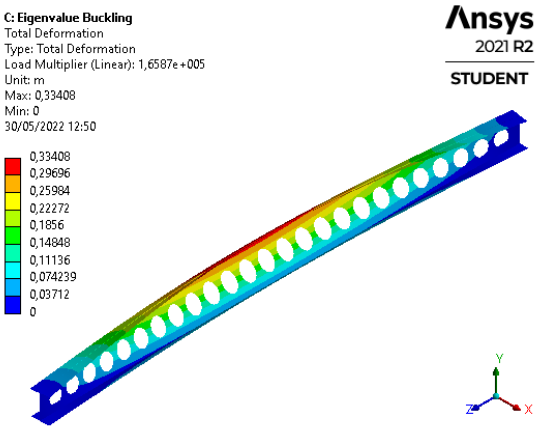

L=5.5 [m]

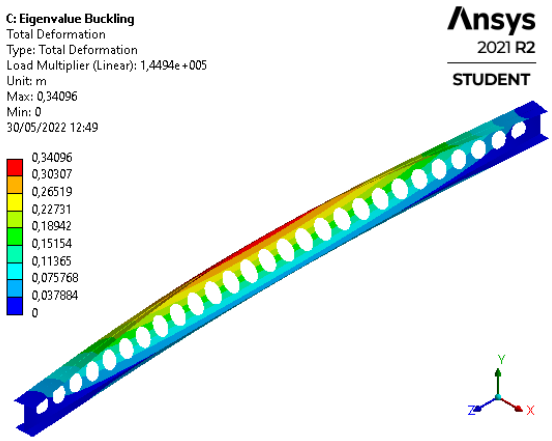

L=6 [m]

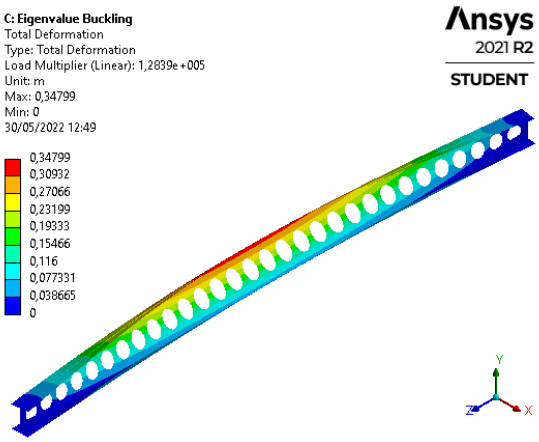

L=6.5 [m]

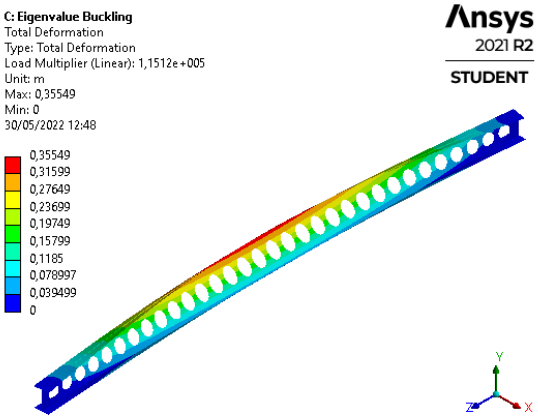

L=7 [m]

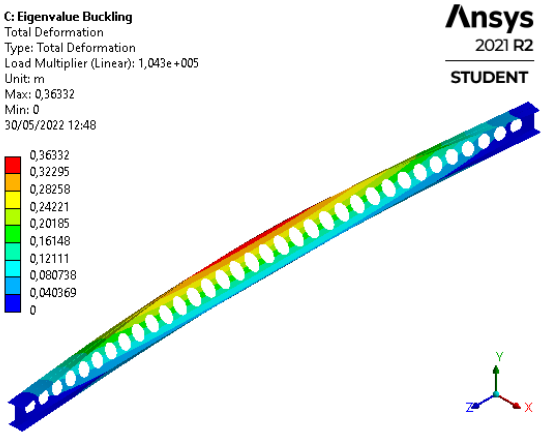

L=7.5 [m]

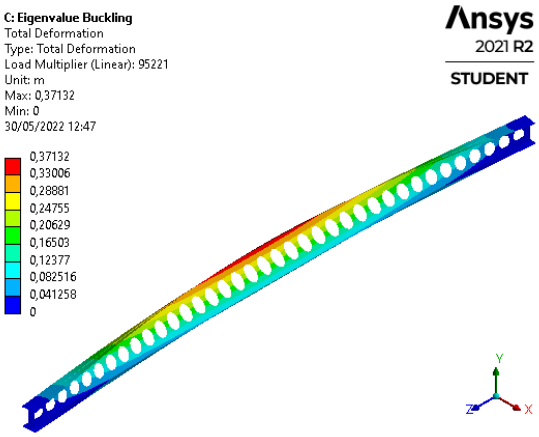

L=8 [m]

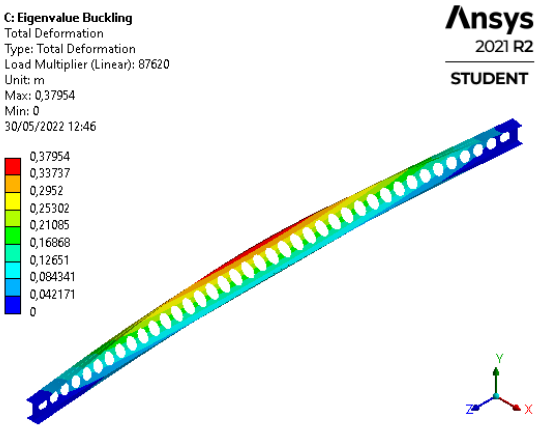

L=8.5 [m]

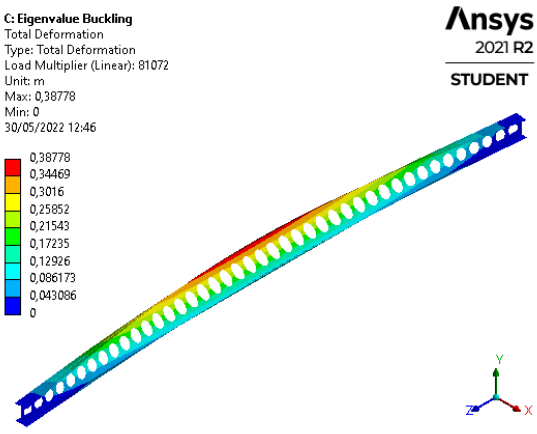

L=9 [m]

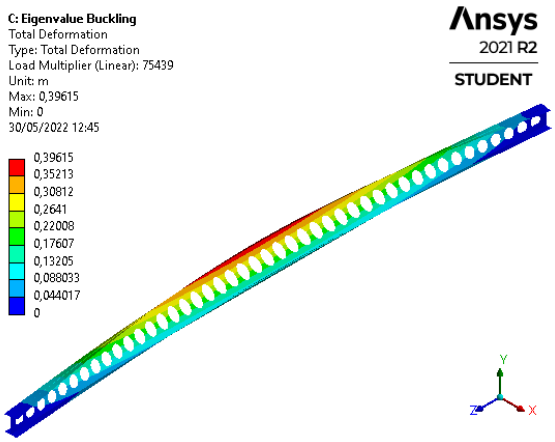

L=9.5 [m]

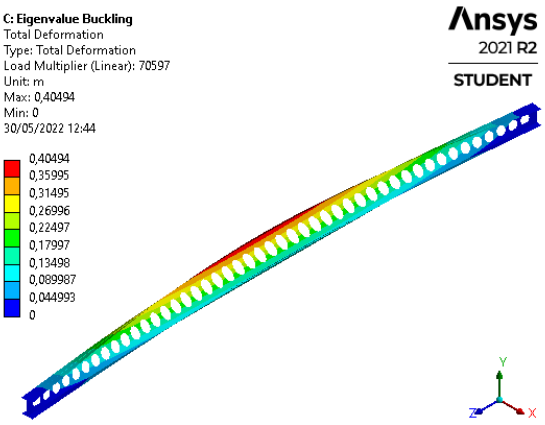
C: Eigenvalue Buckling
Total Deformation
Type: Total Deformation
Load Multiplier (Linear): 70597
Unit: m
Max: 0,40494
Min: 0
30/05/2022 12:44
0,40494
0,35995
0,31495
0,26996
0,22497
0,17997
0,13498
0,089987
0,044993
0
Ansys
2021 R2
STUDENT
Y
Z
X

L=10 [m]

$$a_0 = 1.3h$$

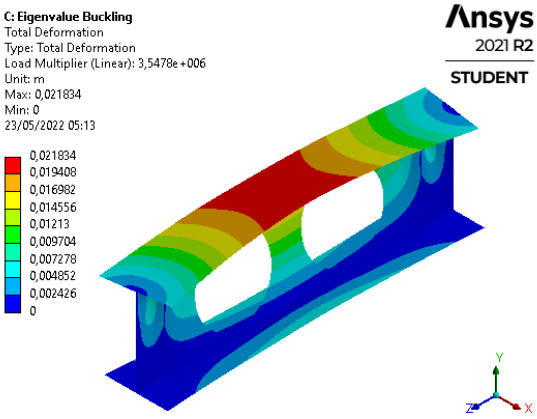

L=1 [m]

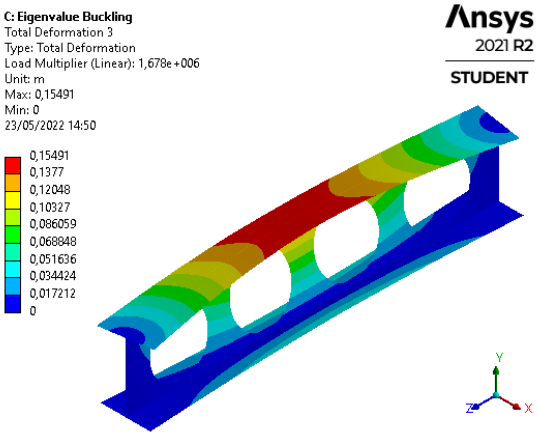

L=1.5 [m]

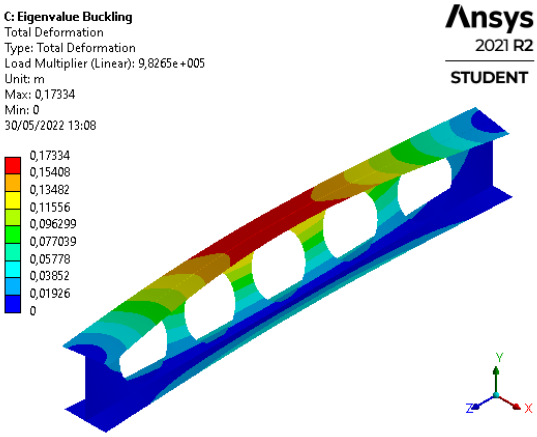

L=2 [m]

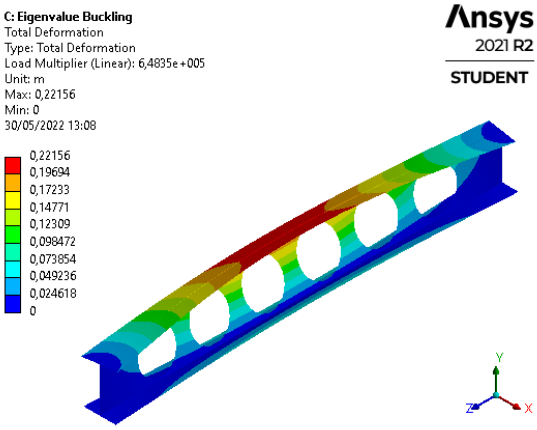

L=2.5 [m]

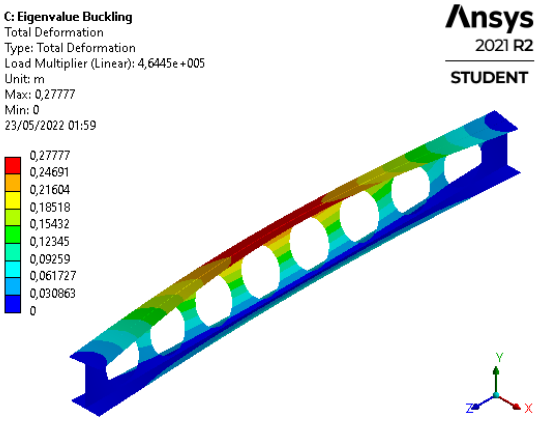

L=3 [m]

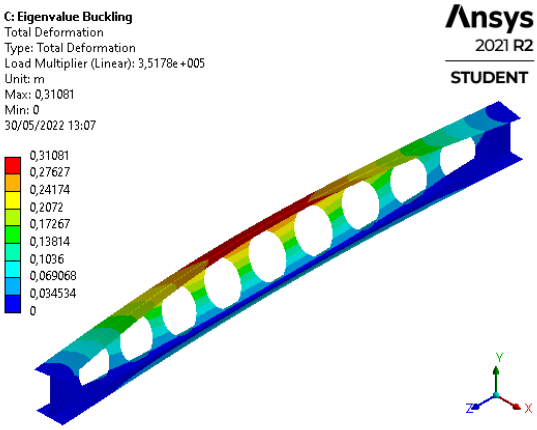

L=3.5 [m]

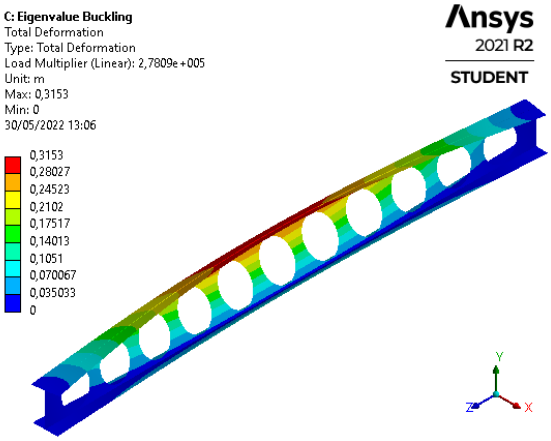

L=4 [m]

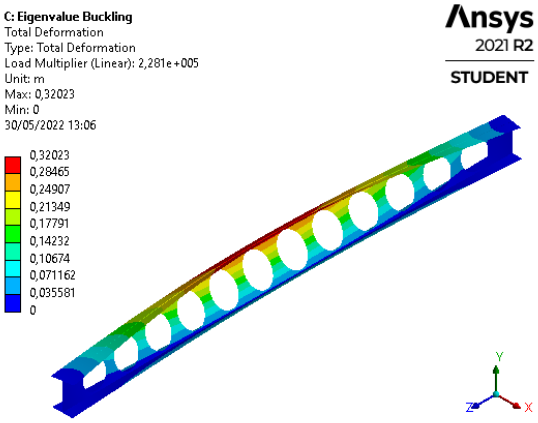

L=4.5 [m]

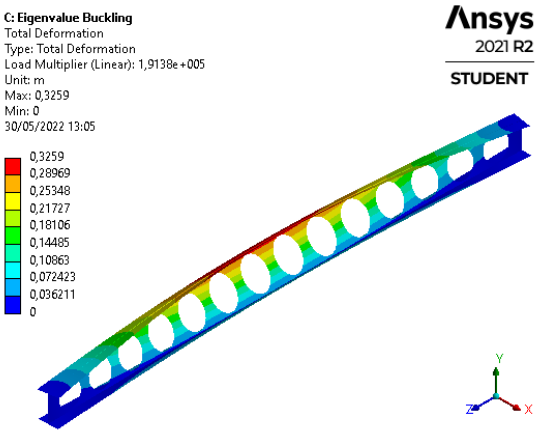

L=5 [m]

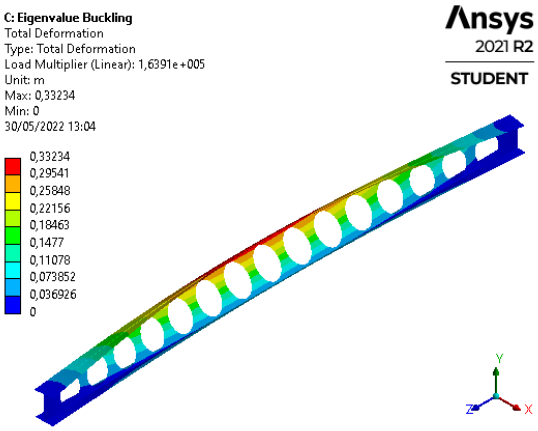

L=5.5 [m]

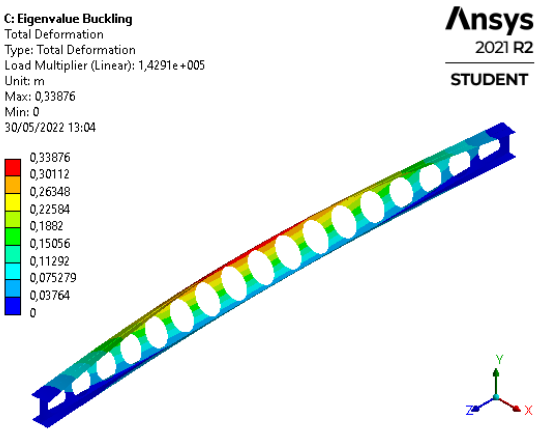

L=6 [m]

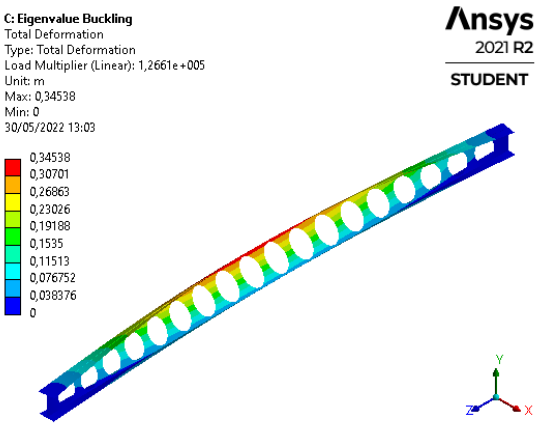

L=6.5 [m]

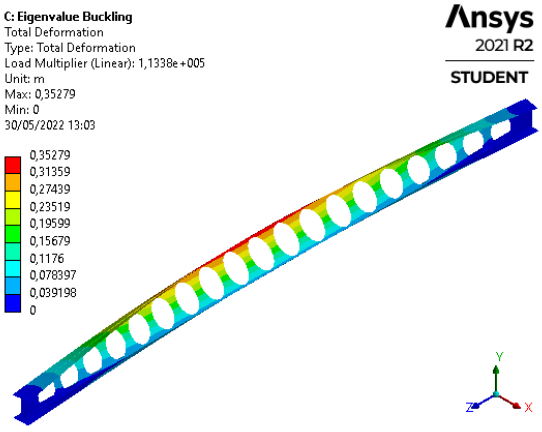

L=7 [m]

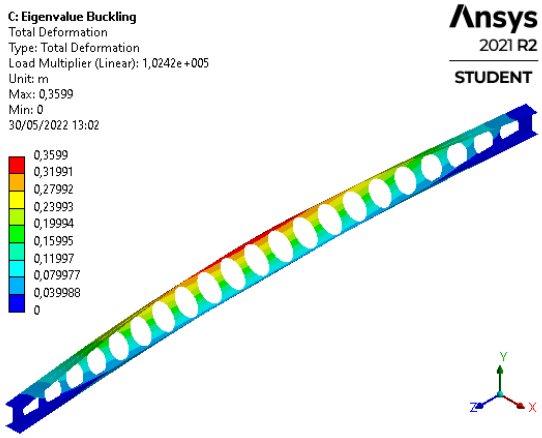

L=7.5 [m]

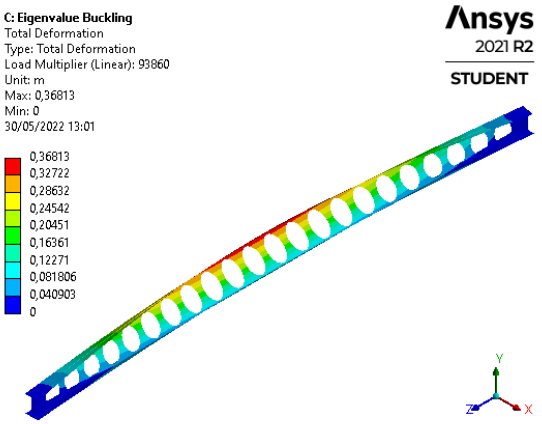

L=8 [m]

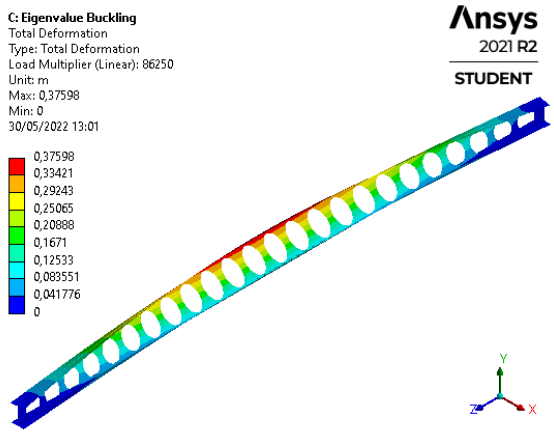

L=8.5 [m]

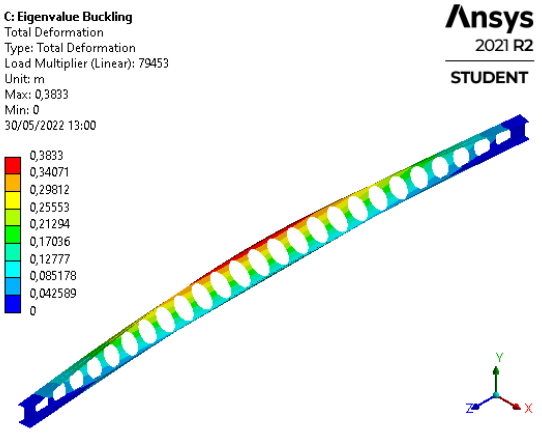

L=9 [m]

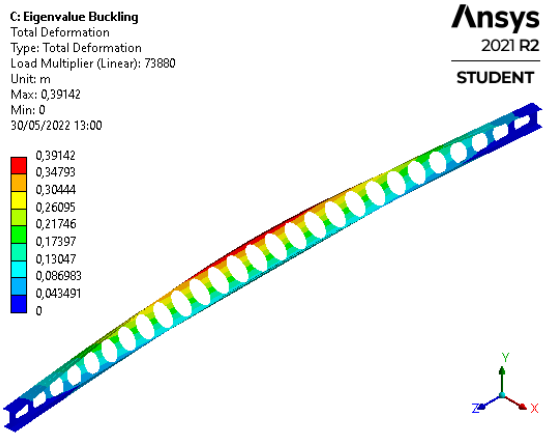

L=9.5 [m]

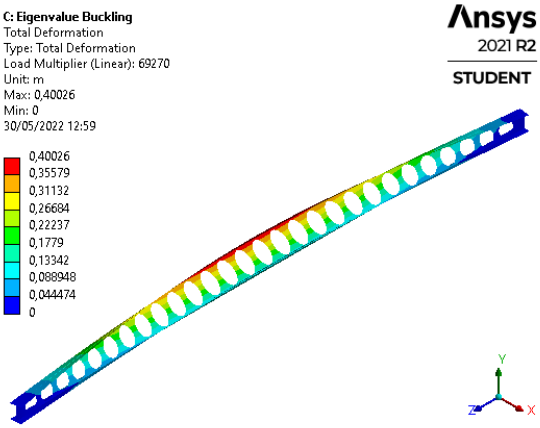
C: Eigenvalue Buckling
Total Deformation
Type: Total Deformation
Load Multiplier (Linear): 69270
Unit: m
Max: 0,40026
Min: 0
30/05/2022 12:59
0,40026
0,35579
0,31132
0,26684
0,22237
0,1779
0,13342
0,088948
0,044474
0
Ansys
2021 R2
STUDENT
Y
Z
X

L=10 [m]

$$S = 1.1a_0$$

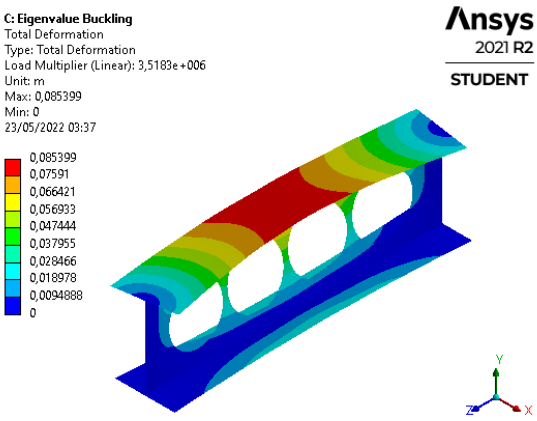

L=1 [m]

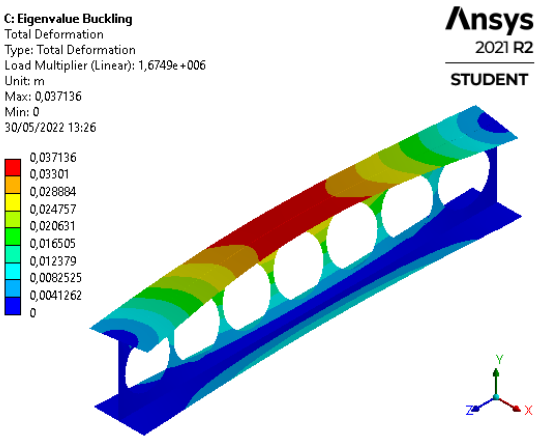

L=1.5 [m]

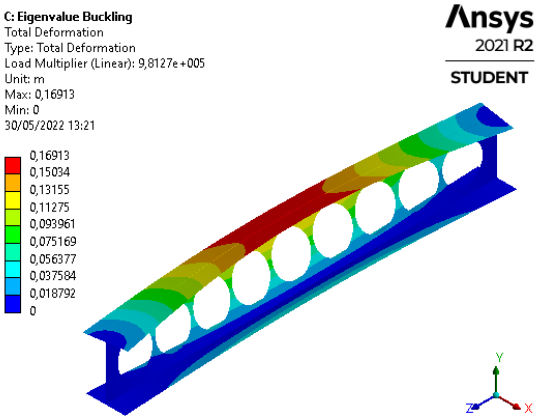

L=2 [m]

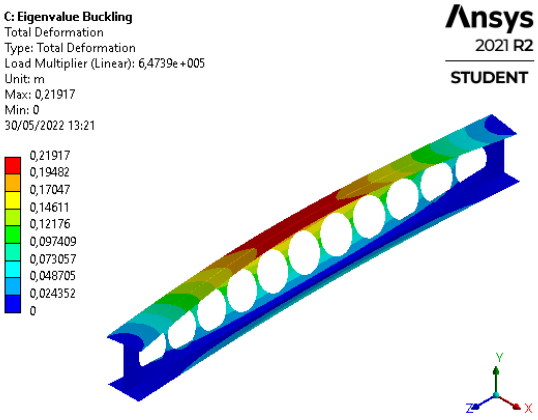

L=2.5 [m]

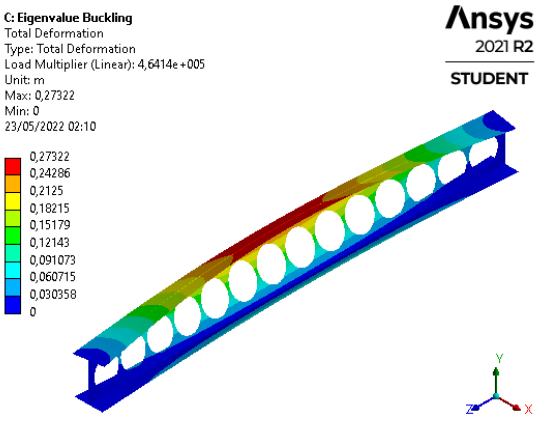

L=3 [m]

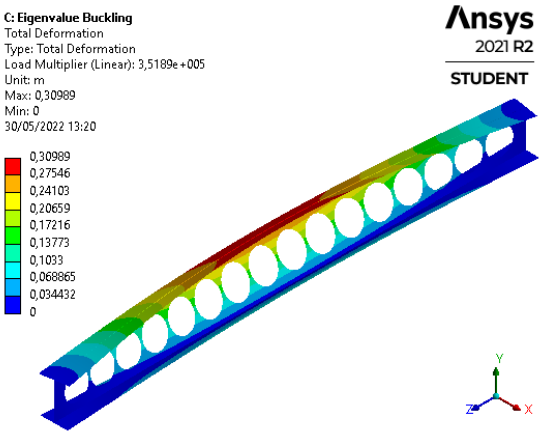

L=3.5 [m]

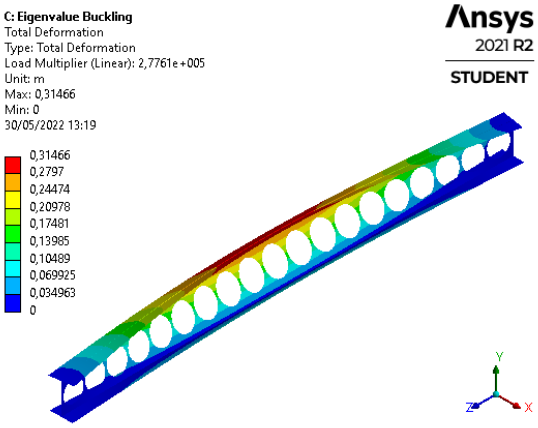

L=4 [m]

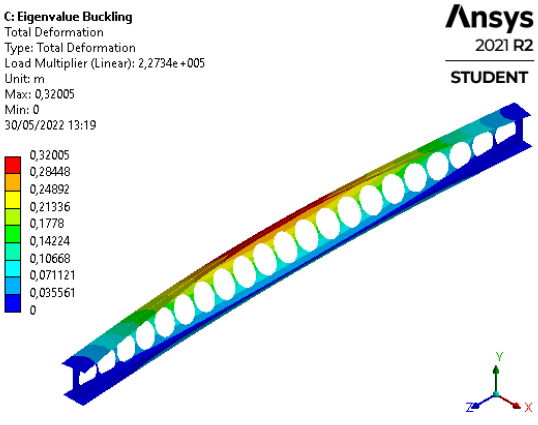

L=4.5 [m]

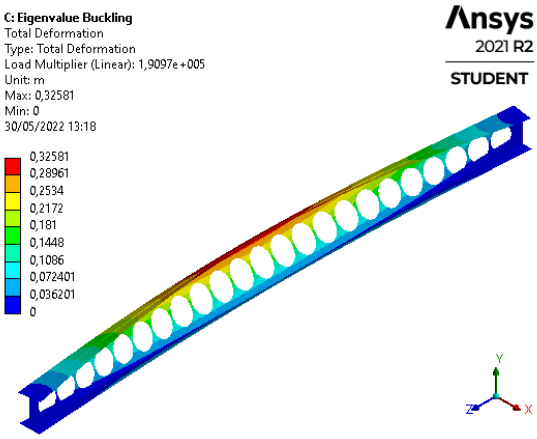

L=5 [m]

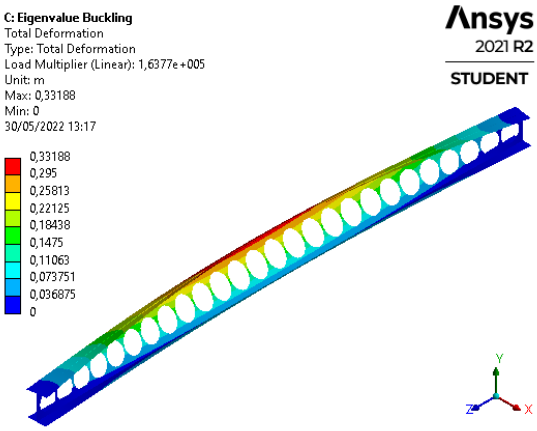

L=5.5 [m]

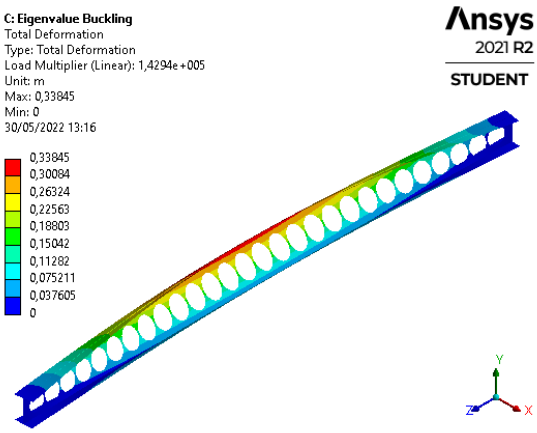

L=6 [m]

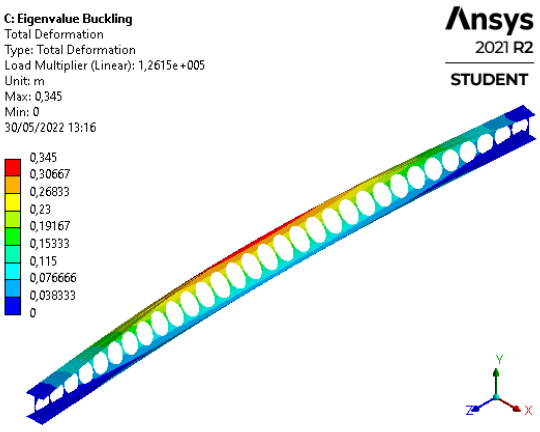

L=6.5 [m]

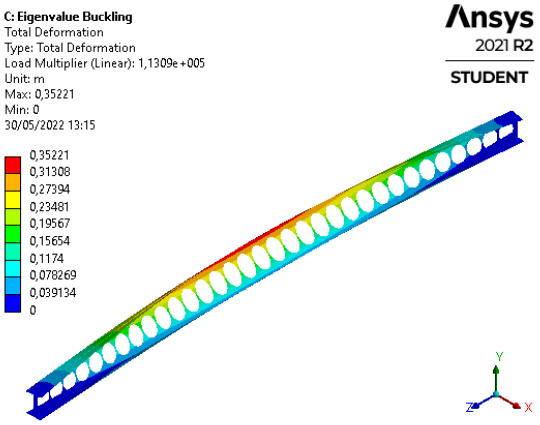

L=7 [m]

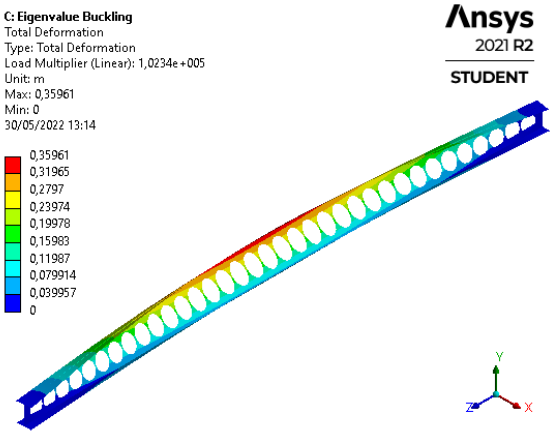

L=7.5 [m]

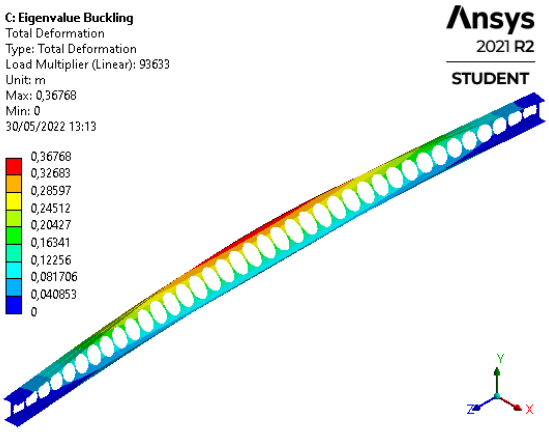

L=8 [m]

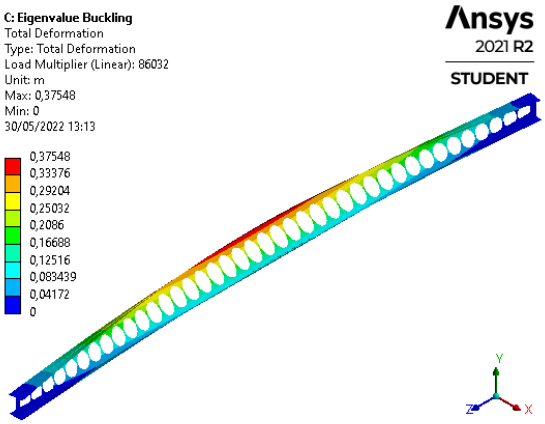

L=8.5 [m]

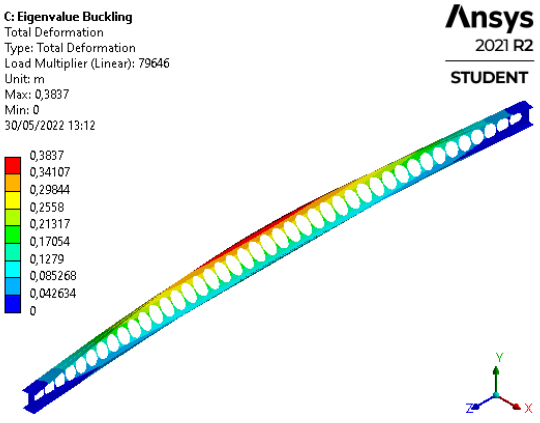

L=9 [m]

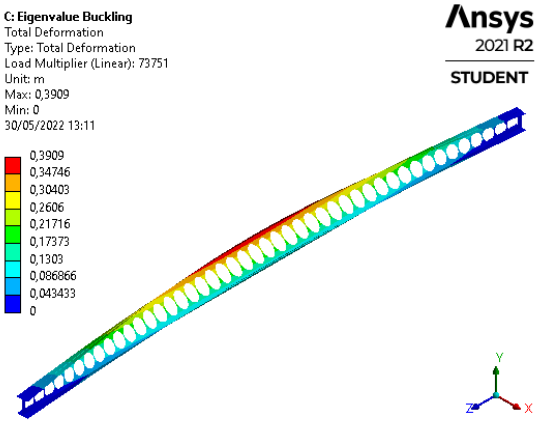

L=9.5 [m]

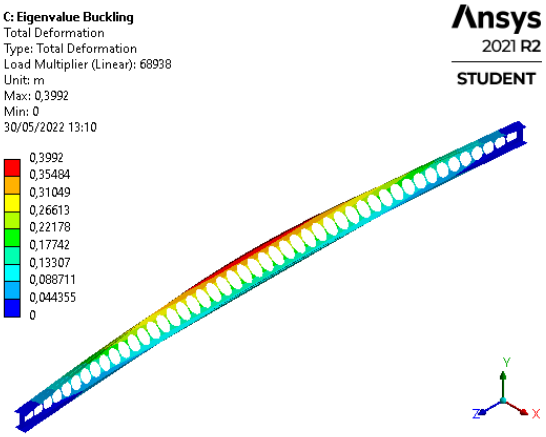
C: Eigenvalue Buckling
Total Deformation
Type: Total Deformation
Load Multiplier (Linear): 68938
Unit: m
Max: 0,3992
Min: 0
30/05/2022 13:10
0,3992
0,35484
0,31049
0,26613
0,22178
0,17742
0,13307
0,088711
0,044355
0
Ansys
2021 R2
STUDENT
Y
Z
X

L=10 [m]

$$S = 1.7a_0$$

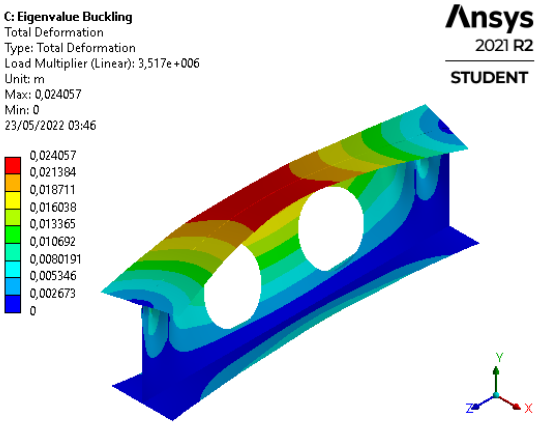

L=1 [m]

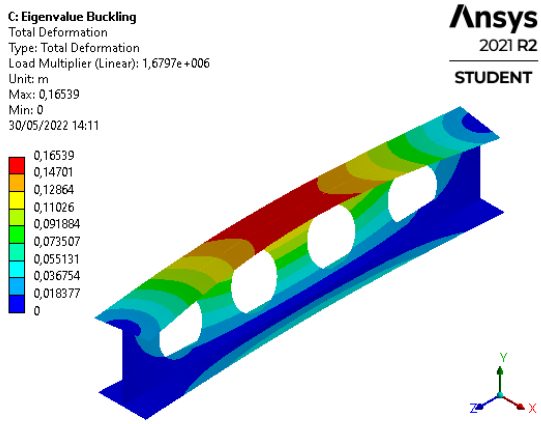

L=1.5 [m]

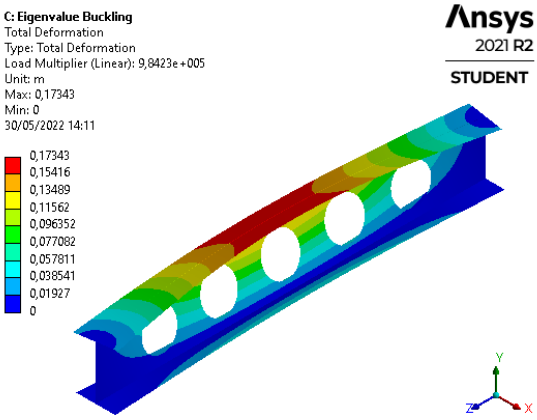

L=2 [m]

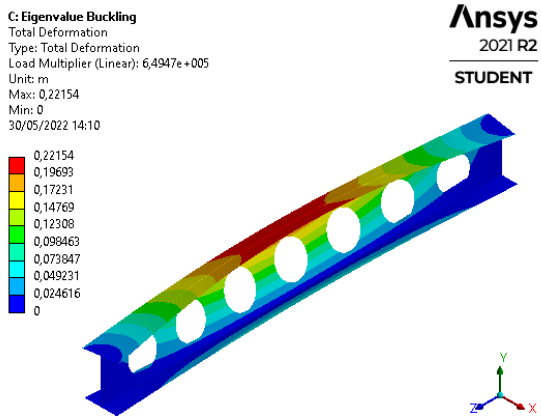

L=2.5 [m]

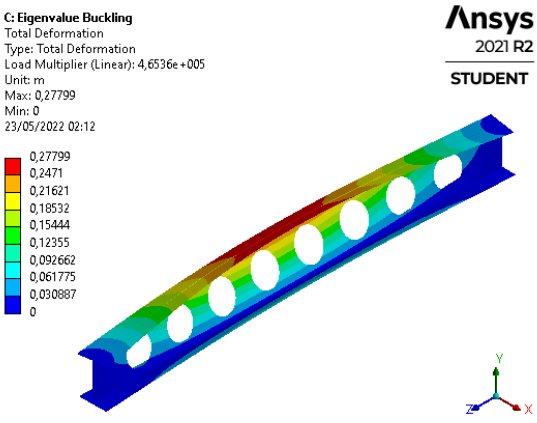

L=3 [m]

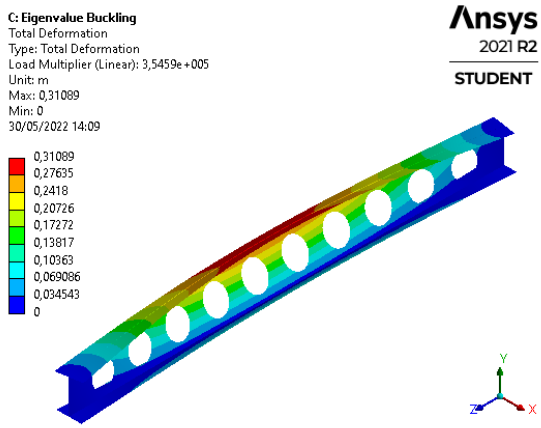

L=3.5 [m]

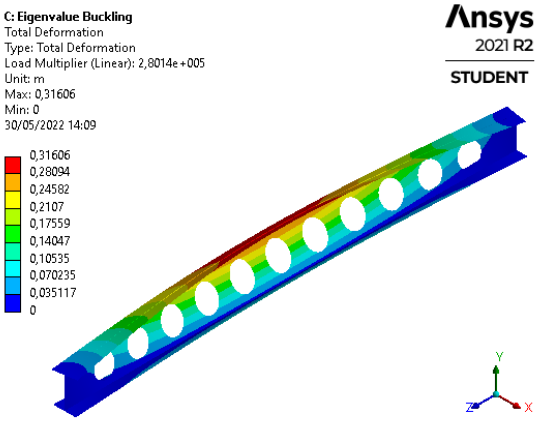

L=4 [m]

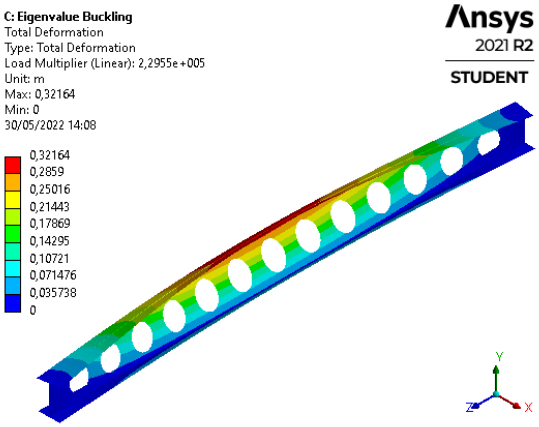

L=4.5 [m]

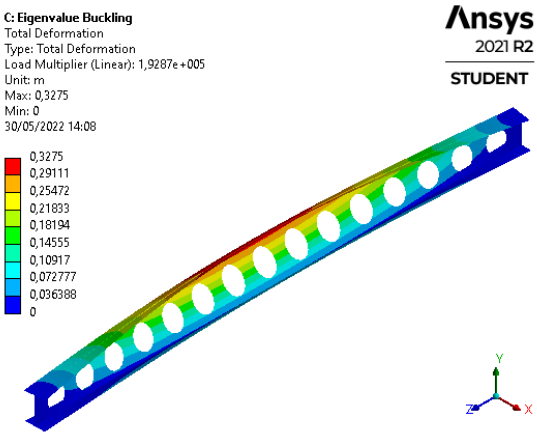

L=5 [m]

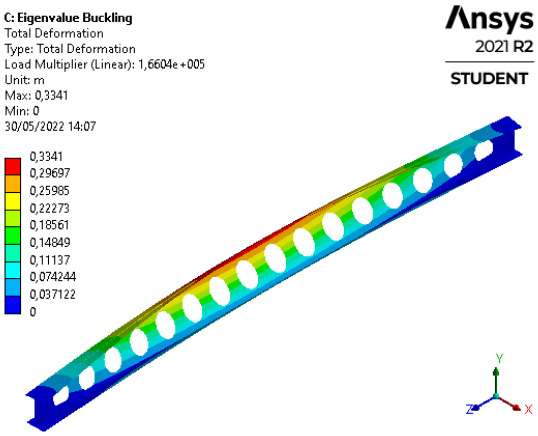

L=5.5 [m]

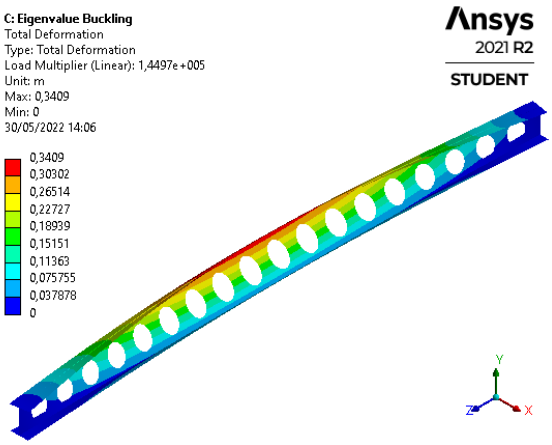

L=6 [m]

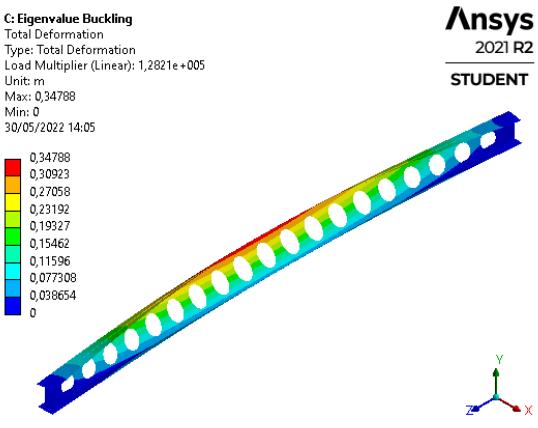

L=6.5 [m]

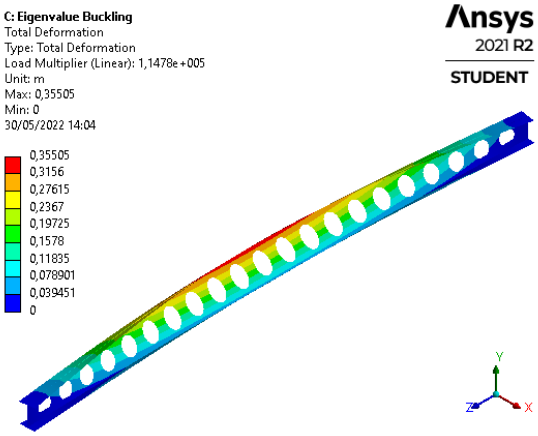

L=7 [m]

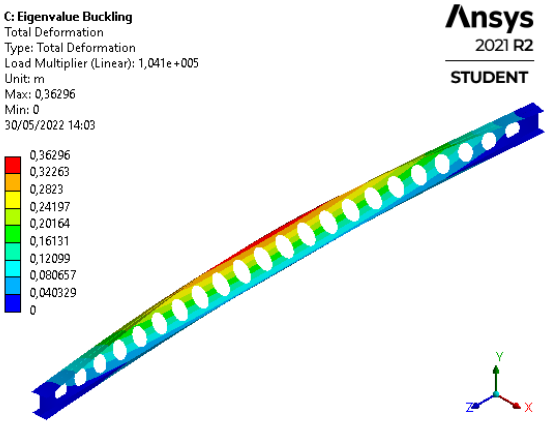

L=7.5 [m]

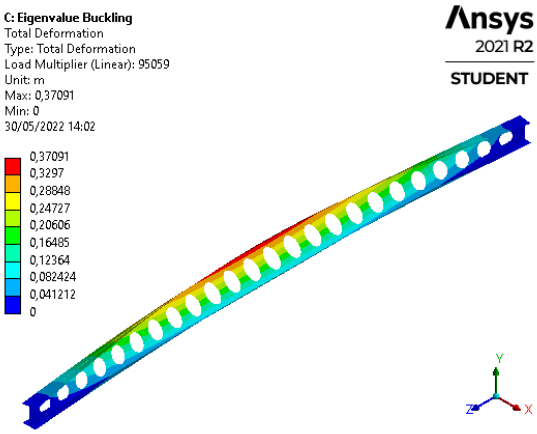

L=8 [m]

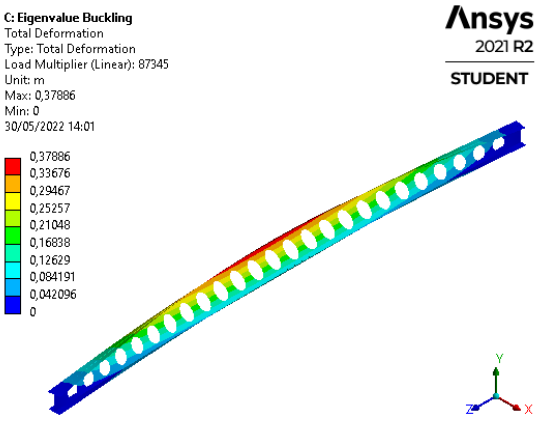

L=8.5 [m]

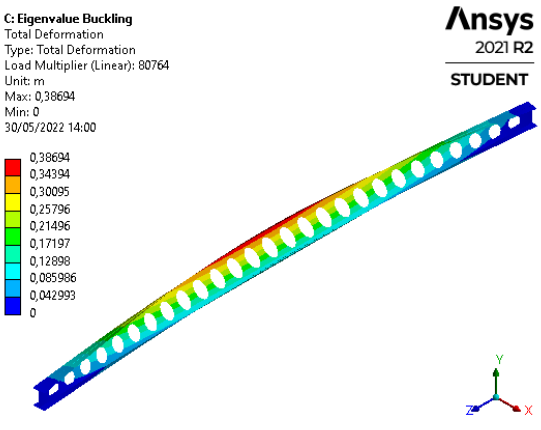

L=9 [m]

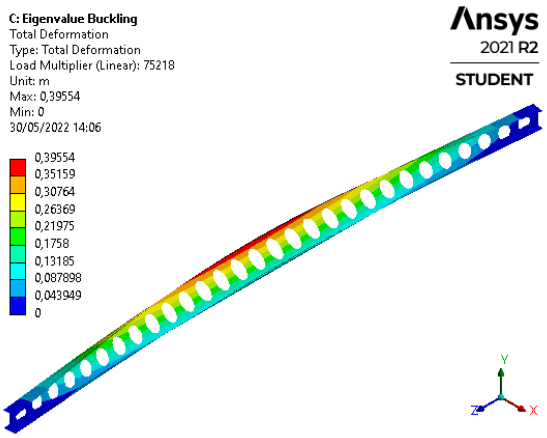

L=9.5 [m]

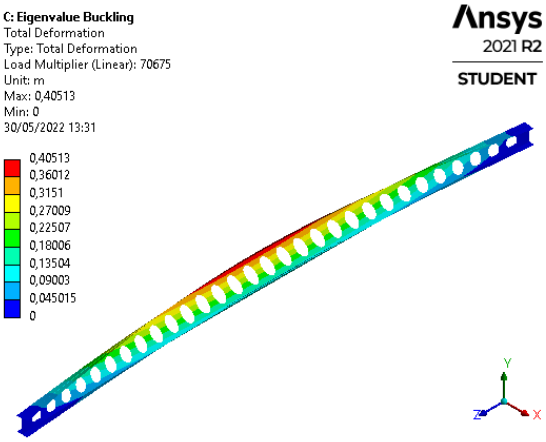
C: Eigenvalue Buckling
Total Deformation
Type: Total Deformation
Load Multiplier (Linear): 70675
Unit: m
Max: 0,40513
Min: 0
30/05/2022 13:31
0,40513
0,36012
0,3151
0,27009
0,22507
0,18006
0,13504
0,09003
0,045015
0
Ansys
2021 R2
STUDENT
Y
Z
X

L=10 [m]

$$H = 1.3h$$

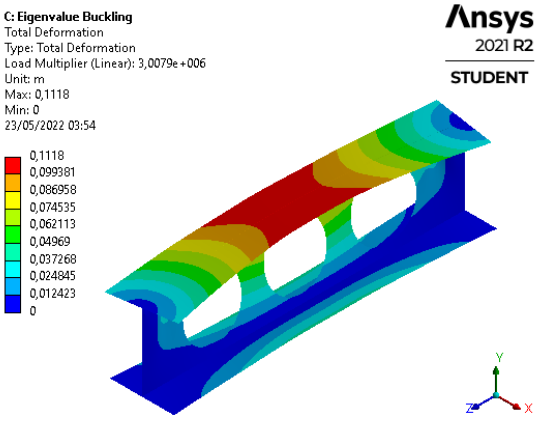

L=1 [m]

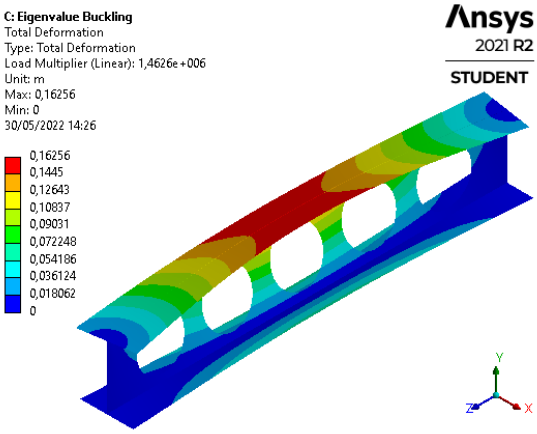

L=1.5 [m]

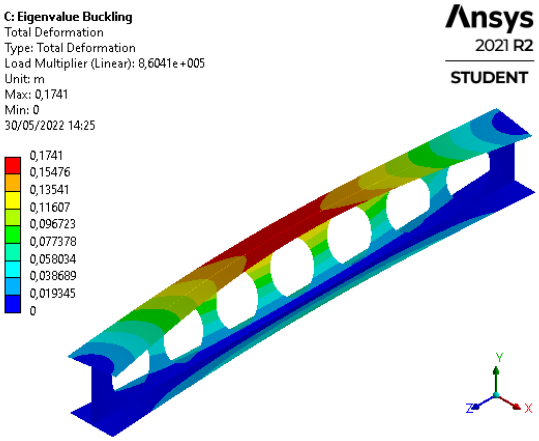

L=2 [m]

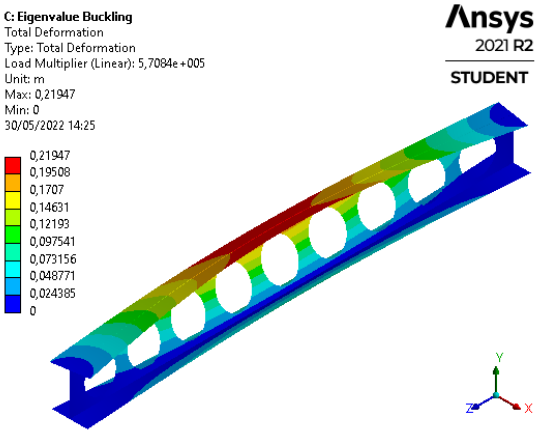

L=2.5 [m]

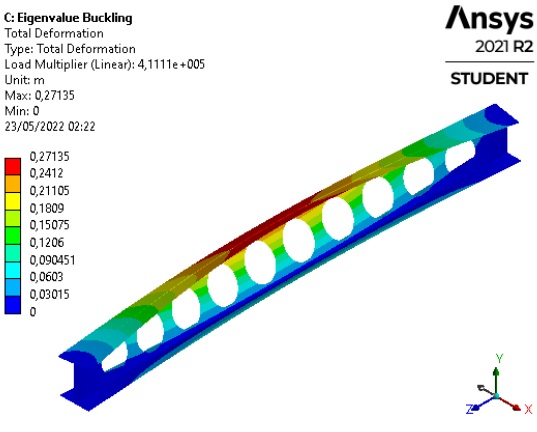

L=3 [m]

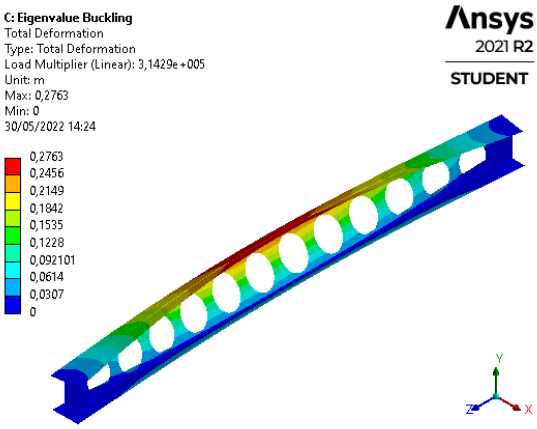

L=3.5 [m]

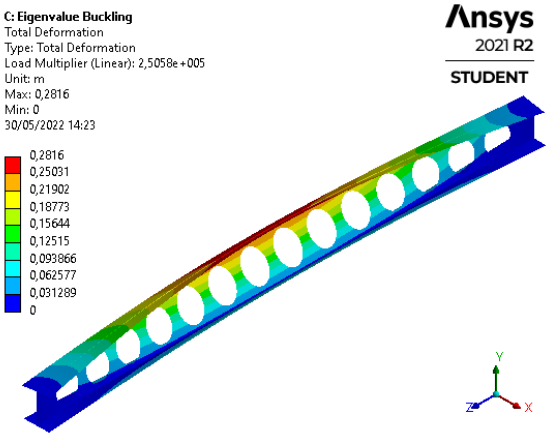

L=4 [m]

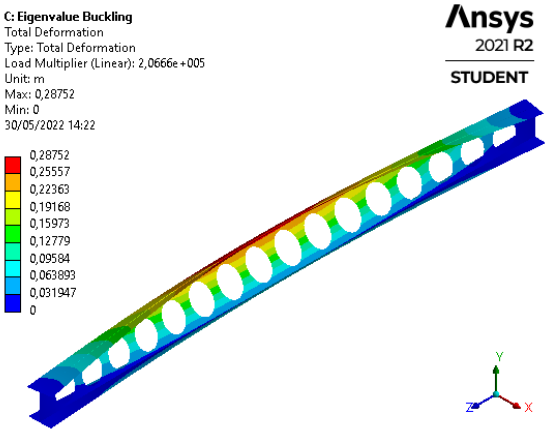

L=4.5 [m]

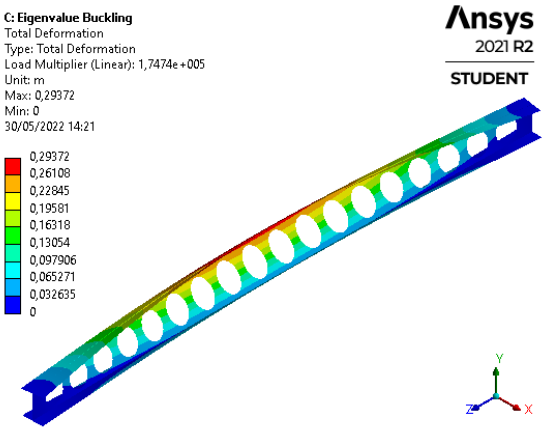

L=5 [m]

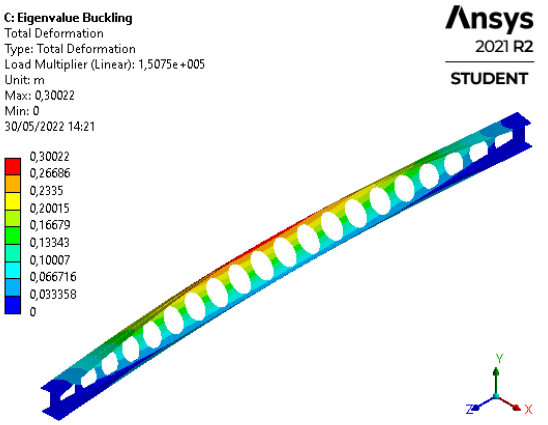

L=5.5 [m]

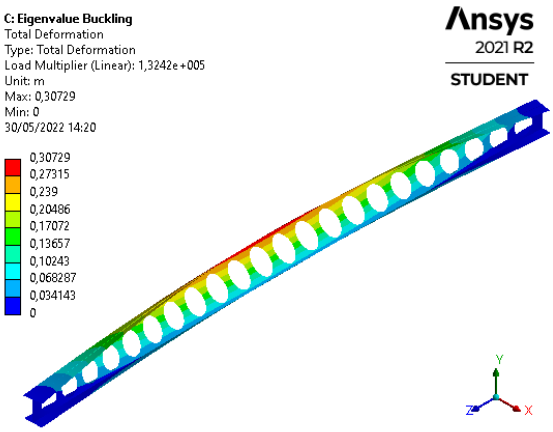

L=6 [m]

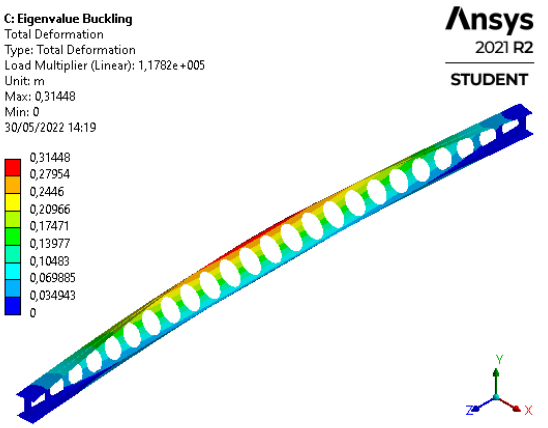

L=6.5 [m]

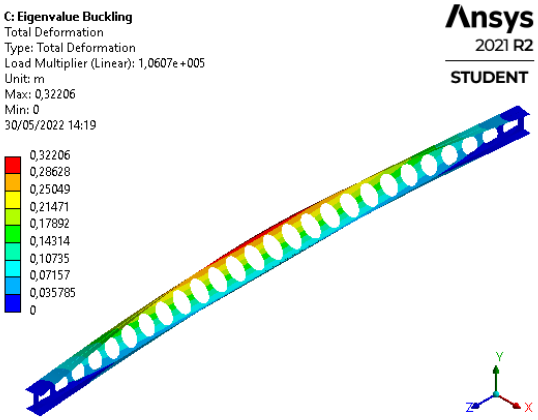

L=7 [m]

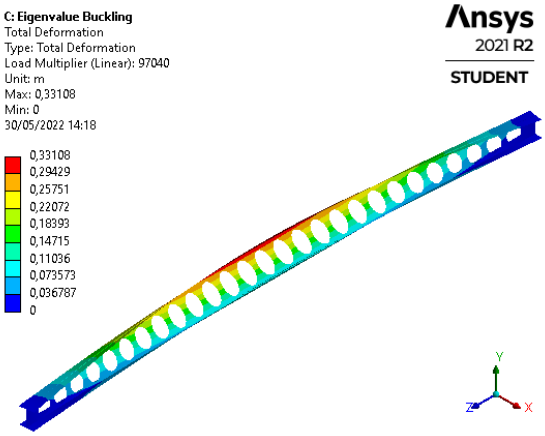

L=7.5 [m]

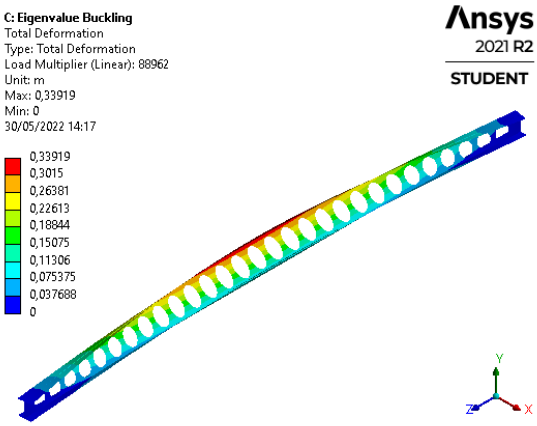

L=8 [m]

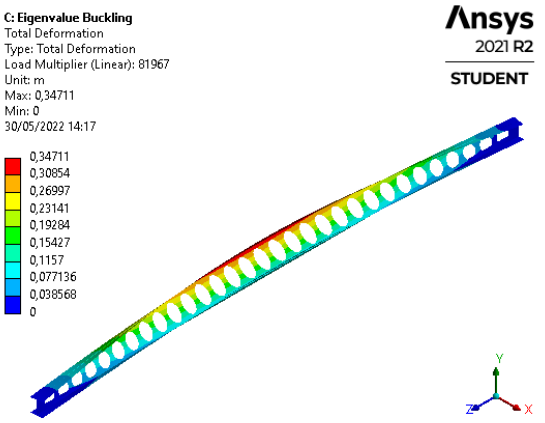

L=8.5 [m]

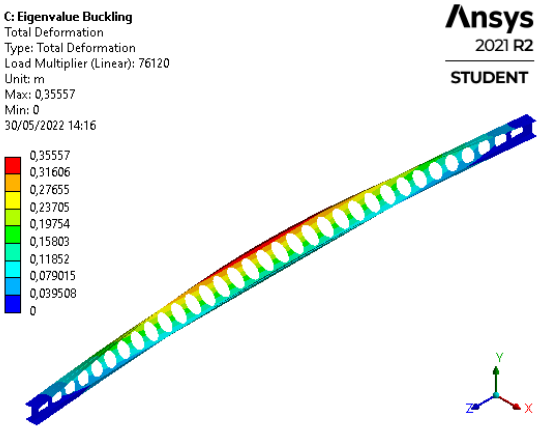

L=9 [m]

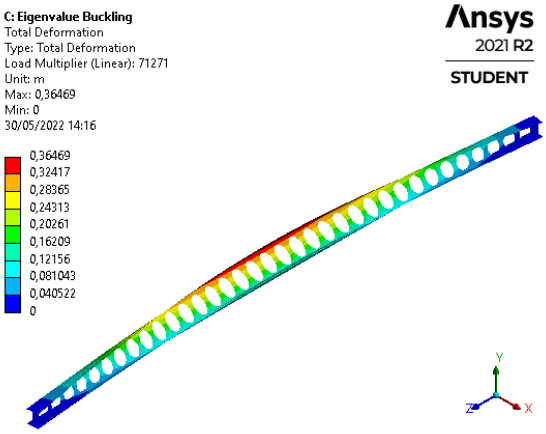

L=9.5 [m]

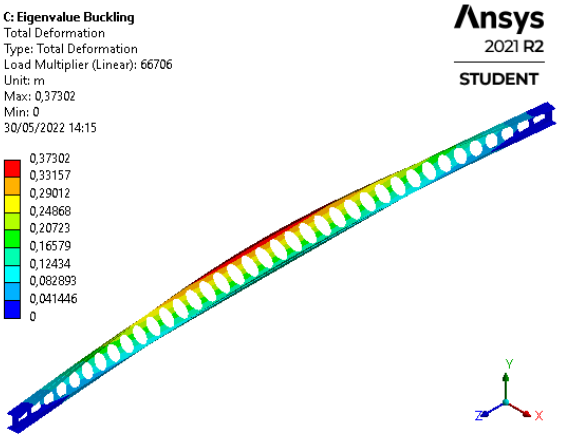
C: Eigenvalue Buckling
Total Deformation
Type: Total Deformation
Load Multiplier (Linear): 66706
Unit: m
Max: 0,37302
Min: 0
30/05/2022 14:15
0,37302
0,33157
0,29012
0,24868
0,20723
0,16579
0,12434
0,082893
0,041446
0
Ansys
2021 R2
STUDENT
Y
Z
X

L=10 [m]

$$H = 1.6h$$

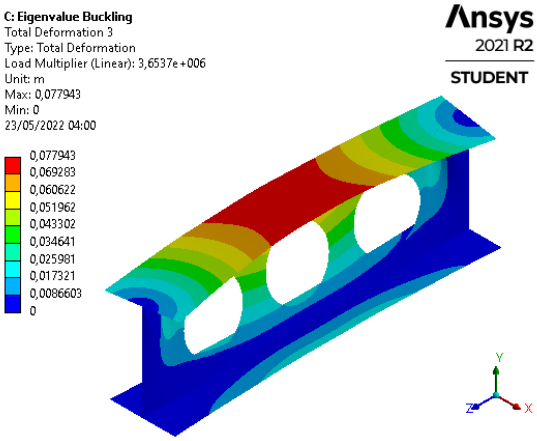

L=1 [m]

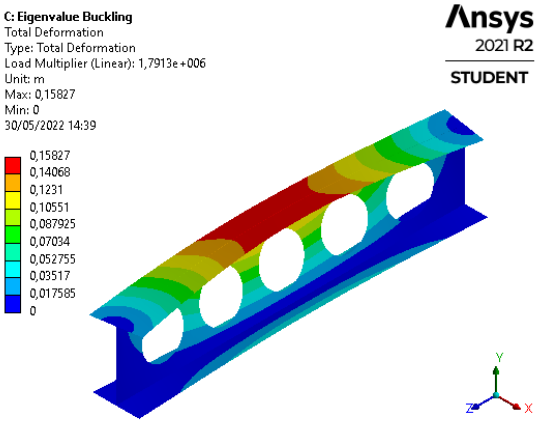

L=1.5 [m]

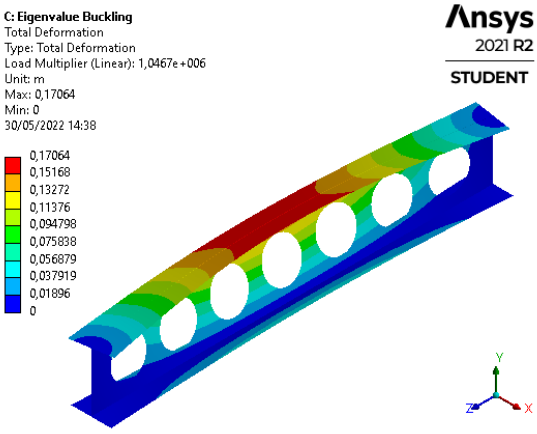

L=2 [m]

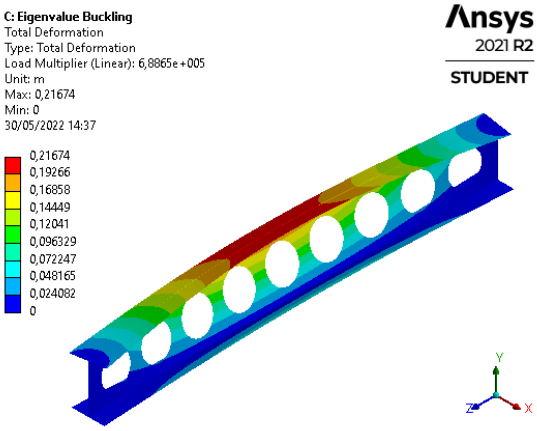

L=2.5 [m]

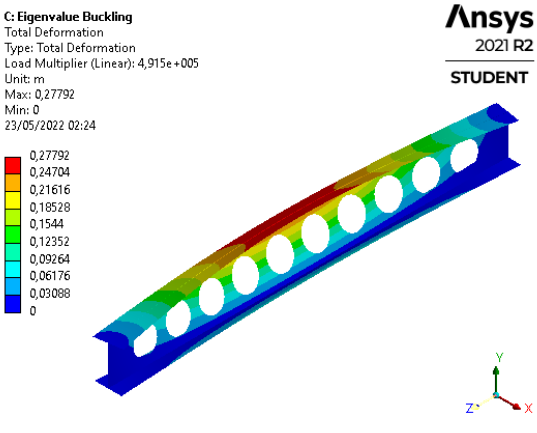

L=3 [m]

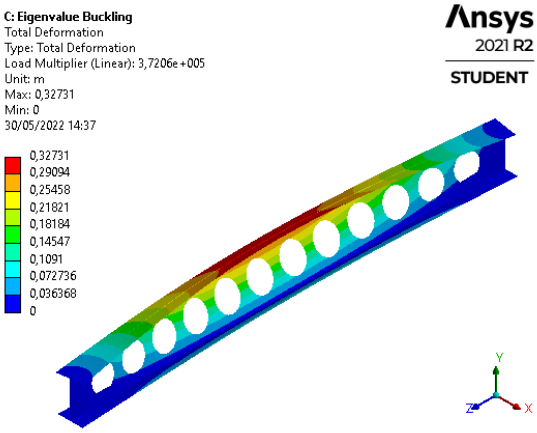

L=3.5 [m]

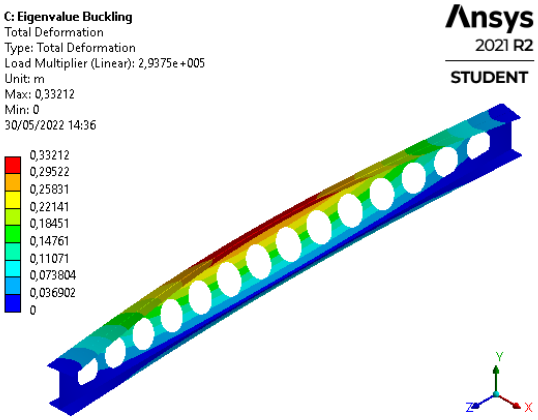

L=4 [m]

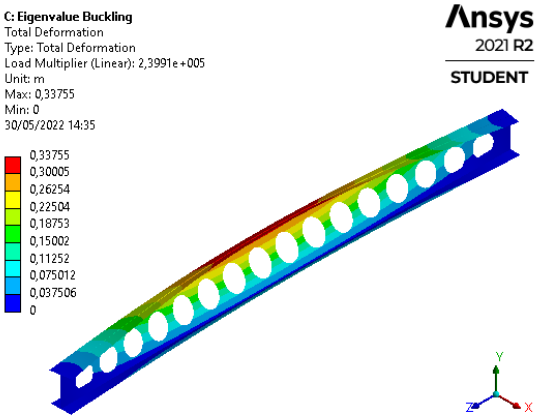

L=4.5 [m]

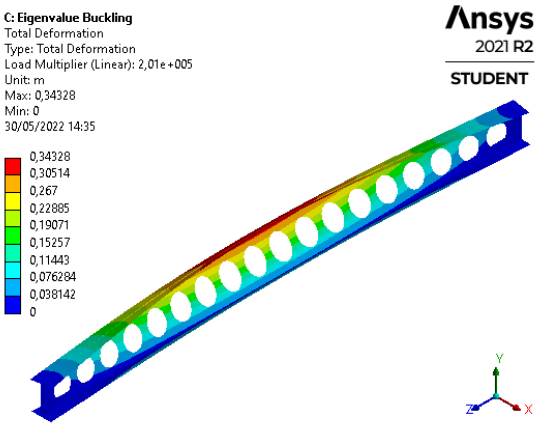

L=5 [m]

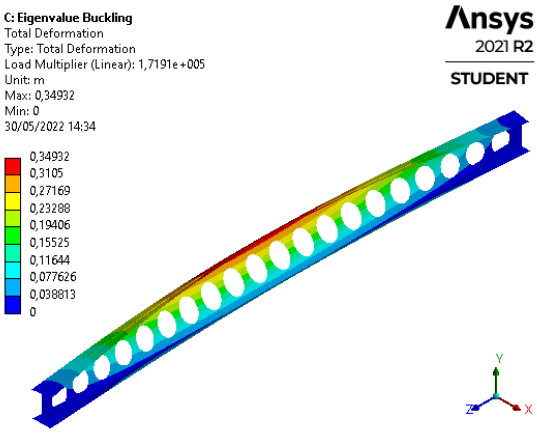

L=5.5 [m]

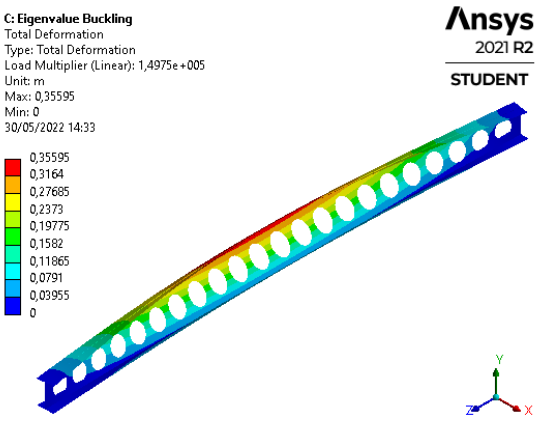

L=6 [m]

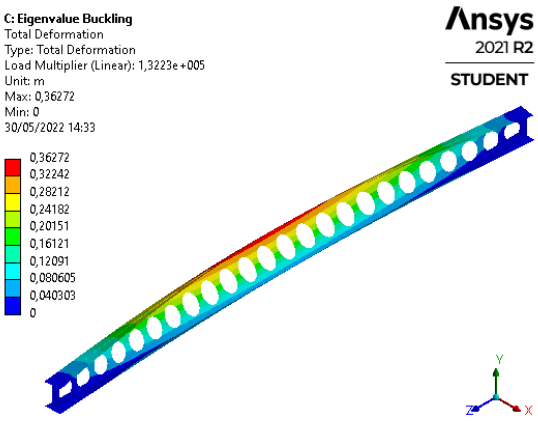

L=6.5 [m]

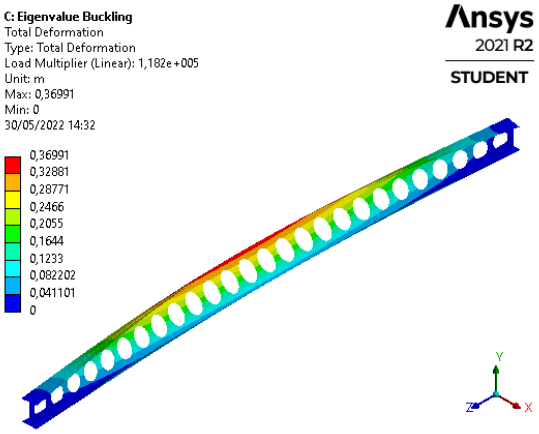

L=7 [m]

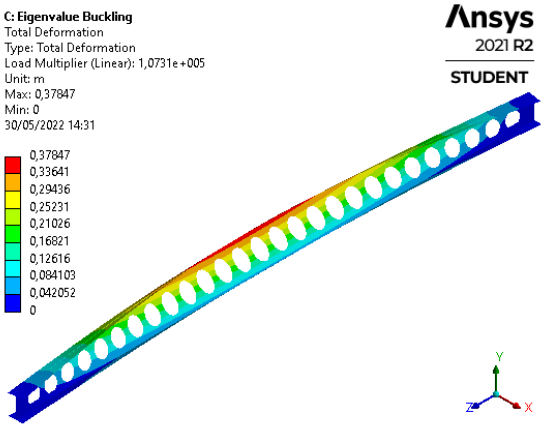

L=7.5 [m]

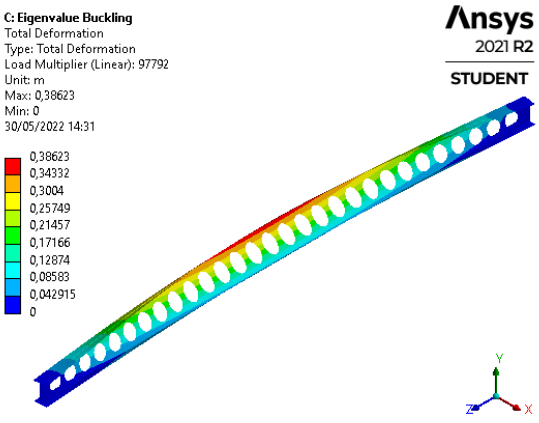

L=8 [m]

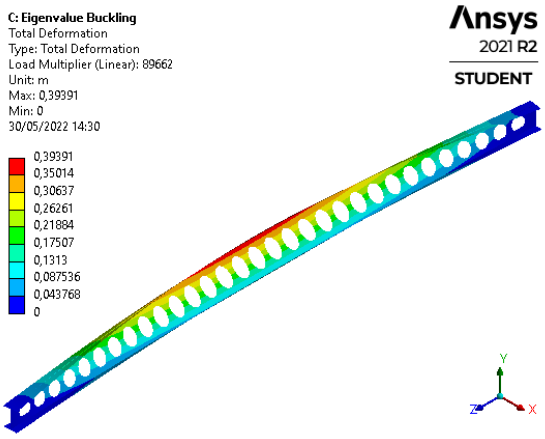

L=8.5 [m]

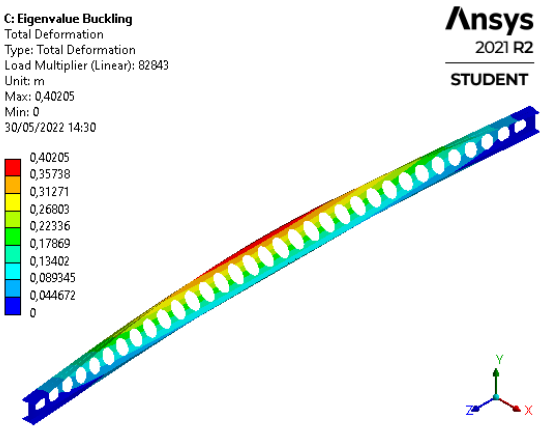

L=9 [m]

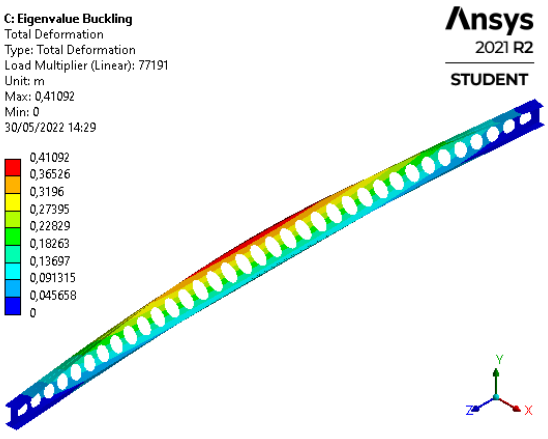

L=9.5 [m]

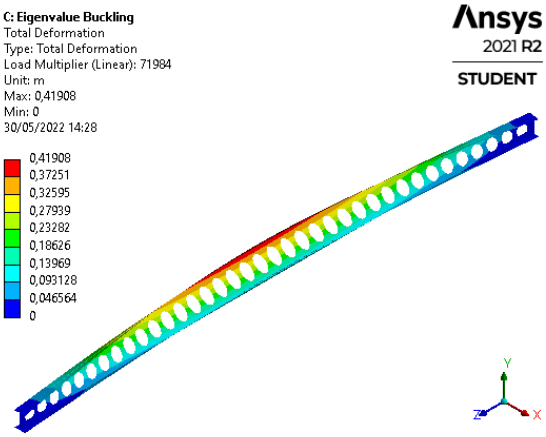
C: Eigenvalue Buckling
Total Deformation
Type: Total Deformation
Load Multiplier (Linear): 71984
Unit: m
Max: 0,41908
Min: 0
30/05/2022 14:28
0,41908
0,37251
0,32595
0,27939
0,23282
0,18626
0,13969
0,093128
0,046564
0
Ansys
2021 R2
STUDENT
Y
Z
X

L=10 [m]

ANNEX H – Non-uniform torsion of solid and cellular beam cases based on RM1

Solid beams

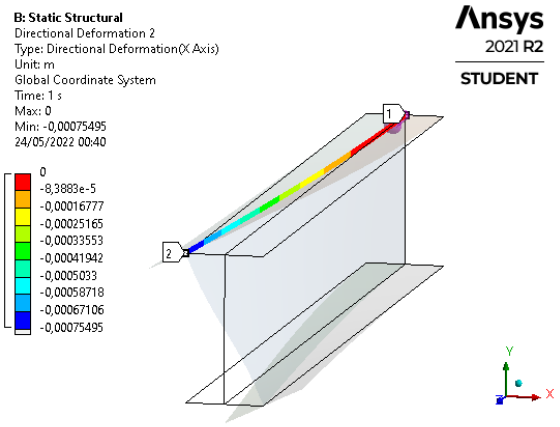

L=1 [m]

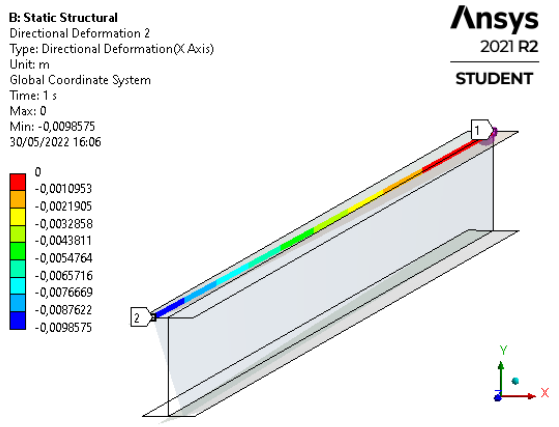

L=5 [m]

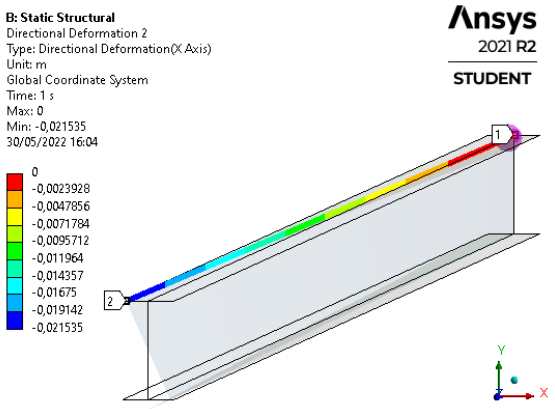

L=10 [m]

$a_0 = 1.0h$ - $S = 1.4a_0$ - $H = 1.0h$ - RM1

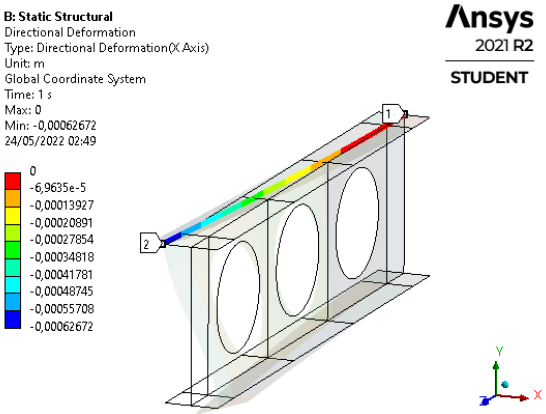

L=1 [m]

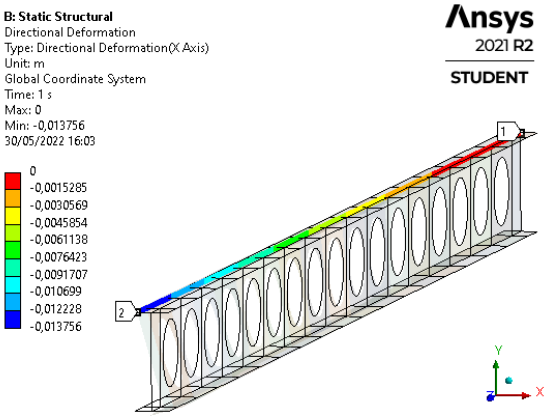

L=5 [m]

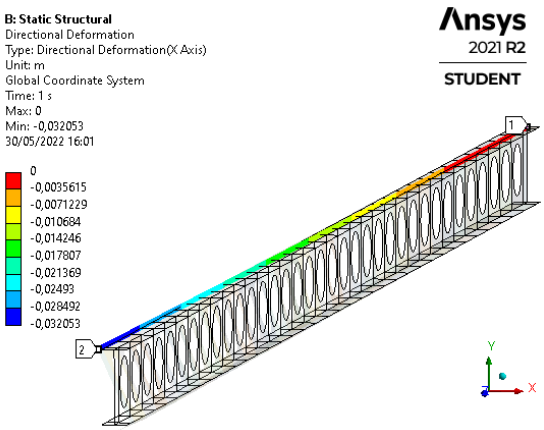

L=10 [m]

ANNEX I– Non-uniform torsion of solid and cellular beam cases based on RM2

Solid beams

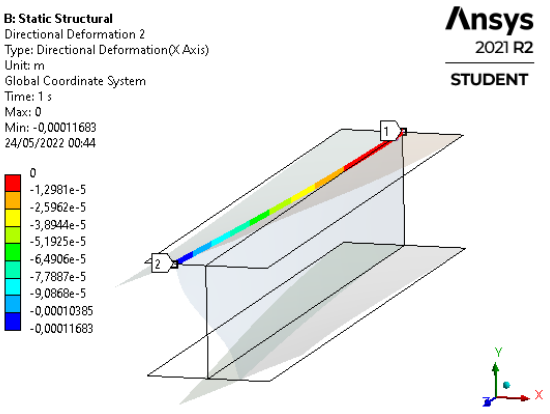

L=1 [m]

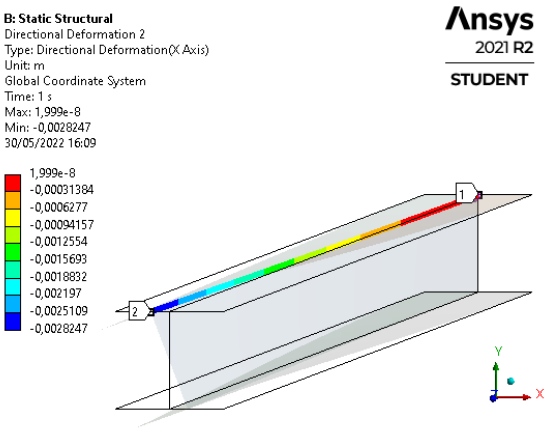

L=5 [m]

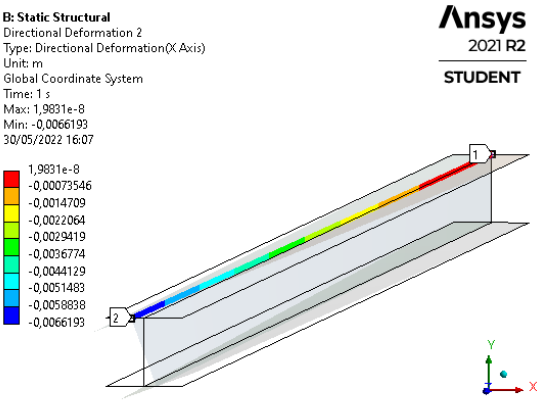

L=10 [m]

$a_0 = 1.0h$ - $S = 1.4a_0$ - $H = 1.0h$ - RM2

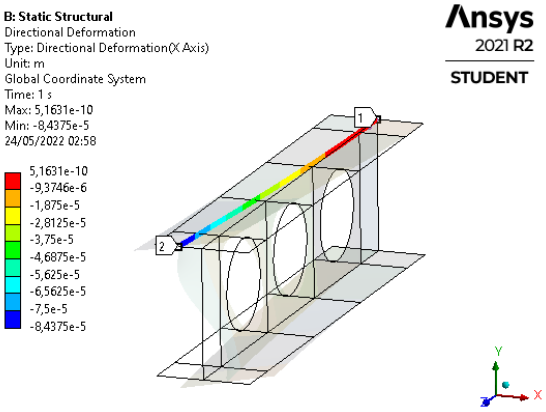

L=1 [m]

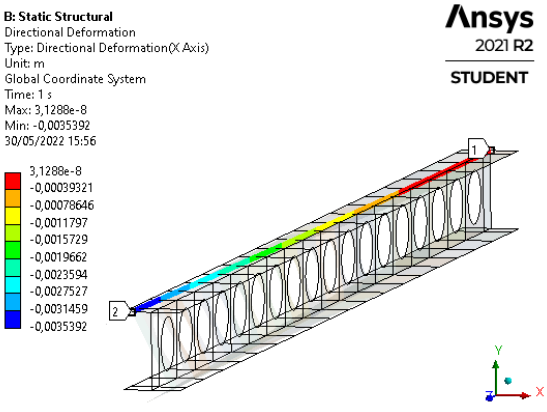

L=5 [m]

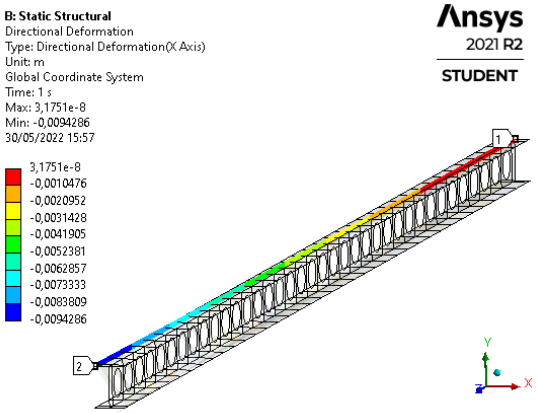

L=10 [m]